STRUCTURE AND FUNCTION ANALYSIS OF THE NATURAL PRODUCT PLANTAZOLICIN, A *BACILLUS ANTHRACIS*-SPECIFIC ANTIBIOTIC

BY

KATIE JO MOLOHON

DISSERTATION

Submitted in partial fulfillment of the requirements
for the degree of Doctor of Philosophy in Microbiology
in the Graduate College of the
University of Illinois at Urbana-Champaign, 2015

Urbana, Illinois

Doctoral Committee:

Associate Professor Douglas A. Mitchell, Chair
Professor Steven R. Blanke
Professor Andrei Kuzminov
Professor Gary J. Olsen

ABSTRACT

Bacteria are a fruitful source of metabolites, many of which have been the scaffolds for the majority of approved antibiotic compounds. In this dissertation, I present the discovery and characterization of a bacterial natural product from *Bacillus methylotrophicus* FZB42, a Gram-positive, rod-shaped bacterium that stimulates plant growth. A prolific producer of secondary metabolites, FZB42 excretes a compound bearing the molecular mass of 1335 Daltons called plantazolicin (PZN). I describe the genetic locus responsible for the biosynthesis of PZN, which is ribosomally synthesized via an amino acid precursor peptide and post-translationally modified to contain thiazoles and (methyl)oxazoles. This group of compounds, known as thiazole/oxazole-modified microcins (TOMMs), exhibit disparate biological activities and complex chemical structures. Using high-resolution mass spectrometry, chemoselective modification, genetic interruptions, and various spectroscopic tools, I report the molecular structure of PZN. PZN contains two conjugated polyazole moieties and an N^{α},N^{α}-dimethylarginine on the amino terminus. By altering oxygenation levels during fermentation, PZN analogs were produced that bear variability in their heterocycle content, which yielded insight into the order of biosynthetic events. Extensive tailoring of PZN endows it with not only a rigid, polyheterocyclic structure, but also antibacterial activity. After screening numerous microorganisms, PZN exhibited highly selective antibiotic activity against *Bacillus anthracis*. This remarkably discriminatory activity rivals a previously-described *B. anthracis*-specific gamma (γ) phage lysis assay in distinguishing *B. anthracis* from other members of the *Bacillus cereus* group. I evaluate this unusually selective activity by measuring the RNA expression profile of PZN-treated *B. anthracis*, which revealed significant upregulation of genes within the cell envelope stress response. Using fluorescence microscopy, PZN localizes to distinct ~200 nm wide foci within the envelope; furthermore, like other cell envelope-acting compounds, PZN depolarizes the *B. anthracis* membrane. Upon selection and whole-genome sequencing of PZN-resistant mutants of *B. anthracis*, I implicate a

relationship between the action of PZN and the phospholipid cardiolipin within the membrane. Exogenous cardiolipin increases the potency of PZN in wild type *B. anthracis* and promotes the incorporation of fluorescently tagged PZN in the cell envelope. I propose that PZN localizes to and exacerbates structurally compromised regions of the bacterial membrane, which ultimately results in cell lysis.

To my brother and sister-in-law for living their motto. “No matter what, keep going.”

ACKNOWLEDGMENTS

With so many people to thank along my journey, I first extend my gratitude toward my advisor, Professor Doug Mitchell. It has been a pleasure to brainstorm with you about a project in which we are both so passionate. You have been the fire under many experimental, collaborative, and funding opportunities, all of which helped me become a better scientist. I am honored to be a part of your scientific family tree. I am thankful to my thesis committee, Professors Steve Blanke, Andrei Kuzminov, Gary Olsen, and Steve Farrand, who have graciously tackled a project that hugs the fringe of the typical microbiology realm, but nonetheless provided me with critical feedback to shape my research. I am also grateful to my collaborators, Dr. Brad Evans, Dr. James Doroghazi, Patti Blair, and Tucker Maxson, without whom my research would be incomplete.

Work hard. Play hard. Many wonderful friends and colleagues have been there to get me through the highs and lows of research. The original Douglings, Courtney Cox, Kate Woodall, Kyle Dunbar, and Joel Melby, have been my accomplices in mischief and shenanigans since the beginning. I will also forever cherish the celebrations with Carleigh Hebbard, Chelsea Lloyd, Caitlin Deane, Michelle Goettge, Brian San Francisco, Tucker Maxson, and Patti Blair, to name a few. As for my hometown gals, Rebecca Crowley and Laura Blumenstock, I am grateful for our long weekends, especially the camping and canoeing trips, where I learned my degree cannot assist me in building a fire.

Lastly, my family has been so instrumental to me during my time in graduate school. Mama, my rock, my counselor, my best friend: I'm so blessed to have you as a confidant, sounding board, and role model. Thank you for the laughs throughout the journey. Daddio, my first science/math instructor, my movie director, my go-kart pusher: your support never goes unnoticed. Every "I'm so proud of you" sent my way demonstrates your love and boosts my confidence. I strive to always make you proud. Ryan and Crystal, you have never let life get in your way of a great day. Together, you live every day to the fullest and demonstrate to me the

most important things to obtain: love and laughter. To my husband, Nick, you have supported me and kept me laughing for the majority of my graduate school career. I will be so fortunate to laugh with you for the rest of my life.

TABLE OF CONTENTS

CHAPTER I: INTRODUCTION

1.1 Bacteria as Abundance Sources of Natural Products

Bacteria harbor extensive capabilities to synthesize structurally complex and useful natural products. Roughly two thirds of approved antibiotics are natural products or natural product derivatives/mimics (Newman and Cragg, 2012), with such notable examples as chloramphenicol (protein synthesis inhibitor) (Gottlieb *et al.*, 1954) and rifampicin (RNA polymerase inhibitor) (Sensi *et al.*, 1959). Past success with natural products as antimicrobial compounds warrants the exploration into uncharted biosynthetic territory to discover new natural products.

Antibiotics have traditionally been discovered by large screening endeavors, examining the bioactivity of bacterial crude extracts for compounds harboring antibiotic activity (Figure 1.1A). While this method has produced a number of useful compounds, the methodologies are tedious and limited. Frequent compound rediscovery, the lack of laboratory culturable organisms, and extensive screening time limit the usefulness of the forward discovery approach (Baltz, 2006).

Low-cost next-generation DNA sequencing technology is responsible for the surge in genomic data mining. The availability of nearly 2,000 new microbial genomes has rekindled interest in the biosynthetic capabilities of bacteria (Bachmann *et al.*, 2014; Challis, 2008; Gross, 2009; Melby *et al.*, 2011; Peric-Concha and Long, 2003; Van Lanen and Shen, 2006), reducing the need for timely screening procedures. Recent studies, making use of newly sequenced bacterial genomes, have demonstrated the enormous, largely untapped potential of microbes as a source of natural products (Bachmann *et al.*, 2014; Bentley *et al.*, 2002; Challis, 2008; Deane and Mitchell, 2014; Doroghazi *et al.*, 2014; Doroghazi and Metcalf, 2013; Velasquez and van der Donk, 2011).

Reverse genetics approaches have demonstrated that *Streptomyces coelicolor*, one of the most studied organisms for natural product/antibiotic research, harbors the genetic capacity to produce many additional secondary metabolites of potential importance (Deane and Mitchell, 2014). This phenomenon extends to the microbial population as a whole (Baltz, 2008; Bentley *et al.*, 2002; Deane and Mitchell, 2014; Fischbach and Walsh, 2009; Jensen *et al.*, 2014). Bioinformatic tools and databases help to organize the abundance of data that has emerged on these previously undescribed biosynthetic pathways (Blin *et al.*, 2013; de Jong *et al.*, 2006; Li *et al.*, 2012; Mohimani *et al.*, 2014). Reverse genetics reconciles some of the unfortunate downfalls of the forward genetic approach, *e.g.* a lack of culturable organisms, biosynthetic pathways that are silent under laboratory conditions, and compound rediscovery. By making use of the vast genomic sequence data available, researchers can enrich for a specific compound class, predict chemical structures, biological activities, and manipulate growth conditions to maximize natural product potential (Figure 1.1B).

1.2 Ribosomally Synthesized and Post-Translationally Modified Peptide Natural Products

Natural product research and antibiotic discovery encompass numerous classes of bacterial compounds (of nonribosomal and ribosomal origin); of primary interest to this research is a relatively newly defined class of natural products referred to as the ribosomally synthesized and post-translationally modified natural products (RiPPs) (Arnison *et al.*, 2013; Haft *et al.*, 2010; Lee *et al.*, 2008; Letzel *et al.*, 2014; Maksimov and Link, 2014; Velasquez and van der Donk, 2011). RiPPs comprise a diverse natural product landscape, encompassing lanthipeptides, linear azol(in)e-containing peptides, lasso peptides, and linaridins, among others. In all cases, a ribosomally produced precursor peptide undergoes modification including, but not limited to, cyclizations, dehydrations, methylations, and disulfide bond formations (Arnison *et al.*, 2013; Dunbar and Mitchell, 2013b). The diverse modifications give rise to an expanse of chemical structures and numerous biological activities. The genomic sequence of the precursor peptide and

homology of the tailoring enzymes bring forth predictions of the chemical structure of the post-translationally modified natural product. Furthermore, the microbial and scientific communities can "evolve" RiPPs by manipulating either the peptide precursor destined for tailoring or the tailoring enzymes themselves.

1.3 Thiazole/Oxazole-Modified Microcins (TOMMs)

One region of largely uncharted biosynthetic RiPP natural product space is the thiazole/oxazole-modified microcin (TOMM) family, which is classified by conserved chemical modifications and genetic layout (Figure 1.2A) (Haft *et al.*, 2010; Lee *et al.*, 2008; Scholz *et al.*, 2011). Each TOMM precursor peptide harbors an *N*-terminal leader region that serves as the binding site for enzymes that post-translationally modify a *C*-terminal core region (Madison *et al.*, 1997; Mitchell *et al.*, 2009). The distinguishing chemical feature of a TOMM is the installation of heterocycles that are derived from Cys, Ser, and Thr residues, which are abundant in the core region of the precursor peptides. During processing by a genetically conserved cyclodehydratase, select Cys and Ser/Thr amino acids undergo peptide backbone cyclization to become thiazoline and (methyl)oxazoline heterocycles (Figure 1.2B) (Dunbar *et al.*, 2014; Dunbar *et al.*, 2012; Dunbar and Mitchell, 2013a). A subset of these are further subjected to a flavin mononucleotide (FMN)-dependent dehydrogenation, which yields the fully oxidized thiazole and (methyl)oxazole heterocycles (Melby *et al.*, 2014). Together, the TOMM cyclodehydratase and dehydrogenase comprise a functional thiazole/oxazole synthetase. The genes encoding the synthetase are typically located as adjacent open reading frames in bacterial genomes, making such biosynthetic clusters relatively easy to identify using routine bioinformatic methods (Donia *et al.*, 2008; Lee *et al.*, 2008; Velasquez and van der Donk, 2011; Wieland Brown *et al.*, 2009). TOMM biosynthetic clusters often contain ancillary tailoring enzymes that increase the chemical complexity of this natural product family, in addition to leader peptide proteolysis (Figure 1.2C) (Datta *et al.*, 2005; Kelly *et al.*, 2009; Liao *et al.*, 2009; Morris *et al.*,

2009; Wieland Brown *et al.*, 2009). In many cases, the fully mature TOMM natural product is then actively exported from the cell through an ABC transport system.

Although the unification of the TOMM family of natural products has only recently emerged, the molecular structure and biological function of some TOMMs have long been established. Examples include microcin B17 (DNA gyrase inhibitor) (Belshaw *et al.*, 1998), the cyanobactins (eukaryotic cytotoxins) (Schmidt and Donia, 2009), streptolysin S (virulence-promoting cytolysin) (Mitchell *et al.*, 2009; Molloy *et al.*, 2011), and the thiopeptides (ribosome inhibitors) (Just-Baringo *et al.*, 2014; Melby *et al.*, 2011).

1.4 Natural Product Isolation and Structure Elucidation

Genetic deletions and chemical investigation often prime natural product discovery. Armed with the genetic context of a natural product, the compound is subjected to isolation and purification from the crude bacterial cellular extract, which contains multiple metabolic compounds. Structure elucidation typically occurs on the purified compound, but can begin in crude form if the compound can be properly separated from the remaining bacterial metabolites.

1.4.1 Natural product identification via genetic deletions and heterologous production

The reverse genetic approach to natural product discovery seeks to identify a connection between genes and metabolites. The most definitive method to link genes to molecules is through genetic deletion of the implicated genes. Then, by comparing the mutant to the parent strain, whether by mass spectrometry or activity screening, natural products can be identified and characterized. Heterologous expression of the target gene clusters can enhance this methodology, given the natural product remains expressed in the new, genetically amenable host (Ongley *et al.*, 2013). There are numerous examples of successful natural product identification that rely on both native producer and heterologous host expression. Native producer approaches typically involve improvement of the host strain to achieve greater natural product yields, including manipulation

of drug efflux pumps or deletion of undesired natural products that convolute compound identification (Ongley *et al.*, 2013).

1.4.2 Mass spectrometry-guided structure elucidation

Mass spectrometry (MS), alone or in conjunction with nuclear magnetic resonance (NMR), provides structural information and characterization of peptidic natural products. High resolution MS provides an accurate compound mass, which is then used to determine a chemical formula within the error of the MS instrument. Tandem MS results in fragmentation of the molecule of interest, breaking the compound into segments from which the structure of the full peptide can be deduced (Kind and Fiehn, 2010). Competing chemical formulas can often be eliminated by integrating knowledge of the chemical modification potentially encoded within the gene cluster. In 2011, a MS method was created specifically for linking biosynthetic genes to molecules (Kersten *et al.*, 2011). MS data from an organism of interest is subjected to tandem MS, and the fragmentation pattern of peptidic compounds is assembled into a sequence tag, providing information on the amino acid sequence of the compound. The genome of the producing organism can then be searched for loci corresponding to that particular amino acid sequence. The assembled fragmentation database includes common post-translational modifications, expanding the method's utility for natural product discovery. In 2013, this method was extended to tandem MS networks, relating all metabolites of an organism to their fragmentation spectra (Nguyen *et al.*, 2013). This method can even be extrapolated to include unsequenced organisms by comparing fragmentation of chemical standards or sequenced organisms.

1.5 Determining the Mode of Action of Antibiotics

Determining the mode of action (MOA) (or molecular target) of bioactive compounds can be challenging, especially if the compound does not have activity similar to other known compounds. There exist some typical methodologies for the mechanistic evaluation of antibiotics.

1.5.1 MOA determination bolstered by genomic sequencing

After establishing a compound as an antibiotic, MOA research is typically initiated by treating a susceptible strain with the compound of interest and isolating resistant mutants (Arias *et al.*, 2011; Friedman *et al.*, 2006; Hachmann *et al.*, 2009; Palmer *et al.*, 2011). Resistant mutants can be generated in a variety of ways, whether it be spontaneous adaptation or via mutagenesis (Price *et al.*, 2003; Vogler *et al.*, 2002). The resistant strains are then bioinformatically mined for the genomic polymorphisms endowing them with resistance; oftentimes, the genetic mutations provide evidence suggestive of a certain MOA. Validation via engineering genetic deletions or overexpression of the suspected target supports the involvement of the genes of interest.

An orthogonal approach to MOA determination is analyzing the changes in gene expression upon exposure to the antibiotic of interest. Transcriptional profiling via RNA-Seq or microarray can reveal the metabolic adjustments an affected organism must make in order to tolerate the harmful compound (Dengler *et al.*, 2011; Muthaiyan *et al.*, 2008; Shaw and Morrow, 2003; Wecke *et al.*, 2009). Transcriptome studies provide essential information on how the entire bacterium responds to the compound of interest. Sub-inhibitory antibiotic treatment stimulates rapid transcriptional responses in bacteria (Goh *et al.*, 2002) and the induced/repressed genes are oftentimes indicative of MOA (Brazas and Hancock, 2005; Freiberg *et al.*, 2005; Hutter *et al.*, 2004).

1.5.2 Macromolecular synthesis

Often, antibiotic classes are known to target major pathways within primary metabolism. Utilizing radioactive precursors to RNA, DNA, protein, peptidoglycan, and fatty acids, researchers can assess the biosynthesis of cellular macromolecules in the presence of the compound of interest (Cotsonas King and Wu, 2009; Silver, 2011). Bacteria are grown in the presence of the radioactive macromolecular precursors (*e.g.* nucleotides or amino acids), and treated with the tested antibiotic. As the cells grow, radiolabelled precursors are incorporated into

their respective macromolecules. Inhibition of radioactive incorporation in cells treated with the compound of interest, relative to untreated cells, can thereby inform about the MOA of the antibiotic. This protocol can be adapted for high throughput use, providing a way to measure the effect of a compound over time and in different concentrations.

1.5.3 Cytological profiling

A more recently-described method of analyzing MOA is cytological profiling. Cytological profiling uses fluorescence microscopy to reveal how fluorescently tagged compounds influence cellular morphology (Nonejuie *et al.*, 2013). The authors use bioinformatics to compare numerous morphological characteristics. This method not only distinguishes between compounds acting on different cellular pathways, but it can even separate inhibitors that target different points along the same pathway. Compounds can be classified by their molecular target or provide evidence for a new MOA, based on their fluorescence patterns.

1.5.4 Difficulties of mode of action determination

The methodologies described above are not always fruitful, especially for compounds with unique MOAs, like daptomycin and nisin. Based on current research, in a calcium-dependent manner, daptomycin oligomerizes and displaces phospholipids in the bacterial membrane. Daptomycin oligomers assemble into a pore structure that depolarizes the membrane, disrupting cell integrity (Pogliano *et al.*, 2012; Silverman *et al.*, 2003; Straus and Hancock, 2006; Zhang *et al.*, 2014). However, despite over two decades of research, the exact MOA and stoichiometry of daptomycin oligomerization is still debated, illustrating the difficulty in characterizing antibiotics that do not target the major biosynthetic pathways. Nisin, on the other hand, exhibits at least two MOAs, targeting lipid II, as well as forming pores across the cytoplasmic membrane (Brotz and Sahl, 2000). Never-before-seen MOAs can easily convolute target determination of unique compounds, and require further experimentation.

1.6 Model Organisms

TOMM natural products are common among bacterial and archaeal species. Here we introduce one TOMM producer, *Bacillus methylotrophicus* FZB42. Chapter 2 will describe the genetic context for the TOMM biosynthetic cluster in FZB42, and Chapter 4 will discuss the bacterium of most relevance to the determination of its MOA, *Bacillus anthracis*.

1.6.1 *Bacillus methylotrophicus* FZB42

*Bacillus methylotrophicus** FZB42 [previously named *Bacillus amyloliquefaciens* FZB42 (Dunlap *et al.*, 2015)] is a Gram-positive, plant growth-promoting bacterium with an impressive capacity to produce secondary metabolites with antimicrobial activity (Chen *et al.*, 2007). The nonribosomal synthesis of polyketides (bacillaene, difficidin, and macrolactin), lipopeptides (surfactin, fengycin, and bacillomycin D), and siderophores (bacillibactin and the product of the *nrs* cluster) are carried out by large gene clusters distributed over the entire genome of FZB42. In total, 8.5% of the entire genomic capacity of FZB42 is devoted to the nonribosomal synthesis of secondary metabolites, exceeding that of the model Gram-positive bacterium *Bacillus subtilis* 168 by more than 2-fold (Chen *et al.*, 2009). Prophage sequences that often harbor RiPP biosynthetic gene clusters, of which are common in *B. subtilis* strains, were not previously detected within the FZB42 genome. This finding underscores the diversity of biosynthetic strategies employed by FZB42 and offers new possibilities for discovering novel natural products with biomedically relevant activities. Specifically, studying the metabolites of soil-dwelling bacteria like FZB42 can reveal a number of products that may be useful for combating infectious disease. While most of the described natural products from FZB42 are classified as non-ribosomal peptides and polyketides, this strain has been recently demonstrated to produce a TOMM which is now referred to as plantazolicin (PZN) (Scholz *et al.*, 2011).

1.6.2 *Bacillus anthracis*: disease and differentiation

Bacillus anthracis is the causative agent of anthrax. Of clear interest to bioterrorism, the bacterial spores responsible for the disease can also be encountered by the consumption of contaminated meat of grazing livestock or direct contact with infected animals. Preventative measures include a variety of bacterial vaccines. Currently, the vaccines used are only administered to those with routine exposure (military, veterinarians, researchers), as safety concerns and production/storage costs are high (Beierlein and Anderson, 2011; Spencer, 2003). The components of the vaccines differ from lot to lot, which may cause complications and reactivity after dosage. Furthermore, the vaccines in present circulation are not approved for post-exposure; therefore, anthrax infections are treated with intense, prolonged antibiotic regimens. A 60-day course of penicillin, doxycycline, and/or ciprofloxacin is the chosen treatment for the most serious manifestation; inhalational anthrax (Inglesby *et al.*, 1999). Antibiotic resistance is a logical concern after such prolonged periods of antibiotic treatment, and resistance has been documented for the above-mentioned compounds (Brook *et al.*, 2001; Pomerantsev *et al.*, 1992; Price *et al.*, 2003). Further, secondary infections like *Clostridium difficile*-associated diarrhea are not uncommon after treatment with quinolones such as ciprofloxacin (Yip *et al.*, 2001). Antibiotics, while extremely useful in fighting infections, can actually be harmful to our wellbeing due to misuse and overprescribed practices in medical facilities today. We must continue to develop and implement new treatment options if we plan to combat these diseases while minimizing drug resistance in future generations

B. anthracis is a Gram-positive bacterium and is a member of the *B. cereus sensu lato* group, which includes *B. cereus*, *B. anthracis*, *B. thuringiensis*, and *B. mycoides* (Jensen *et al.*, 2003; Rasko *et al.*, 2005). Microbiologists have debated whether these organisms should be considered as one species, given that they can be greater than 99% identical at the DNA level. Despite being grouped with other *Bacillus* species, *B. anthracis* harbors a number of features that

set it apart from other members of the *B. cereus* group. As the causative agent of anthrax and a category A priority pathogen, fully virulent *B. anthracis* contains two conserved plasmids, pXO1 and pXO2. The genes responsible for producing the anthrax toxin and poly-D-glutamic acid capsule are encoded on pXO1 and pXO2, respectively. Importantly though, plasmid content cannot be relied upon as a definitive indicator for *B. anthracis*, as a growing number of *B. cereus* and *B. thuringiensis* strains are known to carry homologous plasmids (Kolsto *et al.*, 2009; Wright *et al.*, 2011). Beyond characteristic plasmid content, *B. anthracis*, unlike other members of the *B. cereus* group, harbors a nonsense mutation in *plcR* (phospholipase C regulator), which yields a truncated and inactive protein. *B. anthracis* is therefore devoid of phospholipase C activity, but also, owing to the pleiotropic regulation of several other virulence factor genes, *plcR* dysfunction renders *B. anthracis* non-motile and non-hemolytic (Agaisse *et al.*, 1999).

Exterior to the cell wall, *B. anthracis* displays a two-dimensional protein lattice that encompasses the entire cell surface. This surface layer (S-layer) is non-covalently attached to the cell by lectin-like interactions with a secondary cell wall polysaccharide (SCWP) (Wang *et al.*, 2013; Zheng *et al.*, 2013), which is covalently tethered to the peptidoglycan and radiates outwards. The S-layer is decorated with surface associated proteins in a *csaB* (cell surface attachment)-dependent manner (Mesnage *et al.*, 2000). The *B. anthracis* SCWP is species-specific (Choudhury *et al.*, 2006; Weidenmaier and Peschel, 2008) and serves as the binding site for gamma (γ) phage (Ganguly *et al.*, 2013; Schuch *et al.*, 2013) and previously described *B. anthracis* typing antibodies (Ezzell *et al.*, 1990). γ phage produces a peptidoglycan hydrolase, PlyG, which specifically recognizes the terminal galactoses of the *B. anthracis* SCWP and subsequently hydrolyzes the cell wall (Ganguly *et al.*, 2013). The vast majority of non-*B. anthracis* members within the *B. cereus sensu lato* group bear terminal glucose moieties in their SCWP and thus are resistant to γ phage lysis. However, there exist atypical *B. anthracis* strains which lack the galatose-forming UDP-glucose 4-epimerase. Such *B. anthracis* strains are resistant

to γ phage lysis and would constitute false-negatives in any diagnostic assay based on γ phage (Abshire *et al.*, 2005). Additionally, atypical strains of *B. cereus* exist that encode the galatose-forming UDP-glucose 4-epimerase, rendering the strain susceptible to γ phage (a false-positive in the diagnostic assay) (Hoffmaster *et al.*, 2006). Wip1, another *B. anthracis*-specific phage, is even more selective than γ phage, but yet certain *B. cereus* strains remain sensitive (Kan *et al.*, 2013). Similarly taking advantage of differences in the SCWP, the above-mentioned typing method uses monoclonal antibodies to the galactose-bearing SCWP. As expected, this assay suffers from the same selectivity issues as the γ phage lysis assay (Ezzell *et al.*, 1990).

1.7 Summary and Outlook

For more than a century, natural product researchers have extracted thousands of structurally complex compounds from living organisms, most of them bacteria. Many of these natural products have clinical utility and form the foundation of our modern chemotherapeutic arsenal. The most prolific producers of such compounds are soil-dwelling, Gram-positive bacteria. Today, antibiotic resistance is on the rise, and the need for antibiotics with novel MOA is pressing (Clatworthy *et al.*, 2007).

TOMMs are a large and expanding category of peptide natural products that are post-translationally modified to contain heterocycles. A variety of structural scaffolds and chemical modifications, installed by conserved tailoring enzymes, endow TOMMs with disparate biological activities. A growing number of TOMM natural products have been structurally and functionally assessed, but the majority are unknown compounds that have yet to reveal their potential utility. In 2008, a predicted TOMM precursor peptide was discovered in *Bacillus methylotrophicus* FZB42. In Chapter 2, we introduce a novel natural compound, a TOMM produced by FZB42, referred to as plantazolicin (PZN) and report the initial findings on PZN purification and production. We investigate the biosynthetic cluster responsible for the production of PZN, and engineer genetic deletions in the native producer to confirm the genes required for

biosynthesis, export, and potential self-immunity. In Chapter 2, we begin to explore the bioactivity of PZN, screening a panel of Gram-positive and Gram-negative strains for antibacterial activity.

TOMM natural products are characterized by their short unstructured leader peptide that undergoes post-translational modification. This endows the peptide with structural rigidity (conferred by heterocycle incorporation) and a resultant biological function. At the end of Chapter 2, we divulge the precursor peptide sequence of PZN and establish the initial biological activity. In Chapter 3, we present the high resolution mass of PZN which, in conjunction with tandem MS, NMR, and chemoselective modification, reveals the chemical structure of PZN. Bioinformatic analysis of the PZN gene cluster establishes a small family of PZN or PZN-like bacterial natural products, demonstrating the potential for compound evolution and chemical modification. We further assess the biological activity of PZN, validating the limited spectrum of its biological activity.

Until now, the biological activity of PZN has been only minimally described. In Chapter 4, we examine the unique specificity of PZN for *B. anthracis*, the causative agent of anthrax. We present a large panel of PZN-treated strains that establish PZN as a *B. anthracis* specific compound at clinically relevant concentrations (1 μg/mL). We investigate the molecular target of PZN by assessing the gene expression of *B. anthracis* upon PZN treatment, as well as analyzing the genomic sequences of PZN-resistant *B. anthracis* mutants. These studies, along with confocal localization and synergistic activity with cell envelope-acting antibiotics, provide evidence that PZN targets the *B. anthracis* membrane.

The current rate of antibiotic discovery is one of many factors hindering our fight in the arms race against bacteria. Natural products, which comprise the overwhelming majority of antibiotics, are a plentiful source for new medicinal compounds. The reverse genetics discovery method has provided a way to tap into this resource by accelerating the identification of new

compound classes and inspiring ingenious chemical engineering of our existing arsenal. The discovery of PZN provides a chemical and biological scaffold to advance natural product research as a whole.

1.8 Acknowledgments

Thank you to Dr. Brian San Francisco and Nicholas Hess for critically editing this chapter.

1.9 Figures

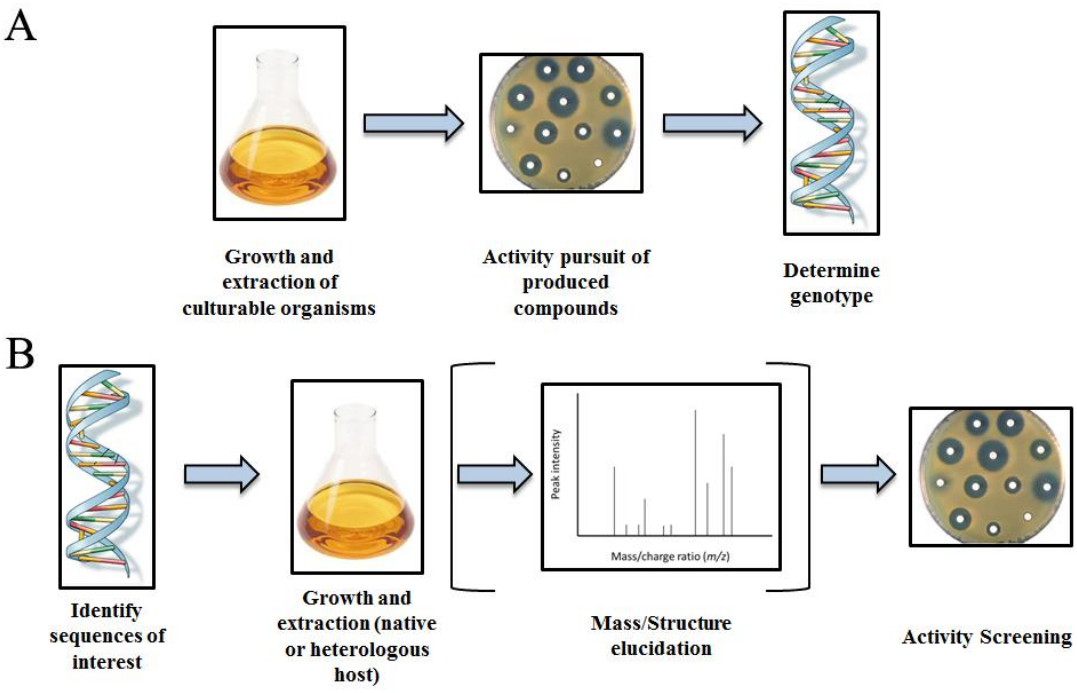

Figure 1.1 | Forward/reverse genetic approaches to natural product discovery. (A) Forward natural product discovery begins with bacterial isolation and growth in laboratory culture. Bacterial extracts undergo large screens for biological activity, and compounds of interest are analyzed for genetic characterization. (B) Reverse natural product discovery utilizes the vast genomic sequencing databases in search for specific natural product classes. Compound production via the native or heterologous host is followed by compound characterization. The genomic sequence alludes to predicted structural scaffolds, simplifying mass spectrometry and activity screens.

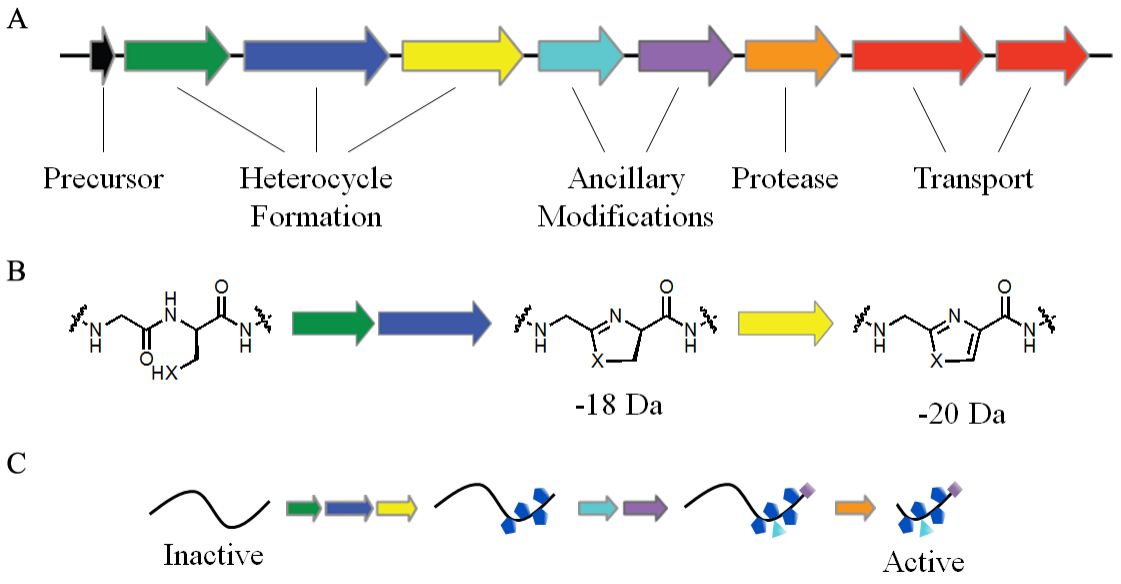

Figure 1.2 | Thiazole/oxazole-modified microcins (TOMMs). (A) Here we depict an example of a TOMM biosynthetic gene cluster. (B) An inactive precursor peptide is ribosomally synthesized and undergoes chemical installation of heterocycles. First, a cyclodehydratase catalyzes the formation of thiazoline/(methyl)oxazoline rings from Cys/Ser/Thr residues in the C-terminal core region (loss of 18 Daltons). Second, a flavin-dependent dehydrogenase oxidizes the heterocycle to afford the thiazole/(methyl)oxazole (additional loss of 2 Daltons, resulting in total loss of 20 Daltons). (C) If encoded, ancillary modifications may be incorporated. A protease cleaves the N-terminal leader region from the core, resulting in an active compound that is then transported to perform its biological activity.

1.10 References

1. Abshire, T.G., Brown, J.E., and Ezzell, J.W. (2005) Production and validation of the use of gamma phage for identification of *Bacillus anthracis*. *J Clin Microbiol*: **43**, 4780-4788.

2. Agaisse, H., Gominet, M., Okstad, O.A., Kolsto, A.B., and Lereclus, D. (1999) PlcR is a pleiotropic regulator of extracellular virulence factor gene expression in *Bacillus thuringiensis*. *Mol Microbiol*: **32**, 1043-1053.

3. Arias, C.A., Panesso, D., McGrath, D.M., Qin, X., Mojica, M.F., Miller, C., Diaz, L., Tran, T.T., Rincon, S., Barbu, E.M., *et al.* (2011) Genetic basis for in vivo daptomycin resistance in Enterococci. *N Engl J Med*: **365**, 892-900.

4. Arnison, P.G., Bibb, M.J., Bierbaum, G., Bowers, A.A., Bugni, T.S., Bulaj, G., Camarero, J.A., Campopiano, D.J., Challis, G.L., Clardy, J., *et al.* (2013) Ribosomally synthesized and post-translationally modified peptide natural products: overview and recommendations for a universal nomenclature. *Nat Prod Rep*: **30**, 108-160.

5. Bachmann, B.O., Van Lanen, S.G., and Baltz, R.H. (2014) Microbial genome mining for accelerated natural products discovery: is a renaissance in the making? *J Ind Microbiol Biotechnol*: **41**, 175-184.

6. Baltz, R.H. (2006) Marcel Faber Roundtable: is our antibiotic pipeline unproductive because of starvation, constipation or lack of inspiration? *J Ind Microbiol Biotechnol*: **33**, 507-513.

7. Baltz, R.H. (2008) Renaissance in antibacterial discovery from actinomycetes. *Curr Opin Pharmacol*: **8**, 557-563.

8. Beierlein, J.M., and Anderson, A.C. (2011) New developments in vaccines, inhibitors of anthrax toxins, and antibiotic therapeutics for *Bacillus anthracis*. *Curr Med Chem*: **18**, 5083-5094.

9. Belshaw, P.J., Roy, R.S., Kelleher, N.L., and Walsh, C.T. (1998) Kinetics and regioselectivity of peptide-to-heterocycle conversions by microcin B17 synthetase. *Chem Biol*: **5**, 373-384.

10. Bentley, S.D., Chater, K.F., Cerdeno-Tarraga, A.M., Challis, G.L., Thomson, N.R., James, K.D., Harris, D.E., Quail, M.A., Kieser, H., Harper, D., *et al.* (2002) Complete genome sequence of the model actinomycete *Streptomyces coelicolor* A3(2). *Nature*: **417**, 141-147.

11. Blin, K., Medema, M.H., Kazempour, D., Fischbach, M.A., Breitling, R., Takano, E., and Weber, T. (2013) antiSMASH 2.0--a versatile platform for genome mining of secondary metabolite producers. *Nucleic Acids Res*: **41**, W204-212.

12. Brazas, M.D., and Hancock, R.E. (2005) Using microarray gene signatures to elucidate mechanisms of antibiotic action and resistance. *Drug Discov Today*: **10**, 1245-1252.

13. Brook, I., Elliott, T.B., Pryor, H.I., 2nd, Sautter, T.E., Gnade, B.T., Thakar, J.H., and Knudson, G.B. (2001) In vitro resistance of *Bacillus anthracis* Sterne to doxycycline, macrolides and quinolones. *Int J Antimicrob Agents*: **18**, 559-562.

14. Brotz, H., and Sahl, H.G. (2000) New insights into the mechanism of action of lantibiotics - diverse biological effects by binding to the same molecular target. *J Antimicrob Chemother*: **46**, 1-6.

15. Challis, G.L. (2008) Genome mining for novel natural product discovery. *J Med Chem*: **51**, 2618-2628.

16. Chen, X.H., Koumoutsi, A., Scholz, R., and Borriss, R. (2009) More than anticipated - production of antibiotics and other secondary metabolites by *Bacillus amyloliquefaciens* FZB42. *J Mol Microb Biotech*: **16**, 14-24.

17. Chen, X.H., Koumoutsi, A., Scholz, R., Eisenreich, A., Schneider, K., Heinemeyer, I., Morgenstern, B., Voss, B., Hess, W.R., Reva, O., *et al.* (2007) Comparative analysis of the complete genome sequence of the plant growth-promoting bacterium *Bacillus amyloliquefaciens* FZB42. *Nat Biotechnol*: **25**, 1007-1014.

18. Choudhury, B., Leoff, C., Saile, E., Wilkins, P., Quinn, C.P., Kannenberg, E.L., and Carlson, R.W. (2006) The structure of the major cell wall polysaccharide of *Bacillus anthracis* is species-specific. *J Biol Chem*: **281**, 27932-27941.

19. Clatworthy, A.E., Pierson, E., and Hung, D.T. (2007) Targeting virulence: a new paradigm for antimicrobial therapy. *Nat Chem Biol*: **3**, 541-548.

20. Cotsonas King, A., and Wu, L. (2009) Macromolecular synthesis and membrane perturbation assays for mechanisms of action studies of antimicrobial agents. *Curr Protoc Pharmacol*: **Chapter 13**, Unit 13A 17.

21. Datta, V., Myskowski, S.M., Kwinn, L.A., Chiem, D.N., Varki, N., Kansal, R.G., Kotb, M., and Nizet, V. (2005) Mutational analysis of the group A Streptococcal operon encoding streptolysin S and its virulence role in invasive infection. *Mol Microbiol*: **56**, 681-695.

22. de Jong, A., van Hijum, S.A., Bijlsma, J.J., Kok, J., and Kuipers, O.P. (2006) BAGEL: a web-based bacteriocin genome mining tool. *Nucleic Acids Res*: **34**, W273-279.

23. Deane, C.D., and Mitchell, D.A. (2014) Lessons learned from the transformation of natural product discovery to a genome-driven endeavor. *J Ind Microbiol Biotechnol*: **41**, 315-331.

24. Dengler, V., Meier, P.S., Heusser, R., Berger-Bachi, B., and McCallum, N. (2011) Induction kinetics of the *Staphylococcus aureus* cell wall stress stimulon in response to different cell wall active antibiotics. *BMC Microbiol*: **11**, 16.

25. Donia, M.S., Ravel, J., and Schmidt, E.W. (2008) A global assembly line for cyanobactins. *Nat Chem Biol*: **4**, 341-343.

26. Doroghazi, J.R., Albright, J.C., Goering, A.W., Ju, K.S., Haines, R.R., Tchalukov, K.A., Labeda, D.P., Kelleher, N.L., and Metcalf, W.W. (2014) A roadmap for natural product discovery based on large-scale genomics and metabolomics. *Nat Chem Biol*: **10**, 963-968.

27. Doroghazi, J.R., and Metcalf, W.W. (2013) Comparative genomics of actinomycetes with a focus on natural product biosynthetic genes. *BMC Genomics*: **14**, 611.

28. Dunbar, K.L., Chekan, J.R., Cox, C.L., Burkhart, B.J., Nair, S.K., and Mitchell, D.A. (2014) Discovery of a new ATP-binding motif involved in peptidic azoline biosynthesis. *Nat Chem Biol*: **10**, 823-829.

29. Dunbar, K.L., Melby, J.O., and Mitchell, D.A. (2012) YcaO domains use ATP to activate amide backbones during peptide cyclodehydrations. *Nat Chem Biol*: **8**, 569-575.

30. Dunbar, K.L., and Mitchell, D.A. (2013a) Insights into the mechanism of peptide cyclodehydrations achieved through the chemoenzymatic generation of amide derivatives. *J Am Chem Soc*: **135**, 8692-8701.

31. Dunbar, K.L., and Mitchell, D.A. (2013b) Revealing nature's synthetic potential through the study of ribosomal natural product biosynthesis. *ACS Chem Biol*: **8**, 473-487.

32. Dunlap, C.A., Kim, S.J., Kwon, S.W., and Rooney, A.P. (2015) Phylogenomic analysis shows that Bacillus amyloliquefaciens subsp. plantarum is a later heterotypic synonym of Bacillus methylotrophicus. *Int J Syst Evol Microbiol*: **65**, 2104-2109.

33. Ezzell, J.W., Abshire, T.G., Little, S.F., Lidgerding, B.C., and Brown, C. (1990) Identification of *Bacillus anthracis* by using monoclonal antibody to cell wall galactose-N-acetylglucosamine polysaccharide. *J Clin Microbiol*: **28**, 223-231.

34. Fischbach, M.A., and Walsh, C.T. (2009) Antibiotics for emerging pathogens. *Science*: **325**, 1089-1093.

35. Freiberg, C., Fischer, H.P., and Brunner, N.A. (2005) Discovering the mechanism of action of novel antibacterial agents through transcriptional profiling of conditional mutants. *Antimicrob Agents Chemother*: **49**, 749-759.

36. Friedman, L., Alder, J.D., and Silverman, J.A. (2006) Genetic changes that correlate with reduced susceptibility to daptomycin in *Staphylococcus aureus*. *Antimicrob Agents Chemother*: **50**, 2137-2145.

37. Ganguly, J., Low, L.Y., Kamal, N., Saile, E., Forsberg, L.S., Gutierrez-Sanchez, G., Hoffmaster, A.R., Liddington, R., Quinn, C.P., Carlson, R.W., *et al.* (2013) The secondary cell wall polysaccharide of *Bacillus anthracis* provides the specific binding ligand for the C-terminal cell wall-binding domain of two phage endolysins, PlyL and PlyG. *Glycobiology*: **23**, 820-832.

38. Goh, E.B., Yim, G., Tsui, W., McClure, J., Surette, M.G., and Davies, J. (2002) Transcriptional modulation of bacterial gene expression by subinhibitory concentrations of antibiotics. *Proc Natl Acad Sci U S A*: **99**, 17025-17030.

39. Gottlieb, D., Carter, H.E., Legator, M., and Gallicchio, V. (1954) The biosynthesis of chloramphenicol. I. Precursors stimulating the synthesis. *J Bacteriol*: **68**, 243-251.

40. Gross, H. (2009) Genomic mining--a concept for the discovery of new bioactive natural products. *Curr Opin Drug Discov Devel*: **12**, 207-219.

41. Hachmann, A.B., Angert, E.R., and Helmann, J.D. (2009) Genetic analysis of factors affecting susceptibility of *Bacillus subtilis* to daptomycin. *Antimicrob Agents Chemother*: **53**, 1598-1609.

42. Haft, D.H., Basu, M.K., and Mitchell, D.A. (2010) Expansion of ribosomally produced natural products: a nitrile hydratase- and Nif11-related precursor family. *BMC Biol*: **8**, 70.

43. Hoffmaster, A.R., Hill, K.K., Gee, J.E., Marston, C.K., De, B.K., Popovic, T., Sue, D., Wilkins, P.P., Avashia, S.B., Drumgoole, R., *et al.* (2006) Characterization of *Bacillus cereus* isolates associated with fatal pneumonias: strains are closely related to *Bacillus anthracis* and harbor *B. anthracis* virulence genes. *J Clin Microbiol*: **44**, 3352-3360.

44. Hutter, B., Schaab, C., Albrecht, S., Borgmann, M., Brunner, N.A., Freiberg, C., Ziegelbauer, K., Rock, C.O., Ivanov, I., and Loferer, H. (2004) Prediction of mechanisms of action of antibacterial compounds by gene expression profiling. *Antimicrob Agents Chemother*: **48**, 2838-2844.

45. Inglesby, T.V., Henderson, D.A., Bartlett, J.G., Ascher, M.S., Eitzen, E., Friedlander, A.M., Hauer, J., McDade, J., Osterholm, M.T., O'Toole, T., *et al.* (1999) Anthrax as a biological weapon: medical and public health management. Working Group on Civilian Biodefense. *JAMA*: **281**, 1735-1745.

46. Jensen, G.B., Hansen, B.M., Eilenberg, J., and Mahillon, J. (2003) The hidden lifestyles of *Bacillus cereus* and relatives. *Environ Microbiol*: **5**, 631-640.

47. Jensen, P.R., Chavarria, K.L., Fenical, W., Moore, B.S., and Ziemert, N. (2014) Challenges and triumphs to genomics-based natural product discovery. *J Ind Microbiol Biotechnol*: **41**, 203-209.

48. Just-Baringo, X., Albericio, F., and Alvarez, M. (2014) Thiopeptide antibiotics: retrospective and recent advances. *Mar Drugs*: **12**, 317-351.

49. Kan, S., Fornelos, N., Schuch, R., and Fischetti, V.A. (2013) Identification of a ligand on the Wip1 bacteriophage highly specific for a receptor on *Bacillus anthracis*. *J Bacteriol*: **195**, 4355-4364.

50. Kelly, W.L., Pan, L., and Li, C. (2009) Thiostrepton biosynthesis: prototype for a new family of bacteriocins. *J Am Chem Soc*: **131**, 4327-4334.

51. Kersten, R.D., Yang, Y.L., Xu, Y., Cimermancic, P., Nam, S.J., Fenical, W., Fischbach, M.A., Moore, B.S., and Dorrestein, P.C. (2011) A mass spectrometry-guided genome mining approach for natural product peptidogenomics. *Nat Chem Biol*: **7**, 794-802.

52. Kind, T., and Fiehn, O. (2010) Advances in structure elucidation of small molecules using mass spectrometry. *Bioanal Rev*: **2**, 23-60.

53. Kolsto, A.B., Tourasse, N.J., and Okstad, O.A. (2009) What sets *Bacillus anthracis* apart from other Bacillus species? *Annu Rev Microbiol*: **63**, 451-476.

54. Lee, S.W., Mitchell, D.A., Markley, A.L., Hensler, M.E., Gonzalez, D., Wohlrab, A., Dorrestein, P.C., Nizet, V., and Dixon, J.E. (2008) Discovery of a widely distributed toxin biosynthetic gene cluster. *Proc Natl Acad Sci U S A*: **105**, 5879-5884.

55. Letzel, A.C., Pidot, S.J., and Hertweck, C. (2014) Genome mining for ribosomally synthesized and post-translationally modified peptides (RiPPs) in anaerobic bacteria. *BMC Genomics*: **15**, 983.

56. Li, J., Qu, X., He, X., Duan, L., Wu, G., Bi, D., Deng, Z., Liu, W., and Ou, H.Y. (2012) ThioFinder: a web-based tool for the identification of thiopeptide gene clusters in DNA sequences. *PLoS One*: **7**, e45878.

57. Liao, R., Duan, L., Lei, C., Pan, H., Ding, Y., Zhang, Q., Chen, D., Shen, B., Yu, Y., and Liu, W. (2009) Thiopeptide biosynthesis featuring ribosomally synthesized precursor peptides and conserved posttranslational modifications. *Chem Biol*: **16**, 141-147.

58. Madison, L.L., Vivas, E.I., Li, Y.M., Walsh, C.T., and Kolter, R. (1997) The leader peptide is essential for the post-translational modification of the DNA-gyrase inhibitor microcin B17. *Mol Microbiol*: **23**, 161-168.

59. Maksimov, M.O., and Link, A.J. (2014) Prospecting genomes for lasso peptides. *J Ind Microbiol Biotechnol*: **41**, 333-344.

60. Melby, J.O., Li, X., and Mitchell, D.A. (2014) Orchestration of enzymatic processing by thiazole/oxazole-modified microcin dehydrogenases. *Biochemistry*: **53**, 413-422.

61. Melby, J.O., Nard, N.J., and Mitchell, D.A. (2011) Thiazole/oxazole-modified microcins: complex natural products from ribosomal templates. *Curr Opin Chem Biol*: **15**, 369-378.

62. Mesnage, S., Fontaine, T., Mignot, T., Delepierre, M., Mock, M., and Fouet, A. (2000) Bacterial SLH domain proteins are non-covalently anchored to the cell surface via a conserved mechanism involving wall polysaccharide pyruvylation. *EMBO J*: **19**, 4473-4484.

63. Mitchell, D.A., Lee, S.W., Pence, M.A., Markley, A.L., Limm, J.D., Nizet, V., and Dixon, J.E. (2009) Structural and functional dissection of the heterocyclic peptide cytotoxin streptolysin S. *J Biol Chem*: **284**, 13004-13012.

64. Mohimani, H., Kersten, R.D., Liu, W.T., Wang, M., Purvine, S.O., Wu, S., Brewer, H.M., Pasa-Tolic, L., Bandeira, N., Moore, B.S., *et al.* (2014) Automated genome mining of ribosomal peptide natural products. *ACS Chem Biol*: **9**, 1545-1551.

65. Molloy, E.M., Cotter, P.D., Hill, C., Mitchell, D.A., and Ross, R.P. (2011) Streptolysin S-like virulence factors: the continuing sagA. *Nat Rev Microbiol*: **9**, 670-681.

66. Morris, R.P., Leeds, J.A., Naegeli, H.U., Oberer, L., Memmert, K., Weber, E., LaMarche, M.J., Parker, C.N., Burrer, N., Esterow, S., *et al.* (2009) Ribosomally synthesized thiopeptide antibiotics targeting elongation factor Tu. *J Am Chem Soc*: **131**, 5946-5955.

67. Muthaiyan, A., Silverman, J.A., Jayaswal, R.K., and Wilkinson, B.J. (2008) Transcriptional profiling reveals that daptomycin induces the *Staphylococcus aureus* cell wall stress stimulon and genes responsive to membrane depolarization. *Antimicrob Agents Chemother*: **52**, 980-990.

68. Newman, D.J., and Cragg, G.M. (2012) Natural products as sources of new drugs over the 30 years from 1981 to 2010. *J Nat Prod*: **75**, 311-335.

69. Nguyen, D.D., Wu, C.H., Moree, W.J., Lamsa, A., Medema, M.H., Zhao, X., Gavilan, R.G., Aparicio, M., Atencio, L., Jackson, C., *et al.* (2013) MS/MS networking guided analysis of molecule and gene cluster families. *Proc Natl Acad Sci U S A*: **110**, E2611-2620.

70. Nonejuie, P., Burkart, M., Pogliano, K., and Pogliano, J. (2013) Bacterial cytological profiling rapidly identifies the cellular pathways targeted by antibacterial molecules. *Proc Natl Acad Sci U S A*: **110**, 16169-16174.

71. Ongley, S.E., Bian, X., Neilan, B.A., and Muller, R. (2013) Recent advances in the heterologous expression of microbial natural product biosynthetic pathways. *Nat Prod Rep*: **30**, 1121-1138.

72. Palmer, K.L., Daniel, A., Hardy, C., Silverman, J., and Gilmore, M.S. (2011) Genetic basis for daptomycin resistance in enterococci. *Antimicrob Agents Chemother*: **55**, 3345-3356.

73. Peric-Concha, N., and Long, P.F. (2003) Mining the microbial metabolome: a new frontier for natural product lead discovery. *Drug Discov Today*: **8**, 1078-1084.

74. Pogliano, J., Pogliano, N., and Silverman, J.A. (2012) Daptomycin-mediated reorganization of membrane architecture causes mislocalization of essential cell division proteins. *J Bacteriol*: **194**, 4494-4504.

75. Pomerantsev, A.P., Shishkova, N.A., and Marinin, L.I. (1992) [Comparison of therapeutic effects of antibiotics of the tetracycline group in the treatment of anthrax caused by a strain inheriting tet-gene of plasmid pBC16]. *Antibiot Khimioter*: **37**, 31-34.

76. Price, L.B., Vogler, A., Pearson, T., Busch, J.D., Schupp, J.M., and Keim, P. (2003) In vitro selection and characterization of *Bacillus anthracis* mutants with high-level resistance to ciprofloxacin. *Antimicrob Agents Chemother*: **47**, 2362-2365.

77. Rasko, D.A., Altherr, M.R., Han, C.S., and Ravel, J. (2005) Genomics of the *Bacillus cereus* group of organisms. *FEMS Microbiol Rev*: **29**, 303-329.

78. Schmidt, E.W., and Donia, M.S. (2009) Chapter 23. Cyanobactin ribosomally synthesized peptides--a case of deep metagenome mining. *Methods Enzymol*: **458**, 575-596.

79. Scholz, R., Molohon, K.J., Nachtigall, J., Vater, J., Markley, A.L., Sussmuth, R.D., Mitchell, D.A., and Borriss, R. (2011) Plantazolicin, a novel microcin B17/streptolysin S-like natural product from *Bacillus amyloliquefaciens* FZB42. *J Bacteriol*: **193**, 215-224.

80. Schuch, R., Pelzek, A.J., Raz, A., Euler, C.W., Ryan, P.A., Winer, B.Y., Farnsworth, A., Bhaskaran, S.S., Stebbins, C.E., Xu, Y., *et al.* (2013) Use of a bacteriophage lysin to identify a novel target for antimicrobial development. *PLoS One*: **8**, e60754.

81. Sensi, P., Greco, A.M., and Ballotta, R. (1959) Rifomycin. I. Isolation and properties of rifomycin B and rifomycin complex. *Antibiot Annu*: **7**, 262-270.

82. Shaw, K.J., and Morrow, B.J. (2003) Transcriptional profiling and drug discovery. *Curr Opin Pharmacol*: **3**, 508-512.

83. Silver, L.L. (2011) Challenges of antibacterial discovery. *Clin Microbiol Rev*: **24**, 71-109.

84. Silverman, J.A., Perlmutter, N.G., and Shapiro, H.M. (2003) Correlation of daptomycin bactericidal activity and membrane depolarization in *Staphylococcus aureus*. *Antimicrob Agents Chemother*: **47**, 2538-2544.

85. Spencer, R.C. (2003) *Bacillus anthracis*. *J Clin Pathol*: **56**, 182-187.

86. Straus, S.K., and Hancock, R.E. (2006) Mode of action of the new antibiotic for Gram-positive pathogens daptomycin: comparison with cationic antimicrobial peptides and lipopeptides. *Biochim Biophys Acta*: **1758**, 1215-1223.

87. Van Lanen, S.G., and Shen, B. (2006) Microbial genomics for the improvement of natural product discovery. *Curr Opin Microbiol*: **9**, 252-260.

88. Velasquez, J.E., and van der Donk, W.A. (2011) Genome mining for ribosomally synthesized natural products. *Curr Opin Chem Biol*: **15**, 11-21.

89. Vogler, A.J., Busch, J.D., Percy-Fine, S., Tipton-Hunton, C., Smith, K.L., and Keim, P. (2002) Molecular analysis of rifampin resistance in *Bacillus anthracis* and *Bacillus cereus*. *Antimicrob Agents Chemother*: **46**, 511-513.

90. Wang, Y.T., Oh, S.Y., Hendrickx, A.P., Lunderberg, J.M., and Schneewind, O. (2013) *Bacillus cereus* G9241 S-layer assembly contributes to the pathogenesis of anthrax-like disease in mice. *J Bacteriol*: **195**, 596-605.

91. Wecke, T., Zuhlke, D., Mader, U., Jordan, S., Voigt, B., Pelzer, S., Labischinski, H., Homuth, G., Hecker, M., and Mascher, T. (2009) Daptomycin versus Friulimicin B: in-depth profiling of *Bacillus subtilis* cell envelope stress responses. *Antimicrob Agents Chemother*: **53**, 1619-1623.

92. Weidenmaier, C., and Peschel, A. (2008) Teichoic acids and related cell-wall glycopolymers in Gram-positive physiology and host interactions. *Nat Rev Microbiol*: **6**, 276-287.

93. Wieland Brown, L.C., Acker, M.G., Clardy, J., Walsh, C.T., and Fischbach, M.A. (2009) Thirteen posttranslational modifications convert a 14-residue peptide into the antibiotic thiocillin. *Proc Natl Acad Sci U S A*: **106**, 2549-2553.

94. Wright, A.M., Beres, S.B., Consamus, E.N., Long, S.W., Flores, A.R., Barrios, R., Richter, G.S., Oh, S.Y., Garufi, G., Maier, H., *et al.* (2011) Rapidly progressive, fatal, inhalation anthrax-like infection in a human: case report, pathogen genome sequencing, pathology, and coordinated response. *Arch Pathol Lab Med*: **135**, 1447-1459.

95. Yip, C., Loeb, M., Salama, S., Moss, L., and Olde, J. (2001) Quinolone use as a risk factor for nosocomial Clostridium difficile-associated diarrhea. *Infect Control Hosp Epidemiol*: **22**, 572-575.

96. Zhang, T., Muraih, J.K., Tishbi, N., Herskowitz, J., Victor, R.L., Silverman, J., Uwumarenogie, S., Taylor, S.D., Palmer, M., and Mintzer, E. (2014) Cardiolipin prevents membrane translocation and permeabilization by daptomycin. *J Biol Chem*: **289**, 11584-11591.

97. Zheng, J., Peng, D., Song, X., Ruan, L., Mahillon, J., and Sun, M. (2013) Differentiation of *Bacillus anthracis*, *B. cereus*, and *B. thuringiensis* on the basis of the csaB gene reflects host source. *Appl Environ Microbiol*: **79**, 3860-3863.

CHAPTER II: PLANTAZOLICIN, A NOVEL MICROCIN B17/STREPTOLYSIN S-LIKE NATURAL PRODUCT FROM *BACILLUS METHYLOTROPHICUS* FZB42

This chapter was adapted from Scholz, R., Molohon, K.J., Nachtigall, J., Vater, J., Markley, A.L., Sussmuth, R.D., Mitchell, D.A., and Borriss, R. (2011). Copyright © American Society for Microbiology, *J. Bacteriology*, Vol 193, 2011, pp 215-224, doi:10.1128/JB.00784-10.

For this publication, I critically revised the manuscript, figures, and performed the reverse transcriptase PCR (RT-PCR, Figure 2.6).

2.1 Abstract

Here we report on a novel thiazole/oxazole-modified microcin (TOMM) from *Bacillus methylotrophicus* FZB42, a Gram-positive soil bacterium. This organism is well known for stimulating plant growth and biosynthesizing complex small molecules that suppress the growth of bacterial and fungal plant pathogens. Similar to microcin B17 and streptolysin S, the TOMM from *B. methylotrophicus* FZB42 undergoes extensive posttranslational modification to become a bioactive natural product. Our data show that the modified peptide bears a molecular mass of 1335 Da and displays antibacterial activity towards closely related Gram-positive bacteria. A cluster of twelve genes that covers ~10 kb is essential for the production, modification, export, and self immunity of this natural product. We have named this compound plantazolicin (PZN), based on the association of several producing organisms with plants and the incorporation of azole heterocycles, which derive from Cys, Ser, and Thr residues of the precursor peptide.

2.2 Introduction

Bacillus methylotrophicus FZB42 [previously named *Bacillus amyloliquefaciens* FZB42 (Dunlap *et al.*, 2015)] is a Gram-positive, plant-growth promoting bacterium with an impressive capacity to produce secondary metabolites with antimicrobial activity (Chen *et al.*, 2007). The nonribosomal syntheses of polyketides (bacillaene, difficidin, and macrolactin), lipopeptides (surfactin, fengycin, and bacillomycin D), and siderophores (bacillibactin and the product of the *nrs*-cluster) are carried out by large gene clusters distributed over the entire genome of *B.*

methylotrophicus FZB42. While these compounds are biosynthesized in a 4'-phosphopantetheine transferase (Sfp)-dependent fashion, the production of the antibacterial dipeptide, bacilysin, is independent of Sfp (Chen *et al.*, 2009b; Chen *et al.*, 2009c). In total, 8.5% of its entire genomic capacity is devoted to the non-ribosomal synthesis of secondary metabolites, exceeding that of the model Gram-positive bacterium *Bacillus subtilis* 168 by more than two-fold (Chen *et al.*, 2009a). Prophage sequences that often harbor biosynthetic gene clusters of ribosomally synthesized peptides (microcins, lantibiotics/lantipeptides), which are common in *B. subtilis* strains, were not previously detected within the FZB42 genome. However, the presence of antimicrobial compound(s) active against *sigW* mutant strain HB0042 of *B. subtilis* has been reported. SigW is an extracytoplasmic sigma factor that provides intrinsic resistance to antimicrobial compounds produced by other *Bacilli* (Butcher and Helmann, 2006).

The driving force for the current report was the finding that FZB42 mutant RS6, which is deficient in the Sfp-dependent synthesis of lipopeptides, polyketides, and in Sfp-independent bacilysin production (Chen *et al.*, 2009c), still produced an antibacterial substance active against *Bacillus subtilis* HB0042. This finding underscores the diversity of biosynthetic strategies employed by FZB42 and offers new possibilities to discover novel natural products with biomedically relevant activities. Recent genomic analysis of FZB42 revealed a ribosomally encoded biosynthetic gene cluster that is conserved among many species across two domains of life (Lee *et al.*, 2008). This cluster encodes a small precursor peptide that is posttranslationally modified to contain thiazole and (methyl)oxazole heterocycles (Figure 2.1). These rings are derived from Cys and Ser/Thr through the action of a trimeric 'BCD' synthetase complex, which consists of a cyclodehydratase complex (CD) and dehydrogenase (B) (Dunbar *et al.*, 2014; Dunbar *et al.*, 2012; Dunbar and Mitchell, 2013; Lee *et al.*, 2008). This mechanism of modification is utilized in the biosynthetic pathway for streptolysin S (SLS, *Streptococcus pyogenes*) (Datta *et al.*, 2005), microcin B17 (Li *et al.*, 1996), the patellamides (Schmidt *et al.*,

2005), and the thiopeptides (Kelly *et al.*, 2009; Liao *et al.*, 2009; Morris *et al.*, 2009; Wieland Brown, 2009). The products of these clusters have been collectively classified as thiazole/oxazole-modified microcins (TOMMs) due to their genetic and chemical structure conservation (Haft *et al.*, 2010).

During TOMM biosynthesis, the precursor peptide is bound by the BCD synthetase complex through specific motifs within the N-terminal leader sequence (Mitchell *et al.*, 2009; Roy *et al.*, 1999). After substrate recognition, heterocycles are synthesized on the C-terminal core peptide over two enzymatic steps. The first is carried out by a cyclodehydratase, which converts Cys and Ser/Thr residues into the corresponding thiazolines and (methyl)oxazolines. A dehydrogenase then oxidizes the 'azoline' rings to yield 'azole' rings [thiazoles and (methyl)oxazoles], resulting in a net loss of 20 Da. The completion of TOMM biosynthesis includes the incorporation of ancillary modifications (*e.g.* dehydrations, methylations, macrocyclization, *etc*.) and leader peptide proteolysis (Datta *et al.*, 2005), (Kelly *et al.*, 2009; Liao *et al.*, 2009; Morris *et al.*, 2009; Wieland Brown, 2009). In many cases, the fully mature TOMM natural product is then actively exported from the cell through the use of an ABC transport system. In this work, we describe the discovery, production, isolation, and initial genetic and chemical characterization of a novel TOMM from *B. methylotrophicus* FZB42. This natural product compound has a molecular mass of 1335 Da (cpd1335) and has been named plantazolicin (PZN).

2.3 Results

2.3.1 MALDI TOF-MS detection of a new metabolite from FZB42

B. methylotrophicus FZB42 is a prolific producer of antibacterial and antifungal natural products. To date, nonribosomally produced peptides, including three antimicrobial lipopeptides (surfactin, bacillomycin D, and fengycin), three polyketide antibiotics (bacillaene, difficidin, and macrolactin), the antibacterial dipeptide bacilysin, and two siderophores (bacillibactin and the

putative product of the *nrs*- gene cluster) have been identified (Chen *et al.*, 2007). In addition to these compounds, small molecule metabolite screening of FZB42 by MALDI-TOF-MS revealed a metabolite with a molecular mass of $[M+H]^+$ = 1336 Da (Figure 2.2A, cpd1335). The visible species at m/z = 1354 Da indicates that this compound also appears in a hydrated form (Figure 2.2A, +18 Da). This may be attributed to a hydrolysis product given that the +18 Da signal progressively dominates after extensive sample manipulation (data not shown). Similar to the lipopeptide products, mass spectrometric signals from this compound were detected in surface extracts and in the culture filtrate. Based on our previous work on small molecule metabolites from FZB42 (Chen *et al.*, 2009a), we surmise that after biosynthesis, cpd1335 is actively transported out of the cell. After export, the product presumably accumulates in the peptidoglycan layer of FZB42, with a portion being spontaneously released into the culture medium. Thus, we set out to determine the biosynthetic origin of cpd1335.

Previously, we generated a strain of FZB42, dubbed RS6, that is deficient in the production of all Sfp-dependent lipopeptides, polyketides, and the Sfp-independent synthesis of bacilysin (*sfp*::*ermAM, bac*::*cm*, Table 2.1) (Chen *et al.*, 2009c). We were initially surprised when strain RS6 was still capable of producing cpd1335, as assessed by MALDI-TOF-MS (Figure 2.2B). Clearly, this natural product is not being assembled by typical non-ribosomal machinery, such as the non-ribosomal peptide synthetase (NRPS) and polyketide synthase (PKS) biosynthetic pathways. This suggested that FZB42 was either assembling cpd1335 using an unrecognized Sfp or that cpd1336 was of ribosomal origin (*i.e*. a bacteriocin). Despite the absence of all known, non-ribosomally synthesized secondary metabolites (Chen *et al.*, 2009c), supernatants of the RS6 mutant strain retained antagonistic activity towards closely related *Bacilli*, such as *B. megaterium*, *B. subtilis* 168 (*trpC2*), and a *sigW* mutant of *B. subtilis* designated as strain HB0042 (Table 2.2). Butcher and Helmann have reported that the growth of *B. subtilis* HB0042 was inhibited by an unknown substance, a potential bacteriocin, produced by FZB42 (Butcher and Helmann, 2006).

Further, BLAST searching returns only one copy of Sfp in the FZB42 genome (Altschul *et al.*, 1997). These findings led us to favor the hypothesis that cpd1335 was a ribosomally synthesized antibacterial substance, which heretofore have not been reported in FZB42.

2.3.2 Preliminary characterization of cpd1335

The non-concentrated, cell surface extract of RSpMarA2, the strain which bears a mariner transposon insertion in the *degU* global transcriptional regulator gene (Koumoutsi *et al.*, 2007), contains significantly higher levels of cpd1335 relative to wild type and the RS6 mutant strain (Table 2.1, Figure 2.3A). Due to the elevated production level of cpd1335, strain RSpMarA2 was employed for further characterization. The dialyzed surface extract of RSpMarA2 was separated by tris-tricine-SDS-PAGE and stained with Coomassie Blue (Figure 2.4A). While the Coomassie stain was relatively weak, we were able to achieve an improved visualization of the peptide-sized band (1-2 kDa) by double staining with Schiff's reagent after oxidation with periodic acid (Figure 2.4B). Periodic acid oxidizes alcohols to aldehydes, which then react with Schiff's reagent (Hardonk and Van, 1964). The band, which presumably contained cpd1335 based on electrophoretic migration, was excised for further characterization. After extraction from the gel, MALDI-TOF-MS identified m/z = 1354 Da as the most intense ion in the monitored mass window (Figure 2.4C), corresponding to the hydrated form $[M+H_2O+H]^+$ of cpd1335. Given that this apparent hydrated product was detected earlier (Figure 2.2), it was not surprising that after extensive sample preparation (gel electrophoresis and extraction), the hydrated product was the major species. Cpd1335 was found to be growth inhibitory towards closely related Gram-positive *Bacilli*, but no activity was observed towards Gram-negative bacteria, such as *E. coli* K12, *Klebsiella terrigena*, *Erwinia carotovora*, and *Pseudomonas* sp. (Table 2.2).

Solubility profiling of purified cpd1335 revealed that this natural product is extractable with chloroform, separable by reverse-phase HPLC-chromatography, and insoluble in water at

high concentrations (Figure 2.3). Taken together, our solubility data and production from strain RS6 suggest that cpd1335 is a relatively hydrophobic, extensively modified peptide of ribosomal origin.

2.3.3 Bioinformatic assessment of the cpd1335 biosynthetic genes

Supported by the above preliminary characterization of cpd1335, we performed a literature search for small, hydrophobic, modified, antibacterial peptides produced by Gram-positive bacteria. Research on thiopeptides revealed similar characteristics to cpd1335 (Kelly *et al.*, 2009; Liao *et al.*, 2009; Morris *et al.*, 2009; Wieland Brown, 2009). Interestingly, several orthologs to the genes involved in thiopeptide biosynthesis can be found clustered in FZB42, suggesting that cpd1335 may be synthesized by a related route. Introduction of a spectinomycin antibiotic cassette within one of these orthologous genes (RBAM_007480, a putative flavin mononucleotide-dependent dehydrogenase) resulted in mutant RS26, which was unable to produce cpd1335, as assessed by mass spectrometry (Figure 2.3A). This result strongly suggested that cpd1335 was a thiazole/oxazole-modified microcin (TOMM).

In addition to their similarity to proteins involved in thiopeptide biosynthesis, protein BLAST (Altschul *et al.*, 1997) and ClustalW (Thompson, 1994) sequence alignment have demonstrated that the FZB42 TOMM biosynthetic proteins also exhibit modest similarity to a previously characterized TOMM from *Streptococcus pyogenes* (Lee *et al.*, 2008). The TOMM biosynthetic locus from *S. pyogenes* is referred to as the *sag* cluster, for SLS-associated genes. SagB (dehydrogenase), SagC and SagD(cyclodehydratase), are homologous to RBAM_007480 (20% identical, 53% similar) RBAM_007460 (13% identical, 50% similar), and RBAM_007470 (19% identical, 58% similar), respectively. Also bearing similarity to the SLS biosynthetic cluster are RBAM_007490 (SagE, Caax protease; 16% identical, 54% similar), RBAM_007420 (SagG, ABC transporter; 15% identical, 53% similar) and RBAM_007430 (SagH, ABC transporter; 22% identical, 63% similar) (Datta *et al.*, 2005; Lee *et al.*, 2008). Due to this similarity, we have

adopted the *sag* lettering nomenclature for this biosynthetic cluster (Figure 2.5). Despite the genetic similarities between SLS and cpd1335, there is no difference in the hemolytic activity of RSpMarA2 (cpd1335 overproducer) and mutant RS26 (devoid of cpd1335 production) on blood agar plates using the concentrated, dialysed cell surface extract (Figure 2.3B). This demonstrates that cpd1335 is not required for the hemolytic activity of FZB42 and suggests cpd1335 exhibits other biological activity.

2.3.4 Preliminary biological activity for cpd1335

It is important to note that although there is remarkable similarity in the genetic organization of the TOMM biosynthetic clusters, the chemical structure and biological targets of the resultant natural products vary widely (*e.g.* SLS, cellular membrane; microcin B17, DNA gyrase; thiostrepton/thiocillin, 50S ribosome; cyanobactins, anticancer activity). Previous data have shown that the specific biological activity of the TOMM product is encoded by the sequence of the precursor peptide and that the cyclodehydratase and dehydrogenase are functionally redundant (Lee *et al.*, 2008). Although this study has not elucidated the molecular target of cpd1335, we have determined that the purified compound is growth inhibitory towards most of the Gram-positive *Bacilli* surveyed, especially *B. megaterium* and *B. subtilis* HB0042 (Figure 2.3C, Table 2.2). Interestingly, extracts of mutant RS26, which do not contain cpd1335, were still capable of suppressing the growth of *B. subtilis* HB0042. This shows that cpd1335 was not solely responsible for the specific antibiotic activity previously observed in FZB42 culture fluid (Butcher and Helmann, 2006). These results demonstrate that FZB42 biosynthesizes at least one additional narrow-spectrum antibiotic, which like cpd1335, is likely synthesized by ribosomes.

As demonstrated by our mass spectrometry studies (Figure 2.2), cpd1335 requires a TOMM-type dehydrogenase for production (Figures 2.1 and 2.5). RBAM_007480 is a *sagB*-like gene, embedded within a cluster of 12 genes involved in the biosynthesis, export, and immunity of a posttranslationally modified, hydrophobic natural product (Figure 2.5). The defining feature

of all TOMM natural products is the incorporation of Cys- and Ser/Thr-derived heterocycles onto a ribosomally synthesized, peptidic backbone. To highlight these suspected modifications, we hereafter refer to cpd1335 as plantazolicin (PZN). The PZN biosynthetic 12-gene cluster spans nearly 10 kb of the FZB42 chromosome (Figure 2.5). Akin to SLS and microcin B17 production, a trimeric thiazole/oxazole BCD synthetase complex is present. Based on similarity to these systems, all three genes (*pznBCD*) will be required for heterocycle formation (*pznC,* RBAM_007460; *pznD,* RBAM_007470) (Figure 2.5).

2.3.5 Reverse Transcriptase-PCR

Transcription of all 12 *pzn* genes in M9 minimal media was confirmed by RT-PCR (Figure 2.6). All amplicons migrated with their expected sizes (Table 2.3). In addition to confirming transcription, we also assessed the intergenic regions of the PZN biosynthetic cluster to determine if the mRNA was polycistronic. Using the appropriate primers from adjacent genes, we determined that the biosynthetic genes are transcribed into two polycistronic mRNAs (*pznFKGHI* and *pznJCDBEL*) and a monocistronic mRNA for *pznA* (Figure 2.6). Amplification of the region between *pznE* and *pznL* resulted in a band that was visible only under extreme contrast (data not shown). Numerous attempts to amplify the *pznIJ* junction were unsuccessful.

2.3.6 Functional analysis of the PZN gene cluster by gene targeted mutagenesis

Precursor peptide gene. Like many TOMM clusters, the gene encoding the precursor peptide is not annotated as an open reading frame (ORF) in the FZB42 genome (gb CP000560.1) (Lee *et al.*, 2008). This gene was identified by a manual ORF search and found to be encoded between *pznI* (RBAM_007440) and *pznJ* (RBAM_007450) in the opposite direction. Although unannotated, this ORF (*pznA*) bears a robust Shine-Dalgarno sequence, AGGAGG, which is found 8 bp upstream of an AUG start codon. *pznA* is predicted to encode for only 41 amino acids (Figure 2.5A), which is 6 shorter than previously reported (Lee *et al*., 2008). The C-terminal region, also known as the core peptide (Oman and van der Donk, 2009), is rich in residues that

can be enzymatically cyclized to thiazoles and (methyl)oxazoles (2 Cys, 4 Thr, and 4 Ser). This feature is a clear indicator of TOMM precursor peptides (Haft *et al.*, 2010; Lee *et al.*, 2008; Wieland Brown, 2009) (Figure 2.1). As expected, the *pznA* mutant RS32, was also deficient in synthesis of PZN (Figure 2.3A, 2.5).

Operon structure and transcriptional regulation. The *pzn* biosynthetic gene cluster is partitioned into three sections. The first operon (*pznFKGHI*) consists of genes predicted to be involved in immunity, regulation, and transport (Figure 2.5). The product of *pznK* (RBAM_007410) is related to homodimeric repressor proteins of the ArsR family (Busenlehner *et al.*, 2003). This protein possibly regulates the expression of other *pzn* genes through an unexplored mechanism. The second operon (*pznJCDBEL*) harbors the genes encoding for the enzymes responsible for converting the inactive PznA precursor peptide into the mature, bioactive natural product. A summary of the putative function of the members of the *pzn* gene cluster in *B. methylotrophicus* FZB42 is given in Figure 2.5B.

Enzymatic processing of PznA. The enzymes dedicated to the modification and processing of the PznA precursor peptide are encoded by the second operon of the PZN biosynthetic cluster (*pznJCDBEL*) (Figure 2.5). The function of the first gene, *pznJ*, is not known; however, uncharacterized orthologs can also be found in two plant-associated, Gram-positive organisms, *Bacillus pumilus* and *Clavibacter michiganensis*. In the latter organism, *pznJ* is annotated as a putative hydroxylase. Sequence analysis and literature searching fail to substantiate this designation. As with the creation of other mutant strains, we applied the splicing by overlapping extension (SOE) method (Horton *et al.*, 1990) to replace *pznJ* with a spectinomycin resistance gene. The resulting mutant, RS28, did not produce PZN (Figures 2.3A and 2.5), demonstrating that PznJ plays a vital biosynthetic role.

Based on sequence alignment, PznC is related to the TOMM cyclodehydratase present in *S. pyogenes*, SagC. Previous research on SagC revealed its importance in substrate (SagA)

recognition, in addition to its ability to catalyze the peptide backbone cyclization of Cys, Ser, and Thr residues (Mitchell *et al.*, 2009). Based on this information, we generated a mutant interrupted in *pznC*, RS31 (Table 2.1). As expected, this mutant does not produce PZN (Figure 2.3A). We did not prepare a deletion mutant of *pznD* (RBAM_007470) or *pznE* (RBAM_007490). PznD is highly similar to SagD from the SLS biosynthetic cluster and contains the ATP binding domain necessary for heterocycle formation (Dunbar *et al.*, 2014; Dunbar *et al.*, 2012; Dunbar and Mitchell, 2013). Therefore, PznD is expected to be of significant importance in the maturation process of PznA. PznE belongs to the type II Caax protease family (Pei and Grishin, 2001). As predicted by OCTOPUS (Viklund and Elofsson, 2008), PznE contains 4 transmembrane domains, similar to the type II Caax proteases from *S. pyogenes*, *C. botulinum*, *S. aureus*, and *L. monocytogenes* (Lee *et al.*, 2008). We hypothesize that this protein will function as a leader peptidase, proteolytically processing the PznA peptide at PMAA/R (Figure 2.5A). Two arguments supporting this site as the putative leader peptide processing site are: *i.* cleavage between or before the Ala residues is unlikely given the molecular mass of the resultant peptide and the number of modifiable residues, and *ii*. bacteriocin leader peptides are most often processed after a Gly-Gly sequence, but other small residues, such as Ser and Ala, can be found directly N-terminal to the scissile bond (Dirix *et al.*, 2004; Oman and van der Donk, 2009; van Belkum *et al.*, 1997).

The product of the last gene within the cluster, PznL (RBAM_007500), was identified by sequence analysis to be a S-adenosylmethionine (SAM)-dependent methyltransferase (Figure 2.5). Mutant RS33, devoid in *pznL* (Table 2.1), produced a compound with m/z = 1308.5 Da, indicating a loss of 28 Da relative to wild type. Based on this data, PznL is responsible for the transfer of two methyl groups to PZN [CH_3 = 15 Da; (2 x 15) – 2H = 28 Da] (Figure 2.3A, right inset).

Natural product export and immunity. As mentioned above, *pznG* (RBAM_007420) and *pznH* (RBAM_007430) are homologous to ABC transporters, with PznG being responsible for

binding ATP and PznH carrying out the permease activity. ABC transporters are common constituents of TOMM biosynthetic gene clusters and are present across many taxa of bacteria and archaea (Lee *et al.*, 2008). The function of the *pznF* (RBAM_007400) and *pznI* (RBAM_007440) gene products are more convoluted. It has previously been hypothesized that one or both of these gene products could be involved in self-immunity of FZB42 against PZN (Lee *et al.*, 2008). While a protein BLAST database search on PznF yields homology to putative membrane proteins, PznI is annotated as a pentapeptide repeat protein. Research on other proteins of the pentapeptide repeat family has revealed that they play important signaling roles via coordinating protein-protein interactions (Vetting *et al.*, 2006) and also can confer resistance to quinolone antibiotics (Rodriguez-Martinez *et al.*, 2009). To address their potential role in PZN production/immunity, the *pznI* and *pznF* genes were individually replaced with the spectinomycin resistance gene. Although both of these mutants were still able to produce PZN (Figure 2.3A), they displayed different growth characteristics. Neither mutant exhibited visible growth defects during growth on LB agar plates. In liquid LB media, the *pznI* mutant (RS27) growth curve was indistinguishable from the background strain (RS6). However, the *pznF* mutant (RS29) displayed markedly different growth behavior. Upon reaching a maximum culture density, which was equal to that of RS6, RS29 appeared to undergo lysis instead of maintaining a high culture density (Figure 2.3D). Mature PZN is present at sufficient quantity to be detected by MALDI mass spectrometry during the early stationary growth phase (Figure 2.2), but not at earlier time points (data not shown). This suggests that the *pznF* mutant is more susceptible to the actions of an antimicrobial compound produced in higher abundance during later growth phases. Upon treating RS6 and RS29 with purified PZN, a larger zone of inhibition was visible for the RS29 strain, confirming that the above growth phenotype was indeed PZN-dependent (data not shown). Given the observation that FZB42 requires an immunity gene (*pznF*) for fully competent growth, and

that PZN exhibits activity against only select Gram-positive bacteria (Table 2.2), we conclude that PZN acts as a narrow spectrum antibacterial compound.

2.4 Summary and Outlook

A novel, antibacterial, microcin B17/streptolysin-like compound with a molecular mass $[M+H]^+$ of 1336 Da (plantazolicin, PZN) was identified in culture supernatant and cell surface extract from *B. methylotrophicus* FZB42. We postulate that the core peptide consists of 14 amino acids (RCTCTTIISSSSTF), 10 of which potentially serve as a site of heterocycle formation (Cys, Ser/Thr). Although we have not yet ascertained the precise chemical structure of PZN, supportive evidence is available that demonstrates this natural product undergoes extensive posttranslational modification (Figures 2.2-2.4). Numerous attempts to elucidate the structure of PZN by LC ESI-MS/MS (tandem) analysis showed an unusually incomplete fragmentation pattern (data not shown). Such tandem MS analysis (*i.e.* collision-induced dissociation) tends to fragment parent ions at the amide bond, leading to a series of ions containing the N-terminus (b ion series) and the C-terminus (y ion series). If contiguous heterocycles were indeed formed on adjacent residues of PznA, an incomplete tandem spectrum would be the expected outcome. A full structural elucidation of PZN by other spectroscopic methods is currently underway and will be the subject of a future publication.

A previous bioinformatics survey revealed modest similarity of a putative biosynthetic locus from FZB42 with the streptolysin S (SLS) biosynthetic operon from *Streptococcus pyogenes* (Lee *et al.*, 2008). Genes from this operon are designated as SLS-associated genes (*sag*), of which there are a total of 9 (*sagA-I*). Related gene clusters have been widely disseminated among bacteria and archaea. The genetic and biochemical conservation within this particular natural product family has led to a new classification of small, highly modified bacteriocins, the thiazole/oxazole-modified microcins (TOMMs) (Haft *et al.*, 2010; Lee *et al.*, 2008). Genetic ablation of RBAM_007480, a gene homologous to *sagB*, resulted in the inability

of FZB42 to synthesize PZN (Figure 2.3). Thus, the FZB42 TOMM cluster appeared to be responsible for the synthesis of PZN. Analysis of the local genomic context of RBAM_007480 identified a 12-gene biosynthetic cluster, encoding hypothetical genes involved in the TOMM biosynthesis, immunity, and export (Figure 2.5). The TOMM precursor gene, *pznA*, encodes a small peptide consisting of 41 amino acids. Like *pznB* (the *sagB* ortholog), deletion of *pznA*, among other essential genes (*e.g. pznC*), abolishes the production of PZN. After PznBCD-dependent heterocycle formation, dimethylation (PznL), and N-terminal processing by a protease, (possibly PznE), the core peptide of modified PznA is secreted into the exterior environment via the ABC transporters, PznG and PznH. In addition to establishing the order and location of all posttranslational events, the biosynthetic role of the requisite PznJ protein is also under investigation in our laboratory.

Several gene clusters encoding TOMMs have been detected in the genomes of plant-associated bacteria, such as *Bradyrhizobium japonicum*, *Pseudomonas putida*, and *Clavibacter michiganensis* (Lee *et al.*, 2008). Performing a protein BLAST search using each PZN gene product as the query sequence returns orthologous protein matches from *Bacillus pumilus* ATCC 7061 as the top hit after FZB42 itself. The thiazole/oxazole synthetase proteins (PznBCD) from *B. pumilis* (protein IDs: EDW22765.1, EDW22903.1, and EDW23125.1, respectively) demonstrated a remarkable degree of amino acid identity to those from FZB42 (PznB, 77%; PznC, 63%, and PznD, 82%). Moreover, the *pzn* genes from *B. pumilis* are found clustered and in identical order to that found in FZB42. Also like FZB42, *B. pumilis* is a plant saprophyte that produces an array of antibacterial and antifungal natural products (Choudhary and Johri, 2009). Further, the PznA core peptide sequences from FZB42 and *B. pumilis* (unannotated, located between EDW23486.1 and EDW22932.1) are 100% identical. Taken together, we predict that *B. pumilis* is also a PZN producer.

Interestingly, the *pzn* gene cluster was absent from the genome of *B. amyloliquefaciens* type strain DSM7^{T} (EMBL identifier FN597644), a non-plant-associated bacterium. It is plausible that the *pzn* gene cluster in FZB42 has been horizontally transferred between members of the plant rhizosphere. To bolster this possibility, we performed a protein BLAST search of three draft genomes of plant-associated *B. methylotrophicus* strains, which became recently available (Borriss *et al.*, 2010). Within the *B. methylotrophicus* CAU-B946 genome, we found the complete 12-gene PZN biosynthetic cluster, displaying 95-100% amino acid identity with that of FZB42. The genomes of strains *B. methylotrophicus* YAU-Y2 and NAU-B3 did not possess the complete set of genes for the PZN cluster, but did harbor a portion of the immunity/transport operon, *pznFKGH*. These genes displayed 95-100% identity with the corresponding genes from FZB42. Although the YAU-Y2 and NAU-B3 genomes lack an intact PZN biosynthetic cluster, the genetic composition of these strains implies that the plant-associated members of the *B. methylotrophicus* (plantarum) taxon are at least immune towards, and/or capable of *de novo* synthesis of PZN.

A detailed biological function for PZN has yet to be established. Unlike some TOMMs, a functional prediction cannot reliably be made based on the sequence of *pznA* due to its lack of homology to other TOMM precursors with known functions. In other words, TOMM precursor peptides similar in sequence to SagA are cytolysins (Cotter *et al.*, 2008; Mitchell *et al.*, 2009), while unrelated sequences do not encode cytolytic activity (*i.e*. the precursors for microcin B17, patellamides, thiostrepton, *etc*.). Our preliminary results demonstrate that PZN functions as a narrow-spectrum, antibacterial compound. Presumably, this natural product is meant to suppress the growth of taxonomically related competitors within the plant rhizosphere. Independent of function, PZN should be highly protected from degradation by peptidases within the plant rhizosphere due to an extensive degree of modification.

2.5 Experimental

2.5.1 Strain construction

The *B. methylotrophicus* strains and plasmids used in this study are summarized in Table 2.1. *Bacillus* and indicator strains were cultivated routinely on Luria-Bertani broth (LB) medium solidified with 1.5% agar. For production of PZN, a medium containing: 40 g soy peptone, 40 g dextrin 10, 1.8 g KH_2PO_4, 4.5 g K_2HPO_4, 0.3 g $MgSO_4$ x 7 H_2O, and 0.2 ml KellyT trace metal solution per L was used. KellyT trace metal solution: 25 mg EDTA disodium salt dihydrate, 0.5 g $ZnSO_4$ x 7 H_2O, 3.67 g $CaCl_2$ x 2 H_2O, 1.25 g $MnCl_2$ x 4 H_2O, 0.25 g $CoCl_2$ x 6 H_2O, 0.25 g ammonium molybdate, 2.5 g $FeSO_4$ x 7H_2O, 0.1 g $CuSO_4$ x 5 H_2O; adjust to pH 6 with NaOH, 500 ml H_2O.

The media and buffers used for DNA transformation of *Bacillus* cells were prepared according to Kunst and Rapoport (Kunst, 1995). Competent cells were prepared as previously described (Koumoutsi *et al.*, 2004). Mutants were obtained after transformation of the FZB42 derivatives with linearized, integrative plasmids containing resistance cassettes flanked by DNA regions homologous to the FZB42 chromosome. The oligonucleotides used for strain construction are listed in Table 2.3. Spectinomycin (90 µg/ml) was used for selecting transformants. Gene interruption strains were obtained as follows: *PznB* RS26: A 2.7 kb PCR fragment was amplified from FZB42 chromosomal DNA using primers pznB-fw and pznB-rv. The fragment was then cloned into pGEM-T, yielding plasmid pRS26a. Plasmid pRS26b was obtained by insertion of a spectinomycin resistance cassette, which was subcloned by PCR using the spc-fw and spc-rv primers and the pIC333 plasmid as a template. The cassette was placed into the central region of the insert and digested with BglII and BamHI. *PznC* RS31: With primers pznC-fw and pznC-rv, a 2.6 kb fragment containing *pznC* was amplified by PCR and cloned into vector pGEM-T-Easy yielding plasmid pRS31a. A central fragment of the insert was removed by digestion with Eco105I and replaced with the spectinomycin resistance cassette, yielding pRS31b. *PznA* RS32:

With primers 007400cst-fw and 007400cst-rv, a 2.3 kb fragment encoding the unannotated precursor peptide, *pznA*, was amplified by PCR and cloned into vector pGEM-T-Easy, yielding plasmid pRS32a. The precursor peptide gene was cleaved by Bsp1407I and interrupted by insertion of a spectinomycin resistance cassette, yielding pRS32b.

The mutants RS27, RS28, RS29 and RS33 were generated by gene splicing using the overlapping extension (SOE) method (Horton *et al.*, 1990). This method assists in avoiding possible polar effects caused by interrupted reading frames. SOE PCR fusion products were generated using the primers listed in Table 2.3 and the spectinomycin gene of pIC333. A-tailing of the *Pfu*-PCR product was performed according to the Promega pGEM-T protocol and ligated into pGEM-T yielding pRS27, pRS28 and pRS29. For mutant RS33, the PCR product was used directly for transformation.

Mutant RSpMarA2 was isolated from a mariner-based (pMarA) transposon library prepared in strain CH5 according to Breton *et al.* (Le Breton *et al.*, 2006). In this transposon mutant, pMarA was integrated into the *degU* gene, which is a global transcriptional regulator that activates the bacillomycin D promoter (Koumoutsi *et al.*, 2007). Coincidentally, we observed by HPLC-ESI-MS that PZN is overproduced by this strain (Figure 2.3A).

2.5.2 Bioassay

LB-Agar (20 ml) was mixed with 0.5 ml of the indicator strain (OD_{600} ~1.0). 10 µl of purified PZN suspended in water was spotted on the agar and incubated for 16 h at 22 °C. The growth suppression activity of PZN was observed as clear zone.

2.5.3 Cell surface extract

The extract was prepared in the following way: Cells of strain RSpMarA2 and RS26 were grown using production media containing 1.5% agar for 24 h at 37 °C. Cells were removed from the plates and treated with 50 ml of 70% acetonitrile : 30% water with 0.1% formic acid. After centrifugation (7000 rpm, 20 min, 22 °C), the extract was passed through a 0.45 µm filter and

concentrated to 2 ml using a rotary evaporator. The extract was dialyzed overnight against 5 L distilled water using a 1 kDa membrane (Zellutrans V, Roth).

2.5.4 HPLC-ESI-MS

Bacterial strains were grown for 24 h at 37 °C on solid production media containing 1.5% agar. One square centimeter of the bacterial lawn culture was extracted with 50 µl of 70% acetonitrile : 30% water with 0.1% formic acid for 30 s with vortexing. After centrifugation (14,000 rpm, 5 min) the solution was analyzed by an online HPLC (1100 series HPLC system, Agilent Technologies) coupled to a QTRAP 2000 mass spectrometer (Applied Biosystems). A sample of extract (4 µl) was separated by HPLC using a Luna C_{18} 100Å 50 x 1 mm column (Phenomenex) at a flow rate of 60 µl/min and a linear gradient of 5% to 100% acetonitrile with 0.1% formic acid in 10 min. MS analysis was performed in positive ion mode. MS settings: mass window was from 500 - 1400 Da, ion spray voltage was 4500, and ion source temperature was 300 °C.

2.5.5 Purification of cpd1335

A cell surface extract from a 250 ml culture of strain RSpMarA2 was collected using the previous method. During concentration under reduced pressure, cpd1335 precipitated. The precipitate was washed 3 times with deionized water, resulting in crude, desalted cpd1335. Pure cpd1335 was obtained using RP-HPLC (Grom-Sil ODS-5 ST, 20 x 250 mm, Alltech-Grom, Rottenburg-Hailfingen) with a linear gradient elution of 40 - 70% aqueous acetonitrile with 0.1% v/v formic acid over 40 min at a flow rate of 15 ml/min.

2.5.6 MALDI-TOF mass spectrometric analysis

Strains were grown for 16 h at 37 °C on production media solidified with 1.5% agar. For preparation of surface extracts, colonies were picked from the agar plates and extracted by vortexing for 30 sec with 50 µl 70% acetonitrile : 30% water with 0.1% formic acid. MALDI-TOF mass spectra were recorded using a Bruker Autoflex MALDI-TOF instrument containing a

337 nm nitrogen laser for desorption and ionization. 2 µl samples were mixed with the same volume of matrix solution (a saturated solution of α-cyano-4-hydroxycinnamic acid in 50% aqueous acetonitrile containing 0.1% v/v trifluoroacetic acid), spotted on the target, air-dried, and measured as described previously (Vater *et al.*, 2002). Spectra were obtained by positive ion detection and reflector mode MS.

2.5.7 RT-PCR

Total RNA was isolated with the Qiagen RNeasy Mini Kit. Cells (1.0 OD_{600}) were harvested from M9 minimal media supplemented with BME vitamin mix (Cat. No. B6891) and ATCC trace mineral solution (Cat. No. MD-TMS) and treated with the Qiagen RNAprotect Bacteria Reagent. Harvested cells were resuspended in 250 µl of 10 mM tris (pH 8.5) with 15 mg/ml lysozyme and 5 µl proteinase K (20 mg/ml) and digested for 1 h at 22 °C with gentle agitation. A DNase I digestion was performed for *pznE* and *pznL* using the Qiagen RNase Free DNase set. DNase I (7 µl) and RDD DNA digest buffer (7 µl) were used to hydrolyze contaminating DNA for 20 min at 22 °C. The RNA isolation protocol was then followed to manufacturer's instructions. To minimize background, a DNase I digestion (5 µl) was executed to the RNA samples and placed at 37 °C for 20 min. Note that this was the second DNase I digest for *pznE* and *pznL*. Samples were column purified using the RNA cleanup protocol in the RNeasy Mini Handbook (Qiagen). Digestion and cleanup were repeated for all RNA samples, excluding those used to analyze *pznE* and *pznL*. cDNA was prepared with commercially available RT-PCR kits using 1 µg of RNA and the primers listed in Table 2.3.

2.5.8 Tris-Tricine SDS-PAGE

Gels (18%) were prepared according to Schägger and Jagow (Schägger and von Jagow, 1987) with water instead of glycerol and without a spacer gel. Cellular extracts (100 µl) were mixed with 5x SDS sample buffer (20 µl) and then heated at 100 °C for 5 min prior to gel loading, along with a Ultra-low Range Molecular Weight Marker (Sigma). The peptides were

separated by low current (30 mA) electrophoresis. The gel was subsequently washed with destaining solution (10 ml ethanol, 10 ml acetic acid, 50 ml water) for 20 min (x3), and in deionized water for 20 min (x3). The gel was stained with Coomassie (EZBlue, Sigma) and/or Schiff's reagent (Sigma) after 1 h oxidation with 0.7% v/v periodic acid. The Coomassie stained band was excised from the gel and extracted with 50 µl 70% acetonitrile:30% water with 0.1% v/v formic acid for 24 h. The supernatant was used for MALDI-TOF MS measurement.

2.6 Acknowledgments

The strains CU1065 and HB0042 were kindly provided by J. Helmann (Cornell Univ. Ithaca, NY). *B. methylotrophicus* strains CAU-B946, YAU-Y2, and NAU-B3 were obtained from Q. Wang (Chinese Agricultural Univ., Beijing, China), Y. He (Yunnan Agricultural Univ., Kunming, China), and X. Gao (Nanjing Agricultural Univ., Nanjing, China), respectively. D. Naumann, P. Lasch (Robert Koch-Institut Berlin), and J. Melby (University of Illinois) assisted with mass spectrometry. Members of the Mitchell lab are acknowledged for critical review of the manuscript.

2.7 Figures

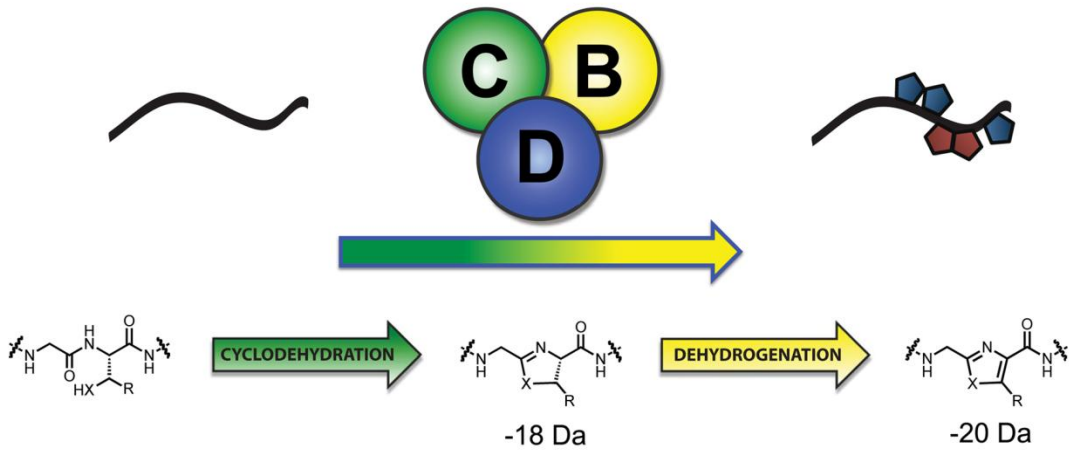

Figure 2.1 | Thiazole/oxazole-modified microcin (TOMM) biosynthesis. Through the action of a trimeric "BCD" complex, consisting of a cyclodehydratase (CD, green/blue), dehydrogenase (B, yellow), thiazoles and (methyl)oxazoles are incorporated onto a peptidic scaffold (black). These heterocycles are synthesized from serine/threonine (X = O; R = H/CH_3) and cysteine (X = S; R = H) residues of the inactive precursor peptide and yield a bioactive natural product. The chemical transformations carried out by the cyclodehydratase and the dehydrogenase are shown, along with the corresponding mass change from the parent peptide in Daltons.

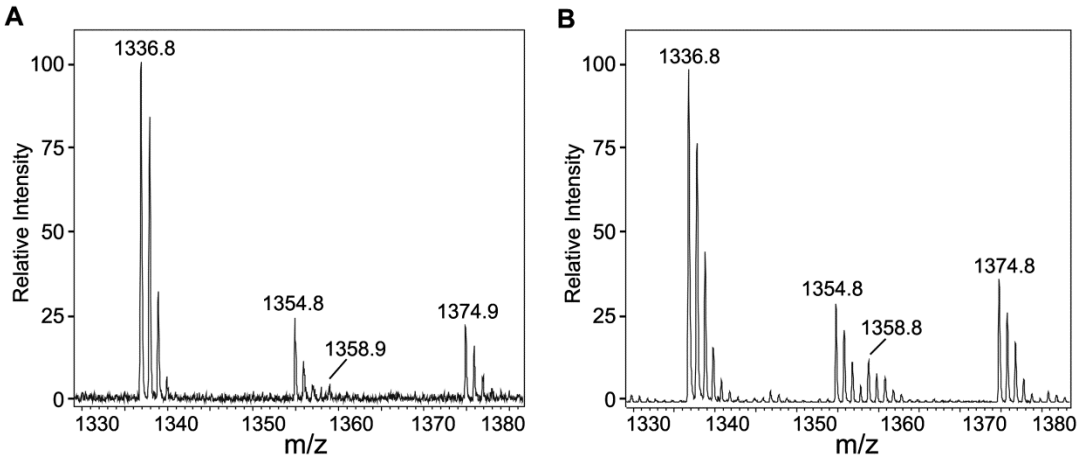

Figure 2.2 | MALDI-TOF mass spectra of *B. methylotrophicus* surface extracts. The samples were prepared from FZB42 (A) and RS6 (B) cells. Surface extracts were prepared and measured as described in the Material and Methods section. Peaks at 1336.8 $[M+H]^+$, 1354.8 $[M+H_2O+H]^+$, 1358.8 $[M+Na]^+$, and 1374.8 $[M+K]^+$ Da indicate the presence of PZN in the wild type strain, and in the Δ*sfp/* Δ*bac* mutant strain, RS6.

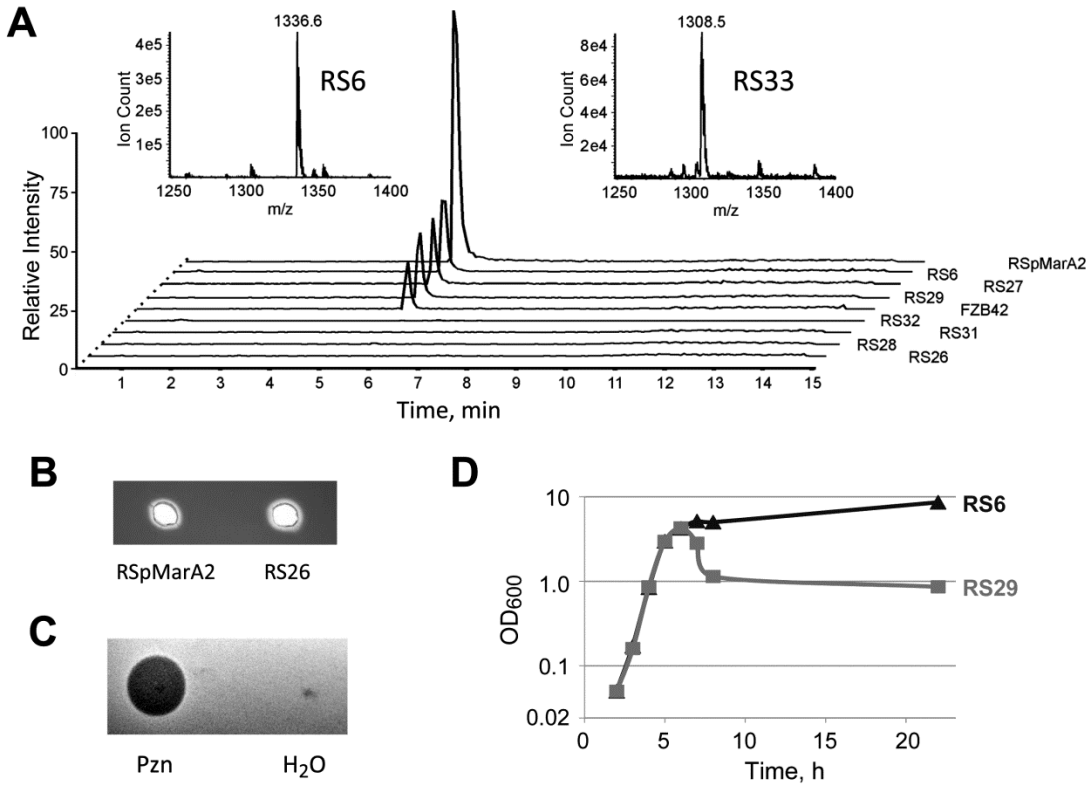

Figure 2.3 | Effect of mutations in the *pzn* gene cluster on biological activity. (A) Extracted ion chromatogram of PZN ($[M+H]^+$ 1336 Da) of FZB42 and mutant strains. This compound (m/z = 1336.6 Da, left inset) is synthesized by wild-type FZB42, and by the mutant strains RS6 *(*Δ*sfp/* Δ*bac*), RS27, and RS29. RSpMarA2 (Δ*degU*) overproduces PZN. Strains RS26, RS28, RS31, and RS32 were deficient in PZN production. Strain RS33 (right inset) produced a compound with m/z = 1308.5 Da, suggesting the loss of two methyl groups ($-H_2 + C_2H_6$, -28 Da). (B) Hemolytic activity of 100 µl extract from RSpMarA2 and RS26 on blood-agar plates. (C) Antibacterial activity of PZN. Left: HPLC purified PZN (10 µl of 100 µg/µl suspended in water) was spotted onto an agar plate of *B. subtilis* HB0042 (*sigW* null) and incubated for 16 h to assess growth inhibition. Right: 10 µl of water (negative control). (D) Growth curves of strains RS6 and *pznF* mutant RS29. After approximately 20 h of growth, the RS29 culture density is 9 log units lower than RS6.

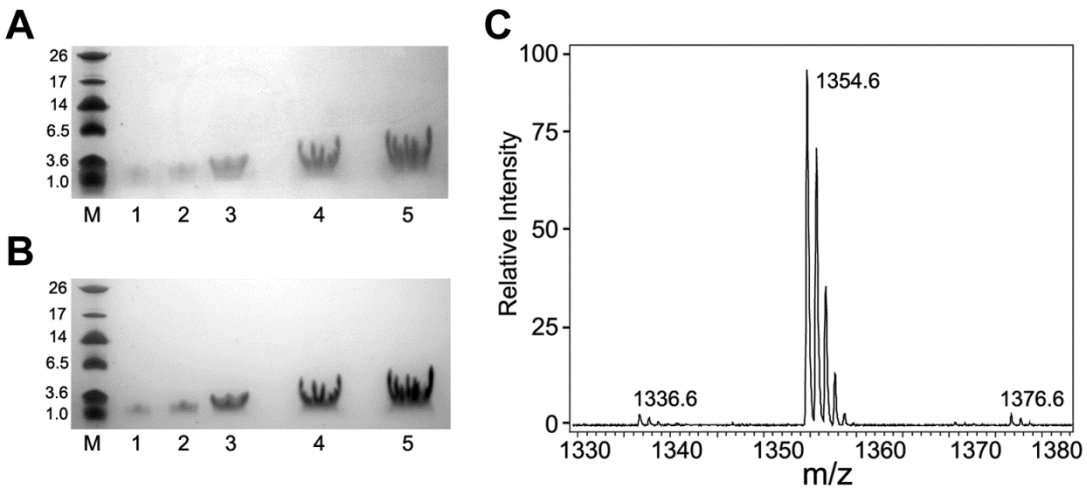

Figure 2.4 | Characterization of cell surface extract. Samples were prepared from RSpMarA2 and separated by 18% tris-tricine SDS-PAGE stained with either Coomassie EZBlue (A) or double-stained with Coomassie EZBlue and Schiff's reagent (B). M: size marker; 1-5: 1 µL, 2 µL, 5 µL, 10µL and 20 µL surface extract. (C) MALDI-TOF mass spectrum of the hydrated form of PZN (m/z: 1336 + 18 = 1354 Da) obtained by excising the peptide band from the tris-tricine SDS-PAGE gel.

A

B

Pzn	Locus (RBAM)	Proposed Function	Deletion	m/z
F	007400	immune function?	F	1336
K	007410	putative repressor		
GH	007420-007430	ABC transporters		
I	007440	unknown	I	1336
A	Unannotated	precursor peptide	A	-
J	007450	maturation	J	-
C	007460	cyclodehydratase	C	-
D	007470	docking scaffold		
B	007480	dehydrogenase	B	-
E	007490	zinc protease		
L	007500	methyltransferase	L	1308

Figure 2.5 | Plantazolicin gene cluster. (A) FZB42 PZN gene cluster (9892 bp) and amino acid sequence of the precursor peptide. (-) putative leader peptide processing site. (B) Proposed function of individual PZN genes. Upon deletion of *pznF* and *pznI*, cpd1336 (PZN) was detected by mass spectrometry. Deletion of *pznL* resulted in desmethyl PZN (m/z = 1308 Da) while individual inactivation of all other tested genes (*pznABCJ*) did not produce PZN. The functions of *pznF*, *pznI*, and *pznJ* require further exploration, but preliminary data suggests that *pznF* plays a role in immunity, *pznI* encodes a pentapeptide repeat protein, and *pznJ* is required for PZN maturation.

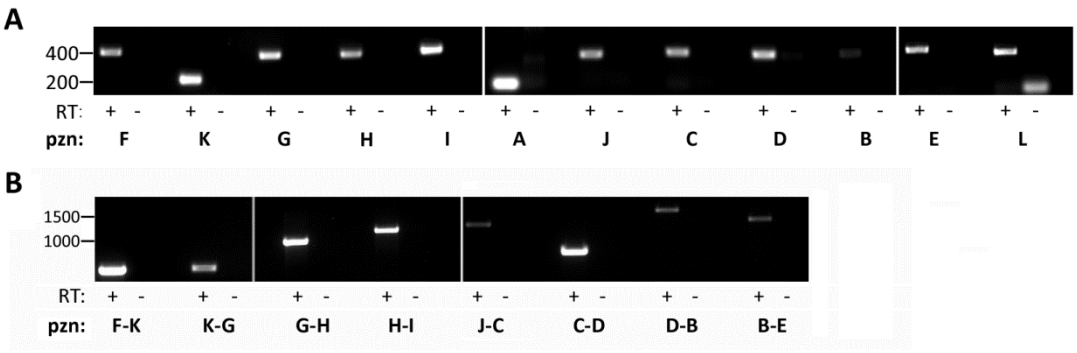

Figure 2.6 | RT-PCR reveals polycistronic mRNAs. Reverse transcriptase PCR was performed using 1 μg of FZB42 RNA isolated from stationary phase using a commercially available kit. PCR products were analyzed in comparison to a negative control lacking reverse transcriptase (-RT). (A) All genes in the putative PZN cluster are transcribed under the culturing conditions employed. Cells (1.0 OD_{600}) were removed from a stationary culture growing at 37 °C 24 h after inoculation. Total RNA was isolated and converted to cDNA by RT-PCR. cDNA (500 ng) was added to each reaction, excluding *pznE* and *pznL* (750 ng each). Gene fragments were then amplified using specific primers and PCR. Amplicons were assessed by separation on 1.1% agarose gels containing ethidium bromide and visualized by UV illumination. (B) Amplification of adjacent *pzn* genes reveals polycistronic mRNA. Not shown: junction A-J did not reveal a significant band; junction E-L was visible under extreme contrast. All amplicons migrate with their expected sizes.

2.8 Tables

Table 2.1 | Bacterial strains and plasmids used in this study

Strains	Description	Source / reference
Bacillus subtilis		
DSM10^T	168, *trp*C2, type strain	DSMZ Braunschweig
CU1065	168, *trpC2 attSP*β	(Butcher and Helmann, 2006)
HB0042	168, *trpC2 attSP*β *sigW*::*kan*	(Butcher and Helmann, 2006)
Bacillus megaterium		
7A/1	Indicator strain for polyketides	Laboratory stock
Bacillus methylotrophicus		
FZB42	Wild type	(Idriss *et al.*, 2002)
CH5	FZB42 *sfp*::*ermAM yczE*::*cm*	(Chen, 2009)
RSpMarA2	Insertion of pMarA in CH5: *degU*::*kan*	this work
RS6	*sfp*::*ermAM*, *bac*::*cmR*, deficient in lipopeptides, polyketides and bacilysin	(Chen *et al.*, 2009c)
RS26 (Δ*pznB*)	RS6 Δ*RBAM_007480*::*spc* does not produce PZN	this work
RS27 (Δ*pznI*)	RS6 Δ*RBAM_007440*::*spc* produces PZN	this work
RS28 (Δ*pznJ*)	RS6 Δ*RBAM_007450*::*spc* does not produce PZN	this work
RS29 (Δ*pznF*)	RS6 Δ*RBAM_007400*::*spc* produces PZN	this work
RS31 (Δ*pznC*)	RS6 Δ*RBAM_007460*::*spc* does not produce PZN	this work
RS32 (Δ*pznA*)	RS6 Δ*pznA*::*spc* does not produce PZN	this work
RS33 (Δ*pznL*)	RS6 Δ*RBAM_007500*::*spc* produces desmethyl-PZN, 1308 Da	this work
Plasmids		
pGEM-T	Ap^r, lacZ`	Promega
pMarA	plasmid containing mariner transposon TnYLB-1	(Le Breton *et al.*, 2006)
pIC333	plasmid with *spc* cassette	T. Msadek, Institute Pasteur, Paris, France
pRS26a	pGEM-T with 2700bp *pznB*	this work
pRS26b	pGEM-T with *pznB*::*spc*	this work
pRS27	pGEM-T with SOE fusion-product *RBAM_007440/spc*	this work
pRS28	pGEM-T with SOE fusion-product *RBAM_007450/spc*	this work
pRS29	pGEM-T with SOE fusion-product *RBAM_007400/spc*	this work
pRS31a	pGEM-T with 2600 bp *pznC*	this work
pRS31b	pGEM-T with *pznC*::*spc*	this work
pRS32a	pGEM-T with 2300 bp flanking region pznA	this work
pRS32b	pGEM-T with *pznA*::*spc*	this work

Table 2.2 | Activity spectrum of plantazolicin

Indicator strain	Result[a]	Source or reference[b]
Bacillus brevis ATCC8246	+	ATCC
Bacillus subtilis 168	+	(Butcher and Helmann, 2006)
Bacillus cereus ATCC14579	+	ATCC
Bacillus licheniformis ATCC9789	+	ATCC
Micrococcus luteus	+	Laboratory collection
Bacillus pumilus	-	Laboratory collection
Bacillus subtilis CU1065	+	(Butcher and Helmann, 2006)
Bacillus subtilis HB0042	++	(Butcher and Helmann, 2006)
Bacillus sphaericus	+	Laboratory collection
Paenibacillus polymyxa	-	Laboratory collection
Paenibacillus granivorans	+	Laboratory collection
Bacillus megaterium 7A1	++	Laboratory collection
Arthrobacter sp.	-	Laboratory collection
Staphylococcus aureus	-	Laboratory collection
E. coli K12	-	Laboratory collection
Klebsiella terrigena	-	Laboratory collection
Pseudomonas sp.	-	Laboratory collection
Erwinia caratovora	-	Laboratory collection

[a] Degree of inhibition in a bioassay: ++: inhibition; +: weak inhibition; -: no inhibition [b] ATCC: American Type Culture Collection

Table 2.3 | Oligonucleotides used for gene replacement and SOE PCR

Oligonucleotide	Sequence (5' to 3')
Spectinomycin resistance cassette	
Spc-fw	CTCAGTGGAACGAAAACTCACG
Spc-rv	TAAGGTGGATACACATCTTGTC
pRS26a/b	
pznB-fw	ATCCATATCGCCAATCATACGG
pznB-rv	GGAATCAATACCTGTCAGTTCG
pRS31a/b	
pznD-fw	ATTGACTAGGAGGTATTGGACG
pznD-rv	TTCTATTGAATAGGAGGAGGCG
pRS32a/b	
007400cst-fw	TGGAATGCTCTTTCCGCAGTAC
007400cst-rv	GTAACTCTGTTTCCACGTAACC
SOE PCR	
7400 rv	TCTTCATCACGCAAATCAGTGC
7400 fw	CCGCATAAACGGGAATTGGAAG
Spc in 7410	TCTATAGAAACTTCTCTCAATTAGAA AAGAAAAGGGCAAGGAAATGAG
7410 in spc	ACTCATTTCCTTGCCCTTTTCTTTTCT AATTGAGAGAAGTTTCTATAG
Start in spc	CTTTGTAAAAAGAGGAGCCTGTCTTA TGAGCAATTTGATTAACGG
Spc in start	TTTTTCCGTTAATCAAATTGCTCATA AGACAGGCTCCTCTTTTTACAAAG
7430 in spc	GCTGGGACTAAAAGGAGAGCGGGAA ATGAGCAATTTGATTAACGG
Spc in ORF2	TTCTATAGAAACTTCTCTCAATTAGA TTTAATATAAAGAAGCATAGACC
Spc in 7430	TTTTTCCGTTAATCAAATTGCTCATTT CCCGCTCTCCTTTTAGTCCCAGC
ORF2 in spc	TGGTCTATGCTTCTTTATATTAAATCT AATTGAGAGAAGTTTCTATAG
7440 rv	TCACGTCCAATACCTCCTAGTC
7440 fw	ATCGACAGAGGGCAGATTATCG
ORF2 in spc for 7450 fw	GATTATTGACTAGGAGGTATTGGACA TGAGCAATTTGATTAACGG
7460 in spc for 7450 rv	GTTTGTTGAGACATCTGTATTCCTCC CTAATTGAGAGAAGTTTCTATAG
7450 rv	TAATGTCGTCCATTTACTCACC
7450 fw	TTGGCTCGAATAAATGTTGACC

Table 2.3 (continued)

Spc in ORF2 for 7450 rv	TTTTTCCGTTAATCAAATTGCTCATGT CCAATACCTCCTAGTCAATAATC
Spc in 7460 for 7450 fw	TTCTATAGAAACTTCTCTCAATTAGG GAGGAATACAGATGTCTCAACAAAC
End in spc for 7500 rv	CGCTTAGACCCTAAAGATATACTTTC TCTAATTGAGAGAAGTTTCTATAG
7490 in spc for 7500 fw	AACTCTTTGGAGGTGTCACAGTTATA TGAGCAATTTGATTAACGG
7500 fw	AAGGTCCTAGACGCCCTATTCC
7500 rv	GATGTGTAGTTTTCAACGCTCG
Spc in end for 7500 fw	CTATAGAAACTTCTCTCAATTAGAGA AAGTATATCTTTAGGGTCTAAGCG
Spc in 7490 for 7500 rv	CCGTTAATCAAATTGCTCATATAACT GTGACACCTCCAAAGAGTTTACC
RT-PCR	
pznF-fw	GGATTATTGCGTACTCCGTTTC
pznF-rv	CTGCCTCCGCCAATAAATG
pznK-fw	ATGCCAAAGTACGGTTGGG
pznK-rv	CTCCTTGTAGGCTGCTTTCC
pznG-fw	CCACAGGATATCAGCCTTGAAG
pznG-rv	CGATAATCTGCCCTCTGTCG
pznH-fw	CGCTCGCTCAAATTGAAACG
pznH-rv	ACAACAACCCACAGATACGC
pznI-fw	TAGCCTGGAAGCAGAGGGTA
pznI-rv	ACTTTTGGCAGGTGACAACC
pznA-fw	GGAGGAGGTAACAATTATGACTCAA
pznA-rv	GGTACAGGTACAGCGTGCAG
pznJ-fw	TTGGATATCGGAATCGAGTTG
pznJ-rv	CGGATGCCCAATTATCTGTT
pznC-fw	TCATGTCCCTTGGTTGTGTG
pznC-rv	GCCGTGATACCATACTTGAGG
pznD-fw	CGCGATGTAGATGACGTTTG
pznD-rv	GATTGGCGATATGGATTAGTTG
pznB-fw	AAGGCATGCCACTAATTTGG
pznB-rv	GATAAAGAGCTCCGCCAGAA
pznE-fw	CATAGCAATAATGCGTACGGTG
pznE-rv	GAGACATTGTCGGCGAAGA
pznL-fw	GATGAGAGGGAAACCTCATCC
pznL-rv	CTCCCAAACTGTTCCTGTCC

2.9 References

1. Altschul, S.F., Madden, T.L., Schaffer, A.A., Zhang, J., Zhang, Z., Miller, W., and Lipman, D.J. (1997) Gapped BLAST and PSI-BLAST: a new generation of protein database search programs. *Nucleic Acids Res*: **25**, 3389-3402.

2. Borriss, R., Chen, X., Rueckert, C., Blom, J., Becker, A., Baumgarth, B., Fan, B., Pukall, R., Schumann, P., Sproer, C., *et al.* (2010) Relationship of *Bacillus amyloliquefaciens* clades associated with strains DSM7T and FZB42: a proposal for *Bacillus amyloliquefaciens* subsp. *amyloliquefaciens* subsp. nov. and *Bacillus amyloliquefaciens* subsp. *plantarum* subsp. nov. based on their discriminating complete genome sequences. *Int J Syst Evol Microbiol*: **61**, 1786-1801.

3. Busenlehner, L.S., Pennella, M.A., and Giedroc, D.P. (2003) The SmtB/ArsR family of metalloregulatory transcriptional repressors: Structural insights into prokaryotic metal resistance. *FEMS Microbiol Rev*: **27**, 131-143.

4. Butcher, B.G., and Helmann, J.D. (2006) Identification of *Bacillus subtilis* sigma-dependent genes that provide intrinsic resistance to antimicrobial compounds produced by Bacilli. *Mol Microbiol*: **60**, 765-782.

5. Chen, X. (2009) Whole genome analysis of the plant growth-promoting Rhizobacteria *Bacilllus amyloliquefaciens* FZB42 with focus on its secondary metabolites. *Dissertation*: **HU-Berlin**.

6. Chen, X.H., Koumoutsi, A., Scholz, R., and Borriss, R. (2009a) More than anticipated - production of antibiotics and other secondary metabolites by Bacillus amyloliquefaciens FZB42. *J Mol Microbiol Biotechnol*: **16**, 14-24.

7. Chen, X.H., Koumoutsi, A., Scholz, R., Eisenreich, A., Schneider, K., Heinemeyer, I., Morgenstern, B., Voss, B., Hess, W.R., Reva, O., *et al.* (2007) Comparative analysis of the complete genome sequence of the plant growth-promoting bacterium *Bacillus amyloliquefaciens* FZB42. *Nat Biotechnol*: **25**, 1007-1014.

8. Chen, X.H., Koumoutsi, A., Scholz, R., Schneider, K., Vater, J., Sussmuth, R., Piel, J., and Borriss, R. (2009b) Genome analysis of *Bacillus amyloliquefaciens* FZB42 reveals its potential for biocontrol of plant pathogens. *J Biotechnol*: **140**, 27-37.

9. Chen, X.H., Scholz, R., Borriss, M., Junge, H., Mogel, G., Kunz, S., and Borriss, R. (2009c) Difficidin and bacilysin produced by plant-associated *Bacillus amyloliquefaciens* are efficient in controlling fire blight disease. *J Biotechnol*: **140**, 38-44.

10. Choudhary, D.K., and Johri, B.N. (2009) Interactions of *Bacillus* spp. and plants--with special reference to induced systemic resistance (ISR). *Microbiol Res*: **164**, 493-513.

11. Cotter, P.D., Draper, L.A., Lawton, E.M., Daly, K.M., Groeger, D.S., Casey, P.G., Ross, R.P., and Hill, C. (2008) Listeriolysin S, a novel peptide haemolysin associated with a subset of lineage I *Listeria monocytogenes*. *PLoS Pathog*: **4**, e1000144.

12. Datta, V., Myskowski, S.M., Kwinn, L.A., Chiem, D.N., Varki, N., Kansal, R.G., Kotb, M., and Nizet, V. (2005) Mutational analysis of the group A Streptococcal operon encoding streptolysin S and its virulence role in invasive infection. *Mol Microbiol*: **56**, 681-695.

13. Dirix, G., Monsieurs, P., Marchal, K., Vanderleyden, J., and Michiels, J. (2004) Screening genomes of Gram-positive bacteria for double-glycine-motif-containing peptides. *Microbiology*: **150**, 1121-1126.

14. Dunbar, K.L., Chekan, J.R., Cox, C.L., Burkhart, B.J., Nair, S.K., and Mitchell, D.A. (2014) Discovery of a new ATP-binding motif involved in peptidic azoline biosynthesis. *Nat Chem Biol*: **10**, 823-829.

15. Dunbar, K.L., Melby, J.O., and Mitchell, D.A. (2012) YcaO domains use ATP to activate amide backbones during peptide cyclodehydrations. *Nat Chem Biol*: **8**, 569-575.

16. Dunbar, K.L., and Mitchell, D.A. (2013) Insights into the mechanism of peptide cyclodehydrations achieved through the chemoenzymatic generation of amide derivatives. *J Am Chem Soc*: **135**, 8692-8701.

17. Dunlap, C.A., Kim, S.J., Kwon, S.W., and Rooney, A.P. (2015) Phylogenomic analysis shows that Bacillus amyloliquefaciens subsp. plantarum is a later heterotypic synonym of Bacillus methylotrophicus. *Int J Syst Evol Microbiol*: **65**, 2104-2109.

18. Haft, D.H., Basu, M.K., and Mitchell, D.A. (2010) Expansion of ribosomally produced natural products: a nitrile hydratase- and Nif11-related precursor family. *BMC Biol*: **8**, 70.

19. Hardonk, M.J., and Van, D. (1964) The mechanism of the Schiff reaction as studied with histochemical model systems. *J Histochem Cytochem*: **12**, 748-751.

20. Horton, R.M., Cai, Z.L., Ho, S.N., and Pease, L.R. (1990) Gene splicing by overlap extension: tailor-made genes using the polymerase chain reaction. *Biotechniques*: **8**, 528-535.

21. Idriss, E.E., Makarewicz, O., Farouk, A., Rosner, K., Greiner, R., Bochow, H., Richter, T., and Borriss, R. (2002) Extracellular phytase activity of *Bacillus amyloliquefaciens* FZB45 contributes to its plant-growth-promoting effect. *Microbiology*: **148**, 2097-2109.

22. Kelly, W.L., Pan, L., and Li, C. (2009) Thiostrepton biosynthesis: prototype for a new family of bacteriocins. *J Am Chem Soc*: **131**, 4327-4334.

23. Koumoutsi, A., Chen, X.H., Henne, A., Liesegang, H., Hitzeroth, G., Franke, P., Vater, J., and Borriss, R. (2004) Structural and functional characterization of gene clusters directing nonribosomal synthesis of bioactive cyclic lipopeptides in *Bacillus amyloliquefaciens* strain FZB42. *J Bacteriol*: **186**, 1084-1096.

24. Koumoutsi, A., Chen, X.H., Vater, J., and Borriss, R. (2007) DegU and YczE positively regulate the synthesis of bacillomycin D by *Bacillus amyloliquefaciens* strain FZB42. *Appl Environ Microbiol*: **73**, 6953-6964.

25. Kunst, F., and G. Rapoport. (1995) Salt stress is an environmental signal affecting degradative enzyme synthesis in *Bacillus subtilis*. *J Bacteriol*: **177**, 2403–2407.

26. Le Breton, Y., Mohapatra, N.P., and Haldenwang, W.G. (2006) In vivo random mutagenesis of *Bacillus subtilis* by use of TnYLB-1, a mariner-based transposon. *Appl Environ Microbiol*: **72**, 327-333.

27. Lee, S.W., Mitchell, D.A., Markley, A.L., Hensler, M.E., Gonzalez, D., Wohlrab, A., Dorrestein, P.C., Nizet, V., and Dixon, J.E. (2008) Discovery of a widely distributed toxin biosynthetic gene cluster. *Proc Natl Acad Sci U S A*: **105**, 5879-5884.

28. Li, Y.M., Milne, J.C., Madison, L.L., Kolter, R., and Walsh, C.T. (1996) From peptide precursors to oxazole and thiazole-containing peptide antibiotics: microcin B17 synthase. *Science*: **274**, 1188-1193.

29. Liao, R., Duan, L., Lei, C., Pan, H., Ding, Y., Zhang, Q., Chen, D., Shen, B., Yu, Y., and Liu, W. (2009) Thiopeptide biosynthesis featuring ribosomally synthesized precursor peptides and conserved posttranslational modifications. *Chem Biol*: **16**, 141-147.

30. Mitchell, D.A., Lee, S.W., Pence, M.A., Markley, A.L., Limm, J.D., Nizet, V., and Dixon, J.E. (2009) Structural and functional dissection of the heterocyclic peptide cytotoxin streptolysin S. *J Biol Chem*: **284**, 13004-13012.

31. Morris, R.P., Leeds, J.A., Naegeli, H.U., Oberer, L., Memmert, K., Weber, E., LaMarche, M.J., Parker, C.N., Burrer, N., Esterow, S., *et al.* (2009) Ribosomally synthesized thiopeptide antibiotics targeting elongation factor Tu. *J Am Chem Soc*: **131**, 5946-5955.

32. Oman, T.J., and van der Donk, W.A. (2009) Insights into the mode of action of the two-peptide lantibiotic haloduracin. *ACS Chem Biol*: **4**, 865-874.

33. Pei, J., and Grishin, N.V. (2001) Type II CAAX prenyl endopeptidases belong to a novel superfamily of putative membrane-bound metalloproteases. *Trends Biochem Sci*: **26**, 275-277.

34. Rodriguez-Martinez, J.M., Briales, A., Velasco, C., Conejo, M.C., Martinez-Martinez, L., and Pascual, A. (2009) Mutational analysis of quinolone resistance in the plasmid-encoded pentapeptide repeat proteins QnrA, QnrB and QnrS. *J Antimicrob Chemother*: **63**, 1128-1134.

35. Roy, R.S., Gehring, A.M., Milne, J.C., Belshaw, P.J., and Walsh, C.T. (1999) Thiazole and oxazole peptides: biosynthesis and molecular machinery. *Nat Prod Rep*: **16**, 249-263.

36. Schägger, H., and von Jagow, G. (1987) Tricine-sodium dodecyl sulfate-polyacrylamide gel electrophoresis for the separation of proteins in the range from 1 to 100 kDa. *Anal Biochem*: **166**, 368-379.

37. Schmidt, E.W., Nelson, J.T., Rasko, D.A., Sudek, S., Eisen, J.A., Haygood, M.G., and Ravel, J. (2005) Patellamide A and C biosynthesis by a microcin-like pathway in *Prochloron didemni*, the cyanobacterial symbiont of *Lissoclinum patella*. *Proc Natl Acad Sci U S A*: **102**, 7315-7320.

38. Thompson, J.D., D.G. Higgins, and T.J. Gibson. (1994) CLUSTAL W: improving the sensitivity of progressive multiple sequence alignment through sequence weighting, position-specific gap penalties and weight matrix choice. *Nucleic Acids Res*: **22**, 4673-4680.

39. van Belkum, M.J., Worobo, R.W., and Stiles, M.E. (1997) Double-glycine-type leader peptides direct secretion of bacteriocins by ABC transporters: colicin V secretion in *Lactococcus lactis*. *Mol Microbiol*: **23**, 1293-1301.

40. Vater, J., Kablitz, B., Wilde, C., Franke, P., Mehta, N., and Cameotra, S.S. (2002) Matrix-assisted laser desorption ionization-time of flight mass spectrometry of lipopeptide biosurfactants in whole cells and culture filtrates of *Bacillus subtilis* C-1 isolated from petroleum sludge. *Appl Environ Microbiol*: **68**, 6210-6219.

41. Vetting, M.W., Hegde, S.S., Fajardo, J.E., Fiser, A., Roderick, S.L., Takiff, H.E., and Blanchard, J.S. (2006) Pentapeptide repeat proteins. *Biochemistry*: **45**, 1-10.

42. Viklund, H., and Elofsson, A. (2008) OCTOPUS: improving topology prediction by two-track ANN-based preference scores and an extended topological grammar. *Bioinformatics*: **24**, 1662-1668.

43. Wieland Brown, L.C., et al. (2009) Thirteen posttranslational modifications convert a 14-residue peptide into the antibiotic thiocillin. *Proc Natl Acad Sci U S A*: **106**, 2549-2553.

CHAPTER III: STRUCTURE DETERMINATION AND INTERCEPTION OF BIOSYNTHETIC INTERMEDIATES FOR THE PLANTAZOLICIN CLASS OF HIGHLY DISCRIMINATING ANTIBIOTICS

This chapter was adapted with permission from Molohon, K.J., Melby, J.O., Lee, J., Evans, B.S., Dunbar, K.L., Bumpus, S.B., Kelleher, N.L., and Mitchell, D.A. (2011) *ACS Chem Biol*: 6, 1307-1313. doi: 10.1021/cb200339d.

3.1 Abstract

The soil dwelling, plant-growth promoting bacterium, *Bacillus methylotrophicus* FZB42, is a prolific producer of complex natural products. Recently, a new FZB42 metabolite, plantazolicin (PZN), has been described as a member of the growing thiazole/oxazole-modified microcin (TOMM) family. TOMMs are biosynthesized from inactive, ribosomal peptides and undergo a series of cyclodehydrations, dehydrogenations, and other modifications to become bioactive natural products. Using high-resolution mass spectrometry, chemoselective modification, genetic interruptions, and other spectroscopic tools, we have determined the molecular structure of PZN. In addition to two conjugated polyazole moieties, the amino-terminus of PZN has been modified to N^{α},N^{α}-dimethylarginine. PZN exhibited a highly selective antibiotic activity towards *Bacillus anthracis*, but no other tested human pathogen. By altering oxygenation levels during fermentation, PZN analogs were produced that bear variability in their heterocycle content, which yielded insight into the order of biosynthetic events. Lastly, genome-mining has revealed the existence of four additional PZN-like biosynthetic gene clusters. Given their structural uniqueness and intriguing antimicrobial specificity, the PZN class of antibiotics may hold pharmacological value.

3.2 Introduction

With facile access to low-cost next-generation DNA sequencing technology, there has been a recent surge in genome sequencing. The availability of nearly 2,000 microbial genomes has rekindled interest in the biosynthetic capabilities of bacteria (Challis, 2008; Gross, 2009; Melby *et al.*, 2011; Peric-Concha and Long, 2003). Given the status of natural products and their

derivatives as the largest source of all medicines, exploring uncharted biosynthetic territory holds vast potential (Newman and Cragg, 2007). One such region of natural product space includes the thiazole/oxazole-modified microcin (TOMM) family (Haft *et al.*, 2010; Lee *et al.*, 2008; Scholz *et al.*, 2011). Unlike the well-known non-ribosomal peptides and polyketides, TOMMs are derived from inactive, ribosomally synthesized precursor peptides. Each TOMM precursor peptide harbors an N-terminal leader region that serves as the binding site for enzymes that posttranslationally modify a C-terminal core region (Madison *et al.*, 1997; Mitchell *et al.*, 2009). The distinguishing chemical features of a TOMM are heterocycles that derive from Cys, Ser, and Thr residues, which are abundant in the core region of the precursor peptide. During processing by a genetically conserved cyclodehydratase, select Cys and Ser/Thr amino acids undergo peptide backbone cyclization to become thiazoline and (methyl)oxazoline heterocycles (Dunbar *et al.*, 2014; Dunbar *et al.*, 2012; Dunbar and Mitchell, 2013). A subset of these are further subjected to a flavin mononucleotide (FMN)-dependent dehydrogenation, which yields the aromatic thiazole and (methyl)oxazole heterocycles. Together, the TOMM cyclodehydratase (CD) and dehydrogenase (B) comprise a functional, heterotrimeric thiazole/oxazole synthetase. The genes encoding for this synthetase are typically located as adjacent open reading frames in bacterial genomes, making such biosynthetic clusters relatively easy to identify using routine bioinformatic methods (Donia *et al.*, 2008; Lee *et al.*, 2008; Wieland Brown *et al.*, 2009). TOMM biosynthetic clusters often contain ancillary tailoring enzymes that increase the chemical complexity of this natural product family.

Although the unification of the TOMM family of natural products has only recently emerged, the molecular structure and biological function of some TOMMs have long been established. Examples include microcin B17 (DNA gyrase inhibitor), the cyanobactins (eukaryotic cytotoxins), streptolysin S (disease-promoting cytolysin), and the thiopeptides (ribosome inhibitors) (Melby *et al.*, 2011). As reported in early 2011, a plant-growth promoting

bacterium, *Bacillus methylotrophicus* FZB42 [previously named *Bacillus amyloliquefaciens* FZB42 (Dunlap *et al.*, 2015)], produces a TOMM with antimicrobial activity towards select Gram-positive bacteria (Scholz *et al.*, 2011). In this work, we report the structure and antimicrobial specificity of a TOMM natural product from FZB42. In addition to the natural production of PZN variants by FZB42, we discovered that other Gram-positive bacteria also contain PZN biosynthetic clusters. We further demonstrate the *in vivo* biosynthesis of PZN in one of these newly identified producers.

3.3 Results

3.3.1 High resolution mass spectrometry of PZN

Very recently, the structure of PZN from FZB42 was reported by Süssmuth and co-workers, primarily using 2D-NMR (Kalyon *et al.*, 2011). Independently, we employed mass spectrometry (MS) as our principle spectroscopic tool and arrived at the same structure. Through the use of high-resolution, linear ion trap Fourier Transform hybrid MS (LTQ-FT) operating at 11 tesla, we measured the mass of the protonated form of PZN to be 1336.4783 Da (Figures. 3.1a and 3.2). Due to the high mass accuracy of FT-MS and the known sequence of the core region of the precursor peptide ($_{1}$RCTCTTIISSSSTF$_{14}$) (Lee *et al.*, 2008; Scholz *et al.*, 2011), the molecular formula of $[PZN+H]^{+}$ can be deduced ($C_{63}H_{70}N_{17}O_{13}S_{2}$; theoretical monoisotopic mass = 1336.4780 Da; error, 0.22 ppm). This formula required that 9 out of 10 heterocyclizable residues (Cys, Ser, Thr) in the core region of the precursor peptide were converted to the azole heterocycle (Figure 3.1a). Due to their adjacent positions, these processed residues form a contiguous polyazole, which was supported by spectrophotometric analysis. PZN gave absorption bands at 260 nm (λ_{max}), 310 nm (minor shoulder), and 370 nm (weak), indicating the presence of a complex chromophore (Figure 3.3). The remaining heterocyclizable residue was left at the azoline (thiazoline, oxazoline, or methyloxazoline) oxidation state. Also, this formula required leader peptide cleavage after Ala-Ala and two methylation events, consistent with earlier deletion

studies (Scholz *et al.*, 2011). Collision induced dissociation (CID) was then used to localize the site(s) of dimethylation and the azoline heterocycle. Analysis of the doubly charged PZN ion using in-line HPLC-FTMS resulted in a spectrum that was featureless from *m/z* ~700-1100 as a result of contiguous heterocycle formation (Figure 3.2). Nonetheless, we noted the production of several diagnostic fragment ions, including peptide bond cleavage at Ile-Ile. The masses of these resultant ions demonstrated that the N-terminal (b^+ ion) fragment contained both posttranslational methyl groups and that the C-terminal (y^+ ion) fragment contained the azoline (now restricted to oxazoline or methyloxazoline due to the absence of Cys on this fragment). Other informative fragment ions were derived from cleavage between Arg1-Cys2(thiazole) and Thr13(methyloxazoline)-Phe14. The former cleavage event demonstrated that both posttranslational methyl groups were localized to Arg1. Cleavage between Thr13-Phe14 led to the formation of several decomposition products that permitted the localization of the (methyl)oxazoline to Thr13. From the apparently unstable parent ion, we routinely observed formal loss of allene from methyloxazoline (C_3H_4, 40.0313 Da) to yield a C-terminal amide (Figure 3.2). Further support for the location of the azoline heterocycle comes from hydrolysis studies, as discussed below. Proposed structures for all assignable ions are given (Figures. 3.4 and 3.5).

3.3.2 Localization of the dimethylation site

Upon in-depth FTMS analysis of singly charged PZN introduced by direct infusion, we observed larger ions relative to doubly charged PZN parent ions, including ones consistent with the loss of guanidine (-59.0483 Da, *m/z* 1277.4299; error, 0.63 ppm) (Figure 3.1b). This indicated that the site of dimethylation was restricted to either the N-terminal amine or the alkyl sidechain of Arg1. The latter is exceedingly improbable since the enzyme known to catalyze this reaction (PznL) is predicted by sequence alignment to be a *S*-adenosylmethionine (SAM)-dependent methyltransferase. The only SAM-dependent enzymes capable of engaging in C-H bond

activation are the radical SAM enzymes, which are identifiable by numerous conserved Cys lacking in PznL (Frey *et al.*, 2008; Lee *et al.*, 2008; Scholz *et al.*, 2011). Higher order CID was performed on the deguanidinated form of PZN (*m/z* 1277), providing corroborating evidence for N-terminal dimethylation (Figure 3.6). Further support for the N-terminus being the site of dimethylation in PZN comes from chemoselective labeling. We reacted HPLC-purified PZN and desmethylPZN (from the *pznL* deletion strain) with the amine-specific reagent, *N*-hydroxysuccinimide (NHS)-biotin (Scholz *et al.*, 2011). As observed by MALDI-MS, labeling was only successful in the desmethylPZN reaction, indicating the presence of a free amine in this compound, but not in PZN (Figure 3.7). From these studies, we conclude that leader peptide cleavage occurs before methylation and that the ABC transport system does not distinguish between PZN and desmethylPZN. The nucleophilic N-terminus of desmethylPZN will likely be a convenient derivatization point for future structure-activity relationship (SAR) studies.

From the apparent hydrolysis of PZN following SDS-PAGE (Scholz *et al.*, 2011), we were not surprised to find that PZN contained an azoline. Such heterocycles are prone to both acid- and base-catalyzed hydrolysis (Frump, 1971; Martin and Parcell, 1961). Mild acid treatment of PZN yields *m/z* 1354 (+18), which was shown by CID studies to be from the reconstitution of the Thr13 residue of the precursor peptide (Figure 3.1b). Higher order tandem MS experiments further confirmed the location of the PZN methyloxazoline moiety (Figures. 3.5 and 3.6). Since the Thr13(methyloxazoline) is the only heterocycle not processed by the dehydrogenase, PznB displays a high level of regiospecificity.. While our PZN structure is identical to that just published, note that Thr13 has been converted to a methyloxazoline, not a methyloxazolidine as reported (Kalyon *et al.*, 2011).

During our extensive MS analysis of PZN, we noticed that fragmentation of the methyloxazoline moiety gave rise to a characteristic mass loss. CID fragmentation of PZN yielded an intense daughter ion of *m/z* 1292.4519 (Figure 3.1b). The mass difference from the

PZN parent ion is 44.0261 Da, which is consistent with the neutral loss of acetaldehyde (C_2H_4O, exact mass = 44.0262). Loss of acetaldehyde is conceivable from cycloelimination of methyloxazoline to yield a nitrile ylide, which can re-cyclize to form an azirine. The microscopic reverse of this reaction pathway is well known in the chemical literature where azirines are reacted with aldehydes to form oxazolines via 1,3-dipolar cycloaddition (Frump, 1971; Giezenda *et al.*, 1973; Sa and Kascheres, 1996). Importantly, the loss of acetaldehyde was observed only when methyloxazoline was present on the parent ion (compare Figure 3.1b-c and Figures. 3.4-3.6). This observation could potentially be capitalized upon in future studies as a means of screening complex mixtures for the presence of azoline-bearing natural products. (Melby *et al.*, 2011)

3.3.3 Nuclear magnetic resonance (NMR) of PZN

To corroborate the proposed structure elucidated by MS, we performed a series of two-dimensional NMR experiments including ^{1}H-^{1}H-gCOSY, ^{1}H-^{1}H-TOCSY, and ^{1}H-^{13}C-gHMBC on a 600 MHz instrument (Figures. 3.8-3.10). The results of these experiments are compiled in Table 3.1. Briefly, the gCOSY and TOCSY spectra confirmed the following: ***i.*** Due to the absence of NH and $C_\alpha H$ correlations, all Cys, Ser, and Thr must be heterocyclized. The NH and $C_\alpha H$ correlations were readily visible for all internal residues with an intact amide bond (Ile, Ile, Phe). ***ii.*** The carbon framework of the Arg1, Ile7, Ile8, and Phe14 side chains were not modified and, ***iii.*** The sole azoline moiety of PZN occurs on a Thr. The ^{1}H-^{13}C-gHMBC spectrum further validated findings from the ^{1}H-^{1}H experiments, in addition to proving the methylation sites as N^{α},N^{α}-dimethylArg (Figure 3.10). N-terminal methylation of ribosomally produced peptides in bacteria is an exceedingly rare posttranslational modification. While N-terminal dimethylation has been described on Ala (*e.g.* cypemycin) (Claesen and Bibb, 2010) N^{α},N^{α}-dimethylArg appears to be a novel posttranslational modification (Garavelli, 2004). The structure of PZN provides yet

another example of the complex natural product repertoire of *B. methylotrophicus* FZB42 (Chen *et al.*, 2007).

3.3.4 Production of PZN analogs

During the course of optimizing the production of PZN for detailed spectroscopic analysis, we noticed that the level of culture oxygenation had a substantial impact on the production of PZN and derivative metabolites. Under low oxygen fermentation, PZN (*m/z* 1336) was the majority species present after a non-lytic, cell surface extraction procedure, as demonstrated by the UV trace, total ion chromatogram (TIC), and the extracted ion chromatogram (EIC, Figure 3.11a-c). The product of methyloxazoline ring opening (*i.e.* hydrolyzed PZN, *m/z* 1354) was also monitored (Figure 3.11c-d). The *m/z* 1338 species that "coelutes" with 1336 at 19.9 min is actually the second isotope peak of *m/z* 1336 (Figure 3.12). Under oxygen saturated cultivation, UV and TIC monitoring revealed an additional, highly abundant species at 14.7 min (Figure 3.11a-b). MS analysis demonstrated this species was *m/z* 1338, suggestive of a reduced PZN species (dihydroPZN) containing two azolines (Figures. 3.11d and 3.13). The earlier elution time on reverse-phase chromatography suggested that this species was more polar than PZN, which is consistent with the replacement of an aromatic azole with a protonated azoline (expected in 0.1% formic acid). After treatment of *m/z* 1338 with mild aqueous acid, two additions of water were observed (*m/z* 1356 and 1374). Tandem MS was then used to demonstrate that the second azoline was located on the N-terminal half of PZN (Figure 3.14). Higher order CID analysis prompted the neutral loss of acetaldehyde, indicating the heterocycle was derived from Thr, likely the residue directly preceding Ile (Thr6, data not shown). To an approximation, this position is sterically and electronically equivalent to the previously discussed methyloxazoline (Thr13) since both lie between an N-terminal tetra-azole and a C-terminal unmodified, hydrophobic residue (Figure 3.1a). The corresponding desmethylPZN species was observed when oxygenation levels were increased during cultivation

of the methyltransferase deletion strain (Figures. 3.15 and 3.16). It is possible that azoline oxidation is the rate-determining step in PZN biosynthesis. With increased aeration (faster metabolism), partially processed PZN products may be more rapidly produced and accepted as substrates by proteins acting downstream of the dehydrogenase. The biosynthetic implication of observing PZN oxidation intermediates is that the rate of methyloxazoline oxidation at "Thr6" (putative) and Thr13 (Figure 3.1a) must be slower than the dissociation rate from the heterotrimeric synthetase complex and subsequent maturation steps. An additional ramification of intercepting this PZN oxidation intermediate is that cyclodehydration must precede dehydrogenation, as has been previously supported by *in vitro* reconstitution experiments but never before demonstrated *in vivo* (McIntosh and Schmidt, 2010; Milne *et al.*, 1999). While the oxygen-dependency of secondary metabolism is well known (Clark *et al.*, 1995), the precise mechanism accounting for the production of a more reduced PZN species during increased culture aeration is not clear at the present time.

3.3.5 Bioactivity of PZN and PZN analogs

In early 2011, the activity of PZN towards 16 distinct bacterial species (18 strains) was reported (Scholz *et al.*, 2011). It was determined that PZN was growth-suppressive primarily towards *Bacillus* sp., including *B. subtilis*. PZN exhibited no activity against any tested Gram-negative organisms. To further define the selectivity within the Gram-positives, we evaluated the scope of PZN activity towards a panel of ubiquitous human pathogens, including methicillin-resistant *Staphylococcus aureus* (MRSA), vancomycin-resistant *Enterococcus faecalis* (VRE), *Listeria monocytogenes*, *Streptococcus pyogenes*, and *Bacillus anthracis* strain Sterne. Using a microbroth dilution bioassay, we observed potent growth inhibition of *B. anthracis* (Figure 3.17a). All other species were unaffected by PZN, with the exception of *S. pyogenes*, which was only inhibited by very high concentrations of PZN. The specificity for PZN against *B. anthracis* was recapitulated in an agar diffusion bioassay (Figure 3.17a), as inhibition zones were not

observed for any other tested bacterium (data not shown). The action of PZN upon *B. anthracis* was decidedly bactericidal, as reculturing of treated cells in the absence of PZN led to no bacterial growth. Live cell imaging by differential interference contrast (DIC) microscopy revealed that *B. anthracis* treated with PZN at 4 μg mL^{-1} underwent massive lysis, as evidenced by an abundance of cellular debris (data not shown). Of the few remaining non-lysed cells, we observed marked changes in the appearance of the cell surface (Figure 3.17c-d). While the biological target of PZN has yet to be established, the "sidewall spot" phenotype suggests PZN has either directly or indirectly compromised the integrity of the cell wall (Tiyanont *et al.*, 2006). Due to the selective, biomedically relevant bactericidal activity exhibited by PZN, elucidation of the precise mode of action for PZN is ongoing in our laboratory.

Dimethylation of the α-amino group was apparently critical for PZN's antibiotic activity, as desmethylPZN was devoid of activity against *B. anthracis* in both bioassays (Figure 3.17a). While the molecular basis for this effect is not currently known, dimethylation increases amine basicity, increases lipophilicity, and removes two potential H-bond donors. Also tested were the effects of hydrolyzing the methyloxazoline moiety of PZN (hydrolyzed PZN, *m/z* 1354) and the variant with two azolines (dihydroPZN, *m/z* 1338). While hydrolyzed PZN retained measurable activity towards *B. anthracis*, dihydroPZN was devoid of activity. Due to difficulty in separating dihydroPZN from the mono- and dihydrolyzed forms (*m/z* 1356 and 1374), these bioassays were performed using a 1:2:2 mixture (non:mono:di). The lack of activity with this mixture of hydrolyzed, dihydroPZN compounds might be attributable to the fact that hydrolyzed PZN is roughly 8-fold less active than PZN (Figure 3.17a). Although the production of dihydroPZN under oxygen-saturated conditions may be artifactual, it nonetheless raises interesting questions regarding the regiospecificity of azoline oxidation and the substrate tolerance of the downstream tailoring enzymes and export apparatus.

3.3.6 Identification of PZN-like gene clusters across phyla

A targeted bioinformatics survey using the thiazole/oxazole synthetase proteins (cyclodehydratase and dehydrogenase) of PZN yielded four highly related biosynthetic gene clusters (Figure 3.18). The cluster found in *Bacillus pumilus* ATCC 7061 (also a plant-growth promoting saprophyte) is of identical gene order and direction as the cluster from *B. methylotrophicus* FZB42 (Scholz *et al.*, 2011). The remaining three PZN-like biosynthetic clusters were found in the Actinobacteria phylum including *Clavibacter michiganensis* subsp. *sepedonicus* (potato pathogen) (Bentley *et al.*, 2008), *Corynebacterium urealyticum* DSM 7109 (human skin-associated bacterium, causative agent of some urinary tract infections) and *Brevibacterium linens* BL2 (human skin-associated bacterium). The PZN clusters from *C. urealyticum* and *B. linens* have amino acid similarity values much higher with each other than the other PZN producers, which is interesting given their overlapping niche and the absence of TOMM genes in sequenced relatives (Figure 3.19). In each of the five species, the PZN biosynthetic cluster contained the canonical TOMM genes: a precursor peptide, dehydrogenase, and cyclodehydratase complex. Beyond this, all five clusters also include a putative membrane-spanning leader peptidase from the type II CAAX superfamily (Pei *et al.*, 2011), SAM-dependent methyltransferase, and a required protein of unknown function (Scholz *et al.*, 2011). Conversely, homologs of the PznF immunity protein and PznGH transporters were not found in the local genomic context for the PZN biosynthetic gene clusters for *C. urealyticum* and *B. linens* (Figure 3.18a). This suggests a distinct mechanism of immunity and chromosomally distant transporters for these PZN variants. Alternatively, the PZNs from *C. urealyticum* and *B. linens* could act intracellularly or the biosynthetic gene cluster might always be silent (non-product forming).

Based on the identical amino acid sequence of the core regions of the precursor peptides from FZB42 and *B. pumilus*, it would be expected that these species produce identical compounds (Figure 3.18b). To test if *B. pumilus* was indeed producing PZN, stationary phase *B. pumilus*

ATCC 7061 cultures were cell surface extracted in an identical manner as with FZB42. MALDI-TOF-MS of HPLC-purified fractions revealed the presence of *m/z* 1336, and in an earlier fraction, m/z 1354 (+H_2O), supporting the production of PZN and hydrolyzed PZN (Figure 3.20a-b). The identity of this species as PZN was confirmed by high accuracy mass measurement (LTQ-FT-MS) and CID analysis (Figure 3.20c-e). As anticipated, *B. amylo*. FZB42 and *B. pumilus* were not susceptible to the action of PZN (MIC > 128 μg mL^{-1}). A non-plant associated strain of *B. amylo*. (NRRL B-14393), which does not produce PZN, was also completely resistant (data not shown). Resistance within the *Bacillus* genus to PZN is clearly complex, with a few strains being *bona fide* PZN producers and others simply harboring the immunity gene [*e.g. B. amylo*. strains YAU-Y2 and NAU-B3 (Scholz *et al.*, 2011) and *B. atrophaeus* 1942, BATR1942_01200, 94% identical to FZB42]. Early attempts to isolate a PZN-type natural product from the Actinobacteria family members have not yet been successful. The lack of a signal by MALDI-MS and reverse transcriptase-PCR suggested that the biosynthetic genes were not transcribed under our cultivation conditions (data not shown). As with many "silent" gene clusters, highly precise environmental conditions are often necessary for the bacterium to produce particular natural products.

With several PZN-like biosynthetic gene clusters identified in this work, these natural products comprise an entirely new class of antibiotic. Sequence alignment of all five PZN precursor peptides showed that there has been evolutionary pressure to maintain a nearly invariant chemotype giving rise to the PZN structure (from N- to C-terminus): leader peptide cleavage site and N-terminal Arg (FEPxAA*R), five cyclizable residues with position 2 and 4 always Cys and position 6 always Thr, two hydrophobic residues, five cyclizable residues, and a more variable C-terminus that ends with Phe, Trp-Gly, or Gly-Gly (Figure 3.18b). It is probable that more PZN producers will emerge with on-going efforts in genome sequencing. Future work will establish the contribution of these conserved functionalities on the bioactivity of PZN.

3.4 Summary and Outlook

Here we have reported on the structural uniqueness of PZN, production of oxygen-dependent derivatives, distribution of producing species, and a striking human pathogen selectivity for *Bacillus anthracis*. Elucidation of the structure, in conjunction with the interception of dehydrogenase and methyltransferase intermediates, has provided a glimpse into the biosynthetic strategy employed by nature (Figure 3.21). With respect to the bioactivity of PZN, it is noteworthy that strains of *B. anthracis* have been reported to be increasingly resistant to the quinolone, beta-lactam, tetracycline, and macrolide classes of antibiotics, thus new strategies to overcome this NIAID-designated Category A priority pathogen are needed (Athamna *et al.*, 2004; Bryskier, 2002). With improved diagnostic technology, we anticipate that highly discriminating antibiotics will play a large role in our future antibiotic repertoire. The ideal drugs will be capable of distinguishing between pathogenic bacteria and those that live in commensal and/or symbiotic relationships with humans. Selection theory predicts that such drugs will delay the rise of antibiotic resistance, as non-targeted species have no evolutionary benefit to develop/obtain a resistance mechanism. Faced with the never-ending arms race with multiple drug resistant bacteria, novel structural classes of antimicrobials with unique modes of action must continually be discovered and clinically implemented to treat bacterial infections. However, more work is necessary to determine if PZN-like compounds exhibit desirable *in vivo* properties.

3.5 Experimental

3.5.1 Production and purification of PZN

Overnight cultures (4 x 20 mL) of *B. methylotrophicus* FZB42 strain RSpMarA2 (Δ*sfp, yczE, degU*) (Scholz *et al.*, 2011) were used to inoculate 4 x 6 L flasks with 2 L of Luria Burtani (LB) broth supplemented with chloramphenicol (7 μg mL^{-1}) and kanamycin (7 μg mL^{-1}). Cultures were grown with shaking for 48 h at 37 °C. Cells were harvested by centrifugation (4,000 x *g*), washed with Tris-buffered saline (pH 8.0), and harvested a second time. Crude PZN was obtained

by a non-lytic, methanolic extraction of the cellular surface. Cells were resuspended in MeOH (10% culture volume) and anhydrous Na_2SO_4 (5 g/L culture). The cell mixture was agitated by vortex (45 s) and equilibrated for 15 min at 22 °C. The supernatant was retained after centrifugation (4,000 x *g*), vacuum filtered with Whatman filter paper, and rotary evaporated to dryness to yield about 100 mg/L of a yellowish-brown solid. This crude material was dissolved in 80% aqueous MeCN (10 mL for 8 L culture), where the sample separated into two layers. The top organic layer was retained and concentrated for injection onto an Agilent 1200 series liquid chromatograph that was fitted inline to an Agilent 6100 Series Quadrupole LC/MS. For preparative purposes, PZN was reverse phase purified using a Thermo BETASIL C18 column (250 mm x 10 mm; pore size: 100 Å; particle size: 5 μm) at a flow rate of 4 mL min^{-1}. A gradient of 65-85% MeOH with 0.1% formic acid over 32 min was used. The fractions containing PZN (as monitored by A_{266} and MS) were collected into 20 mL borosilicate vials and the solvent removed *in vacuo*. The isolated yield for PZN following this procedure was routinely 150-200 μg L^{-1} culture. Mutant RS33 (Δ*sfp, bac, pznL*) was prepared similarly, with the only exceptions being a 24 h fermentation, substitution of spectinomycin (90 μg mL^{-1}) for kanamycin, and elimination of the TBS wash.

3.5.2 Production of PZN (elevated oxygen)

Increased aeration of *B. methylotrophicus* FZB42 strains RSpMarA2 and RS33 were achieved using a New Brunswick Scientific BioFlo 110 Fermenter system. RSpMarA2 and RS33 (9 L) were cultured at 37 °C with 250 rpm stirring for 24 h. Air was supplied at 5 L/min (saturated in oxygen, ~1 L min^{-1}).

3.5.3 On-line RPLC-FTMS

All reverse phase liquid chromatography (RPLC)-Fourier-transform mass spectrometry (FTMS) was conducted using an Agilent 1200 high performance LC (HPLC) system with an autosampler coupled directly to a ThermoFisher Scientific LTQ-FT hybrid linear ion trap-FTMS

system operating at 11 tesla. The MS was calibrated weekly using the calibration mixture and instructions specified by the manufacturer. All instrument parameters were tuned according to the manufacturer's instructions (employing bovine ubiquitin for tuning purposes). For all analyses of PZN, a 1 mm x 150 mm Jupiter C18 column (Phenomenex, 300 Å, 5 µm) was connected in-line with the electrospray ionization source (operated at ~5 kV with a capillary temperature of 200-250 °C) for the MS system. A typical sample was loaded onto the column using the autosampler and separated using a linear gradient of H_2O/MeCN and 0.1% formic acid with the analytes eluted directly into the MS. All ionized species were subjected to an MS method with five MS and MS/MS events: 1) full scan measurement of all intact peptides (all ions detected in the FTMS in profile mode; resolution: 100,000; *m/z* range detected: 400-2000), 2-5) data-dependent MS/MS on the first, second, third, and fourth most abundant ions from scan (1) using collision induced dissociation (CID) (all ions detected in the FTMS in profile mode; minimum target signal counts: 5,000; resolution: 50,000; *m/z* range detected: dependent on target *m/z*, default charge state: 2, isolation width: 5 *m/z*, normalized collision energy: 35; activation q value: 0.40; activation time: 30 ms). During all analyses, dynamic exclusion was enabled with the following settings: repeat count – 2, repeat duration – 30 s, exclusion list size – 300, exclusion duration – 60 s.

3.5.4 Direct infusion FTMS

After lyophilization for at least 24 h, HPLC purified samples were dissolved in 80% MeOH (to ~0.5 mg mL^{-1}) and then further diluted 10-fold into 50% MeOH supplemented with 0.1% (v/v) formic acid. The diluted samples were directly infused using an Advion Nanomate 100. The singly charged ions were targeted for CID using identical settings as above, except that the resolution was set to 100,000.

3.5.5 N-terminal labeling

Purified PZN and desmethylPZN were dissolved in 80% MeCN, 10 mM MOPS (pH 8.0) to a final concentration of 1.5 mM. An aliquot (5 µL) was transferred to a microfuge tube containing 5 µL of 80% MeCN, 10 mM MOPS (pH 8.0) supplemented with 20 mM EZ-Link® sulfo-NHS-biotin. Control reactions lacked the NHS-biotin reagent. The samples were allowed to react for 3 h at 23 °C prior to analysis on an Applied Biosystems Voyager DE-STR MALDI-TOF-MS.

3.5.6 NMR

PZN was produced from low oxygenation cultures and purified as described in the main text methods. PZN (700 µg) was dissolved in 200 µL of DMSO-d_6 and placed into an Advanced Shigemi 5 mm NMR tube matched to DMSO-d_6. NMR experiments were conducted on a Varian Unity Inova 500 NB (^{1}H-^{1}H-gCOSY) and a Varian Unity Inova 600 spectrometer (^{1}H, ^{1}H-^{1}H-TOCSY and ^{1}H-^{13}C-gHMBC) using a 5 mm Varian ^{1}H{^{13}C/^{15}N} PFG Z probe and 5 mm Varian ^{1}H{^{13}C/^{15}N} XYZ PFG triple resonance probe, respectively. The ^{1}H-NMR, TOCSY and gHMBC experiments were conducted at 25 °C and utilized water suppression. A mixing time of 150 ms was used for the TOCSY. For the gHMBC, ^1J and ^nJ were set to 140 and 8 Hz, respectively. Chemical shifts were referenced using DMSO (δ_H=2.50 and δ_C=39.51), and the spectra were processed and analyzed using MestReC. Stereochemical configuration was assumed to be identical to the ribosomally produced precursor peptide.

3.5.7 Determination of MIC

B. anthracis strain Sterne was grown to stationary phase in a 10 mL LB culture at 37 °C. The culture was adjusted to OD_{600} of 0.01 in LB broth and added to 96-well plates. 2-fold dilutions of PZN (5 mg mL^{-1} in 80% MeCN) were added to the cultures (0.5 – 128 µg mL^{-1}). Kanamycin was added similarly to control samples, with dilutions from 1 – 32 µg mL^{-1}. Covered plates were incubated at 37 °C for 12 h. The minimum inhibitory concentration that suppressed

the growth of at least 99% of the bacteria (MIC_{99}) was established based on culture turbidity. Additional pathogens were grown and prepared similarly as above, with the exception of optimizing the growth media to match an organism's nutritional requirements (*Streptococcus pyogenes*, Todd Hewitt broth; *Listeria monocytogenes*, *Enterococcus faecalis* st. U503 [VRE], and *Staphylococcus aureus* st. NRS384/USA300 [MRSA], brain heart infusion). Positive controls: *S. pyogenes* and *L. monocytogenes*, kanamycin; *E. faecalis*, tetracycline; *S. aureus*, vancomycin. Bactericidal activity was determined by diluting 1 µL of *B. anthracis* strain Sterne grown with 8 µg mL^{-1} PZN into 99 µL of media. The sample was then streaked onto LB agar plates and incubated for 24 h for counting colony-forming units.

3.5.8 Agar diffusion bioassay

B. anthracis strain Sterne was grown as described previously and diluted to OD_{600} of 0.13. The diluted culture (100 µL) was inoculated onto an LB plate and allowed to dry. HPLC-purified PZN (50-200 µg) was added to a paper disk, dried, and added to the plate. Culture were then incubated at 37 °C for 12 h. Kanamycin (8-25 µg) was used as a positive control, and 80% MeCN was the negative (solvent) control.

3.5.9 Microscopy

Differential interference contrast (DIC) microscopy images were obtained by preparing live cell images of *B. anthracis* cultures. Samples were pretreated with or without PZN at 4 µg mL^{-1} (MIC_{99}) and morphology was assessed using a Zeiss LSM 700 microscope. The objective used was a Plan-Apochromat 63x/1.40 Oil DIC M27. The analysis software used was Program Zen 2009 Light Edition.

3.5.10 Production of PZN from *Bacillus pumilus* ATCC 7061

Cultures were prepared as described above, but with the exception no antibiotics were added. The method employed for metabolite extraction and HPLC purification were identical to samples from *B. methylotrophicus*. Purified fractions were analyzed on a Bruker Daltonics

ultrafleXtreme MALDI-TOF/TOF instrument operating in reflector/positive mode. Sinapic acid was used as the matrix.

3.6 Acknowledgments

We are grateful for the gift of *B. methylotrophicus* strains RSpMarA2 and RS33 from R. Borriss (Humboldt Universität Berlin, Germany). VRE strain U503 and *S. aureus* strain NRS384/USA300 were kindly provided by J. Williams and P. Hergenrother (University of Illinois) while *L. monocytogenes* and *B. anthracis* Sterne were from J. Call (USDA-ARS) and S. Stibitz (FDA), respectively. T. Maxson, N. Ethridge, A. Mohan, M. Sivaguru are acknowledged for their technical assistance. Members of the Mitchell lab assisted in the critical review of this manuscript.

3.7 Figures and Tables

Figure 3.1

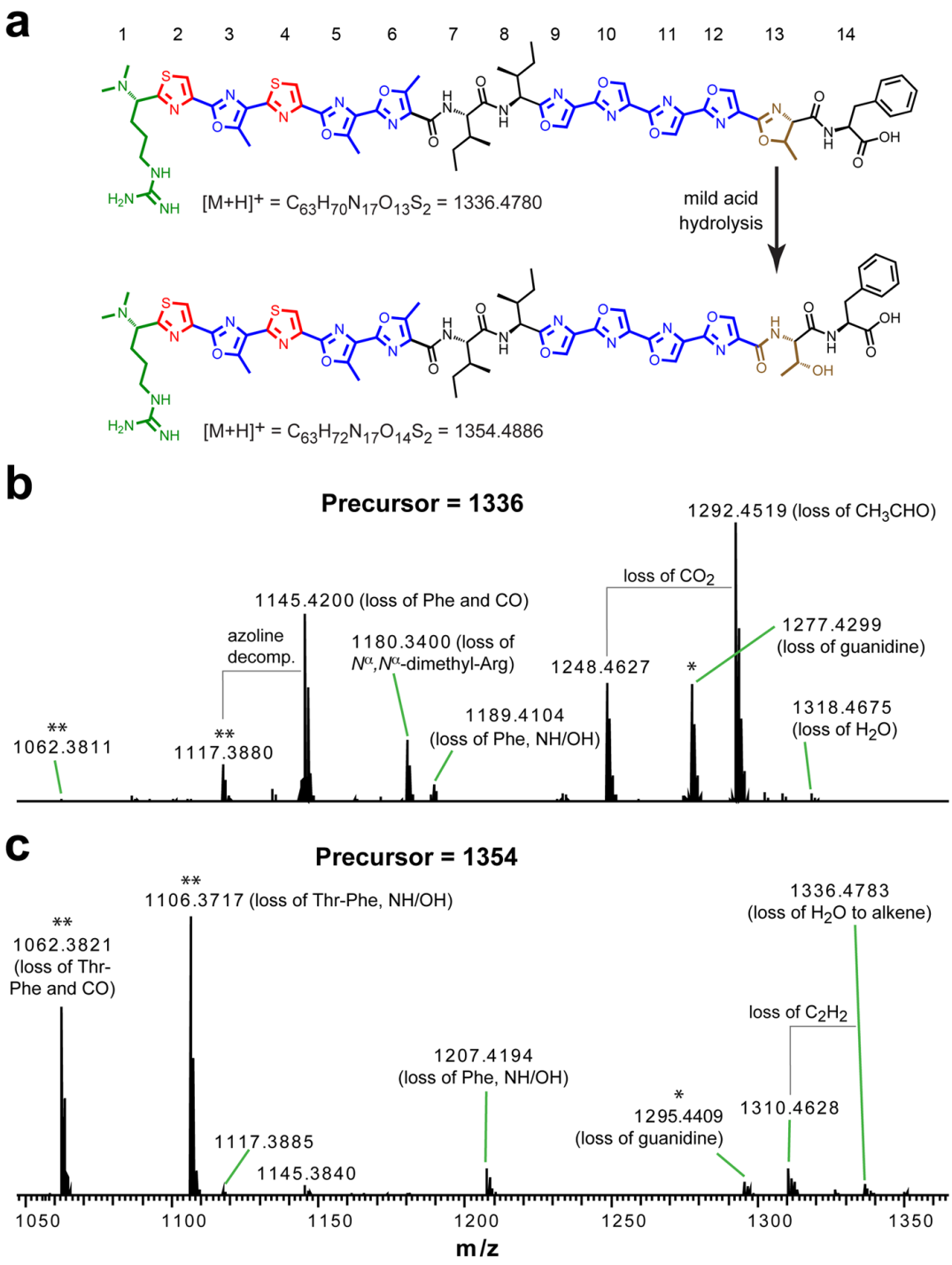

Figure 3.1 (continued)| Mass spectrometry-based structural elucidation of PZN. (a) After biosynthetic processing, the chemical structure of PZN features N^{α},N^{α}-dimethylArg (green), two thiazoles (red), seven (methyl)oxazoles (blue), and one methyloxazoline (brown). The numbering scheme used for each original residue is given at the top of the figure. After treatment with mild acid, azolines undergo hydrolytic ring opening to the original amino acid (in this case, Thr). (b) CID spectrum of the singly charged PZN ion (*m/z* 1336) acquired by LTQ-FT-MS. (c) Same as (b) except the parental ion analyzed was hydrolyzed PZN (*m/z* 1354). *Denotes ions resulting from the loss of guanidine localize the site of dimethylation to the α-amine of Arg. Localization to Arg is further supported by loss of N^{α},N^{α}-dimethylArg (*m/z* 1180). **Denotes ions indicating that the sole azoline moiety of PZN is derived from the most C-terminal Thr residue. All masses are given in Da and represent the singly-charged ion. For proposed structures of the daughter ions, see Fig 3.4 and 3.5.

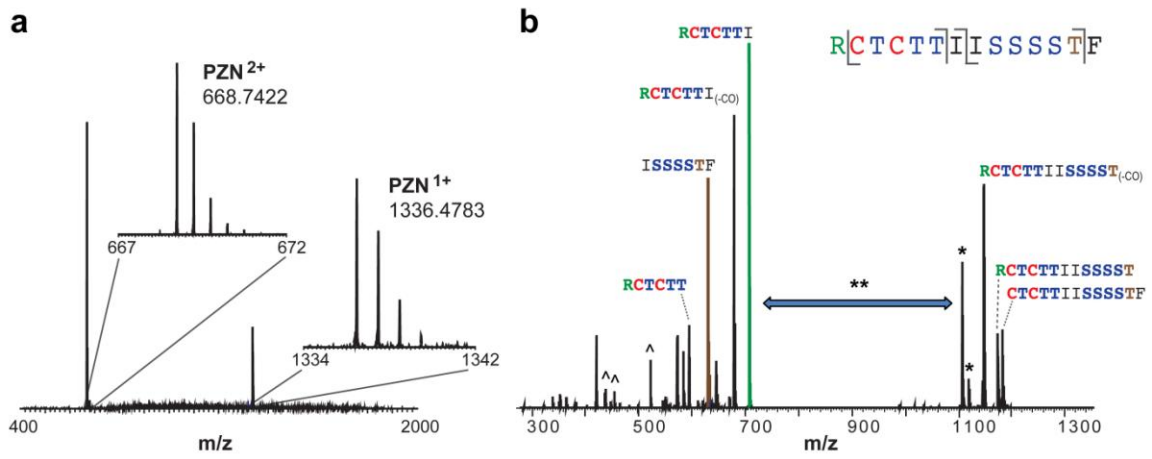

Figure 3.2 | FTICR-MS of PZN (*m/z* 1336, broadband and CID spectrum of 2+ charge state). (a) Broadband spectrum of HPLC-purified PZN on a linear ion trap MS (11 Tesla LTQ-FT). Visible are the singly and doubly charged positive ions of PZN. Due to the high mass accuracy of FT-MS (<5 ppm error) and the known sequence of the precursor peptide (Lee *et al.*, 2008; Scholz *et al.*, 2011), the molecular formula of PZN was deduced from this mass measurement. This formula required that 9 out of the 10 heterocyclizable residues were converted to the azole heterocycle and the remaining residue was left at the azoline oxidation state. Also, this formula required two methylation events (consistent with earlier deletion studies) and leader peptide cleavage after Ala-Ala (see Figure 3.18b). (b) Collision induced dissociation (CID) spectrum of *m/z* 668.7 (PZN^{2+}). The fragmentation pattern of PZN in the doubly charged state is markedly different than that of the singly charged species shown in Figure 3.1b of the main text. The amino acid sequence for the PZN precursor peptide from *B. methylotrophicus* FZB42 (BamA) is color-coded by posttranslational modification as follows: N^{α},N^{α}-dimethylarginine (green), thiazoles (red), methyloxazoles and oxazoles (blue), and methyloxazoline (brown). Identified fragment ions are also plotted onto the BamA precursor sequence. The most diagnostic peaks for localizing posttranslational modifications resulted from Ile-Ile cleavage (green and brown mass peaks). These ions demonstrate that both methylation events are on the N-terminal fragment and that the sole azoline moiety is on the C-terminal fragment. *****Fragment ions with the azoline as the most C-terminal moiety spontaneously decompose, supporting the assignment of the C-terminal Thr as being converted to methyloxazoline in PZN (assigned in Figure 3.4). Under the CID conditions employed, most peptides will fragment at the amide bond. The first step in TOMM biosynthesis, cyclodehydration, removes an amide bond from the peptide backbone. ******Contiguous heterocycles thus preclude the formation of a complete series of y^+ and b^+ ions and results in a CID spectrum that is featureless from *m/z* ~710-1100. One non-amide cleavage is noted between arginine and cysteine (highest mass ion in the spectrum), which permits the methyl groups to both be localized to arginine. ^Internal fragments (assigned in Figure 3.4).

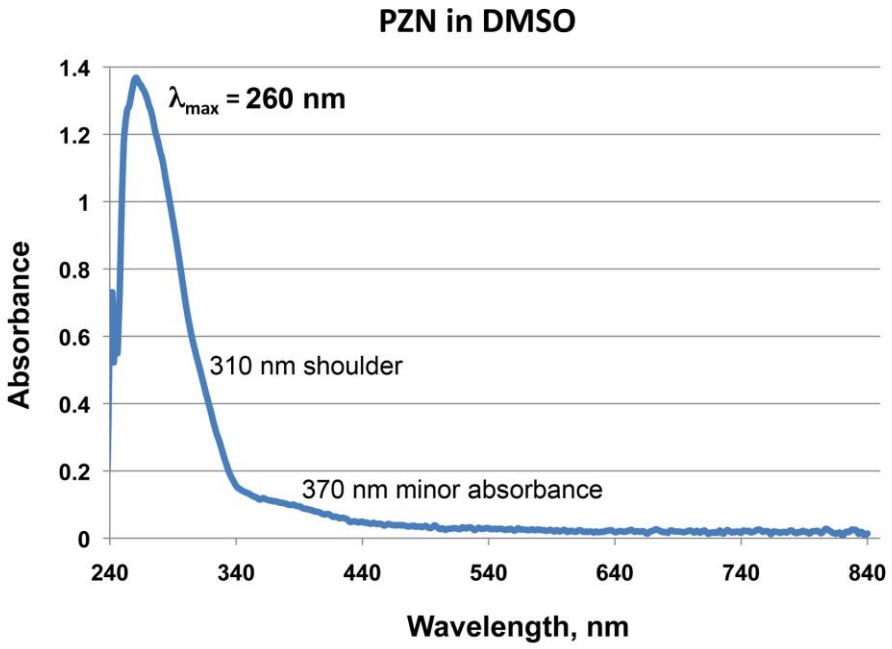

Figure 3.3 | UV-Vis spectrum of HPLC-purified PZN in DMSO acquired on a Nanodrop 2000. The instrument was blanked on DMSO, which has a UV cut-off of approximately 245 nm. The extinction coefficient for PZN in DMSO is ε_{260} = 560 $M^{-1}cm^{-1}$. The λ_{max} in 80% acetonitrile/water is 266 nm.

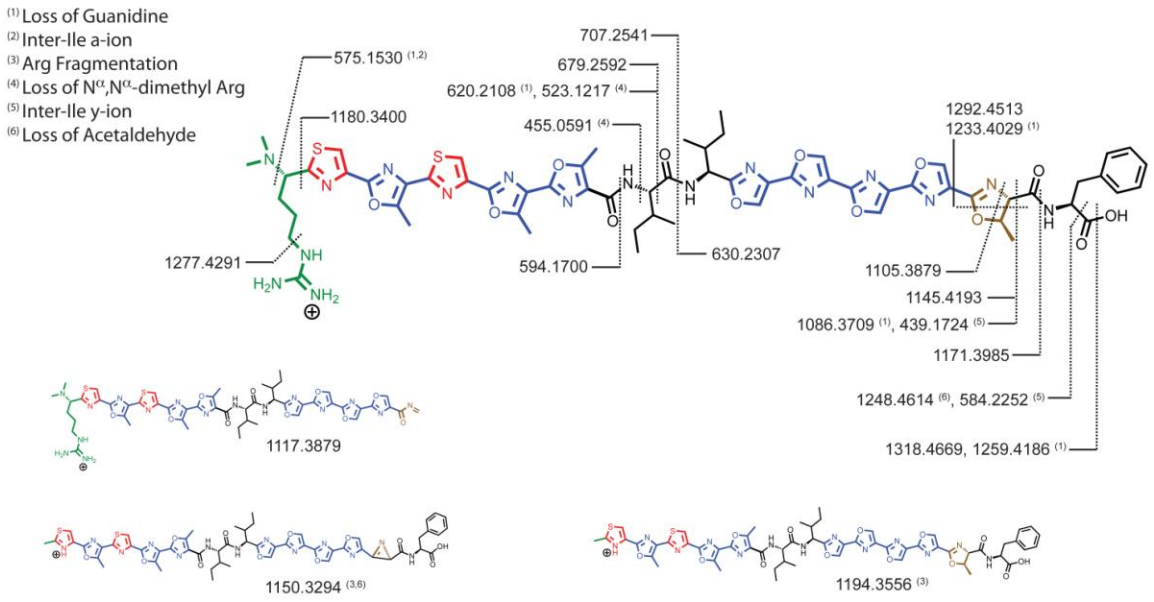

Figure 3.4 | Observed fragments during MS/MS of PZN (*m/z* 1336). Cleavage sites are shown with their corresponding theoretical monoisotopic fragment masses. Some of the observed fragments are derived from multiple bond cleavages, denoted by superscripts (these are not intended to suggest a pathway of fragmentation). In the lower part of the figure, structures with more complex fragmentation pathways are shown with their corresponding masses. The *m/z* 1277 structure permits the localization of both methyl groups to the N-terminus of PZN. The *m/z* 1145 structure results from the loss of the C-terminal Phe residue and CO. In conjunction with selective hydrolysis studies, *m/z* 1145 and the subsequent azoline decomposition ions (1117 and 1105) localize the sole azoline as the C-terminal Thr residue. Further, we note many examples of neutral loss of acetaldehyde (C_2H_4O, exact mass = 44.0262; not to be confused with loss of CO_2, exact mass = 43.9898; >800 ppm difference). See the main text for an explanation of the formation of these ions.

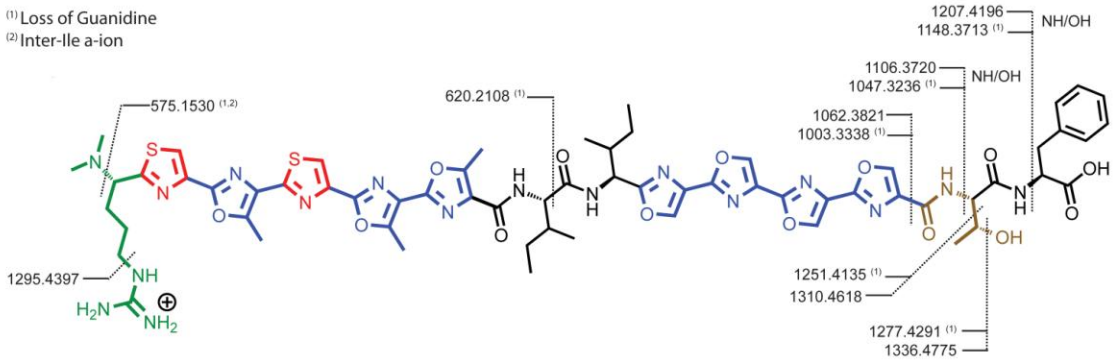

Figure 3.5 | Observed fragments during MS/MS of hydrolyzed PZN (*m/z* 1354). Unlike their aromatic azole counterparts, azoline heterocycles are hydrolytically unstable in mild acid and mild base (Frump, 1971). Selective acidic hydrolysis of PZN was performed to convert the sole azoline heterocycle back to the original amino acid. This reinstates an amide bond that can be located by subsequent MS^n analysis. Observed cleavage sites are shown with their corresponding theoretical monoisotopic fragment masses. Some of the observed fragments are derived from multiple bond cleavages, denoted by superscripts (these are not intended to suggest multiple fragmentation events or a pathway of fragmentation). Note that upon methyloxazoline hydrolysis to threonine, in no cases can neutral loss of acetaldehyde be found. This implies that loss of acetaldehyde (formation of azirine) is specific to methyloxazolines under the CID conditions we employed. Note that loss of C_2H_4O is possible from hydrolyzed (Thr-containing) PZN, but only via dehydration and subsequent loss of acetylene. Other fragment ions of interest in this map confirm the site of dimethylation to be the N-terminal amine.

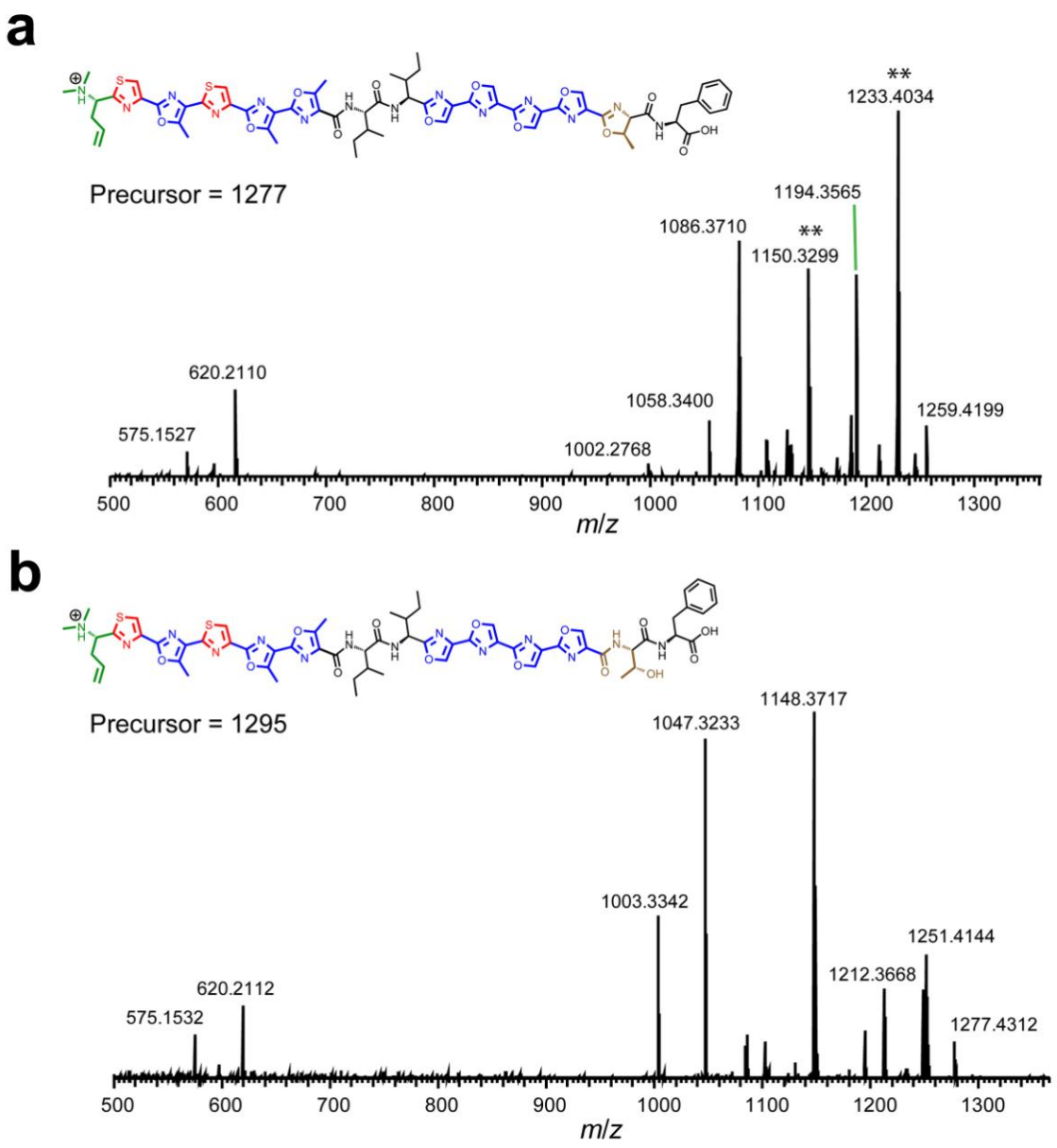

Figure 3.6 | CID spectra for deguanidinated PZN (*m/z* 1277) and deguanidinated hydrolyzed PZN (*m/z* 1295). MS^3 collision induced dissociation (CID) spectra for (a) deguanidinated PZN (*m/z* 1277) and (b) deguanidinated hydrolyzed PZN (*m/z* 1295). **Indicates loss of acetaldehyde (44.0262 Da) from methyloxazoline (1277 – 44 = 1233; 1194 – 44 = 1150). Note that this is only possible in (a) where an intact heterocycle is found. The ions at m/z 575, 1150, and 1194 demonstrate that the Arg was dimethylated on the amino terminus. Structural assignments are given for the fragments of deguanidinated PZN and deguanidinated hydrolyzed PZN in Figure 3.4 and 3.5, respectively.

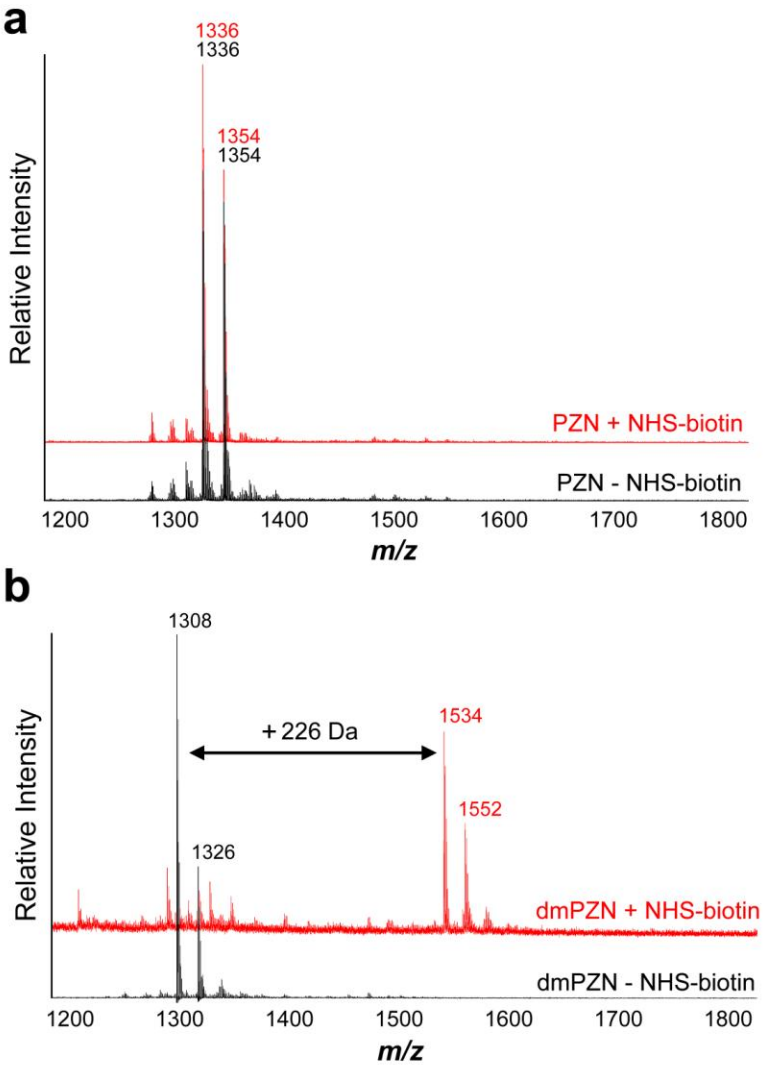

Figure 3.7 | N-terminal labeling of PZN and desmethylPZN using NHS-biotin. MALDI-TOF-MS results of NHS-biotin labeling for (a) PZN (*m/z* 1336) and hydrolyzed PZN (*m/z* 1354) and (b) desmethylPZN (*m/z* 1308) and hydrolyzed desmethylPZN (*m/z* 1326). Abbreviation: desmethylPZN, dmPZN. Red traces are samples that included the NHS-biotin reagent while black traces are from control reactions that lacked NHS-biotin. Labeling was only observed with desmethylPZN, as indicated by the new species at *m/z* 1534 and 1552. Addition of biotin gives a net mass increase of 226 Da ($C_{10}H_{14}N_2O_2S$). Specific labeling reactions are given in the methods section.

Table 3.1 | Complilation of NMR results. Abbreviations: Tz, thiazole; Oz, oxazole; Ozn, oxazoline

Amino acid	Position	δ_H (J in Hz)	^{1}H-^{1}H-gCOSY	^{1}H-^{1}H-TOCSY	^{1}H-^{13}C-gHMBC
Arg[1]	α	3.93; t (6.2)		1.53, 1.85, 1.96,	
	β	1.52; m		3.93, 1.85, 1.98	
	γ	0.87, 1.23; m			24.4, 36.8
	δ	1.86, 1.98; m		3.93	
	ε	n.d.			
	η1, η2	7.63, 7.72; m			
	N,N-dimet	2.26, s			65.6, 41.4
Tz[2]	5	8.41; s			
Me-Oz[3]	5-Met	2.81; s			147.2
Tz[4]	5	8.45; s			
Me-Oz[5]	5-Met	2.74; s			150.5
Me-Oz[6]	5-Met	2.63; s			152.3
Ile[7]	NH	7.88; s (10.2)	4.45	4.44, 0.86, 1.92	
	α	4.45; t (8.4)	1.93	7.88, 1.92, 0.86	
	β	1.93; m	4.45, 0.89	7.88, 4.45, 0.86, 0.81	
	γ^1	1.00; b			178.8
	γ^2	0.87; m	1.93	7.88, 1.93, 4.44	36.8, 56.7
	δ	0.81; m		1.93	22.2
Ile[8]	NH	8.78; d (7.8)	4.9	4.90, 0.84, 2.02	
	α	4.91; t (8.1)	8.8,2.1	8.78, 2.02, 0.84	
	β	2.05; m	4.9,0.85	8.78, 4.91, 0.88, 0.84	
	γ^1	1.00; b			
	$\gamma^{2\text{-met}}$	0.84; m	2.1	8.78, 2.02, 4.90	36.8, 51.3
	δ	0.88; m		2.02	22.6
Oz[9]	5	8.94; s			
Oz[10]	5	9.06; s			
Oz[11]	5	9.08; s			
Oz[12]	5	8.80; s			
Me-Ozn[13]	4	4.22; d (7.8)	4.61	4.6, 1.43	
	5	4.60; m	4.23, 1.44	4.21, 1.43	
	5-Met	1.44; d 6.6	4.61	4.6, 4.22	74.6, 79.5
Phe[14]	NH	7.17; d (7.8)	4.14	4.13, 3.00, 2.90	
	α	4.15; m	7.17, 3.00, 2.92	7.16, 3.00, 2.90	
	β	2.92, 3.02; d (5.4)	4.14	7.17, 4.14	
	δ^1, δ^2	6.94; m	7.02	7.06	125.6
	ε^1, ε^2	7.02; m	6.94	6.98	136.2
	ζ	6.98; m			

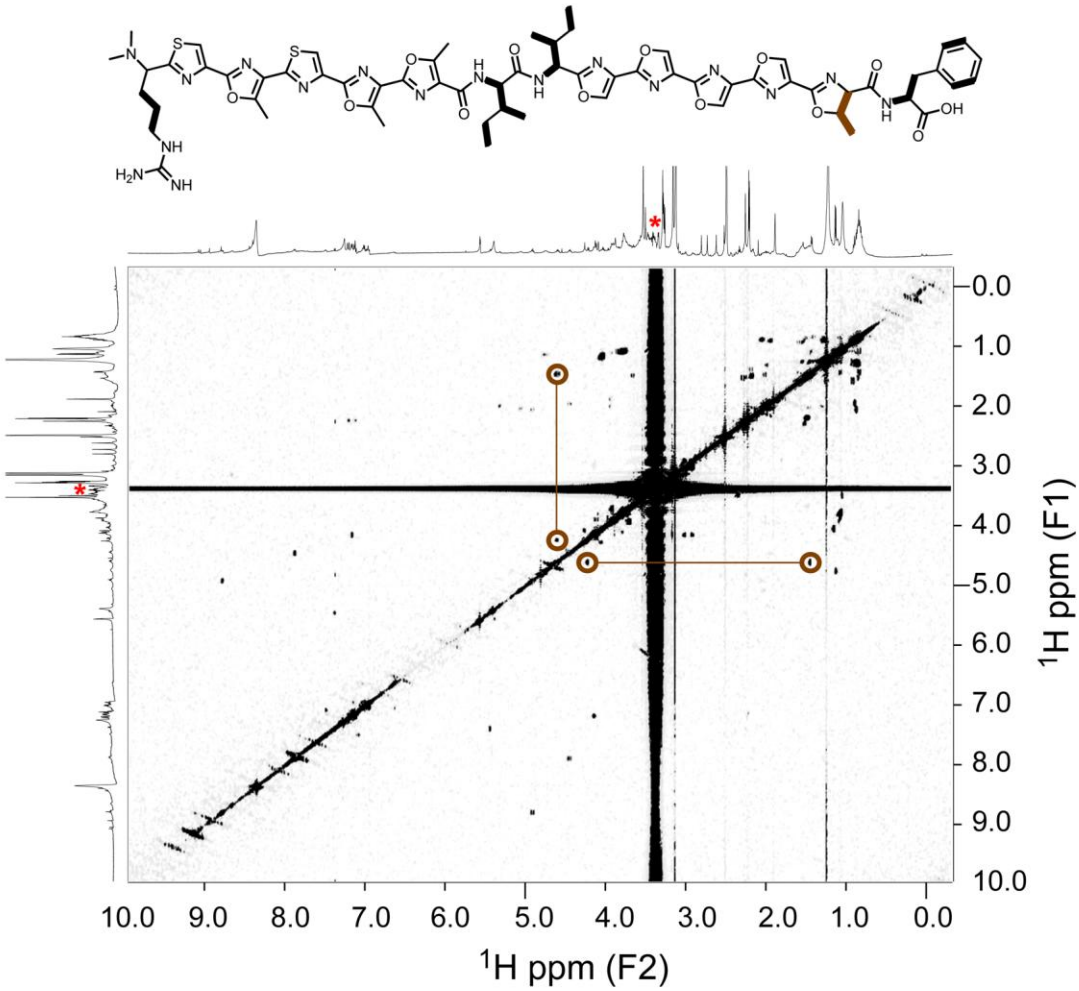

Figure 3.8 | ^{1}H-^{1}H-gCOSY of PZN. Assigned correlations are drawn on the structure of PZN as thickened bonds. The brown circles indicate correlations deriving from the methyloxazoline protons (shown as brown bonds in structure). The red asterisk indicates that in the 1D-^{1}H-spectrum, the signal from water was suppressed. This signal was not suppressed for the 2D experiment.

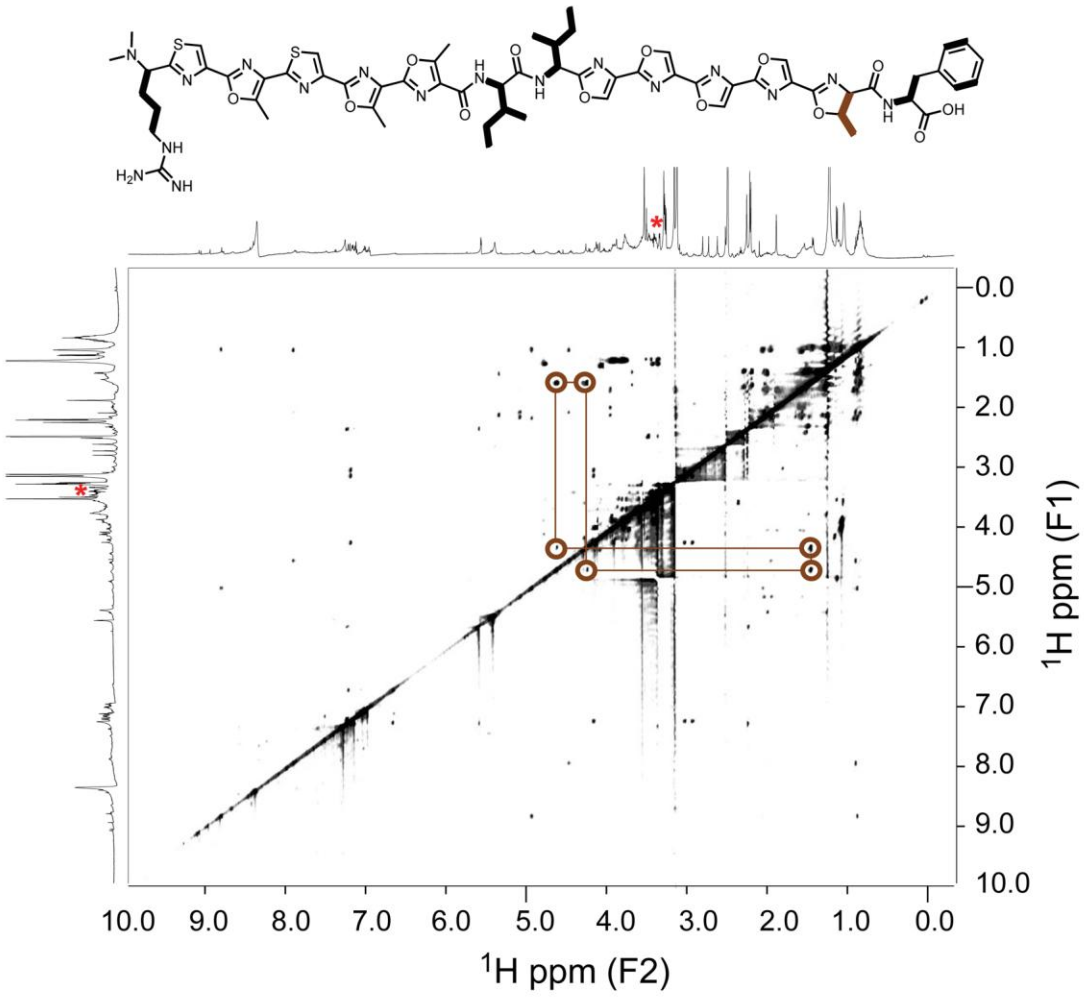

Figure 3.9 | ^{1}H-^{1}H-TOCSY of PZN. Assigned correlations are drawn on the structure of PZN as thickened bonds. The brown circles indicate correlations deriving from the methyloxazoline protons (shown as brown bonds in structure). The red asterisks on the 1D spectra indicate the signal from water suppression. This signal was also suppressed for the 2D experiment.

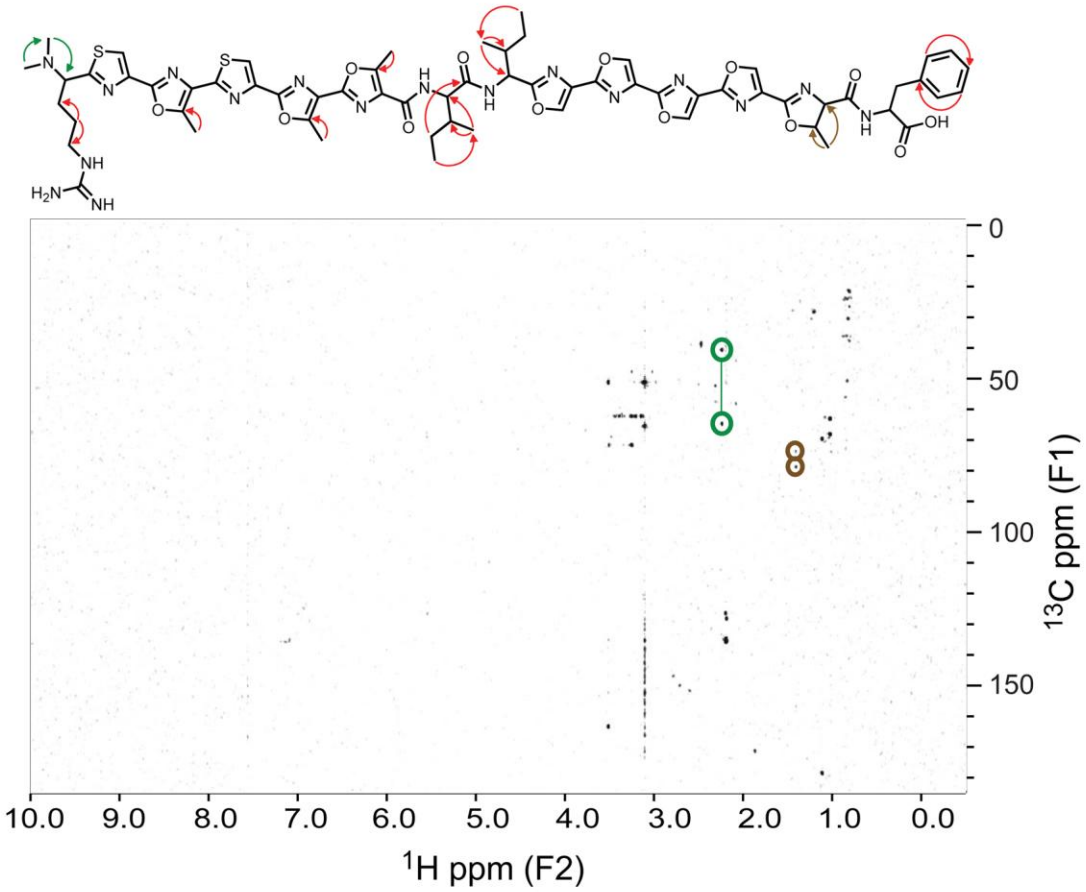

Figure 3.10 | ^{1}H-^{13}C-gHMBC of PZN. Assigned correlations are drawn on the structure of PZN as red arrows. The green arrows/circles indicate correlations that localize the posttranslational methyl groups to the N-terminus. The brown arrows/circles indicate correlations that demonstrate the azoline is methyloxazoline.

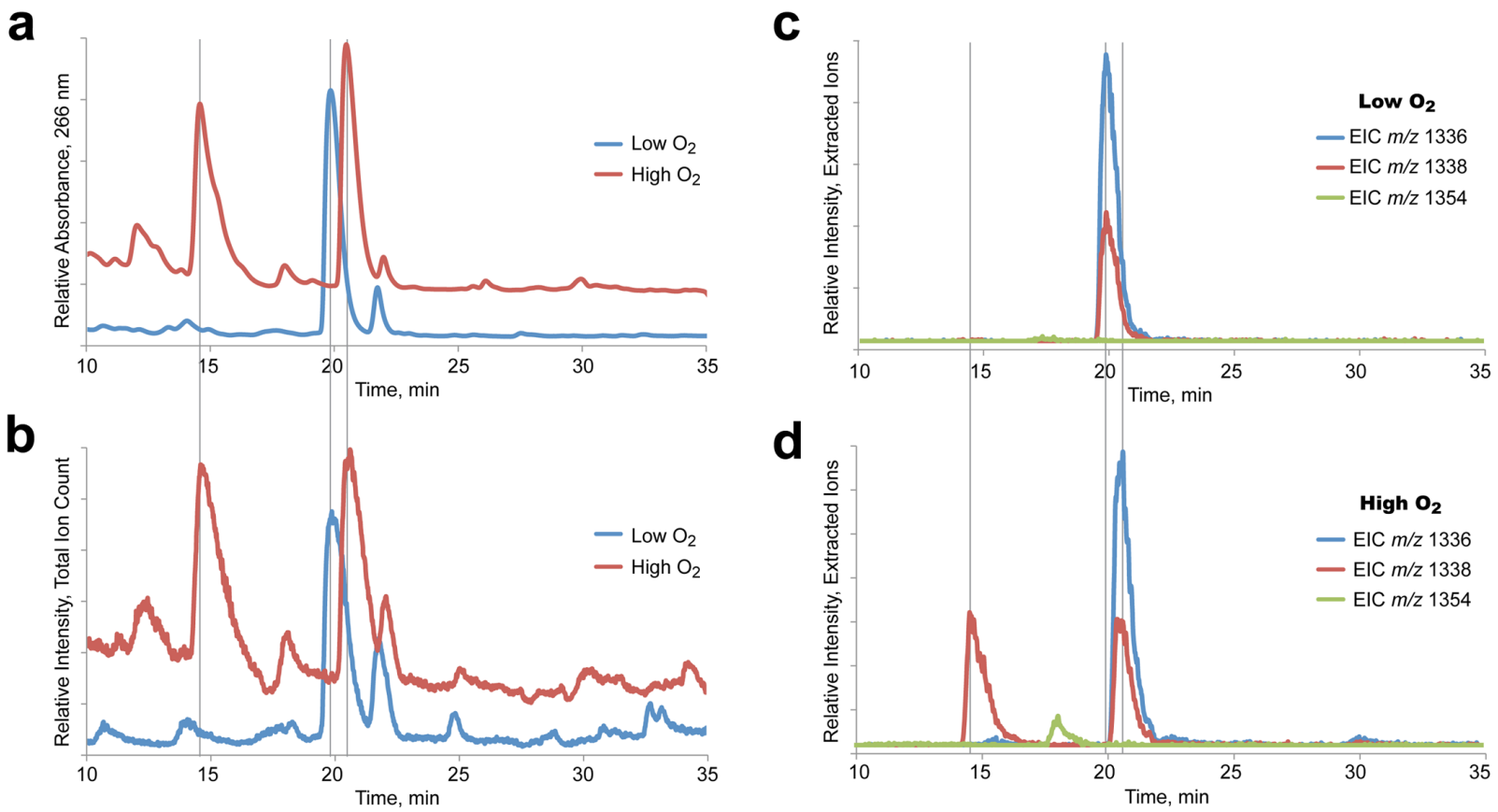

Figure 3.11 | Effect of fermentation oxygenation on PZN production. High and low oxygenation cultures were extracted and subjected to chromatography using an identical procedure. In all panels, vertical lines were drawn at 14.7, 19.9, and 20.5 min. (a) UV chromatogram (Abs 266 nm) of FZB42 strain RSpMarA2 extract from high and low oxygen fermentation. (b) Same as (a) except the trace is the total ion chromatogram (TIC). (c) Extracted ion chromatogram (EIC) of *m/z* 1336, 1338, and 1354 from a low oxygen fermentation. (d) Same as C except under high oxygenation conditions.

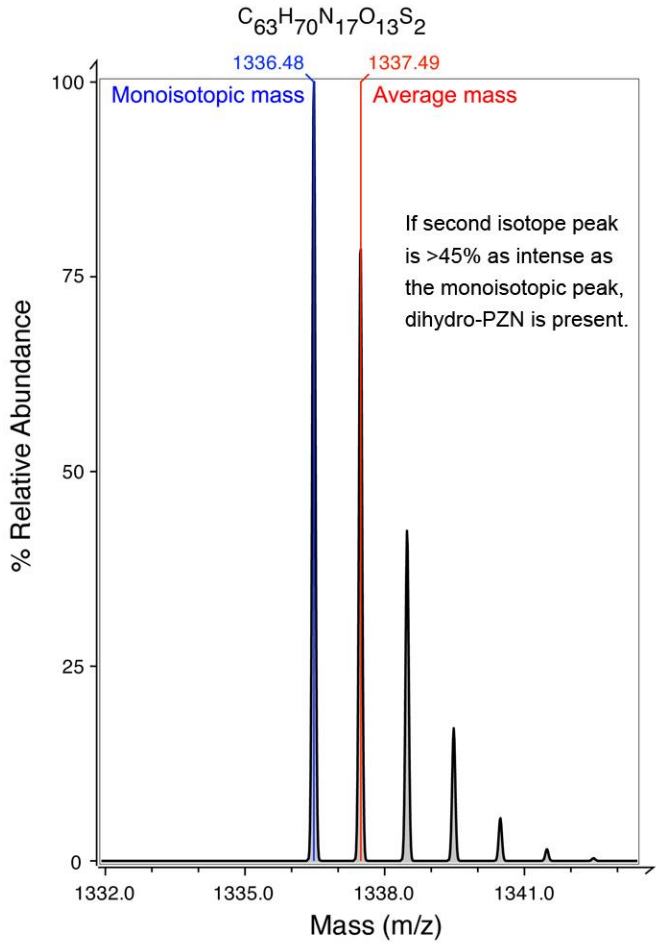

Figure 3.12 | Predicted isotope pattern for PZN (*m/z* 1336). Note that the average mass is slightly heavier than the first isotope mass. This figure was generated using iMass version 1.1 (freeware written by Urs Roethlisberger).

Figure 3.13

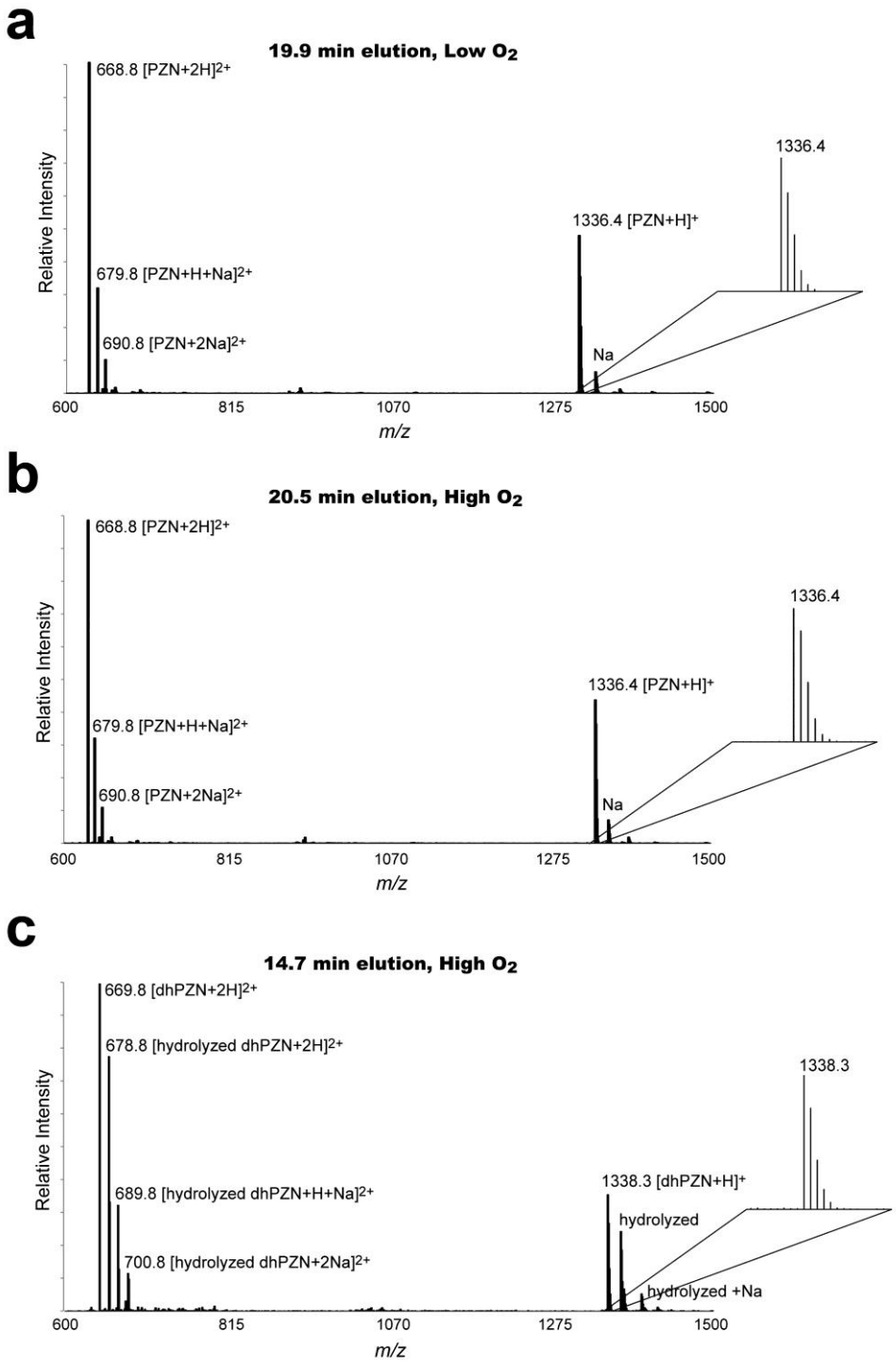
a
19.9 min elution, Low O2
668.8 [PZN+2H]2+
679.8 [PZN+H+Na]2+
690.8 [PZN+2Na]2+
1336.4 [PZN+H]+
1336.4
Na
Relative Intensity
600
815
1070
1275
1500
m/z
b
20.5 min elution, High O2
668.8 [PZN+2H]2+
679.8 [PZN+H+Na]2+
690.8 [PZN+2Na]2+
1336.4 [PZN+H]+
1336.4
Na
Relative Intensity
600
815
1070
1275
1500
m/z
c
14.7 min elution, High O2
669.8 [dhPZN+2H]2+
678.8 [hydrolyzed dhPZN+2H]2+
689.8 [hydrolyzed dhPZN+H+Na]2+
700.8 [hydrolyzed dhPZN+2Na]2+
1338.3 [dhPZN+H]+
1338.3
hydrolyzed
hydrolyzed +Na
Relative Intensity
600
815
1070
1275
1500
m/z

Figure 3.13 (continued) | Effect of oxygen levels during fermentation on the production of PZN. ESI-MS at selected time points from LCMS analysis (UV, TIC, EIC) shown in Figure 3.11. (a) Under low oxygen conditions, PZN (*m/z* 1336) is the only species present in the 19.9 min elution. (b) Under an oxygen saturated fermentation, PZN is found in the 20.5 min elution. (c) As expected from the EIC's shown in Figure 3.11, high oxygen fermentation yields an additional compound eluting at 14.7 min consistent with dihydroPZN (dhPZN, *m/z* 1338). The earlier elution of dhPZN relative to PZN is in agreement with azolines being more hydrophilic and basic than azoles (azoles are not protonated with 0.1% formic acid). Right insets for all panels show a zoomed in spectrum to highlight the isotopic pattern of the singly charged PZN species.

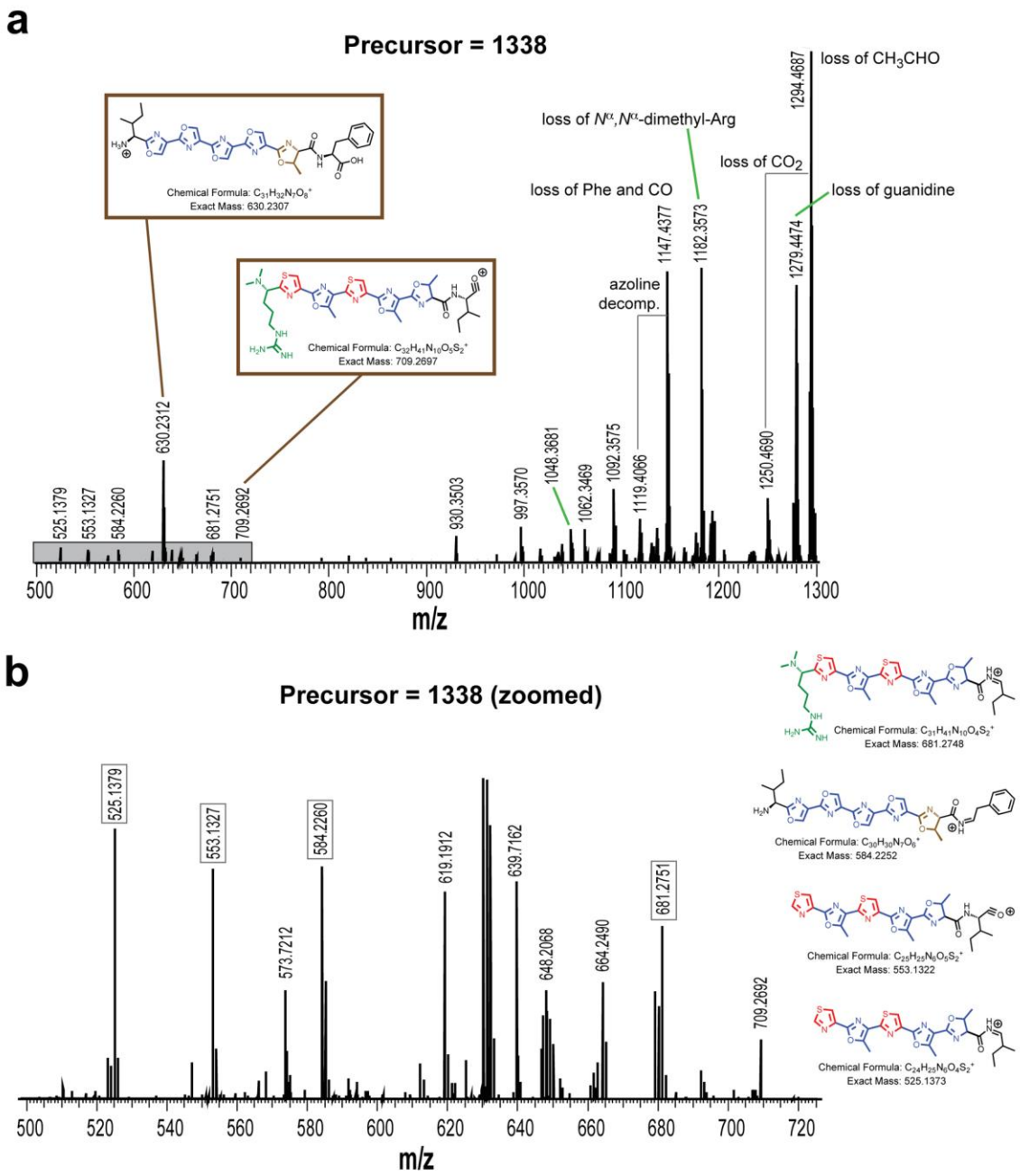

Figure 3.14 | Partial localization of the second azoline in dihydroPZN (dhPZN). (a) CID spectrum of dhPZN (*m/z* 1338) acquired using LTQ-FT-MS. The heavier fragment ions are identical to those shown in Figure 3.1, with the exception of each fragment being 2 Da heavier. The gray box depicts a zoomed in region shown in (b). Brown boxes highlight two ions demonstrating that an azoline heterocycle exists on each side of the Ile-Ile. The location of the C-terminal azoline was localized to the most C-terminal Thr. The location of the N-terminal azoline is likely to be the Thr adjacent to Ile due to similar sterics/electronics. However, the precise position cannot be concluded from this spectrum. (b) Zoomed in region from (a) (gray box). Diagnostic ions are boxed in gray and their respective (predicted) structures drawn in the right margin.

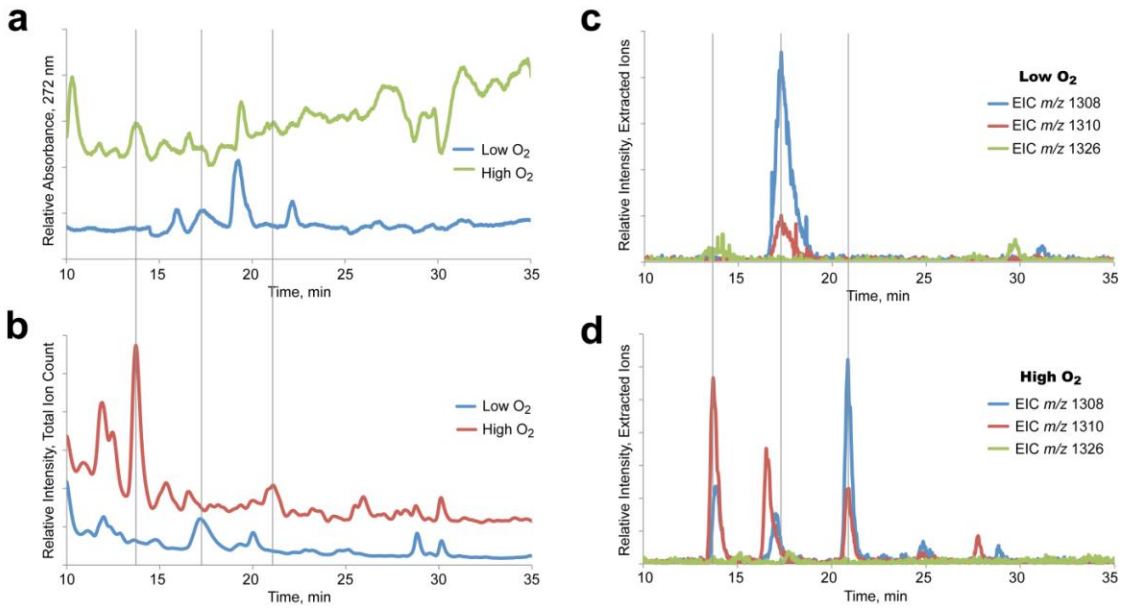

Figure 3.15 | Effect of oxygen levels during fermentation on the production of desmethylPZN. In each case presented, the low oxygen samples were prepared by shake flask fermentation of *B. methylotrophicus* strain RS33 (*pznL* deletion, desmethylPZN producer) in 2 L of LB in 6 L flasks. High oxygen samples were prepared using a biofermentor with 5 L/min air input. Both cultures were grown for 24 h at 37 °C. All samples were extracted in an identical fashion and subjected to identical chromatographic procedures (analytical C_{18}-HPLC) as described in the methods. In all panels, vertical lines are drawn at 14, 17, and 21 min. (a) UV chromatogram (Abs 272 nm) of RS33 extract from high and low oxygen fermentation. This trace shows that more chromophores absorbing light at 272 nm are produced under high oxygen conditions. (b) Same as (a) except the trace is the total ion chromatogram (TIC). (c) Extracted ion chromatogram (EIC) of *m/z* 1308, 1310, and 1326 from low oxygen fermentation. Under these conditions, the majority species is desmethylPZN (1308) with trace amounts of hydrolyzed desmethylPZN (1326). The 1310 trace that appears to "coelute" with 1308 at 17 min is the actually the second isotope peak of 1308, not dihydrodesmethylPZN (see Figure 3.12). (d) Same as C except under high oxygenation conditions. The peaks at 14 and 16 min contain primarily dihydrodesmethylPZN (*m/z* 1310) while the peaks at 17 and 21 min contain primarily desmethylPZN (*m/z* 1308). The species eluting at 14 and 16 min are suspected to be regioisomers, as are the species eluting at 17 and 21 min. ESI-MS at these selected time points are shown in Figure 3.16.

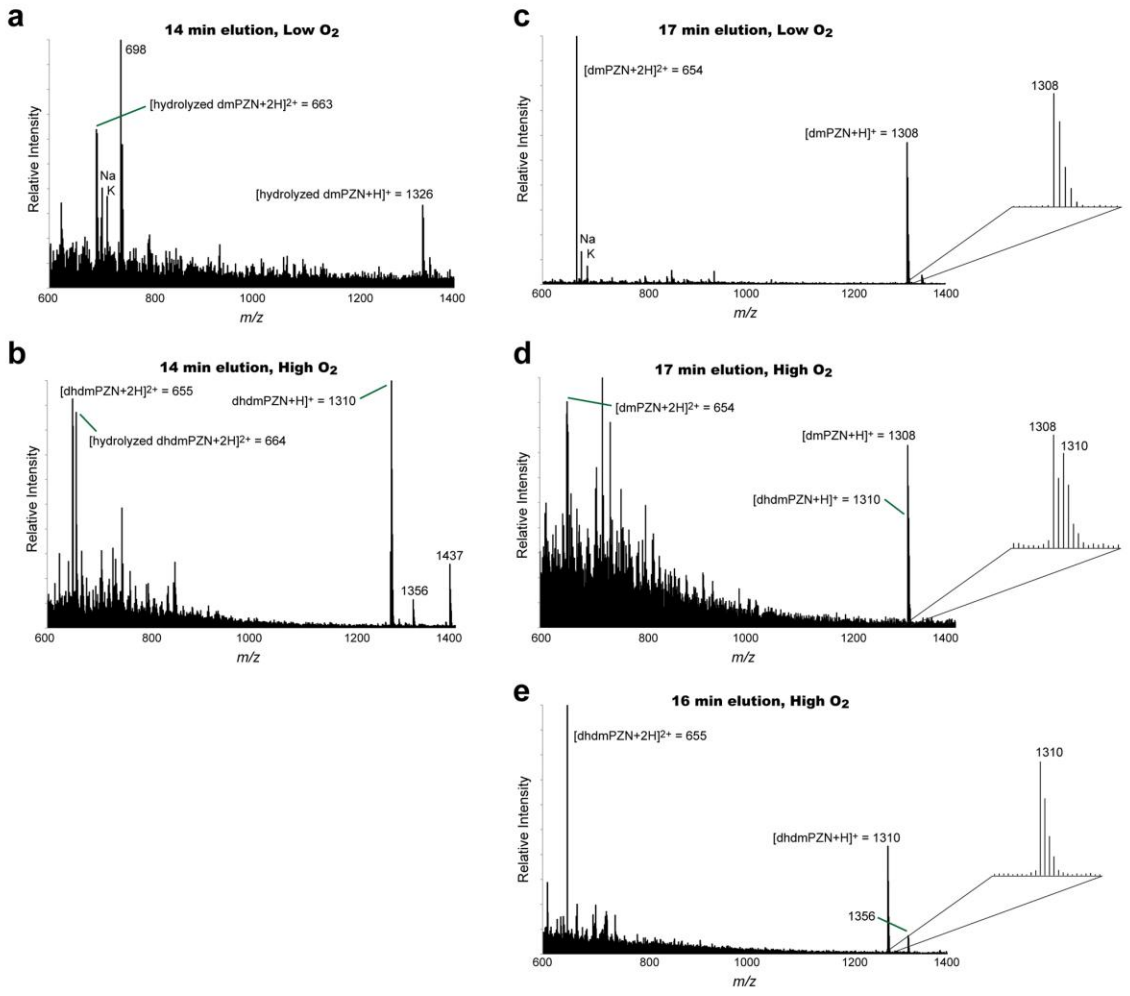

Figure 3.16 | Effect of oxygen levels during fermentation on the production of desmethylPZN. ESI-MS at selected time points from LCMS analysis (UV, TIC, EIC) shown in Figure 3.15. (a) Under low oxygen conditions, hydrolyzed desmethylPZN (*m/z* 1326) is visible in the 14 min elution. (b) As expected from the EIC's shown in Figure 3.15, the 14 min elution is dominated by dihydrodesmethylPZN (*m/z* 1310) at the 14 min elution. (c) Low oxygen fermentation and an elution of 17 min yields exclusively desmethylPZN (*m/z* 1308). As indicated by the ion purity and signal to noise ratio in this spectrum, relative to the other panels, desmethylPZN was a majority product and easily separated under the conditions employed. (d) Same as C but high oxygen conditions led to the production of a mixture of desmethylPZN and dihydrodesmethylPZN (ratio ~60:40, respectively). (e) At 16 min under high oxygen conditions, 1310 is the majority species produced, consistent with azolines being more hydrophilic than azoles. Right insets for panels c-e show a zoomed in spectrum to highlight the isotopic pattern of the singly charged desmethylPZN species. The ratio of intensities given in Figure 3.12 applies.

a

Organism	MIC (μg/mL)	PZN variant	*B. anthracis* MIC (μg/mL)
B. anthracis	2–4	desmethylPZN	>128
E. faecalis (VRE)	>128	dihydroPZN*	>128
L. monocytogenes	>128	hydrolyzed PZN	32
S. aureus (MRSA)	>128		
S. pyogenes	128		

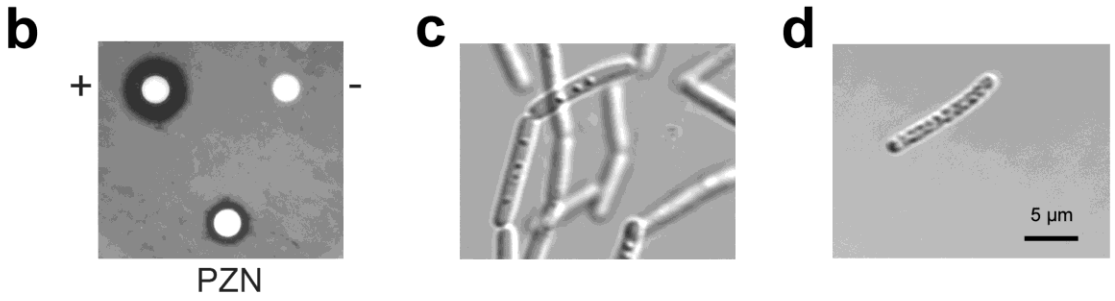

Figure 3.17 | Assessment of PZN antibiotic activity. (a) The minimum inhibitory concentration (MIC) of HPLC-purified PZN was measured against a panel of Gram-positive human pathogens. Values reported were the concentration of PZN that inhibited 99% of the bacteria growth in a microbroth dilution bioassay. *Due to separation difficulties, dihydroPZN was supplied as a 1:2:2 mixture of non-, mono-, and dihydrolyzed species (*m/z* 1338, 1356, 1374). (b) PZN activity in an agar disk diffusion bioassay against *B. anthracis* Sterne. Upper left disk, 8 μg kanamycin control (positive); upper right, solvent control (negative); lower disk, 100 μg PZN (200 μg gave a similar inhibition diameter). (c) Visual appearance of live *B. anthracis* Sterne treated with a solvent control by DIC microscopy. (d) Same as (c) except cells were treated with 4 μg mL^{-1} PZN. Scale bar is the same for panel c.

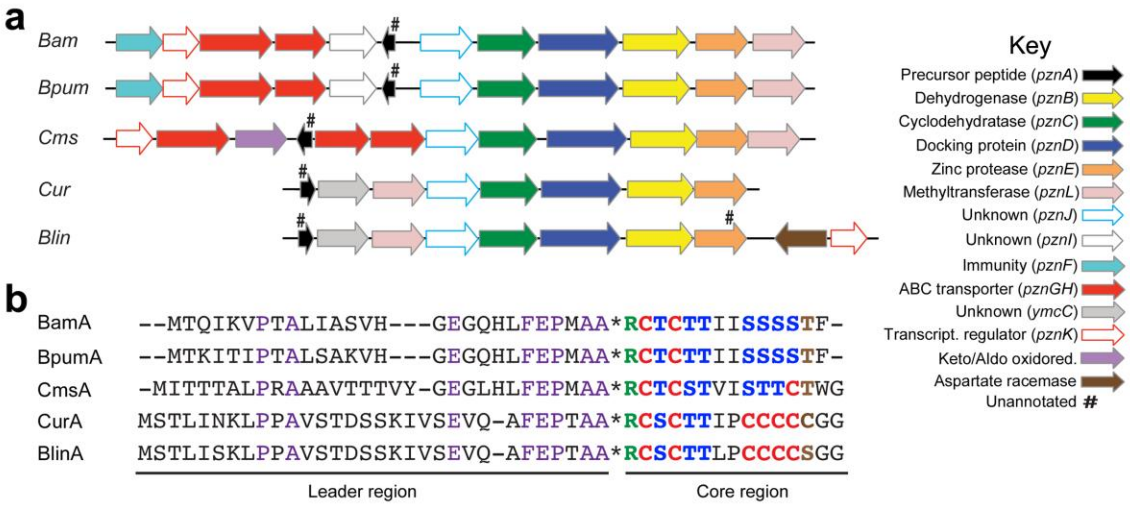

Figure 3.18 | PZN biosynthetic gene clusters. (a) Open-reading frame diagram showing the genetic organization of PZN clusters, which form a subclass of TOMMs. Gene designations and predicted functions are color coded in the provided legend. (b) PZN precursor peptide alignment. Shown in purple are conserved residues within the N-terminal leader region. *Denotes the leader peptide cleavage site, which is known for BamA and BpumA but predicted for the others. Color-coding indicates the posttranslational modifications of the BamA core region, which are extrapolated to the remaining precursor peptides: N^{α},N^{α}-dimethylarginine (green), thiazoles (red), (methyl)oxazoles (blue), and methyloxazoline (brown). Abbrev.: Bam, *Bacillus methylotrophicus* FZB42; Bpum, *Bacillus pumilus* ATCC 7061; Cms, *Clavibacter michiganensis* subsp. *sepedonicus*; Cur, *Corynebacterium urealyticum* DSM 7109; Blin, *Brevibacterium linens* BL2.

PznJ

	Bam	Bpum	Cms	Cur	Blin
Bam	100	63	26	6	10
Bpum	90.1	100	27	8	6
Cms	61.8	61.2	100	13	12
Cur	51.4	49.4	52.7	100	54
Blin	47.2	48.7	54.4	87	100

PznB

	Bam	Bpum	Cms	Cur	Blin
Bam	100	77	57	44	43
Bpum	96.3	100	57	43	42
Cms	87.5	87.1	100	43	42
Cur	78.8	81.3	77.1	100	86
Blin	77.3	78.8	76.7	98.2	100

PznC

	Bam	Bpum	Cms	Cur	Blin
Bam	100	63	41	22	25
Bpum	91.1	100	40	26	27
Cms	77	77.4	100	24	24
Cur	64	66.3	65.1	100	73
Blin	64.7	66.1	66.5	93.2	100

PznE

	Bam	Bpum	Cms	Cur	Blin
Bam	100	44	16	15	14
Bpum	78.1	100	13	13	13
Cms	54.6	56.1	100	20	18
Cur	55.5	48	50	100	52
Blin	49.5	55.9	49	83.7	100

PznD

	Bam	Bpum	Cms	Cur	Blin
Bam	100	82	57	38	38
Bpum	96.8	100	56	38	38
Cms	76	74.2	100	39	38
Cur	73	73.7	64.5	100	79
Blin	71.4	71.1	64	94.6	100

PznL

	Bam	Bpum	Cms	Cur	Blin
Bam	100	48	25	22	18
Bpum	81.6	100	25	21	18
Cms	60.3	59.2	100	20	22
Cur	55.7	54.4	54	100	53
Blin	57.4	54.4	50.5	87.6	100

Order of similarity:
PznB > PznD > PznC > PznL > PznJ > PznE

Order of identity:
PznB > PznD > PznC > PznL > PznJ > PznE

Figure 3.19 | Similarity/identity matrix of related (PZN-producing) biosynthetic proteins. Shown in yellow are amino acid identity scores obtained by pairwise alignment using ClustalW2, which includes the standard parameters for gap penalties. In blue are the corresponding amino acid percent similarity values, obtained by recording the ratio of similar amino acids to the full protein sequence after alignment (no gap penalties). PznJ, required biosynthetic protein of unknown function; PznCD, cyclodehydratase; PznB, FMN-dependent dehydrogenase; PznE, suspected leader peptidase; PznL, SAM-dependent methyltransferase. Abbreviations used are derived from the genus and species name for each organism. Bam, *Bacillus methylotrophicus* FZB42; Bpum, *Bacillus pumilus* ATCC 7061; Cms, *Clavibacter michiganensis* subsp. *sepedonicus*; Cur, *Corynebacterium urealyticum* DSM 7109; Blin, *Brevibacterium linens* BL2. Bam and Bpum are Firmicutes, while the other three species are Actinobacteria.

Figure 3.20

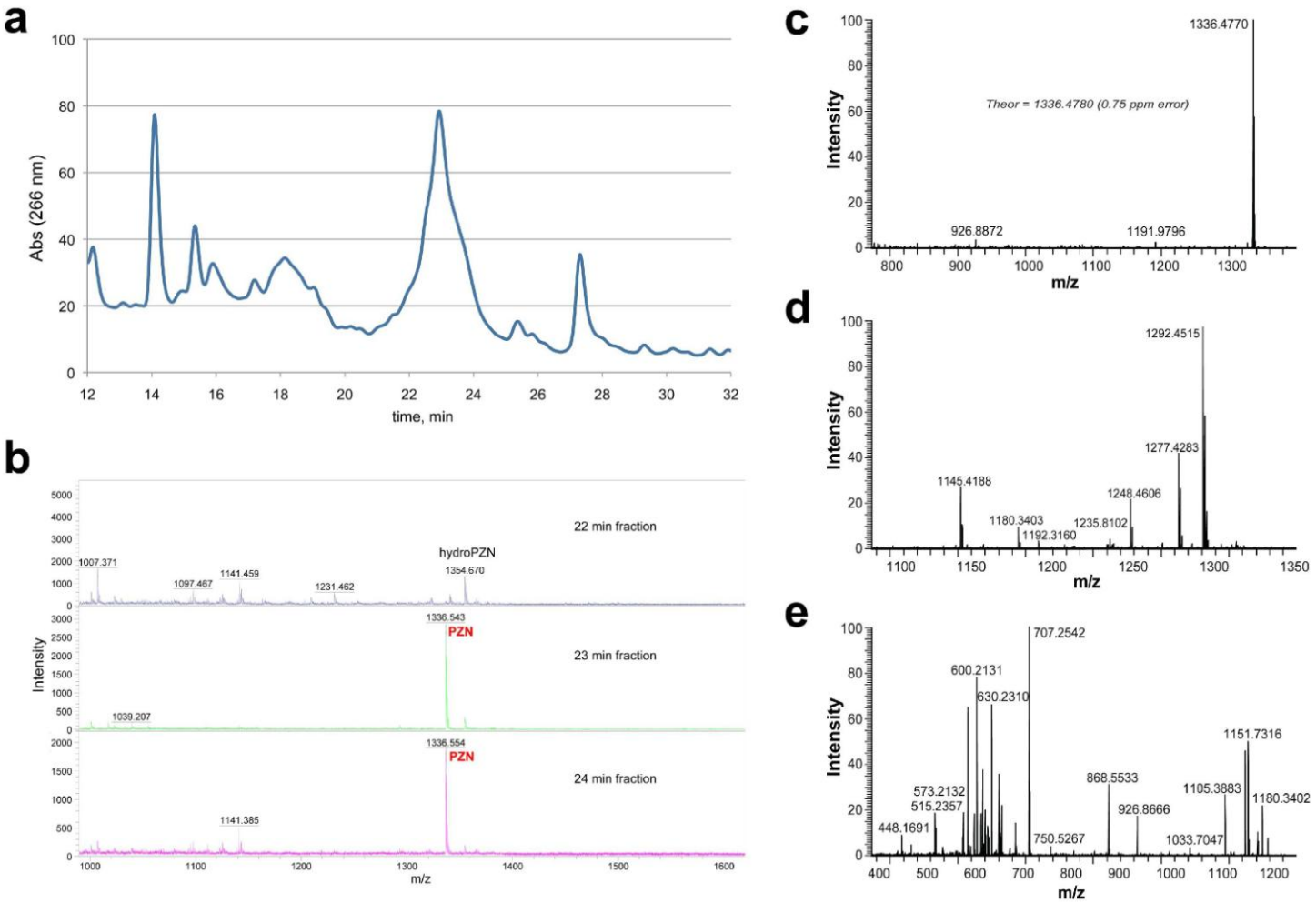
a
Abs (266 nm)
time, min
b
22 min fraction
hydroPZN
1007.371
1097.467
1141.459
1231.462
1354.670
23 min fraction
1336.543
PZN
1039.207
24 min fraction
1336.554
PZN
1141.385
Intensity
m/z
c
1336.4770
Theor = 1336.4780 (0.75 ppm error)
926.8872
1191.9796
Intensity
m/z
d
1292.4515
1277.4283
1145.4188
1248.4606
1180.3403
1235.8102
1192.3160
Intensity
m/z
e
707.2542
600.2131
630.2310
1151.7316
868.5533
573.2132
515.2357
1105.3883
1180.3402
926.8666
448.1691
750.5267
1033.7047
Intensity
m/z

Figure 3.20 (continued) | Demonstration of PZN production from *Bacillus pumilus* ATCC 7061. Cells were grown in an identical fashion to *B. methylotrophicus*. (a) The cell surface metabolites were extracted with methanol, dried, concentrated, and separated on a preparative C_{18}-HPLC column with UV monitoring at 266 nm (λ_{max} for PZN). (b) The 22-min (top), 23-min (middle), and 24-min (bottom) fractions from HPLC purification were concentrated and spotted on to the MALDI target with sinapic acid. In the earliest fraction, m/z 1354 (hydrolyzed PZN is visible). In the latter two fractions, m/z 1336 (PZN) is readily identified, which was pooled for further analysis. (c) HPLC purified PZN from *B. pumilus* was subjected to high-resolution MS (LTQ-FT-MS), which verified the molecular formula to be consistent with PZN within the mass accuracy of the instrument (<5 ppm). (d) CID spectrum obtained upon isolation of the singly charged (*m/z* 1336) precursor ion. This data is analogous to Figure 3.1b (PZN from *B. amylo.* RSpMarA2). Figure 3.1b. (e) CID spectrum obtained upon isolation of the doubly charged (*m/z* 668) precursor ion. This data is analogous to Figure 3.2b (PZN from *B. amylo.* RSpMarA2). However, different instrumental settings had to be employed to visualize the PZN ions, which were less abundant than from the *B. amylo*. overproducer (RSpMarA2) and required summing over many scans. An unidentified contaminant and instrumental noise account for the ions between *m/z* 750-1100.

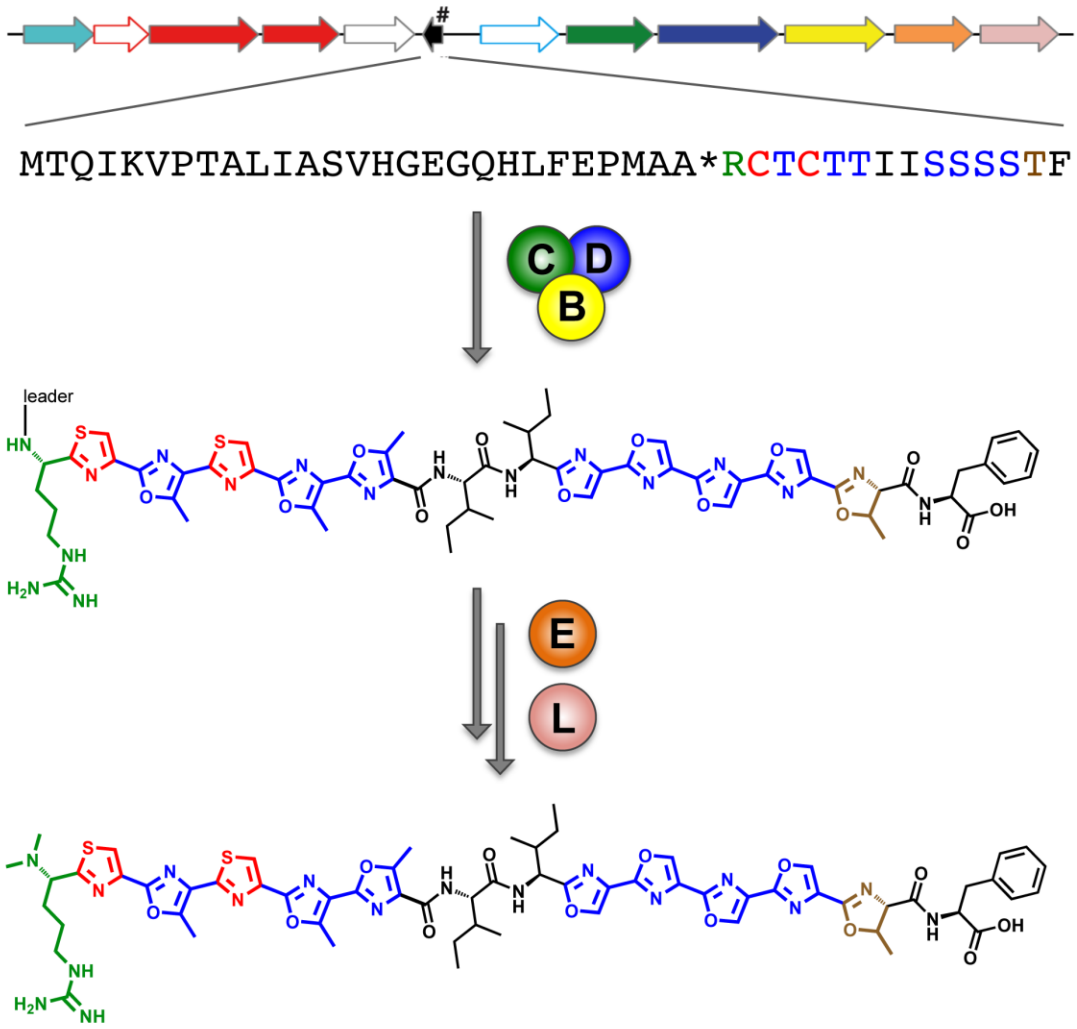

Figure 3.21 | Plantazolicin (PZN) constitutes an entirely new class of highly discriminating antibiotic. PZN produced by *Bacillus methylotrophicus* FZB42 is biosynthesized from a 12 open reading frame biosynthetic gene cluster, which encodes a 41 amino acid precursor peptide and all necessary maturation machinery. One remarkable feature of PZN is the extensive incorporation of thiazole and (methyl)oxazol(in)e heterocycles, which are installed by PznBCD. The final processing steps are likely carried out by PznE (leader peptide cleavage) followed by PznL-dependent dimethylation of the newly formed α-amine group of arginine.

3.8 References

1. Athamna, A., Athamna, M., Abu-Rashed, N., Medlej, B., Bast, D.J., and Rubinstein, E. (2004) Selection of *Bacillus anthracis* isolates resistant to antibiotics. *J Antimicrob Chemother*: **54**, 424-428.

2. Bentley, S.D., Corton, C., Brown, S.E., Barron, A., Clark, L., Doggett, J., Harris, B., Ormond, D., Quail, M.A., May, G., *et al.* (2008) Genome of the actinomycete plant pathogen *Clavibacter michiganensis* subsp. *sepedonicus* suggests recent niche adaptation. *J Bacteriol*: **190**, 2150-2160.

3. Bryskier, A. (2002) *Bacillus anthracis* and antibacterial agents. *Clin Microbiol Infect*: **8**, 467-478.

4. Challis, G.L. (2008) Genome mining for novel natural product discovery. *J Med Chem*: **51**, 2618-2628.

5. Chen, X.H., Koumoutsi, A., Scholz, R., Eisenreich, A., Schneider, K., Heinemeyer, I., Morgenstern, B., Voss, B., Hess, W.R., Reva, O., *et al.* (2007) Comparative analysis of the complete genome sequence of the plant growth-promoting bacterium *Bacillus amyloliquefaciens* FZB42. *Nat Biotechnol*: **25**, 1007-1014.

6. Claesen, J., and Bibb, M. (2010) Genome mining and genetic analysis of cypemycin biosynthesis reveal an unusual class of posttranslationally modified peptides. *Proc Natl Acad Sci U S A*: **107**, 16297-16302.

7. Clark, G.J., Langley, D., and Bushell, M.E. (1995) Oxygen limitation can induce microbial secondary metabolite formation - investigations with miniature electrodes in shaker and bioreactor culture. *Microbiol-Uk*: **141**, 663-669.

8. Donia, M.S., Ravel, J., and Schmidt, E.W. (2008) A global assembly line for cyanobactins. *Nat Chem Biol*: **4**, 341-343.

9. Dunbar, K.L., Chekan, J.R., Cox, C.L., Burkhart, B.J., Nair, S.K., and Mitchell, D.A. (2014) Discovery of a new ATP-binding motif involved in peptidic azoline biosynthesis. *Nat Chem Biol*: **10**, 823-829.

10. Dunbar, K.L., Melby, J.O., and Mitchell, D.A. (2012) YcaO domains use ATP to activate amide backbones during peptide cyclodehydrations. *Nat Chem Biol*: **8**, 569-575.

11. Dunbar, K.L., and Mitchell, D.A. (2013) Insights into the mechanism of peptide cyclodehydrations achieved through the chemoenzymatic generation of amide derivatives. *J Am Chem Soc*: **135**, 8692-8701.

12. Dunlap, C.A., Kim, S.J., Kwon, S.W., and Rooney, A.P. (2015) Phylogenomic analysis shows that Bacillus amyloliquefaciens subsp. plantarum is a later heterotypic synonym of Bacillus methylotrophicus. *Int J Syst Evol Microbiol*: **65**, 2104-2109.

13. Frey, P.A., Hegeman, A.D., and Ruzicka, F.J. (2008) The Radical SAM superfamily. *Crit Rev Biochem Mol Biol*: **43**, 63-88.

14. Frump, J.A. (1971) Oxazolines - their preparation, reactions, and applications. *Chem Rev*: **71**, 483-505.

15. Garavelli, J.S. (2004) The RESID database of protein modifications as a resource and annotation tool. *Proteomics*: **4**, 1527-1533.

16. Giezenda, H., Heimgart, H., Jackson, B., Winkler, T., Hansen, H.J., and Schmid, H. (1973) Photoreactions .31. Photochemical cycloadditions of 3-phenyl-2h-azirines with aldehydes. *Helv Chim Acta*: **56**, 2611-2627.

17. Gross, H. (2009) Genomic mining--a concept for the discovery of new bioactive natural products. *Curr Opin Drug Discov Devel*: **12**, 207-219.

18. Haft, D.H., Basu, M.K., and Mitchell, D.A. (2010) Expansion of ribosomally produced natural products: a nitrile hydratase- and Nif11-related precursor family. *BMC Biol*: **8**, 70.

19. Kalyon, B., Helaly, S.E., Scholz, R., Nachtigall, J., Vater, J., Borriss, R., and Sussmuth, R.D. (2011) Plantazolicin A and B: structure elucidation of ribosomally synthesized thiazole/oxazole peptides from *Bacillus amyloliquefaciens* FZB42. *Org Lett*: **13**, 2996-2999.

20. Lee, S.W., Mitchell, D.A., Markley, A.L., Hensler, M.E., Gonzalez, D., Wohlrab, A., Dorrestein, P.C., Nizet, V., and Dixon, J.E. (2008) Discovery of a widely distributed toxin biosynthetic gene cluster. *Proc Natl Acad Sci U S A*: **105**, 5879-5884.

21. Madison, L.L., Vivas, E.I., Li, Y.M., Walsh, C.T., and Kolter, R. (1997) The leader peptide is essential for the post-translational modification of the DNA-gyrase inhibitor microcin B17. *Mol Microbiol*: **23**, 161-168.

22. Martin, R.B., and Parcell, A. (1961) Hydrolysis of 2-methyl-delta-oxazoline - an intramolecular O-N-acetyl transfer reaction. *J Am Chem Soc*: **83**, 4835-4838.

23. McIntosh, J.A., and Schmidt, E.W. (2010) Marine molecular machines: heterocyclization in cyanobactin biosynthesis. *Chembiochem*: **11**, 1413-1421.

24. Melby, J.O., Nard, N.J., and Mitchell, D.A. (2011) Thiazole/oxazole-modified microcins: complex natural products from ribosomal templates. *Curr Opin Chem Biol*: **15**, 369-378.

25. Milne, J.C., Roy, R.S., Eliot, A.C., Kelleher, N.L., Wokhlu, A., Nickels, B., and Walsh, C.T. (1999) Cofactor requirements and reconstitution of microcin B17 synthetase: a multienzyme complex that catalyzes the formation of oxazoles and thiazoles in the antibiotic microcin B17. *Biochemistry*: **38**, 4768-4781.

26. Mitchell, D.A., Lee, S.W., Pence, M.A., Markley, A.L., Limm, J.D., Nizet, V., and Dixon, J.E. (2009) Structural and functional dissection of the heterocyclic peptide cytotoxin streptolysin S. *J Biol Chem*: **284**, 13004-13012.

27. Newman, D.J., and Cragg, G.M. (2007) Natural products as sources of new drugs over the last 25 years. *J Nat Prod*: **70**, 461-477.

28. Pei, J., Mitchell, D.A., Dixon, J.E., and Grishin, N.V. (2011) Expansion of type II CAAX proteases reveals evolutionary origin of gamma-secretase subunit APH-1. *J Mol Biol*: **410**, 18-26.

29. Peric-Concha, N., and Long, P.F. (2003) Mining the microbial metabolome: a new frontier for natural product lead discovery. *Drug Discov Today*: **8**, 1078-1084.

30. Sa, M.C.M., and Kascheres, A. (1996) Electronically mediated selectivity in ring opening of 1-azirines. The 3-X mode: Convenient route to 3-oxazolines. *J Org Chem*: **61**, 3749-3752.

31. Scholz, R., Molohon, K.J., Nachtigall, J., Vater, J., Markley, A.L., Sussmuth, R.D., Mitchell, D.A., and Borriss, R. (2011) Plantazolicin, a novel microcin B17/streptolysin S-like natural product from *Bacillus amyloliquefaciens* FZB42. *J Bacteriol*: **193**, 215-224.

32. Tiyanont, K., Doan, T., Lazarus, M.B., Fang, X., Rudner, D.Z., and Walker, S. (2006) Imaging peptidoglycan biosynthesis in *Bacillus subtilis* with fluorescent antibiotics. *Proc Natl Acad Sci U S A*: **103**, 11033-11038.

33. Wieland Brown, L.C., Acker, M.G., Clardy, J., Walsh, C.T., and Fischbach, M.A. (2009) Thirteen posttranslational modifications convert a 14-residue peptide into the antibiotic thiocillin. *Proc Natl Acad Sci U S A*: **106**, 2549-2553.

CHAPTER IV: PLANTAZOLICIN IS AN ULTRA-NARROW SPECTRUM ANTIBIOTIC THAT TARGETS THE *BACILLUS ANTHRACIS* MEMBRANE

Manuscript in review at ACS Infectious Diseases

Authors: Katie J. Molohon[#], Patricia M. Blair[#], Seongjin Park, James R. Doroghazi, Tucker Maxson, Jeremy R. Hershfield, Kristen M. Flatt, Nathan E. Schroeder, Taekjip Ha, and Douglas A. Mitchell

[#]These authors contributed equally.

For this chapter, I established the PZN bioactivity (Figures 4.2, 4.3, and Tables 4.1, 4.4, 4.13), performed the radioactivity work (Figure 4.7), RNA experiments and analysis (Figures 4.8, 4.9, Tables 4.5, 4.9, 4.6, and 4.12) (Rockhopper was run by J. Doroghazi), growth curve analysis (Figure 4.10A), isobolograms (Figures 4.11A and 4.18A) generated spontaneous mutants and assembled bacterial genomes (Figure 4.16 and Table 4.14), performed endospore studies (Table 4.2), γ phage sensitivity (Table 4.3), and qualitative reverse transcriptase PCR (qRT-PCR, Table 4.16).

4.1 Abstract

Plantazolicin (PZN) is a ribosomally synthesized and post-translationally modified natural product from *Bacillus methylotrophicus* FZB42 and *Bacillus pumilus*. Extensive tailoring to twelve of the fourteen amino acid residues in the mature natural product endows PZN with not only a rigid, polyheterocyclic structure, but also antibacterial activity. Here we report on the remarkably discriminatory activity of PZN toward *Bacillus anthracis*, which rivals a previously-described *B. anthracis*-specific gamma (γ) phage lysis assay in distinguishing *B. anthracis* from other members of the *Bacillus cereus* group. We evaluate the underlying cause of this selective activity by measuring the RNA expression profile of PZN-treated *B. anthracis*, which, among other clues, revealed significant upregulation of genes within the cell envelope stress response. PZN depolarizes the *B. anthracis* membrane like other cell envelope-acting compounds but uniquely localizes to distinct ~200 nm wide foci within the envelope. Selection and whole-genome sequencing of PZN-resistant mutants of *B. anthracis* implicate a relationship between the action of PZN and cardiolipin (CL) within the membrane. Exogenous CL increases the potency of

PZN in wild type *B. anthracis* and promotes the incorporation of fluorescently tagged PZN in the cell envelope. We propose that PZN localizes to and exacerbates structurally compromised regions of the bacterial membrane, which ultimately results in cell lysis.

4.2 Introduction

The current practice of employing broad-spectrum antibiotics to treat bacterial infections contributes to the rise of antibiotic resistance (de Man *et al.*, 2000). As a countermeasure, species-selective and narrow-spectrum antibacterial compounds are garnering increased attention in the medical community for their potential as therapeutics and diagnostics (Payne, 2008; Wilson *et al.*, 2005). Plantazolicin (PZN) is a polyheterocyclic, linear compound of the ribosomally synthesized and post-translationally modified peptide (RiPP) natural product family with narrow-spectrum antibiotic activity (Figure 4.1) (Scholz *et al.*, 2011). More specifically, PZN is a member of the thiazole/oxazole-modified microcins (TOMMs), a recently grouped and rapidly expanding RiPP class with ~1,500 identified gene clusters (Arnison *et al.*, 2013; Cox *et al.*, 2015). Previously, PZN was described as an antibiotic compound that inhibits Gram-positive organisms closely related to its producing organism, *Bacillus methylotrophicus* FZB42 (Scholz *et al.*, 2011). In 2011, by screening a small panel of microorganisms, we described PZN as having potent activity towards *Bacillus anthracis*, but not other Gram-positive pathogens (Molohon *et al.*, 2011). Several additional PZN-like gene clusters have been identified in six distinct bacterial genera (from three phyla) through genome mining, but experimental data on antibiotic specificity has so far been limited to PZN (Kalyon *et al.*, 2011; Molohon *et al.*, 2011; Scholz *et al.*, 2011). Although PZN has been the subject of total synthesis (Banala *et al.*, 2013; Wilson *et al.*, 2015), heterologous expression (Deane *et al.*, 2013), and enzymological studies (Hao *et al.*, 2015; Lee *et al.*, 2013; Sharma *et al.*, 2013), insight into the mode of action (MOA) of PZN has not been reported in the seven years since the discovery of its biosynthetic gene cluster (Lee *et al.*, 2008).

B. anthracis, the causative agent of anthrax and a category A priority pathogen, is a Gram-positive bacterium and is a member of the *B. cereus sensu lato* group, which includes *B. cereus*, *B. anthracis*, *B. thuringiensis*, and *B. mycoides* (Jensen *et al.*, 2003; Rasko *et al.*, 2005). Microbiologists have debated whether these organisms should be considered as one species, given that some strains share greater than 99% DNA sequence identity. Despite being grouped with other *Bacillus* species, *B. anthracis* harbors a number of features that set it apart from other members of the *B. cereus* group. Fully virulent *B. anthracis* contains two conserved plasmids, pXO1 and pXO2, which harbor the genes responsible for producing the anthrax toxin and poly-D-glutamic acid capsule, respectively. However, homologous plasmids are also found in certain *B. cereus* strains (Kolsto *et al.*, 2009). Beyond characteristic plasmid content, *B. anthracis*, unlike other members of the *B. cereus* group, harbors a nonsense mutation in *plcR* (phospholipase C regulator), rendering *B. anthracis* non-motile and non-hemolytic (Agaisse *et al.*, 1999).

Other defining features of *B. anthracis* that may facilitate species selectivity are exterior to the cell wall. *B. anthracis* displays a two-dimensional protein lattice called the surface layer (S-layer). Decorated with surface-associated proteins in a *csaB* (cell surface attachment)-dependent manner (Mesnage *et al.*, 2000), the S-layer is non-covalently attached to the secondary cell wall polysaccharide (SCWP) (Wang *et al.*, 2013; Zheng *et al.*, 2013), which is covalently tethered to the peptidoglycan. The *B. anthracis* SCWP is structurally unique (Choudhury *et al.*, 2006; Weidenmaier and Peschel, 2008) and serves as the binding site for gamma (γ) phage (Ganguly *et al.*, 2013; Schuch *et al.*, 2013) and previously described *B. anthracis* typing antibodies (Ezzell *et al.*, 1990). γ phage produce a peptidoglycan hydrolase, PlyG, which specifically recognizes the terminal galactoses of the *B. anthracis* SCWP and subsequently hydrolyzes the cell wall (Ganguly *et al.*, 2013). Similarly, typing methods using monoclonal antibodies to the SCWP also exploit differences in the terminal sugar unit. However, there exist atypical *B. anthracis* strains that would constitute false-negatives in any diagnostic assay based on these methods (Abshire *et*

al., 2005; Ezzell *et al.*, 1990). Wip1, another *B. anthracis*-specific phage, is even more selective than γ phage, yet certain *B. cereus* strains remain sensitive (Kan *et al.*, 2013). Thus, the species specificity of PZN is intriguing not just from a MOA standpoint, but also as a means to distinguish *B. anthracis* from other *B. cereus sensu lato* members.

Here we describe PZN as a remarkably selective small molecule antibiotic towards *B. anthracis*. The intriguing specificity was first examined by gene expression profiling, which yielded an expression signature distinct from broader spectrum antibiotics. We have identified and characterized a set of resistant mutants and evaluated their role in PZN resistance, which led to us to further investigate the bacterial membrane as the probable target of PZN. Using fluorescence-based approaches, we confirmed that PZN localizes to the cell envelope and rapidly causes membrane depolarization. Taken together with the observation that PZN interacts synergistically with the negatively charged phospholipid, cardiolipin (CL), we propose that PZN localizes to and aggravates transient weaknesses present in the *B. anthracis* cell membrane.

4.3 Results

4.3.1 Defining the species selectivity of PZN

PZN was originally described as a Gram-positive antibiotic, inhibiting the growth of *B. subtilis*, *B. cereus*, and *B. megaterium* (Scholz *et al.*, 2011). It is important to note, however, that the spot on lawn assay employed to reach this conclusion used an exorbitant amount of purified PZN (1 mg per spot). Using a microbroth dilution assay, the activity of PZN was later revealed to be considerably more selective, in that antibacterial activity was only detected toward *B. anthracis* upon screening a small panel of human pathogens (Molohon *et al.*, 2011; Sterne and Proom, 1957). We continued to establish this unusually narrow-spectrum of activity by screening a larger panel of strains with varying degrees of genetic similarity (Table 4.1). PZN was found to be selective for vegetative *B. anthracis*, including fully virulent biosafety level 3 strains, with minimum inhibitory concentrations (MICs) between 1-16 μg/mL (0.75-12 μM). Endospores, the

dormant phase of the *B. anthracis* life cycle, were resistant to PZN until germination was initiated (Table 4.2). By microbroth dilution, *B. subtilis* and *B. cereus* were not susceptible to PZN at concentrations up to 64 μg/mL, which is in contrast to the previously reported spot on lawn assay (Scholz *et al.*, 2011).

To further investigate the selectivity of PZN towards *B. anthracis*, we conducted a head-to-head comparison using the γ phage assay. Prior to modern genomic methods, γ phage sensitivity and other phenotype testing were popular methods for identifying *B. anthracis* (Abshire *et al.*, 2005). Notwithstanding the reported 96% positive accuracy, non-*B. anthracis* strains that are sensitive to γ phage and true *B. anthracis* strains that are insensitive have been reported (Abshire *et al.*, 2005; Hoffmaster *et al.*, 2006; Schuch and Fischetti, 2006). We obtained a panel of atypical *B. cereus* strains that are sensitive to γ phage and tested them for PZN susceptibility (Table 4.3). *B. cereus* strains that generated a false positive in the γ phage assay were not susceptible to PZN (Kan *et al.*, 2013; Marston *et al.*, 2006; Schuch and Fischetti, 2006).

In an attempt to further define the attributes giving rise to the species selectivity of PZN, we procured various bacterial strains that address key differences between *B. anthracis* and *B. cereus*. *plcR*, encoding the phospholipase C regulator, is nonfunctional in *B. anthracis* but is intact in *B. cereus* (Agaisse *et al.*, 1999). Deletion of *plcR* in *B. cereus* did not increase its susceptibility to PZN (Table 4.1). Additionally, sortase-deficient strains of *B. anthracis*, which lack the ability to anchor various proteins to the cell wall, remain susceptible to PZN (Davison *et al.*, 2005). Similarly, PZN activity was not dependent on the presence or composition of the *B. anthracis* S-layer, as strains deficient in S-layer assembly or decoration, namely those harboring mutations in *csaB*, *sap*, and *eag*, are equally susceptible to PZN (Mesnage *et al.*, 2000). We further confirmed that susceptibility to PZN is plasmid-independent given that the susceptibility of a plasmid-deficient strain, *B. anthracis* LLNL A0517-1. (Table 4.1; Figure 4.2). Wip1 phage and antibody typing have also been used to discriminate *B. cereus sensu lato* strains, but also

have known exceptions to their specificity for *B. anthracis* (Ezzell *et al.*, 1990; Kan *et al.*, 2013). We obtained a "false-positive for *B. anthracis*" strain for each marker: *B. cereus* CDC32805 for Wip1 and *B. cereus* ATCC 7064 for antibody typing. We again observed no measurable PZN susceptibility for either strain (Table 4.1).

After extensive susceptibility testing, the only notable exception to the *B. anthracis* selectivity of PZN was *B. cereus* G9241 (MIC of 8 μg/mL). *B. cereus* G9241 encodes the genes for an anthrax-like toxin on its pBCXO1 plasmid, which is named for its homology to the *B. anthracis* pXO1 plasmid (Hoffmaster *et al.*, 2004). As *B. cereus* G9241 is encapsulated and toxigenic, it causes an anthrax-like disease but is undetectable in the γ phage assay (Hoffmaster *et al.*, 2006). From a pathogen detection perspective, the action of PZN towards G9241 could be considered fortuitous if it were to be further developed as a diagnostic test. Together, these data not only highlight the species discrimination of PZN but also rule out *plcR*-related effects, sortase-mediated proteins, the SCWP, the S-layer, and plasmid-borne entities as targets of PZN.

The spectrum of PZN activity calls into question whether bacteria are the naturally intended target. The canonical PZN-producing strain, *B. methylotrophicus* FZB42, has been described to have antifungal and nematicidal activity and is a prolific producer of other natural products (Burkett-Cadena *et al.*, 2008; Chen *et al.*, 2007). Liu *et al*. assigned a nematicidal activity to PZN, derived from experiments showing that PZN-deficient FZB42 strains exhibit reduced nematicidal activity against *Caenorhabditis elegans* (Liu *et al.*, 2013). Since these experiments employed crude cellular extracts, we evaluated purified PZN in a similar manner, embedding the compound in agar (slow killing assay) or providing PZN in a liquid suspension (liquid fast killing assay). PZN was found to be no more toxic to *C. elegans* than a vehicle control and is clearly not nematicidal in its own right (Figure 4.3). Purified PZN was also not responsible for the antifungal activity of the native producer, leaving the ecological function of PZN unknown (Table 4.1).

After observing the specificity of PZN under one growth medium condition (Luria-Bertani broth, LB), we re-assessed specificity against a smaller but representative panel of strains in two additional growth media (Mueller-Hinton and brain-heart infusion broths, Table 4.4). All tested strains of *B. anthracis* remained equally susceptible, but unexpectedly, some *Staphylococcus aureus* strains were susceptible to PZN under alternative growth media (MICs from 8 – 32 μg/mL). All other tested strains remained non-susceptible to PZN.

4.3.2 Assessing potential macromolecules as the target of PZN

In an attempt to identify the molecular target(s) of PZN, two biotinylated PZN probes were prepared for affinity purification, a standard technique for identifying targets of bioactive small molecules (Ziegler *et al.*, 2013). First, an *N*-terminally biotinylated PZN was prepared from desmethylPZN, which is a biosynthetic intermediate obtainable by fermentation of an expression strain missing the PZN *N*-methyltransferase (Figure 4.1; Figure 4.4) (Molohon *et al.*, 2011). Unfortunately, *N*-biotinylated PZN was devoid of antibiotic activity at the concentrations tested; however, *C*-terminally biotinylated PZN retained bioactivity, albeit with a 16-fold reduction in potency (Figure 4.1; Figure 4.5). For this reason, *C*-terminally labeled PZN-biotin was chosen for affinity-based target identification. Despite numerous attempts, we were unable to identify interactions unique to PZN-biotin compared to the control (data not shown). A photoaffinity tagged derivative of PZN was then prepared on the notion that PZN-biotin may weakly interact with its target, (Figure 4.1, Figure 4.6). To minimally perturb potential interactions, a minimalist, bifunctional analog containing a diazirine and alkyne was employed to enable crosslinking prior to biotinylation and enrichment (Li *et al.*, 2013). Again, no binding partners were identified by either mass spectrometry or western blot.

Because affinity purification-based strategies to identify small molecule targets is most successful when the interaction is proteinaceous and of high-affinity (Burdine and Kodadek, 2004), we next considered the possibility that PZN interacted with a non-protein macromolecule.

We used radiolabeled precursors of the cell wall, fatty acids, and RNA (as well as protein), to assay for their biosynthesis in the presence of PZN. Similar to the nisin-like lanthipeptide Pep5, PZN extensively disrupted macromolecular biosynthesis (Sahl and Brandis, 1982) (Figure 4.7). Interestingly, PZN did not affect cell wall biosynthesis compared to the vancomycin control.

4.3.3 The gene expression signature of PZN

Sub-lethal antibiotic treatment stimulates rapid transcriptional responses in bacteria (Goh *et al.*, 2002) and the induced/repressed genes may be indicative of MOA (Brazas and Hancock, 2005). We thus performed RNA-Seq to evaluate the transcriptional response of *B. anthracis* following exposure to 0.25 μg/mL (0.25 × MIC) PZN for 10 min (Shaw and Morrow, 2003). A total of 74 genes were differentially regulated, including 63 upregulated and 11 downregulated genes, with an adjusted false discovery rate (q-value) of 0.01 (Figure 4.8; Table 4.5). The expression of a subset of these genes was validated by qRT-PCR (Table 4.6; Table 4.7). Fourteen of the upregulated genes were transporter subunits, a common stress response upon antibiotic treatment (Li and Nikaido, 2009). Conversely, PZN treatment led to the downregulation of genes associated with L-lactate metabolism, for which the implications remain unclear.

The most highly upregulated *B. anthracis* genes upon PZN treatment were *bas1344* and *bas1345*, which encode a hypothetical protein and a predicted member of the PspA/IM30 family, respectively (Table 4.6). These genes are homologous to the *B. subtilis* genes *liaI* and *liaH* (lipid II cycle interfering antibiotics), which are involved in the cell envelope stress response. Induction of these genes upon antibiotic treatment is well documented in *B. subtilis*, specifically to antibiotics interacting with lipid II in some capacity (*e.g.*, nisin, vancomycin, and bacitracin) (Jordan *et al.*, 2008). Induction of *lia* is also seen upon treatment of *B. subtilis* with daptomycin, despite the lack of direct interaction between daptomycin and lipid II (Wecke *et al.*, 2009). PZN treatment also results in massive upregulation of *bas5200* and *bas5201*, which are homologous to a *B. subtilis* thermosensor two-component system that regulates the lipid desaturase, *desRK*

(Martin and de Mendoza, 2013). To our knowledge, PZN is the first compound known to alter the expression of *desRK*, further suggestive of a unique MOA.

Recently, we reported on the synthesis of a PZN derivative, Me_2-Arg-Az_5 (Figure 4.1) (Hao *et al.*, 2015). Chemically, Me_2-Arg-Az_5 represents the *N*-terminal half of PZN, but the activity spectrum of Me_2-Arg-Az_5 is broader and includes other *Bacillus* species as well as *S. aureus* (Table 4.8). To investigate their differing spectra of activity, we recorded the gene expression profile of *B. anthracis* treated with Me_2-Arg-Az_5 under otherwise identical conditions (0.25 × MIC, 10 min) by RNA-Seq. The two compounds shared a minor portion of their expression profiles, but each profile was largely independent (Figure 4.9; Tables 4.9-4.10). For example, sub-lethal Me_2-Arg-Az_5 treatment also induced the *desRK* two-component system, but expression of *liaIH* remained unchanged. Additionally, Me_2-Arg-Az_5 failed to induce *B. anthracis* lysis, in contrast to PZN (Figure 4.10). These data, together with strain susceptibility, suggest that PZN and Me_2-Arg-Az_5 pursue independent, but possibly related, targets.

4.3.4 PZN depolarizes the *B. anthracis* membrane

We examined the activity of PZN towards *B. anthracis* in the presence of the membrane disrupting agents nisin and daptomycin. Based on the resulting isobolograms, both compounds elicited strong synergistic activity with PZN (Figure 4.11) (Berenbaum, 1989). Both nisin and daptomycin disrupt membrane potential in Gram-positive organisms, and their synergism with PZN suggests that PZN might also depolarize the *B. anthracis* membrane (Ruhr and Sahl, 1985; Silverman *et al.*, 2003). Thus, $DiOC_2(3)$ (3,3'-diethyloxacarbocyanine iodide) was used to measure the membrane potential of PZN-treated *B. anthracis* cells. As expected, PZN treatment, at both inhibitory and sub-inhibitory concentrations, correlated with a decrease in membrane potential, suggesting that PZN exerts its action by disrupting the integrity of the cell membrane (Figure 4.11).

4.3.5 Subcellular localization of PZN

With mounting evidence that PZN targets the cell membrane, we aimed to determine the subcellular localization of PZN by confocal microscopy. Antibiotics derivatized with fluorescent probes have previously been used to shed light on their MOAs (Bindman and van der Donk, 2013; Tiyanont *et al.*, 2006). Localization of PZN was established by employing a Cy5-labeled PZN derivative (PZN-Cy5) (Figures 4.1, 4.12) that retained much of its anti-*B. anthracis* activity (MIC of 4 μg/mL, 2 μM). PZN-Cy5 localized to distinct ~200 nm wide foci in *B. anthracis* Sterne (Figure 4.13A). To confirm that PZN-Cy5 behaved in a matter identical to unlabeled PZN, we carried out a competition assay where and excess of PZN was applied to *B. anthracis* Sterne followed by addition of PZN-Cy5. Due to the extensive cell lysis elicited by PZN, we employed a later-described spontaneously PZN-resistant Sterne mutant (PR06) for this competition assay. Just as in *B. anthracis* Sterne, PZN-Cy5 localized to distinct foci in *B. anthracis* PR06 (Figure 4.13B). PZN-Cy5 failed to label strain PR06 when an excess of unlabeled PZN was administered first, demonstrating that PZN and the PZN-Cy5 probe identically interact with *B. anthracis* (Figure 4.13C). Due to the photoswitching properties of Cy5, we were able to further investigate PZN-Cy5 localization using stochastic optical reconstruction microscopy (STORM, Figure 4.14) (Huang *et al.*, 2008). Using this super-resolution imaging technique, *B. anthracis* Sterne cells were again confirmed to accumulate PZN-Cy5 at the foci described above. These foci were clearly localized to the surface of the cells, further implicating a component of the cell envelope as the target of PZN (Figure 4.15). *B. anthracis* cells contain 16 ± 2 foci per cell, each with a diameter of 181 ± 7 nm, as determined by analysis of 14 cells treated with PZN-Cy5 (Figure 4.15). Notably, the labeling pattern of PZN-Cy5 is different from BODIPY-vancomycin, which has been shown to localize to bacterial septa at the site of peptidoglycan synthesis (Nguyen-Mau *et al.*, 2012). If PZN were acting on the cell wall, sites of active PG synthesis or the entire cell wall would be labeled with PZN-Cy5. The non-septal, punctate labeling of PZN-Cy5 suggests

that the target of PZN is neither nascent nor existing peptidoglycan, which is congruent with the observation that PZN did not block cell wall biosynthesis (Figure 4.7).

4.3.6 Isolation and characterization of PZN-resistant mutants

An orthogonal strategy for obtaining antibiotic MOA information involves the selection and mapping of resistant mutant polymorphisms (Silver, 2011). The genes containing the resistance-conferring mutations can either be involved directly in the MOA of the antibiotic or in a target-unrelated mechanism of immunity. We isolated PZN-resistant *B. anthracis* by growing the Sterne strain on agar plates containing PZN at 4 × MIC. The resistance frequency was determined to be 2.3×10^{-7}, and the resulting mutants exhibited MICs that were ≥32 μg/mL. Genomic DNA was isolated and sequenced for six independently-selected PZN-resistant strains (PR01 through PR06) and the parent Sterne strain. Comparison of PR01 through PR06 to the parent revealed that all six polymorphisms were confined to a 50-nucleotide section of a single gene, *bas4114*, which is annotated as an AcrR transcriptional repressor (Table 4.11) (Deng *et al.*, 2013). This particular AcrR protein is predicted to contain a single transmembrane domain near the *C*-terminus (Figure 4.16) (Viklund *et al.*, 2008), which is precisely where the PZN-resistance conferring mutations were found, all resulting in premature stop codons. Directly downstream of *bas4114* are two EmrE-type efflux pumps, encoded by *bas4115-4116*. We hypothesized that as an AcrR transcriptional repressor, BAS4114 would negatively regulate *bas4115-4116*, and mutations near the C-terminus of BAS4114 would result in regulator dysfunction and derepression of the efflux pumps. This in turn would increase resistance to PZN. Therefore, RNA-Seq was employed to compare the mRNA expression profiles of PR06 to the parent Sterne strain. This analysis revealed a significant upregulation of *bas4114-4117* (Table 4.12). PR06 and the Sterne parent were equally susceptible to Me_2-Arg-Az_5 (Table 4.8), again underscoring differences between PZN and Me_2-Arg-Az_5. The susceptibility of PR06 to a panel of

mechanistically-diverse antibiotics, including daptomycin, was also assessed (Table 4.13). The PZN resistance-conferring mutation did not alter the susceptibility towards any tested antibiotic.

Mutation of *bas4114* is clearly the favored route for generating PZN-resistance in *B. anthracis*, as shown by the occurrence of multiple independent mutations within the same gene. In order to subvert this resistance mechanism, and to obtain more insightful information about PZN MOA, we deleted *bas4114-4117* from the parental strain by homologous recombination (Figure 4.17) (Janes and Stibitz, 2006). *B. anthracis* Sterne Δ*bas4114-4117* thus became the new parental strain for isolating second-generation PZN-resistant mutants, as the removal of *bas4114-4117* rendered the strain resensitized to PZN at wild type levels (1 μg/mL). This time, two routes were pursued for obtaining PZN-resistant strains. First, we selected spontaneous PZN-resistant mutants by challenging with 4 × MIC. Isolation of the spontaneous mutants resulted in a mutation frequency an order of magnitude lower than before (1.3×10^{-8}). Two independently-selected resistant strains (PR07 and PR08) were subjected to whole-genome sequencing, revealing single point mutations within *ftsE* (Table 4.14). FtsE is an ATP-binding protein that associates with its cognate permease FtsX, which together comprise an ABC transporter that functions during cell wall elongation and septum formation (Yang *et al.*, 2011).

In a second strategy to obtain PZN-resistant mutants, we cultured *B. anthracis* Sterne Δ*bas4114-4117* in the presence of a sub-lethal concentration of PZN. The concentration of PZN was gradually increased with the number of passages (Friedman *et al.*, 2006). We isolated genomic DNA from a 1st passage strain (PR09-1, MIC 16 μg/mL) in addition to two independent 4th passage strains (PR09-4, PR10-4, MICs ≥64 μg/mL) for whole genome sequencing. PR09-1 contained a point mutation in *bas1659*, which is annotated as a CitB-like response regulator (Table 4.14). Downstream of *bas1659* are genes encoding a predicted histidine kinase (*bas1660*), ABC transporter subunits (*bas1661-1663*), and a cardiolipin (CL) synthase gene (*bas1664*). PR09-4 is a descendent of PR09-1, and as such, PR09-4 contained the same *bas1659* mutation as

PR09-1 in addition to another point mutation in *bas1662* (the permease domain of a locally-encoded ABC transporter). PR10-4 contained a similar mutation series (*bas1663*, a second permease gene for what is presumably a trimeric ABC transporter) but had an additional mutation in *bas1842*, which is implicated in petrobactin biosynthesis (Lee *et al.*, 2007). However, deletion of the petrobactin biosynthetic gene cluster did not decrease susceptibility to PZN (Table 4.1).

4.3.7 Cardiolipin increases sensitivity to PZN

We hypothesized that the regulatory- and transport-related mutations upstream of the gene encoding CL synthase could alter CL concentrations and thus, CL may be playing a role in PZN's activity. We first examined the effect of exogenous CL on the interaction of PZN with the *B. anthracis* cell membrane. *B. anthracis* cells were treated with PZN-Cy5 (1 nM) in the presence and absence of exogenous CL (up to 100 µg/mL). Cell-associated PZN was then quantified by flow cytometry. The extent of PZN-Cy5 binding to *B. anthracis* was significantly increased when cells were co-treated with CL (Figure 4.18). This result is in contrast to that with daptomycin, which acts on the bacterial membrane but exhibits an antagonistic relationship with CL (Zhang *et al.*, 2014). As predicted, co-administration of CL did not increase the labeling efficiency of daptomycin-Cy5 on *B. anthracis* cells (Figures 4.1, 4.18, 4.19) (Zhang *et al.*, 2014). Congruent with these data was the observation that CL potentiated the killing activity of PZN towards *B. anthracis*. Indeed, the strongly synergistic behavior with CL enhanced the potency of PZN upwards of 16-fold while CL alone had no antibiotic activity at the concentrations tested (Figure 4.18).

The proportion of CL in cell membranes has been reported to increase during growth in high osmolarity medium, especially for *B. subtilis* (Romantsov *et al.*, 2009). We thus tested whether increasing the osmolarity of the *B. subtilis* medium (and thus the CL content) would induce susceptibility to PZN. When grown in standard LB supplemented with an additional 1.5 M NaCl (final 1.67 M NaCl), PZN was weakly growth-suppressive towards *B. subtilis* (Table 4.15).

By measuring CL from total lipid extractions, CL levels did increase compared to standard growth in LB (Table 4.15). However, exogenous cardiolipin alone does not induce PZN susceptibility in *B. subtilis* (data not shown). Unfortunately, members of *B. cereus sensu lato*, including *B. anthracis*, are not tolerant of high osmolarity media (Peters *et al.*, 1991). Therefore, induced susceptibility to PZN under high osmolarity conditions could not be evaluated for these strains.

As stated previously, the stepwise-selected PZN-resistant mutants accumulated mutations in genes upstream of the CL synthase gene. We next analyzed the transcriptional response within the *cls* locus, including the upstream regulators/transporters and observed a dramatic increase in the expression of several *cls* genes in PR09-1 and PR09-4, including CL synthase itself and the transporters, but not the predicted response regulator and histidine kinase genes (Table 4.16). In contrast, there was no differential expression of any tested gene in the PR10-4 strain. Upon CL quantification, we did not detect differences in CL content between *B. anthracis* and the Δ*bas4114-4117* strain; however, only mutant PR10-4 contained a proportionally increased level of CL (Table 4.15).

4.3.8 PZN colocalizes with cardiolipin and regions of increased fluidity

The genetic and functional association with CL implicates the membrane as the most probable target for PZN. The lipid dye 10-N-nonyl acridine orange (NAO) approximates regions of the cell membrane enriched in CL (Mileykovskaya and Dowhan, 2000; Petit *et al.*, 1992). Alone, NAO staining yielded a patchy appearance on *B. anthracis* membranes (Figure 4.20). We equilibrated *B. anthracis* cells with PZN-Cy5 and NAO to investigate if PZN localized to CL-rich regions in the cell membrane. There existed a clear but imperfect colocalization of the two dyes, suggesting a possible interaction with CL in the bacterial membrane (Figure 4.20). Additionally, 1,1'-Didodecyl-3,3,3',3'-tetramethylindocarbocyanine perchlorate, (DilC12(3)), is a dye reported to associate with regions of increased fluidity (RIF) within cell membranes, which may also be

indicative of CL localization (Strahl *et al.*, 2014). We observed colocalization of DilC12(3) and PZN-Cy5, consistent with PZN and CL co-associating with *B. anthracis* RIFs (Figure 4.20).

4.4 Summary and Outlook

Due to genomic advances, *B. anthracis,* the causative agent of anthrax, can be distinguished from the other members of the *B. cereus sensu lato* group by whole genome sequencing, multi-locus sequence typing (Marston *et al.*, 2006; Tourasse and Kolsto, 2008), the presence of chromosomal lambdoid prophages (Kolsto *et al.*, 2009), and the presence of a characteristic nonsense mutation in *plcR.* An alternative approach to *B. anthracis* identification now includes susceptibility to PZN, which is a natural product exhibiting potent and specific activity for *B. anthracis* under standard laboratory conditions. Our data demonstrate that the species selectivity of PZN is even more discriminating than that of the reputedly selective γ phage (Abshire *et al.*, 2005; Kan *et al.*, 2013; Marston *et al.*, 2006; Schuch and Fischetti, 2006).

B. cereus G9241, which was inhibited by PZN at 8 μg/mL, is a fortuitous exception to PZN selectivity, as it was isolated from a patient exhibiting an anthrax-like disease (Hoffmaster *et al.*, 2004). Upon treatment with high concentrations of PZN in other rich media, namely Mueller-Hinton and brain-heart infusion broths, the spectrum of PZN activity is broadened to include strains of *S. aureus*, a phenomenon that convolutes the search for PZN's precise MOA. Upon testing a panel of Gram-positive strains, no bacterium besides *S. aureus* showed media-dependent susceptibility to PZN.

We were able to rule out certain *B. anthracis*-defining features, namely the SCWP/S-layer, plasmid-borne entities, proteins tethered to the cell wall, and *plcR*-related components as targets of PZN by analyzing select *B. anthracis* strains. Additionally, despite preparing a biotinylated PZN derivative that retained antibacterial activity, no proteinaceous binding partners could be identified. Similarly, a photoaffinity PZN probe was employed in the event that the PZN-biotin probe had decreased affinity for the target, but this too was unsuccessful.

The gene expression profile of PZN suggested a target within the *B. anthracis* cell membrane. Sub-lethal concentrations of PZN resulted in the differential expression of 74 genes within *B. anthracis*. Two of the most upregulated genes in the PZN expression profile are homologs of *liaI* and *liaH*, which are part of a known cell envelope stress response. A number of cell wall- and cell membrane-acting antibiotics induce the *lia* system (*e.g.* bacitracin, nisin, daptomycin, and vancomycin) (Wecke and Mascher, 2011). However, PZN likely has a distinct MOA, given that we observed an overall expression profile different from those reported for other antibiotics. Of particular note is the overexpression of the lipid desaturase (*des*) two-component regulatory system. Cell survival in conditions of increased osmolarity is dependent on membrane fluctuations with an increase in unsaturated fatty acid composition (Lopez *et al.*, 1998). We have demonstrated that by increasing the osmolarity of the growth medium, we can induce, to a modest extent, PZN susceptibility in *B. subtilis*. Increased CL levels are characteristic of osmotic stress in *B. subtilis*, *Escherichia coli*, and *Lactococcus lactis*, among others (Romantsov *et al.*, 2009). Furthermore, excess CL within the membrane results in increased fluidity and lipid bilayer deformation (Unsay *et al.*, 2013). Regulation of the lipid desaturase, Des, influences the composition of phospholipids within the membrane (Aguilar *et al.*, 1998). Thus, PZN induces stress in the cell membrane, inducing the *des* two-component system and likely affecting membrane fluidity.

To further illuminate the MOA of PZN, we deleted four adjacent genes (*bas4114-4117*) involved in endowing *B. anthracis* with spontaneous resistance to PZN. Serially passaging the resulting deletion strain for PZN-resistant mutants yielded an accumulation of point mutations within a regulator (*bas1659*) and transporters upstream (*bas1662-1663*) of a CL synthase gene (*bas1664*). As these are missense mutations, we would not necessarily expect loss of function in the protein products. We observed differential expression of the CL synthase and upstream transporters in the PZN-resistant mutants, but only the PZN-resistant mutant PR10-4 displayed

differential levels of CL in the cell membrane. Increased CL content in the PR10-4 mutant suggests that CL does play a role in the activity of PZN, although there is not a straightforward relationship between CL content composition and PZN susceptibility. Based on our findings, we expect that in addition to CL, other membrane-associated biomolecules contribute to the ability of PZN to destabilize *B. anthracis* cell membranes.

Nonetheless, our results reveal that CL plays an important role in PZN susceptibility, in that CL dramatically increased the potency of PZN without being cytotoxic at the concentrations investigated here. Such synergy was not observed between daptomycin and CL, and according to the available literature, increased CL contributes to daptomycin resistance in Entercocci; thus, although PZN and daptomycin both disrupt membrane function, they exhibit differences in MOA (Palmer *et al.*, 2011; Zhang *et al.*, 2014). CL has the potential to dramatically alter membrane architecture and may contribute to the susceptibility of *B. anthracis* through localization to distinct foci throughout the cell. The link between PZN and CL is further supported by the colocalization of PZN-Cy5 with the quasi-CL-specific dye, NAO, in *B. anthracis* (Mileykovskaya and Dowhan, 2000; Petit *et al.*, 1992). In *B. subtilis*, NAO organizes into distinct foci at the septa and the poles (Matsumoto *et al.*, 2006; Mileykovskaya and Dowhan, 2009), but it appears that in *B. anthracis* Sterne, NAO labels distinct, ~200 nm foci throughout the entirety of the cell membrane. Thus, *B. anthracis* appears to have a unique distribution of CL that facilitates an interaction with PZN and leads to cell death, whereas CL within other species may not be accessible to PZN. In addition to colocalization with NAO, we report that PZN-Cy5 colocalizes with DilC12(3), which is a dye that recognizes regions of increased fluidity (RIFs) in the membrane of *B. subtilis* (Strahl *et al.*, 2014). RIFs are transiently weakened regions within the bacterial membrane that affect lipid homeostasis and membrane fluidity.

In an effort to further understand the remarkable selectivity of PZN susceptibility, we initiated a comparative analysis of PZN and Me_2-Arg-Az_5 activities. Just as the PZN substructure

Me_2-Arg-Az_5 partially resembles PZN, our investigation reveals some similarities but major differences in their activities. Me_2-Arg-Az_5 displayed a broader range of antibiotic activity, including *S. aureus* and multiple *Bacillus* species (Hao *et al.*, 2015). Importantly, mutations conferring PZN resistance did not confer resistance to other antibiotics or to Me_2-Arg-Az_5. Additionally, Me_2-Arg-Az_5 shared a minor portion of its gene expression profile with PZN; together with the evidence that Me_2-Arg-Az_5 does not lyse *B. anthracis* cells, we hypothesize that Me_2-Arg-Az_5 and PZN have distinct MOAs. A possible explanation for the observed differences between PZN and Me_2-Arg-Az_5 is that the *C*-terminal portion of the molecule is responsible for the species selectivity of the mature molecule and the *N*-terminal portion harbors the antibiotic activity, although this remains to be more extensively investigated. Thus, while Me_2-Arg-Az_5 is not useful as a mimic for the full-length natural product, it may represent a way to broaden the spectrum of PZN activity.

In this paper, we report a MOA for PZN bioactivity involving cell membrane depolarization in a CL-enhanced manner. Through extensive testing, we determined that the stringency of PZN for *B. anthracis* is relaxed only in alternative media conditions. Additionally, the compound on its own does not contribute to *B. methylotrophicus* FZB42 antifungal or nematicidal activity. *B. anthracis* is very similar to other members of the *B. cereus sensu lato* family as described, but strains of *B. anthracis* designed to analyze key genetic differences retain their respective susceptibility to PZN. By imaging with confocal and STORM microscopy, PZN-Cy5 was found to localize to the cell envelope and colocalize with RIFs and CL. Gene expression analysis reveals that PZN operates by a different MOA than previously described cell envelope-targeting antibiotics. Thus, we present a model for PZN activity wherein PZN takes advantage of a locally weakened cell membrane, whether due to RIFs, CL-dependent membrane deformation, or some combination thereof. PZN accumulates to such membrane defects, which results in membrane depolarization and eventual cell lysis.

4.5 Experimental

4.5.1 Strain and growth conditions

All strain references are displayed in Table 4.1. All strains were grown in Luria-Bertani (LB) broth unless otherwise described (10 g/L tryptone, 5 g/L yeast extract, 10 g/L (0.34 M) NaCl). Biosafety level 3 strains of *B. anthracis* were grown on Mueller-Hinton agar. *Neisseria* strains were grown in gonococcal medium base supplemented with Kellogg's I and II (Kellogg *et al.*, 1963). *Streptomyces* endospores were isolated on mannitol soybean flour agar (20 g/L mannitol, 20 g/L soybean flour, 1.5% agar) and used to determine PZN susceptibility in ISP2 (4 g/L yeast extract, 10 g/L malt extract, 4 g/L dextrose). Yeast strains were grown in YPD medium (10 g/L yeast extract, 20 g/L peptone, 20 g/L dextrose). *C. elegans* was cultured on nematode growth medium with *E. coli* OP50. Cultures were supplemented with 1.25 mM $CaCl_2$ when assaying daptomycin susceptibility. In cases where increased osmolarity was desired, the LB was supplemented with additional NaCl (final concentration of 1.84 M).

4.5.2 PZN production

Stationary phase cultures of RSpMarA2 (Δ*sfp, yczE, degU*) (Kalyon *et al.*, 2011) were grown in LB with 7 µg/mL kanamycin and 7 µg/mL chloramphenicol. Sterilized aluminum sheet cake pans were prepared with M9 agar medium supplemented with BME vitamin mix and ATCC trace mineral solution and the aforementioned antibiotics. Cake pans were inoculated with 1.5 mL stationary phase RSpMarA2 and incubated 48 h at 37 °C. Bacterial lawns were loosened from the agar and resuspended in Tris-buffered saline (TBS) (150 mL/pan). The bacteria were then harvested via centrifugation (11,000 x *g*, 20 min). The supernatant was decanted and the cell pellets were stored at -20 °C until extraction.

4.5.3 PZN purification

PZN was extracted from bacterial pellets by resuspending in 150 mL MeOH/tray of cells with intermittent vortexing for 15 min at 22 °C. The cells were harvested by centrifugation as

above. The supernatant was vacuum filtered using Whatman filter paper, rotary evaporated, and subsequently lyophilized to dryness. The dried, crude PZN was resuspended in MeOH (1 mL/tray of extract) and centrifuged to remove insoluble debris (4,000 × *g*, 10 min). The supernatant was then injected onto a RediSep R_f High Performance 15.5 g HP C_{18} cartridge (Teledyne Isco) and purified by MPLC using a Combiflash Rf 200 system (25-100% MeOH/10 mM aqueous NH_4HCO_3 over 120 column volumes). The fractions containing PZN were pooled, rotary evaporated, and lyophilized to dryness, yielding roughly 5 mg/tray. PZN was dissolved in DMSO at concentrations of 30-50 mg/mL and stored at -80 ˚C for later use.

4.5.4 PZN bioactivity

PZN and Me_2-Arg-Az_5 bioactivity was determined via microbroth dilution assay as described in the Clinical and Laboratory Standards Institute manual (2006). The optical density (OD_{600}) of a stationary phase culture was adjusted to 0.01 and added to a microtiter plate containing serially diluted PZN. Wells were visually inspected for turbidity, and the minimum inhibitory concentration (MIC) was determined as the lowest compound concentration that incurred no growth after 16 h. MICs were determined in LB unless growth conditions required an alternative medium (see above). The *S. aureus* media-dependent PZN susceptibility was analyzed using LB, Brain-Heart Infusion (BHI, Bacto), and Mueller-Hinton (BBL) broths. When indicated, cardiolipin (CL) was added to the medium at 100 μg/mL.

A *B. anthracis* growth curve was generated using Tecan Infinite M200 Pro. *B. anthracis* Sterne 7702 cultures were grown in LB to stationary phase at 37 ˚C. Cultures were diluted to OD_{600} of 0.05 with fresh LB and allowed to recover to an OD_{600} of 0.35. Cultures were aliquoted into 96-well plates containing PZN and incubated at 37 ˚C with orbital shaking. OD_{600} was measured every 2 min. Values were normalized to an initial OD_{600} of 0.35 and adjusted to a 1 cm path length. Error bars represent standard deviation of two independent experiments.

A growth curve in the presence of Me_2-Arg-Az_5 was generated as described above with the following differences: *B. anthracis* Sterne 7702 and *S. aureus* USA300 cultures were grown in duplicate to OD_{600} 1.0 and aliquoted into 96-well plates. Wells were treated with 1:1 dilutions of Me_2-Arg-Az_5 at a maximum concentration of 12 μM. The plate was incubated at 37 °C with orbital shaking and OD_{600} was measured every 2 min. Values were normalized to an initial OD_{600} of 1.0, adjusted to a 1 cm path length, and averaged at each time point.

4.5.5 Bacterial endospore preparation and susceptibility screening

B. anthracis Sterne 7702 endospores were prepared as described previously (Stojkovic *et al.*, 2008). Briefly, *B. anthracis* Sterne 7702 cells were incubated overnight in LB at 37 °C. Difco Sporulation Media agar plates (8 g Nutrient Broth, 1 g KCl, 0.25 g $MgSO_4$ + $7H_2O$, and 17 g agar, per liter) was inoculated with 150 μL of the stationary phase culture and incubated at 30 °C for 5 days. Lawns were recovered by resuspension in sterile H_2O and filtered using 3.1 and 1.2 μm filters to remove vegetative cells and aggregated endospores. Endospore filtrate was incubated at 65 °C for 1 h to remove any remaining vegetative cells. Endospores were harvested by centrifugation at 8000 × *g* for 25 min at 4 °C. After decanting the supernatant, the endospores were washed 3 times with 40 mL of H_2O, harvesting by centrifugation. Endospores were stored at 4 °C in H_2O and quantified by serial dilution. Endospores were screened for PZN activity by incubating 1×10^9 endospores with PZN (0-16 μg/mL) in H_2O for 20 h at 37 °C. Endospores were subsequently incubated at 65 °C for 1 h to destroy any contaminating vegetative cells, and then 4 °C for 4 h to recover, and followed by serial dilution onto LB agar plates to assess germination. Plate counts represent the average of two trials.

4.5.6 Gamma (γ) phage sensitivity

γ phage were propagated as described previously (Abshire *et al.*, 2005) using *B. anthracis* Sterne 7702 cells on brain heart infusion (BHI) agar plates, with no visible loss in infectivity. Phage infectivity was tested against a panel of *B. cereus* and *B. anthracis* strains using a serial

dilution assay. Stationary phase cultures were adjusted to an OD_{600} of 0.1 and 100 µL was plated on BHI plates. 5 µL of phage stock (2.6×10^8 plaque forming units/mL) was serially diluted (2-fold) and spotted onto the plates and allowed to dry. After incubation at 37 °C for 16 h, plates were removed and visually inspected for plaques.

4.5.7 *C. elegans* nematicidal assays

Wild-type N2 *C. elegans* were cultured on *E. coli* OP50 using standard techniques (Brenner, 1974). Eggs were isolated from gravid hermaphrodites using standard bleaching protocols (Emmons *et al.*, 1979) and incubated for 18 h at 20 °C to obtain synchronized L1 larvae. Cultures were then transferred to new NGM plates seeded with OP50 *E. coli* and incubated for 48 h at 25 °C. Resulting L4 larvae were used for assays adapted from Liu *et al* (Liu *et al.*, 2013).

Slow killing assays were performed using 12-well cell culture dishes with wells containing 1 mL NGM agar amended with 64 µg/mL PZN dissolved in DMSO or an equivalent volume (2 µL) of DMSO alone. One half of the slow killing assay wells were also seeded with 10 µL of OP50 *E. coli*. The effect of DMSO alone on mortality was also tested and found to be negligible. Subsequently, 40-60 L4 hermaphrodites were transferred to each well, incubated at 25 °C and checked every 24 h for 3 days. Each treatment was performed with two biological replicates, each having three technical replicates. Liquid fast killing assays were also performed using 12-well cell culture dishes with wells containing 1 mL M9 buffer combined with 64 µg/mL PZN dissolved in DMSO or DMSO alone. 40-60 L4 larvae were transferred into each well and incubated at 25 °C for 24 h. Fast killing assays were replicated similarly to the slow killing assay (two biological, three technical replicates). For the duplicate assay, an additional control of M9 buffer was included. In both fast and slow killing assays, animals were scored according to criteria shown in Liu *et al*. Mortality rates were also calculated using identical ratios.

4.5.8 RNA isolation and transcriptional profiling of PZN-treated Sterne cells

For the compound-treated samples, independent 3 mL cultures of *B. anthracis* Sterne 7702 cells were grown to an OD_{600} of 0.4, and 0.25 × MIC of PZN, 0.25 × MIC Me_2-Arg-Az_5 (Hao *et al.*, 2015), or an equivalent volume of DMSO was added and allowed to incubate for 10 min at 37 °C. Together with resistant mutant PR06, RNA was isolated and prepared as described previously (Scholz *et al.*, 2011). RNA-Seq libraries were created using the TruSeq Stranded RNA Sample Prep kit (Illumina, San Diego, CA) after rRNA depletion using the RiboZero Bacteria kit (Epicentre, Madison, WI). Sequencing was performed for 1 × 100 cycles on a HiSeq 2000 with Version 3 Chemistry. Transcriptomic data was processed with the Rockhopper version 1.30 pipeline (McClure *et al.*, 2013) using *B. anthracis S*terne and *B. anthracis* Ames Ancestor plasmid pXO1 (NC_007322.2) as references. Default values (allowed mismatches 0.15, minimum seed length 0.33, minimum expression of UTRs and ncRNAs 0.5) were used, with the exception that reverse complement reads were used for mapping. The RNA-Seq data discussed in this publication have been deposited in NCBI's Gene Expression Omnibus (Barrett *et al.*, 2013) and is accessible through GEO Series accession number GSE73343 (http://www.ncbi.nlm.nih.gov/geo/query/acc.cgi?acc=GSE73343).

4.5.9 cDNA construction and qRT-PCR analysis

cDNA was generated using the published protocol from the Promega Improm-II system, replacing the reverse transcriptase with Invitrogen m-MLV reverse transcriptase. qRT-PCR was performed with iTaq universal SYBR Green Supermix and following manufacturer's instructions using a Roche Lightcycler 480 System. Fold changes upon PZN treatment were calculated as described previously (Schmittgen and Livak, 2008).

4.5.10 Membrane depolarization

Three independent stationary phase cultures of *B. anthracis* Sterne 7702 were used to inoculate fresh LB and grown to OD_{600} 0.5 at 37 ˚C with shaking. Aliquots (10 µL) were diluted

to 1 mL in PBS containing 3 mM $DiOC_2(3)$ (3,3'-diethyloxacarbocyanine iodide) and compounds (DMSO - vehicle, 5 µM carbonyl cyanide *m*-chlorophenyl hydrazone (CCCP), 3.0 µM daptomycin, 0.5 µM PZN, 1.0 µM PZN). Cells were mixed at 21 °C for 30 min prior to analysis by flow cytometry (BD LSR II Flow Cytometry Analyzer). Voltages for fluorescein isothiocyanate (FITC) and propidium iodide (PI) fluorescence were set so that average counts per cell were between 10^3 and 10^4. Geometric means for fluorescence ratios were normalized to the control $DiOC_2(3)$ samples.

4.5.11 Compound preparation

Me$_2$-Arg-Az$_5$. Me_2-Arg-Az_5 was synthesized as previously described (Sharma *et al.*, 2013).

PZN-Cy5. PZN (500 µg, 3.74 x 10^{-7} mol) in 20 µL dimethylformamide (DMF) was mixed with 5 µL *N,N'*-diisopropylethylamine (DIPEA), 10 µL of a 190 mM solution of 1-hydroxybenzotriazole (HOBt) in DMF, and 10 µL of a 190 mM solution of 1-ethyl-3-(3-dimethylaminopropyl)carbodiimide (EDC) in DMF for 15 min at 21 °C. Then 29.3 µL of a 10 µg/µL solution of Cy5 amine (Lumiprobe) in DMF was added. The reaction was protected from light and stirred at 22 °C for 24 h. The sample was dried by speed vacuum, redissolved in 5% MeOH, and purified on a Sep-Pak C_{18} cartridge (Waters) on a gradient from 0 – 100% MeOH. Fractions containing PZN-Cy5, as determined by MALDI-TOF mass spectrometry, were combined and their purity assessed by analytical HPLC (Thermo BetaSil C_{18} column [250 mm × 4.6 mm], 40 – 95% MeOH). Concentration was determined using the extinction coefficient of Cy5 in DMSO (ε_{646} = 250,000 L cm^{-1} mol^{-1}).

Daptomycin-Cy5. A 1 mg/mL solution of daptomycin in DMSO was prepared and 33 µL was mixed with 2 µL of 10 mM Cy5 NHS ester (Lumiprobe) and stirred at 22 °C, protected from light, for 4 h. Labeled compound was purified by reverse-phase chromatography on a Perkin Elmer Flexar HPLC outfitted with a Thermo Scientific BetaSil C_{18} column (250 mm × 4.6 mm

I.D., 5 µm particle size) using 10 mM NH_4HCO_3 as the aqueous phase on a 45 min gradient from 25 – 95% MeCN at a flow rate of 1 mL/min. Absorbance monitoring at 647 nm was used to identify the fraction containing daptomycin-Cy5, which was confirmed by MALDI mass spectrometry. Purity was determined by a second analytical HPLC run using the same solvents on a 30 min gradient from 40 – 95% MeOH. Concentration was determined using the extinction coefficient of Cy5 in DMSO.

Biotin-PZN (N-terminal label). A 100 mM solution of EZ-link *N*-hydroxysuccinimide (NHS) Biotin (Thermo Scientific) in 80% MeCN, 10 mM MOPS (pH 8.0) was prepared. DesmethylPZN (200 µg, 1.53×10^{-7} mol) was dissolved in 24 µL of the same buffer and treated with 6 µL EZ-link NHS biotin solution for 4 h at 22 °C. The solvent was removed by speed vacuum and the sample was dissolved in MeOH for purification by HPLC (BetaSil C_{18} column, 250 mm × 4.6 mm, 1 mL/min, 50 – 95% MeOH over 60 min, 10 mM NH_4HCO_3 aqueous phase, monitored at 254 nm). Fractions containing purified biotin-PZN were combined, dried, and redissolved in DMSO. *B. anthracis* Sterne 7702 susceptibility was determined to be >32 µg/mL using a standard microbroth dilution assay.

PZN-Biotin (C-terminal label). PZN (500 µg, 3.74×10^{-7} mol) was dissolved in 10 µL DMF and 1 µL DIPEA was added to the sample. A solution of 2.0 mM EDC and 2.0 mM HOBt in DMF was prepared and 2 µL was added to the PZN. After 5 min stirring, 1.0 mg biotin cadaverine was added to the reaction and allowed to proceed at 22 °C for 30 h. The reaction was dried by speed vacuum, redissolved in MeOH, and purified by HPLC (BetaSil C_{18} column, 250 mm × 4.6 mm, 1 mL/min, 50 – 95% MeOH over 60 min, 10 mM NH_4HCO_3 aqueous phase, monitored at 254 nm). Fractions containing purified PZN-biotin were combined, dried, and redissolved in DMSO. *B. anthracis* Sterne 7702 susceptibility was determined to be 32 µg/mL by a standard microbroth dilution assay.

PZN-diazirine-alkyne. PZN (6.68 mg, 5.0×10^{-6} mol) was dissolved in 75 µL DMF and 1.4 µL Et_3N was added with stirring. The sample was cooled in an ice bath to 0 ˚C. HOBt (0.95 mg, 0.007 mmol) and EDC (1.1 mg, 0.007 mmol) were dissolved in 100 µL DMF and added to the PZN. 2-(2-azidoethyl)-2-(but-3-ynyl)-1,3-dioxolane (0.96 mg, 0.007 mmol) (Li *et al.*, 2013) was dissolved in 200 µL DMF and 24 µL was added after 10 min at 0 ˚C with stirring, protected from light. The reaction was allowed to warm to 22 ˚C and allowed to proceed for 24 h. The solvent was removed by speed vacuum and the sample was redissolved in MeOH. The sample was purified by HPLC (BetaSil C_{18} column, 250 mm × 4.6 mm, 1 mL/min, 50 – 95% MeOH over 60 min, 10 mM NH_4HCO_3 aqueous phase, monitored at 254 nm). Fractions containing purified PZN-diazirine-alkyne were combined, dried, and redissolved in DMSO. *B. anthracis* Sterne 7702 susceptibility was determined to be 32 µg/mL using a standard microbroth dilution assay.

4.5.12 Structural characterization of PZN derivatives

Purified samples were dried by speed vacuum and dissolved in 50% MeCN supplemented with 1% (v/v) acetic acid. The diluted samples were directly infused using an Advion Nanomate 100 to an LTQ-FT hybrid linear ion trap-FTMS system (ThermoFisher) operating at 11 T. The MS was calibrated weekly using calibration mixture following the manufacturer's instructions, and tuned daily with Pierce LTQ Velos ESI Positive Ion Calibration Solution (ThermoFisher). Spectra were collected in profile mode with a resolution of 100,000. The singly charged ions were targeted for CID using an isolation width of 5 *m/z*, a normalized collision energy of 35, an activation q value of 0.4, and an activation time of 30 ms. Data analysis was performed using Thermo Xcalibur software.

4.5.13 Affinity purification using PZN-Biotin

LB (200 mL) was inoculated with 10 mL stationary phase *B. anthracis* Sterne 7702. The culture was grown with shaking at 37 °C to OD_{600} 0.5. The sample was divided into 100 mL aliquots, centrifuged, and individually resuspended in 1.5 mL lysis buffer (50 mM Tris, 500 mM

NaCl, 2.5% v/v glycerol, 0.1% v/v Triton X-100, pH 7.5) with 500 mU mutanolysin. After equilibrating for 30 min at 22 °C, the samples were sonicated (4 × 30 s, 50% amplitude) and harvested by centrifugation (17,000 × *g*, 10 min). The insoluble fractions were resuspended in 1.5 mL 3-[(3-cholamidopropyl)dimethylammonio]-1-propanesulfonate (CHAPS) buffer (50 mM Tris-HCl, 150 mM NaCl, 1% w/v CHAPS, pH 7.5) and sonicated (10 s, 50% amplitude). One sample was treated with 1.0×10^{-7} mol PZN-biotin and the other was treated with vehicle (DMSO). The samples were treated for 30 min at 22 °C before the addition of 100 µL streptavidin-agarose resin suspension (pre-equilibrated with Tris buffer, 50 mM Tris-HCl, 150 mM NaCl, pH 7.5). After mixing for 3 h at 22 °C, samples were applied to Bio-Rad spin columns and the flow through was collected. The resin was washed (5 × 4 mL Tris buffer). The resin was then resuspended in 200 µL 1% SDS in PBS and boiled for 10 min. After cooling, the eluent was collected and analyzed by SDS-PAGE for the presence of unique bands in the sample containing PZN-biotin. Unique bands, as visualized by Coomassie and silver stain, were not found compared to the vehicle-treated sample (data not shown). Samples were also analyzed by Western blot using the following procedure: proteins were transferred by electroblot to a polyvinylidene fluoride (PVDF) transfer membrane (EMD Millipore). The membrane was blocked overnight at 4 °C in TBS containing 0.1% (v/v) Tween-20 (TBST buffer), treated for 1 h at 4 °C with 1/3,000 dilution of streptavidin-HRP in TBST, and then washed (2 × 30 s then 5 × 5 min) with TBST. After washing once in PBS (1 × 30 s), the membrane was treated with 1:1 hydrogen peroxide solution:luminol solution (Bio-Rad) for imaging.

4.5.14 Photoaffinity purification using PZN-diazirine-alkyne

The procedure used for photoaffinity purification studies was similar to that of affinity purification experiments, except that the samples were incubated with PZN-diazirine-alkyne or vehicle (DMSO) for 4 h at 4 °C, protected from light. The cells were then exposed to UV (4 W, 365 nm) for 15 min at 22 °C to induce crosslinking. The samples were pelleted and resuspended

in PBS containing 1 mM $CuSO_4$, 128 µM tris(3-hydroxypropyltriazolylmethyl)amine, 1.2 mM sodium ascorbate, and 50 µM biotin-azide for 1 h at 22 °C. The cells were then centrifuged (4,000 × *g*, 2 min), the supernatant was decanted, and the cells were resuspended in PBS treated with 200 U/mL mutanolysin. After incubation for 1 h at 37 °C, cells were sonicated as previously described. The insoluble fraction was separated by centrifugation and resuspended as previously described. Clarified lysates and insoluble fractions were all enriched with streptavidin-agarose resin as previously described, and eluents were compared by SDS-PAGE followed by Western blot and mass spectrometric analysis.

4.5.15 Macromolecular synthesis assay

Radiolabel incorporation into cellular macromolecules was carried out as previously described (Cotsonas King and Wu, 2009). Briefly, identical *B. anthracis* Sterne 7702 cultures were grown to an OD_{600} of 0.6 in Luria Broth and diluted to a final OD_{600} of 0.3. Radiolabelled precursor was added to a final concentration of 0.1 µCi, and compound (either PZN or control) was added to 1×, or 2× the MIC. Samples were taken at 60 min post-compound addition. OD_{600} at each time point was determined using identically treated cultures lacking radioactive compound. The macromolecules of the cultures treated with radiation were precipitated using trichloroacetic acid on glass filter disks and washed with dilute acid and ethanol successively. The filters were placed in scintillation vials with Ultima Gold scintillation cocktail. Radioactive counts were determined using a liquid scintillation analyzer (PerkinElmer Tri-Carb 2910 TR). The macromolecules, radiolabelled precursors, and their corresponding control antibiotics were as follows:

cell wall: [1,6-^{3}H (N)] N-acetyl-D-glucosamine (ARC, ART 0142), vancomycin control

protein: [U-^{14}C] L-amino acid mixture (MP, 1014750), chloramphenicol control

RNA: [^{14}C(U)] uridine (ARC, ARC 0154), rifampicin control

fatty acid: acetic acid [1-^{14}C] sodium salt (ARC, ARC 0101A), triclosan control

4.5.16 Confocal microscopy

In general, cells were prepared by inoculating 5 mL LB with 200 µL of a stationary phase culture. After growing to an OD_{600} of 0.5 at 37 °C with shaking, 1 mL aliquots were centrifuged (3 min, 8000 × *g*), decanted, and resuspended in sterile PBS. Slides were prepared by mixing 1:1 (v/v) cell suspensions in PBS and liquefied low gelling temperature agarose (Sigma-Aldrich, 2% w/v in water). All microscopy images were obtained using a Zeiss LSM 700 Confocal microscope with a 63×/1.4 Oil DIC objective and processed using Zen 2012 software. Laser intensity and gain were kept at a minimum and held constant for all experiments. Linear contrast was equally applied during image processing. To localize PZN, *B. anthracis* Sterne 7702 was treated in PBS with 0.2 µM PZN-Cy5 for 30 min at 22 °C. After washing in PBS (3 × 500 µL), cells were resuspended in a final volume of 250 µL PBS. Competition experiments were performed using PR06 (PZN-resistant) in PBS treated with DMSO (vehicle) or 1 µM PZN for 20 min at 22 °C before the addition of 0.05 µM PZN-Cy5. After 20 min at 21 °C, the cells were washed in PBS (3 × 500 µL) and resuspended in a final volume of 250 µL PBS. Sterne underwent co-treatment in PBS with 0.2 µM PZN-Cy5 for 25 min before the addition of other fluorescent compounds. After 5 min additional treatment, cells were washed in PBS (5 × 500 µL) and resuspended in a final volume of 250 µL PBS. Concentrations used: NAO (Sigma-Aldrich), 1 µM; Dil-C12, 1 µM; BODIPY-vancomycin, 1 µM; Bocillin-FL, 1 µM. For CL experiments, cells were treated with EtOH (vehicle), 10 µg/mL CL, or 100 µg/mL CL in addition to 0.2 µM PZN-Cy5 for 30 min.

4.5.17 Super-resolution microscopy (STORM)

Cells for 3D super-resolution microscopy were grown and treated with PZN-Cy5 as described for confocal microscopy. The cells were immobilized on Nunc® Lab-Tek® 8-well chambered coverglass (Sigma-Aldrich) coated with 0.1% (w/v) poly-L-lysine (Sigma-Aldrich). After 10 min incubation, unattached cells were removed by washing chambers with sterile PBS.

Chambers were filled with 500 µL imaging buffer (10 mM NaCl, 50 mM Tris-HCl (pH 8.5), 10% w/v glucose). Immediately prior to imaging, cysteamine (Sigma-Aldrich, 10 mM final concentration), catalase (EMD Millipore, 909 U/mL), and pyranose oxidase (Sigma-Aldrich, 4.44 U/mL) were added to the imaging buffer. 3D super-resolution microscopy was performed as described previously (Fei *et al.*, 2015; Rust *et al.*, 2006; Shashikanth *et al.*, 2015). Briefly, samples were imaged using an Olympus IX-71 inverted microscope outfitted with a 100× NA 1.4 SaPo oil objective. Mechanical shutters (LS6T2, Unibliz) were used to alternatively excite the sample with a red laser (DL640-100-AL-O, Crystalaser) and reactivate Cy5 with a violet laser (405 nm, 20 mW, Spectra Physics Excelsor). The lasers were expanded by 7.5×, reflected by a dichoroic mirror (Semrock FF408/504/581/667/762-Di01-25X36), and sent to the sample chamber with a focusing lens that also creates an incidental angle slightly smaller than the total internal reflection angle, reducing the background signal while allowing illumination of several hundred nm along the z-axis. The emission signal from the sample was passed through an emission filter (Semrock FF01-594/730-25) and two additional notch filters (Semrock NF01-568/647-25X5.0 and NF01-568U-25), and was imaged on an EMCCD camera (DV887ECS-BV, Andor Tech). A cylindrical lens (SCX-50.8-1000.0-UV-SLMF-520-820, CVI Melles Griot, 2 m focal length) in the emission beam path induced astigmatism for 3D detection (Huang *et al.*, 2008). ASI CRISP (Applied Scientific Instrumentation) and a piezo-objective (PI P-721.10) were used to compensate for vertical drift during data collection. The horizontal drift was corrected in the post data acquisition step by the analysis software utilizing the correlation function (Bates *et al.*, 2007). The data analysis software was provided by Xiaowei Zhuang (Rust *et al.*, 2006) and modified for 3D imaging.

4.5.18 2D projection analysis

2D projection analysis was used to determine spatial localization of PZN on *B. anthracis* cells. A total of 11 cells imaged by super-resolution microscopy were aligned lengthwise along

the y-axis, and then sectioned to remove poles and septa. Cells were projected onto the XZ plane and divided into units of 30 × 30 nm^2. Within each unit, spot density was determined and color-mapped. The probability of finding a dye molecule a certain distance R from the y-axis was calculated for radial windows with a 20 nm bin size and normalized to the area of the radial window.

4.5.19 PZN-Cy5 cluster analysis

A density-based clustering analysis algorithm, DBSCAN (Daszykowski *et al.*, 2002), was used as previously reported (Fei *et al.*, 2015; Shashikanth *et al.*, 2015) to analyze super-resolution images of PZN-Cy5-treated *B. anthracis*. Briefly, spots in super-resolution images of 14 cells were grouped into clusters based on spatial density. The required *Npts* and *Eps* parameters were set to 19 and 40 nm, respectively, and used to identify core points in high density spots. Parameter values empirically set such that core points within a cluster were within *Eps* distance of each other and surrounded by at least *Npts* points. Cluster borders were defined by points located with *Eps* distance to any core point. Cluster size was calculated as twice the average distance between the cluster center and every point in the cluster.

4.5.20 Selection of spontaneous PZN-resistant mutants

Spontaneous PZN-resistant mutants were generated by plating 2 × 10^8 *B. anthracis* Sterne 7702 cells grown to stationary phase onto a PZN plate containing 4 × PZN MIC. Surviving colonies were tested for sustained PZN resistance via microbroth dilution as described above. Resistant mutants PR01, PR02, PR05, and PR06 were subjected to genomic DNA isolation as follows: 3 × 10 mL cultures of each strain were grown to stationary phase, harvested, and resuspended in 400 µL of water. Cells were lysed with 50 µL of 10% SDS and 5 µL of 20 mg/mL RNase solution at 22 °C for 5 min. DNA was isolated via 25:24:1 phenol/chloroform/isoamyl alcohol extraction, followed by addition of 24:1 chloroform/isoamyl alcohol. DNA precipitation via cold isopropyl alcohol and a subsequent 70% ethyl alcohol wash resulted in purified gDNA.

4.5.21 Whole genome sequencing and assembly

Genomic libraries for resequencing were prepared using the TruSeq DNAseq Sample prep kit (Illumina, San Diego, CA). Sequencing was performed on a HiSeq 2000 with Version 3 Chemistry for 1×100 cycles. SNP and DIP discovery was performed with two different methods. Regarding PR02, PR05, and PR06, CLC Genomics Workbench SNP and DIP discovery pipelines were employed using with the publicly available *B. anthracis* str. Sterne genome NC_005945.1 as a reference. PR01 required de novo assembly with IDBA UD version 1.0.9, followed by whole genome alignment and SNP discovery using Mauve version 2.3.1. Resistant mutants PR03 and PR04 were selected separately and underwent Sanger sequencing after PCR amplification of *bas4114* and sequencing with the BamHI-BAS4114-f primer (Table 4.2). The WGS data discussed in this publication have been deposited in NCBI's GenBank and are accessible via BioProject accession number: PRJNA295544. Within this BioProject are individual accession numbers for each *B. anthracis* strain (taxId:1392) for which whole genome sequencing was performed: CP012720, PR01; CP012721, PR02; CP012722, PR05; CP012723, PR06; CP012724, PR07; CP012725, PR08; CP012726, PR09-1; CP012727, PR09-4; CP012728, PR10-4; CP012730, Parent1 (for PR01 through PR06); CP012729, Parent2 (for PR07 through PR10-4.

4.5.22 Genetic deletion of *bas4114-bas4117*

Markerless genetic deletions were created in *B. anthracis* Sterne 7702 following established protocols (Janes and Stibitz, 2006). The 500 base pairs upstream and downstream the bas4114-4117 gene cluster were cloned into the homologous recombination vector pBKJ236 using Gibson cloning (New England Biolabs) with the BamHI and NotI restriction sites. The pBKJ236 constructs were transformed into the *E. coli dam dcm* strain SCS110. Overnight cultures of the vector-containing SCS110 strain grown in LB containing 500 µg/mL erythromycin were used for conjugation along with overnight cultures of the conjugation helper strain *E. coli* SS1827 grown in LB with 200 µg/mL ampicillin and *B. anthracis* Sterne 7702 grown in BHI.

From the stationary phase cultures, 400 µL were removed and washed twice by pelleting and suspending in 500 µL of LB to remove residual antibiotic. The pellets were resuspended in 200 µL of LB, then mixed thoroughly in equal volumes, and 150 µL of the mixture was inoculated onto a BHI agar plate without spreading. The inoculum was allowed to dry and the plate was incubated at 22 °C for 24 h. The entire growth was then carefully removed from the plate, resuspended in 200 µL of LB, and spotted onto a BHI agar plate containing 5 µg/mL erythromycin and 60 U/mL polymyxin B (BHIep). The culture was allowed to dry and then subsequently plated to achieve single colonies. The plate was incubated at 22 °C until single colonies of *B. anthracis* Sterne 7702 were visible (~48 h). A single colony was used to inoculate a 2 mL culture of BHI containing 5 µg/mL erythromycin, and the culture was incubated with shaking at 22 °C overnight. The saturated culture was used to inoculate a fresh culture of BHI containing 5 µg/mL at a 1:1000 dilution. This culture was incubated at 37 °C with shaking until saturation (~8 h), then 150 µL of the culture was spotted onto a BHIep plate and allowed to dry. The spot was streaked for single colonies and the plate was incubated at 37 °C overnight. A single colony was picked and used to make competent cells as previously described (Quinn and Dancer, 1990). Briefly, a colony was used to inoculate a 1 mL culture of LB containing 0.1% glucose (LBG). The culture was incubated at 37 °C without shaking for 10 min, and then used to inoculate 25 mL of LBG in a 250 mL sealable Erlenmeyer flask. The culture was incubated with shaking at 100 rpm at 37 °C until it reached an OD_{600} of 0.20, at which point it was transferred to a 50 mL conical tube and pelleted at 4000 × *g* at 4 °C for 10 min. The spent media was discarded and the pellet was washed with ice cold electroporation buffer (EB; 10% w/v sucrose, 15% v/v glycerol, 2 mM potassium phosphate, pH 7.8) twice. The cells were resuspended in 400 µL of cold EB, transferred to a 0.4 cm gap electroporation cuvette (USA Scientific), and incubated on ice for 10 min. A plasmid encoding the I-SceI restriction enzyme, pSS4332 (Cybulski *et al.*, 2009), was added as 10 µL of a 500 ng/µL stock and the cells were pulsed one time at 2.5 kV, 25

μF, 200 Ω (mean time constant of 4.4 ms). The cells were then placed on ice for 10 min before being diluted with 600 μL LBG. The cells were recovered at 37 °C for 2 h and then plated on LBG agar plates containing 25 μg/mL kanamycin. Colonies were pooled and passaged repeatedly on BHI agar plates containing 25 μg/mL kanamycin until erythromycin sensitive colonies could be isolated. Sensitive colonies with the desired genes deleted were determined by PCR amplification with the cloning primers and were then repeatedly streaked on antibiotic free BHI agar plates until kanamycin sensitive colonies were isolated. Gene deletion was confirmed by PCR amplification with gene specific primers (Figure 4.17) and the strains were confirmed to be sensitive to both kanamycin and erythromycin by plating on the appropriate antibiotic containing BHI agar plates.

After genetic deletion of *bas4114-4117*, a second round of spontaneously resistant mutants to PZN were selected and isolated as above. Serial-passage mutants were isolated as previously described (Friedman *et al.*, 2006), starting with three independent cultures of an OD_{600} of 0.1 *B. anthracis* Sterne 7702 Δ*bas4114-4117* in 0.25 μg/mL (0.25 × MIC) PZN LB. Cultures that grew were diluted to an OD_{600} of 0.1 and subjected to increased concentrations of PZN, until cultures were resistant to 64 μg/mL. Cultures were serially passaged onto PZN-free medium to confirm mutant stability. Genomic DNA was isolated as described above. All mutants derived from the Δ*bas4114-4117* deletion strain were sequenced as described and assembled via CLC Genomics Workbench and SNP analysis was performed with Mauve version 2.3.1.

4.5.23 Effect of cardiolipin on fluorescence intensity

Three independent stationary phase cultures of *B. anthracis* Sterne 7702 were used to inoculate fresh LB (200 μL into 5 mL LB) and the new cultures were grown to OD_{600} 0.5 at 37 ˚C with shaking. Samples were prepared by diluting 10 μL aliquots of culture to 1 mL in PBS containing 1 nM PZN-Cy5 and vehicle (EtOH), 10 μg/mL CL (Sigma Aldrich), or 100 μg/mL CL. After mixing at 22 °C for 30 min, cells were analyzed by flow cytometry as described above

for differences in PZN-Cy5 fluorescence intensity. Geometric means were normalized to the control samples.

4.5.24 Cardiolipin quantification from total lipid extracts

Cultures of *B. anthracis* Sterne 7702, *B. anthracis* Δ*bas4114-4117*, *B. anthracis* PR09-4, *B. anthracis* PR10-4, *B. subtilis* 168, *E. faecium* U503, and *S. aureus* USA300 (three independent 10 mL cultures for each strain) were grown for 20 h at 37 ˚C. LB containing an additional 1.5 M NaCl was inoculated with 200 µL aliquots of stationary phase cultures of *B. subtilis* 168, *E. faecium* U503, and *S. aureus* USA300 (three independent 10 mL cultures for each strain) and grown for 40 h at 37 °C. The cells were harvested by centrifugation (4000 × *g*, 10 min, 4 °C) and resuspended in 5 mL 2:1 $CHCl_3$:MeOH and 1.25 mL PBS, and then extracted for 1 h at 22 °C. The supernatant was removed after centrifugation (4000 × *g*, 10 min, 4 °C) and layers were washed with 1 mL $CHCl_3$ and 1 mL PBS. The organic layer was removed and dried by speed vacuum. The crude lipids were redissolved in 200 µL $CHCl_3$ and transferred to microfuge tubes, then dried again. The lipids were then dissolved in 20 µL $CHCl_3$ and separated by preparative TLC (Analtech Silica Gel G) using 2:1 $CHCl_3$:MeOH. The CL-containing spots were removed and extracted with 200 µL 2:1 $CHCl_3$:MeOH for 15 min with shaking. The extracts were dried by speed vacuum and redissolved in 20 µL $CHCl_3$. Each sample was spotted (0.5 µL) onto Merck Silica Gel 60 F_{254} analytical TLC plates and separated using 80:20:5 $CHCl_3$:MeOH:AcOH. The plates were developed in iodine and imaged using a Bio-Rad ChemiDoc XRS+. ImageJ was used to subtract background and measure spot density to determine percent CL out of total lipid content.

4.6 Acknowledgments

We are grateful to the Pasteur Institute, BEI Resources, O. Schneewind (U. Chicago), C. Turnbough (U. Alabama Birmingham), U.S. Department of Agriculture, ATCC, The *Caenorhabditis* Genetics Center, The Bacillus Genetic Stock Center, S. Shozhamannan (The

Naval Medical Research Center), V. Fischetti (Rockefeller U.), C. Marston (Center for Disease Control and Prevention), D. de Mendoza (U. Nacional de Rosario), J. Wells (UCSF), J. Helmann (Cornell U.), M. So (U. Arizona), P. Hergenrother (UIUC), H. Zhao (UIUC), P. Hanna (U. Michigan), and S. Leppla (National Institute of Allergy and Infectious Diseases) for providing strains and plasmids used in this study, Dr. Yao Shao Qin and Dr. Li Zhengqiu (National U. of Singapore) for providing 2-(2-azidoethyl)-2-(but-3-ynyl)-1,3-dioxolane, as well as Teresa Abshire, Stephanie Halasohoris, and Lynda Miller (U.S. Army Medical Research Institute for Infectious Diseases, USAMRIID) for providing us with γ phage and their assistance. We also thank Caitlin Deane for critical review of this chapter.

4.7 Figures

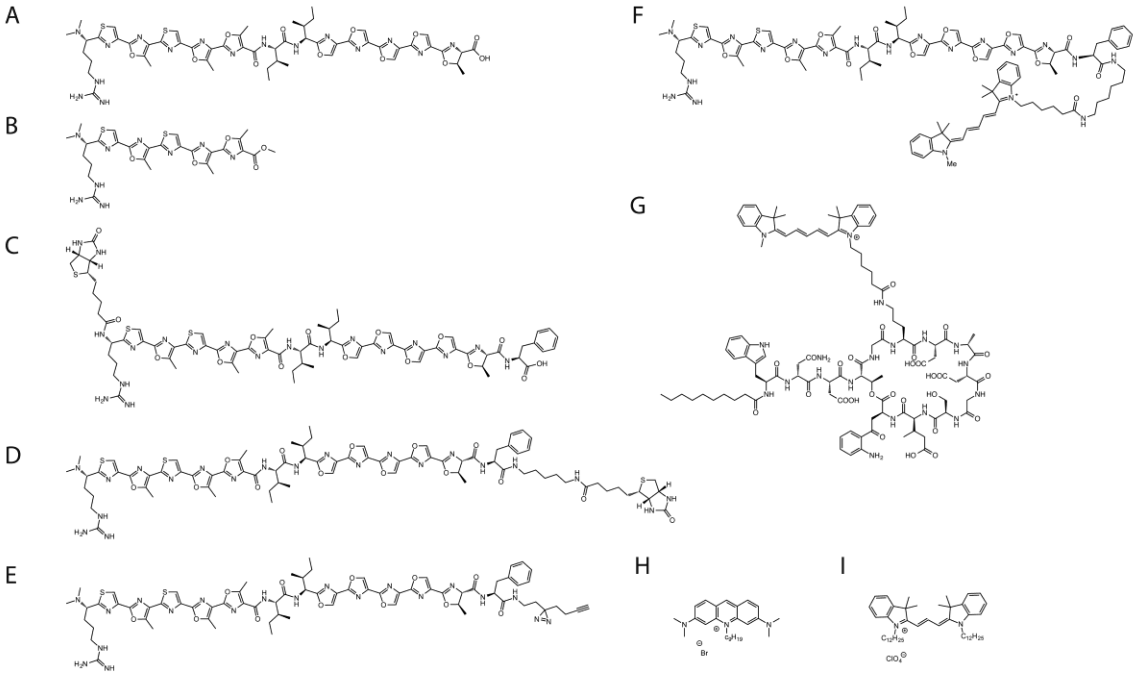

Figure 4.1 | Structures. Chemical structures of plantazolicin (PZN) (A), Me_2-Arg-Az_5 (B), Biotin-PZN (C), PZN-Biotin (D), PZN-photoaffinity probe (E), PZN-Cy5 (F), daptomycin (Dap)-Cy5 (G) NAO, nonyl acridine orange (H), and DilC12(3) perchlorate (I).

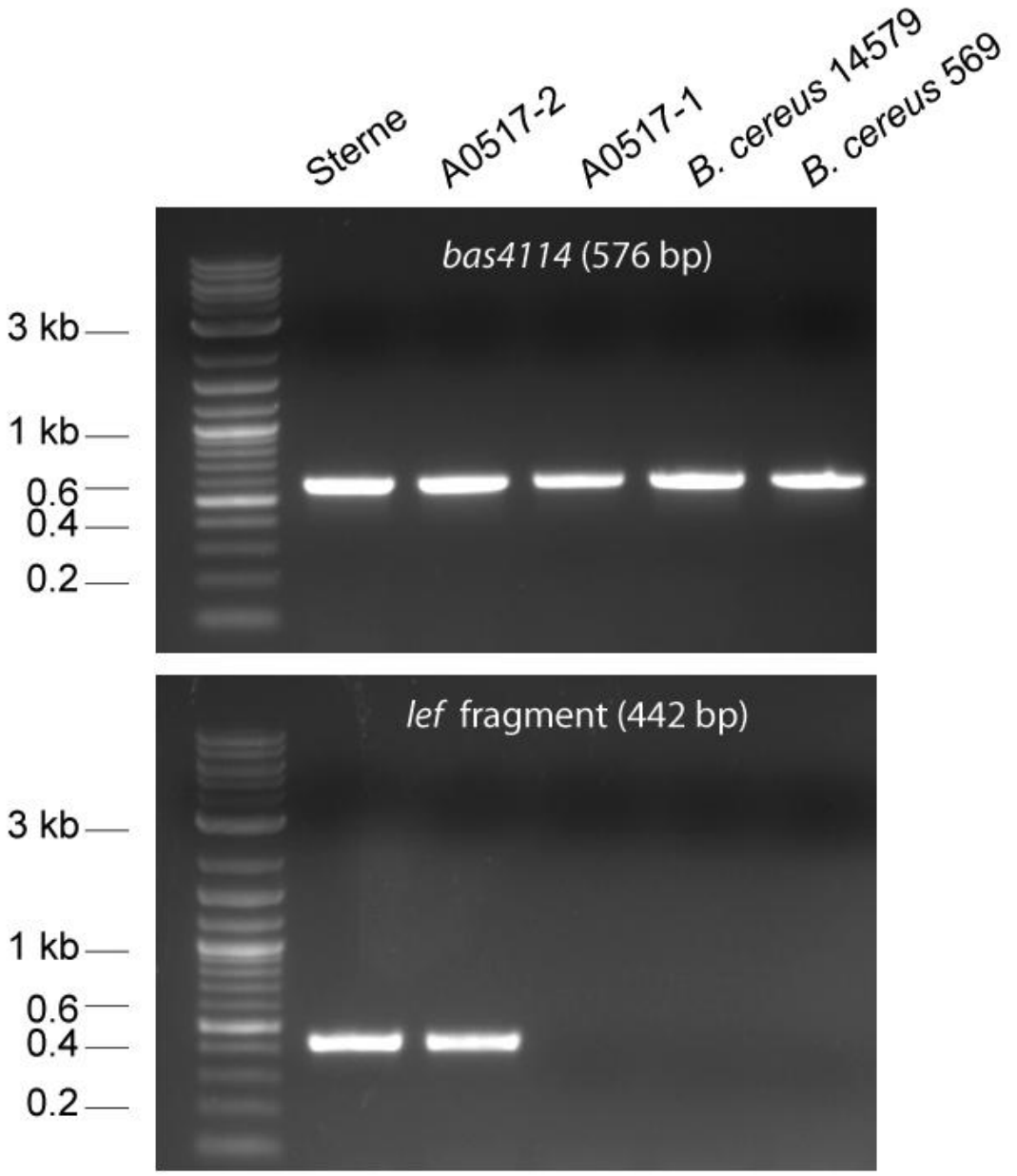

Figure 4.2 | Confirmation of plasmid loss in *B. anthracis* 34F2 LLNL A0517-1. (Top) PCR of a conserved chromosomal gene, *bas4114*. (Bottom) pXO1 encoded gene *lef* is not present in A0517-1 or the select *B. cereus* strains.

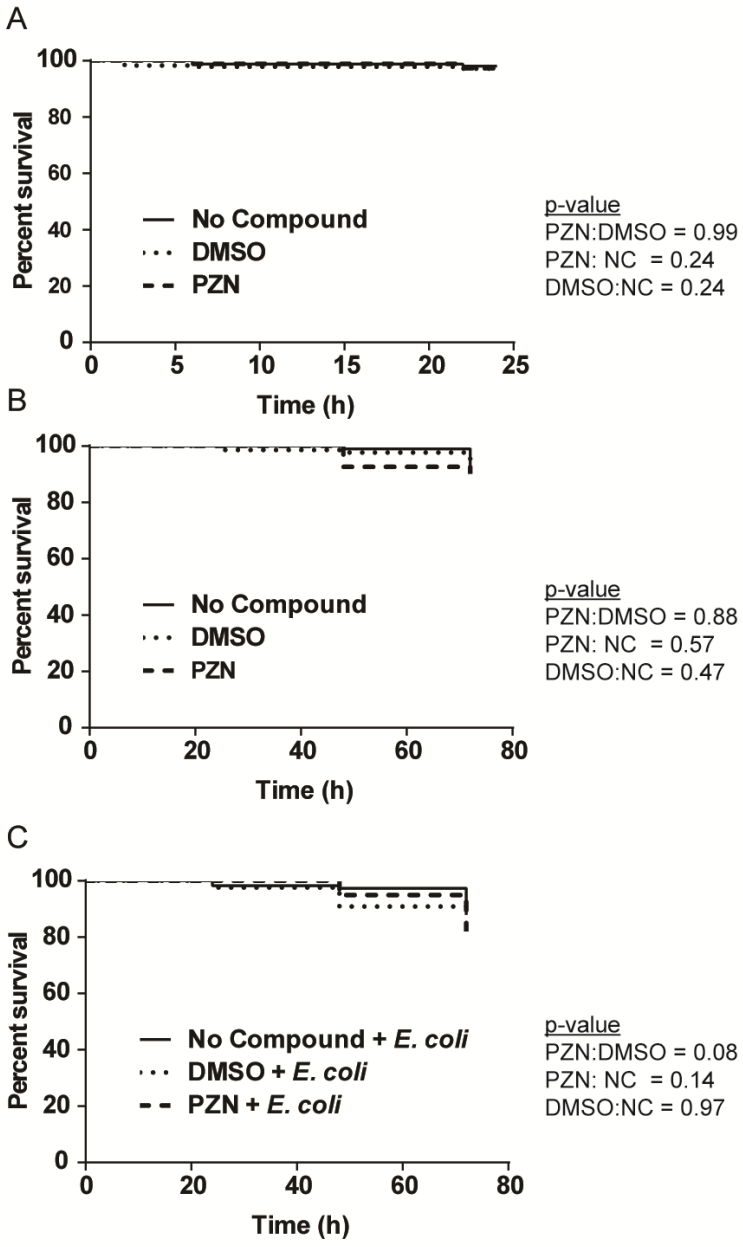

Figure 4.3 | PZN is not toxic to *Caenorhabditis elegans* using two different experiments. PZN was subjected to purified PZN during both liquid fast killing (A) and slow killing assays (B-C). Animals were treated with 64 μg/mL PZN and analyzed by live/dead screening over the course of the experiments. P-values were generated using the Log-rank (Mantel-Cox) test.

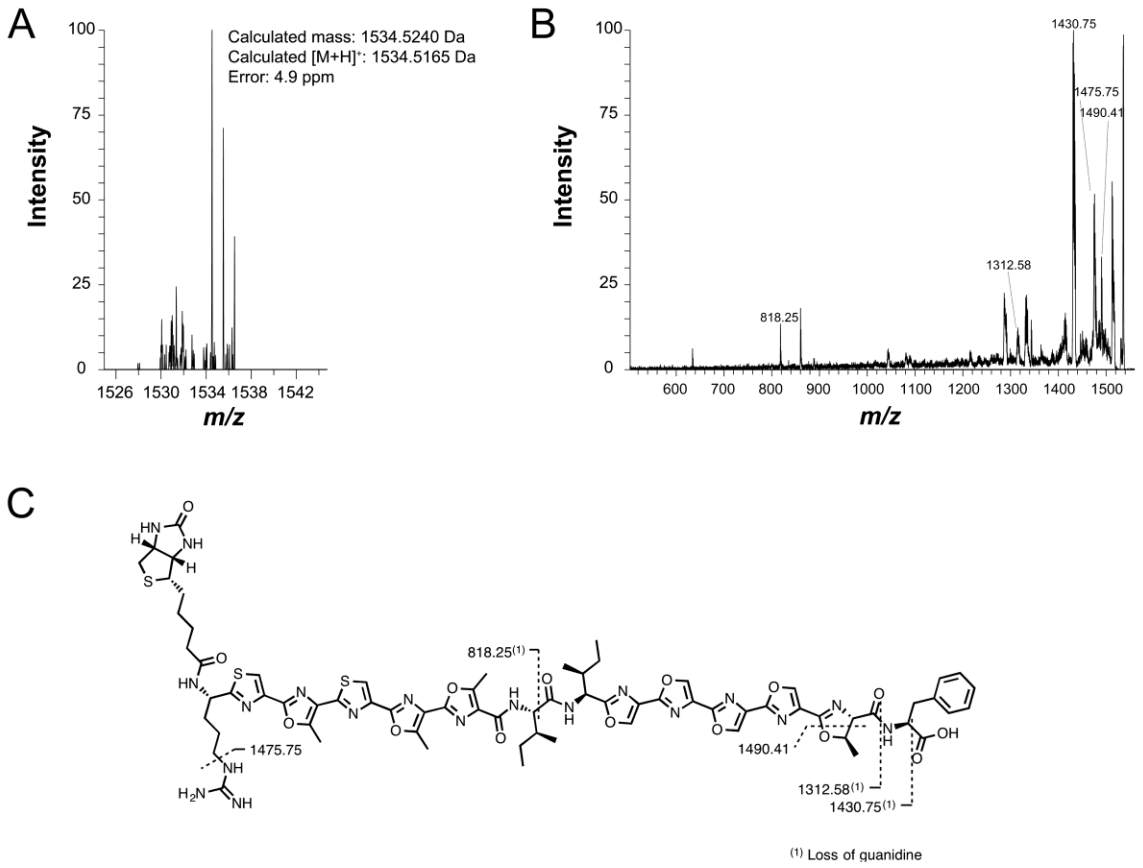

Figure 4.4 | Mass spectrometry structural characterization of biotin-PZN. (A) Mass spectrum of the $[M+H]^{2+}$ species by LTQ-FT-MS, which was used to calculate exact mass. (B) CID spectrum of the singly charged ion acquired by LTQ-FT-MS. Labeled peaks correspond to identified fragments of biotin-PZN, shown on the structure in panel (C).

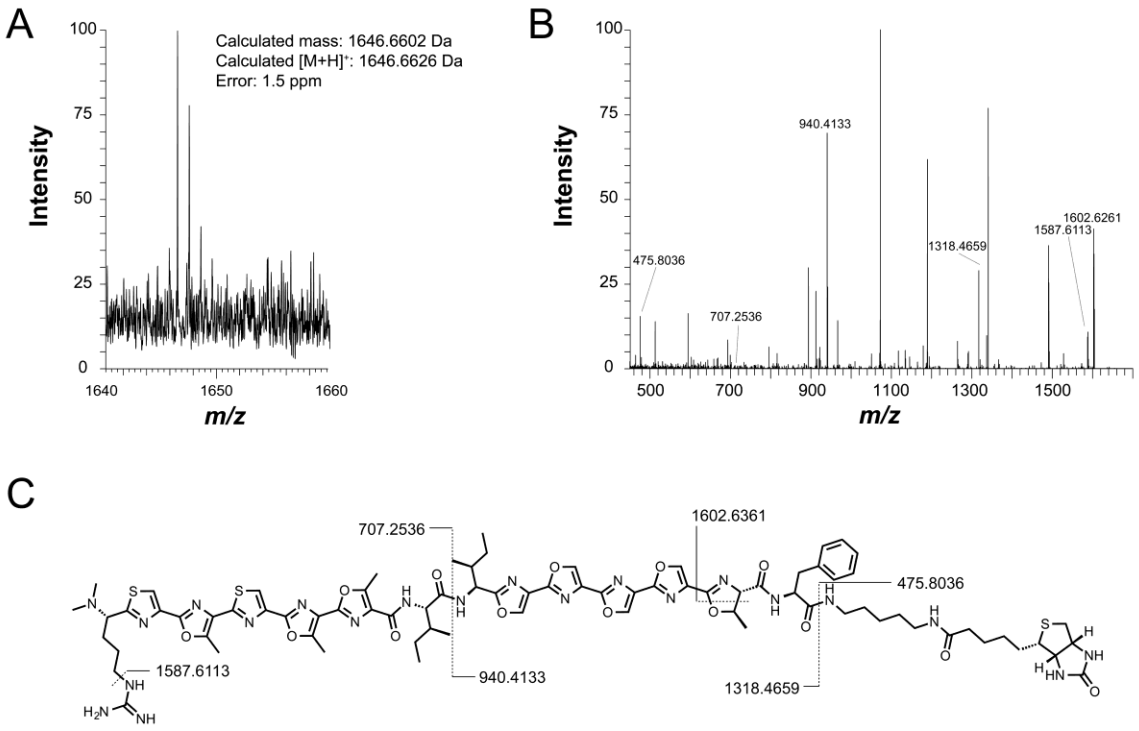

Figure 4.5 | Mass spectrometry structural characterization of PZN-biotin. (A) Mass spectrum of the $[M+H]^{2+}$ species by LTQ-FT-MS, which was used to calculate exact mass. (B) CID spectrum of the singly charged ion acquired by LTQ-FT-MS. Labeled peaks correspond to identified fragments of PZN-biotin, shown on the structure in panel (C).

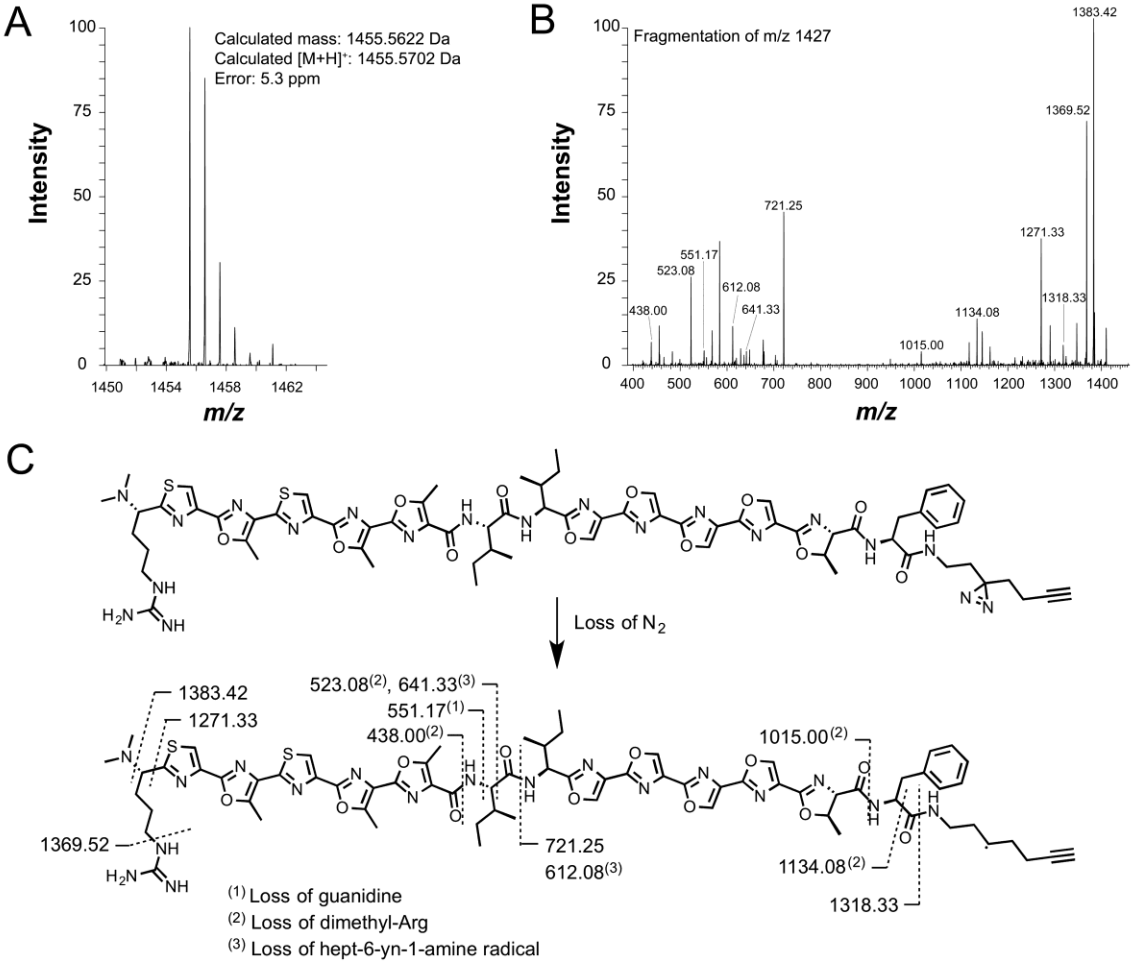

Figure 4.6 | Mass spectrometry structural characterization of PZN-photoaffinity probe. (A) Mass spectrum of the $[M+H]^{2+}$ species by LTQ-FT-MS, which was used to calculate exact mass. (B) CID spectrum of the *m/z* 1427 species, corresponding to the loss of N_2 from the original molecule. Labeled peaks correspond to identified fragments, shown on the structure in panel (C).

Figure 4.7

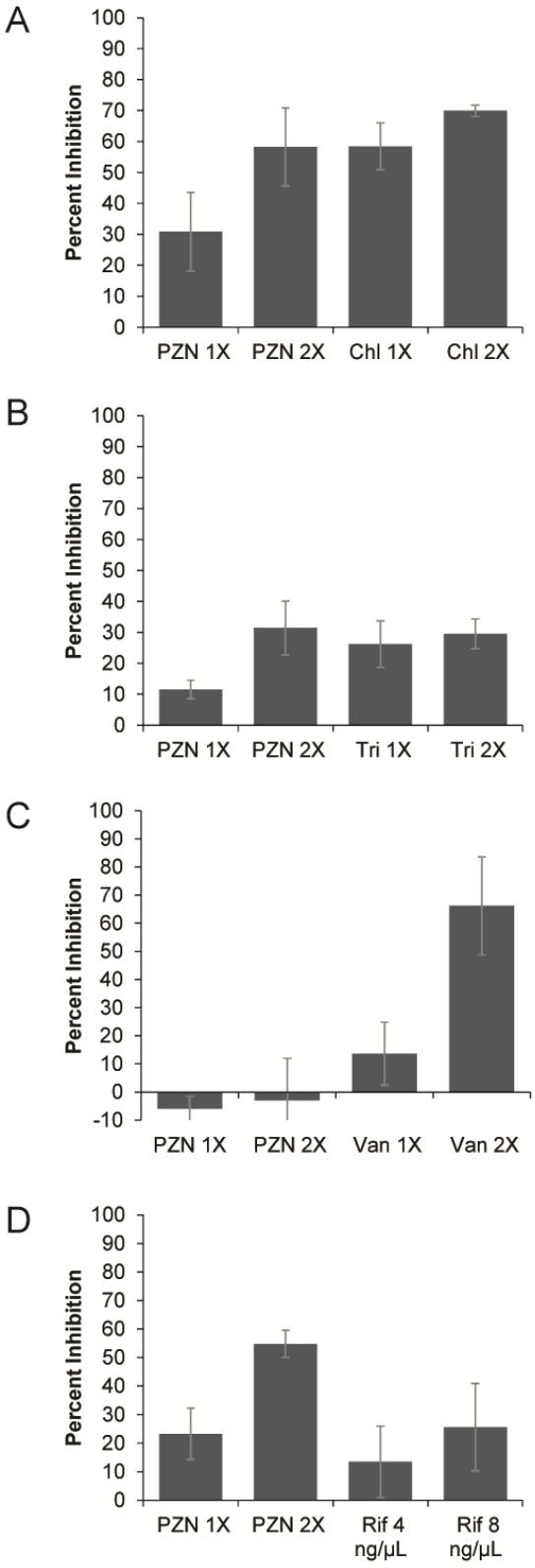
A
Percent Inhibition
100
90
80
70
60
50
40
30
20
10
0
PZN 1X
PZN 2X
Chl 1X
Chl 2X
B
Percent Inhibition
PZN 1X
PZN 2X
Tri 1X
Tri 2X
C
Percent Inhibition
-10
PZN 1X
PZN 2X
Van 1X
Van 2X
D
Percent Inhibition
PZN 1X
PZN 2X
Rif 4 ng/µL
Rif 8 ng/µL

Figure 4.7 (continued) | PZN treatment results in the inhibition of three out of four analyzed macromolecular pathways. *B. anthracis* cells were treated with 1 × or 2 × MIC PZN and the appropriate radiolabelled precursor to the macromolecule of interest. After incubation for 1 h, macromolecules were precipitated and radiolabelled precursor incorporation into protein (A), fatty acid (B), peptidoglycan (C), or RNA (D) was measured. Each experiment included samples treated with a control compound that is known to affect a particular pathway (protein: chloramphenicol; fatty acid: triclosan; peptidoglycan: vancomycin; RNA: rifampicin. All compounds were added at 1 × or 2 × MIC, except rifampicin, which required significantly lower concentrations to achieve medial inhibition. Percent inhibition was determined by comparing radioactive incorporation between cells containing compound vs. vehicle. Error is reported as standard deviation with n = 3.

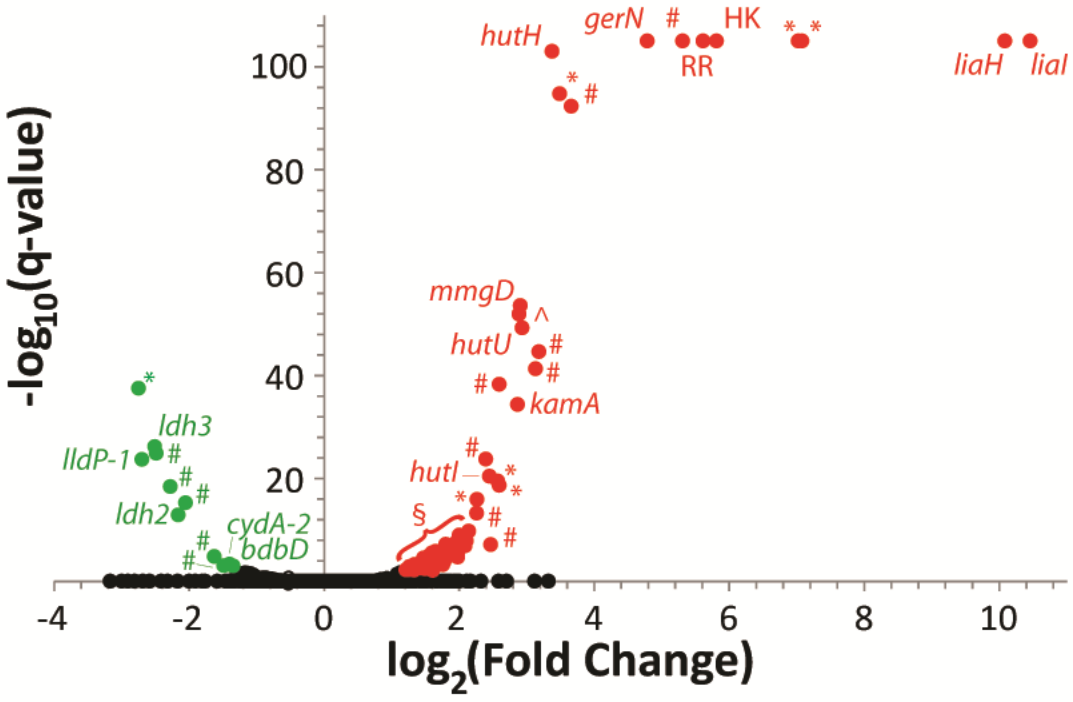

Figure 4.8 | *B. anthracis* gene expression profile when treated with PZN. A volcano plot represents the set of differentially regulated genes in response to treatment with 0.25 × MIC of PZN. Red (upregulated) and green (downregulated) points are genes with significantly altered expression in response to PZN treatment, while black genes did not meet the q-value (< 0.01) threshold. Genes where the q-value = 0 were given a value of 1×10^{-105}. Abbreviations: # – hypothetical, * – transporter, ^ – transcriptional regulator, *bdbD* – *B. subtilis* hypothetical homolog, *lldP-1* – L-lactate permease, *ldh2/3* – L-lactate dehydrogenase, *cydA-2* – cytochrome d ubiquinol oxidase, *mmgD* – citrate synthase 3, *hutHIU* – histidine utilization genes, *gerN* – germination protein, *kamA* – L-lysine 2,3-aminomutase, § – remaining upregulated genes. All differentially expressed genes are summarized in Table 4.5.

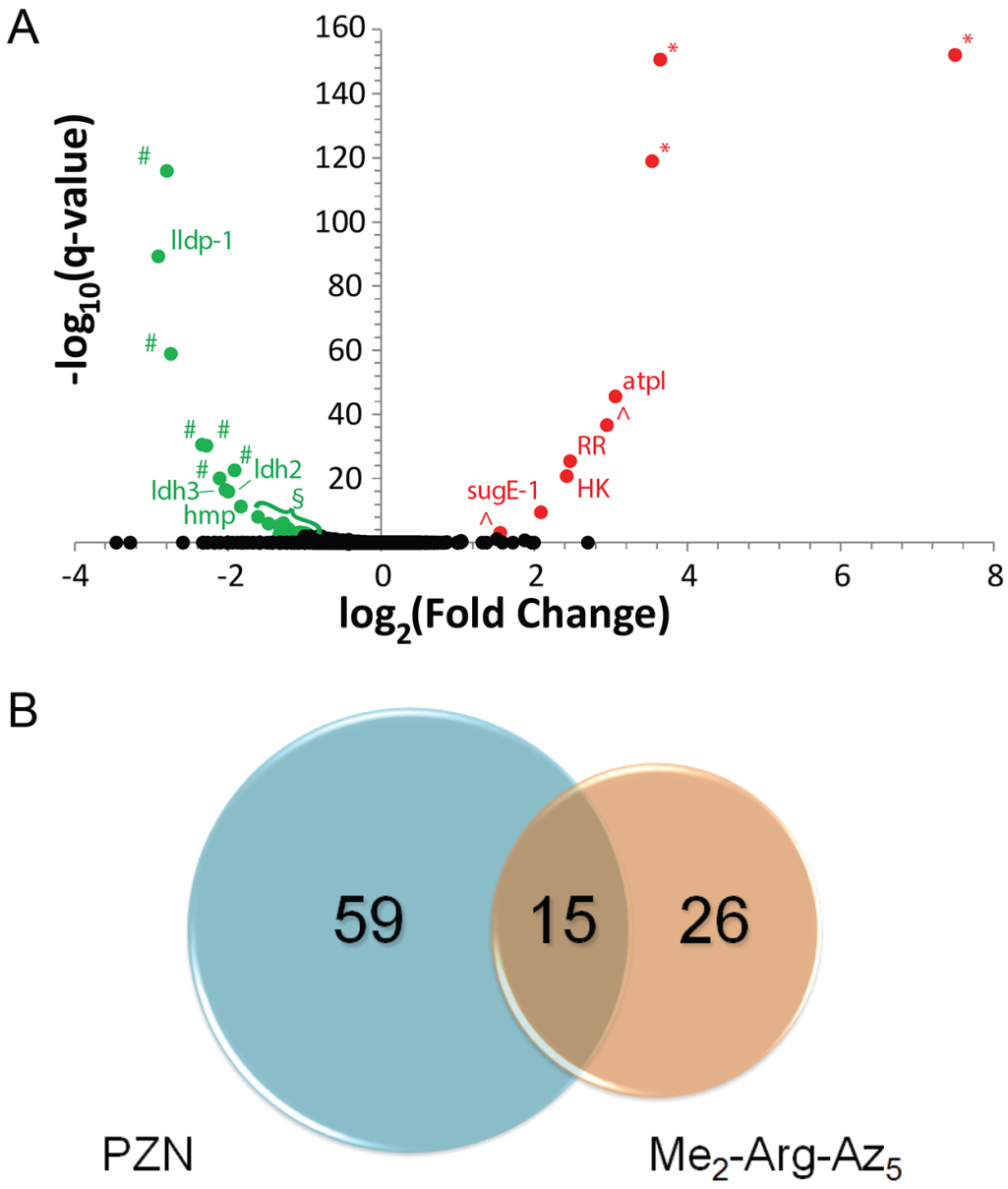

Figure 4.9 | The *B. anthracis* gene expression profile with Me_2-Arg-Az_5 differs from PZN treatment. (A) A volcano plot represents the set of differentially regulated genes in response to treatment with 0.25 × MIC of Me_2-Arg-Az_5. Red (upregulated) and green (downregulated) points are significantly expressed genes in response to Me2-Arg-Az5, while black genes did not meet the q-value (< 0.01) threshold. Genes where the q-value = 0 were given a value of E-155. Abbreviations: # – hypothetical, * – transporter, ^ – transcriptional regulator, atpI – ATP synthase protein I, hmp – nitric oxide dioxygenase, lldP-1 – L-lactate permease, ldh2/3 – L-lactate dehydrogenase, sugE-1 – EmrE protein (cationic drug membrane transporter), RR – response regulator, HK: histidine kinase , § – remaining upregulated. All genes are summarized in Table 4.10. (B) Venn diagram demonstrating the commonality of the PZN and Me_2-Arg-Az_5 expression profiles. The compilation of common genes is located in Table 4.9.

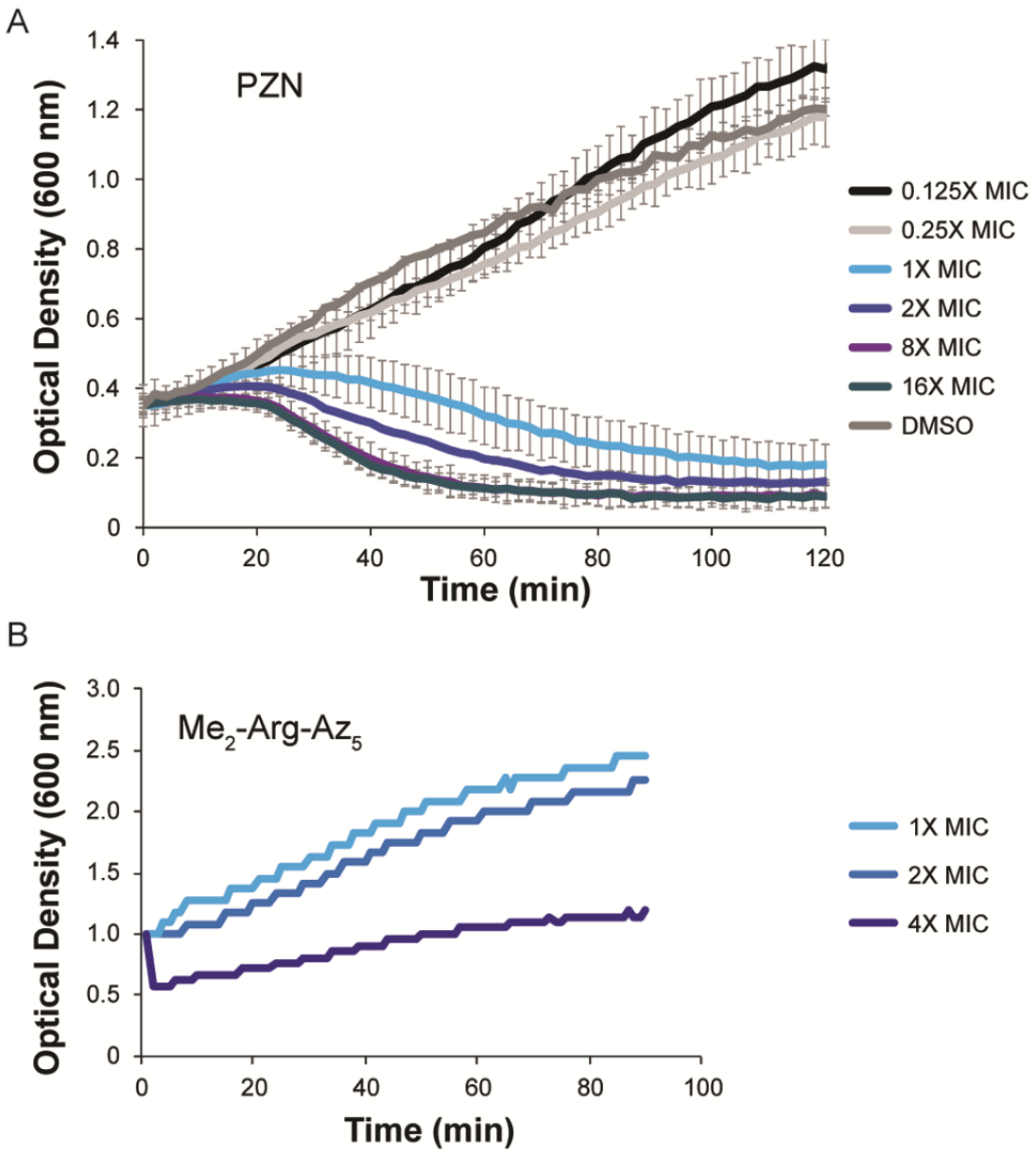

Figure 4.10 | Growth curves of PZN and Me_2-Arg-Az_5 reveal different phenotypes. (A) *B. anthracis* cells treated with PZN undergo rapid decrease in optical density with concentrations above the minimum inhibitory concentration (MIC, determined from microbroth dilution assays). Time points were collected every two minutes and adjusted to a 1-cm path length. Error is reported as standard deviation with n = 3. (B) *B. anthracis* treated with Me_2-Arg-Az_5. Reduction in optical density is observed briefly at 4 × MIC. Both growth curves were measured in duplicate and normalized to OD_{600} 0.35 (A) and 1.0 (B).

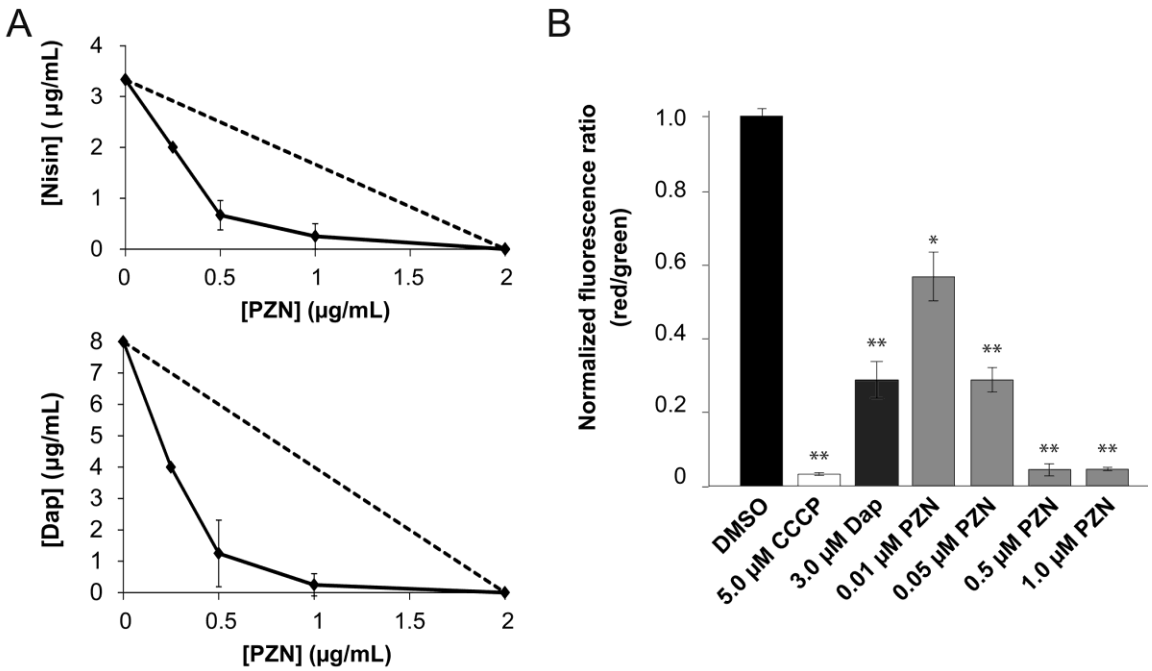

Figure 4.11 | PZN synergizes with cell envelope-acting antibiotics and depolarizes the *B. anthracis* membrane. (A) Isobolograms of the minimum inhibitory concentrations (µg/mL) of PZN with nisin (top) and daptomycin (bottom). Interactions taking place below the dotted line represent synergistic behavior. (B) Detection of membrane potential in *B. anthracis*. Red/green ratios were calculated using mean fluorescence intensities of cells treated for 30 min at RT with 0.1 µM $DiOC_2(3)$ and the vehicle of DMSO (negative control), 0.1 µM $DiOC_2(3)$ and 5.0 µM CCCP (positive control), 0.1 µM $DiOC_2(3)$ and 0.5 µM PZN, and 0.1 µM $DiOC_2(3)$ and 1.0 µM PZN. Data were normalized to the positive control sample of $DiOC_2(3)$ and vehicle (DMSO). Error is given as standard deviation with n = 3. P-values are given relative to the DMSO control with * indicating < 0.0005 and ** indicating < 0.0001. Abbreviations: Dap, daptomycin; $DiOC_2(3)$, 3,3'-diethyloxacarbocyanine iodide; CCCP, carbonyl cyanide *m*-chlorophenyl hydrazone.

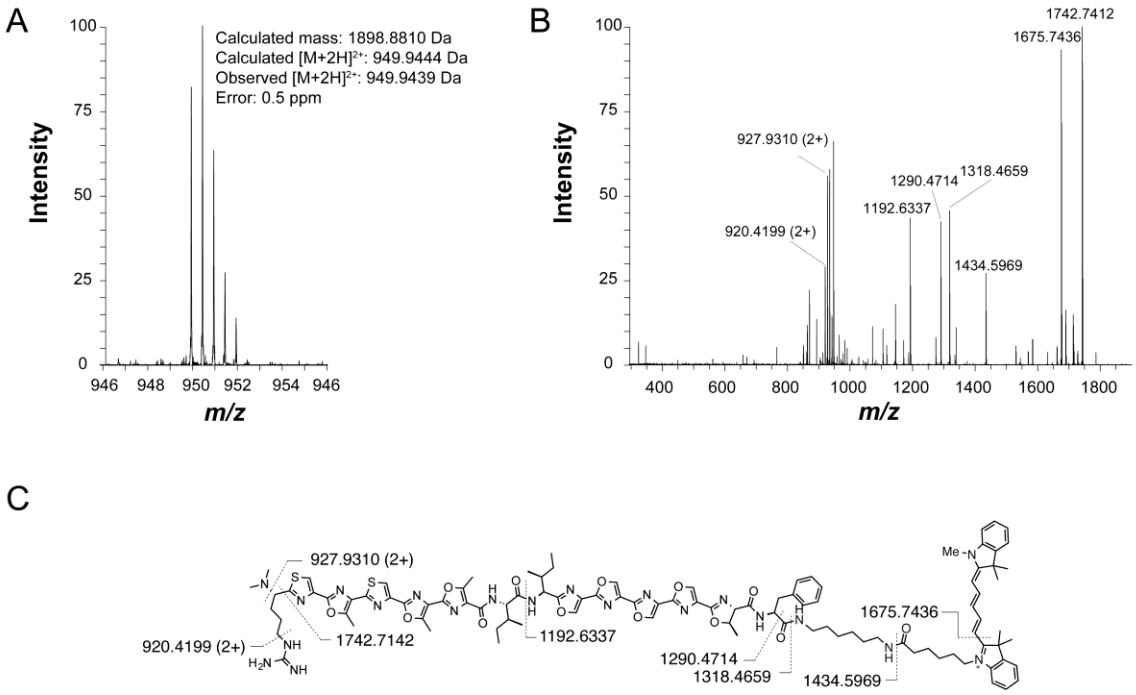

Figure 4.12 | Mass spectrometry characterization of PZN-Cy5. (A) Mass spectrum of the $[M+H]^{2+}$ species by LTQ-FT-MS, which was used to calculate exact mass. (B) CID spectrum of the singly charged ion acquired by LTQ-FT-MS. Labeled peaks correspond to identified fragments of PZN-Cy5, shown on the structure in panel (C).

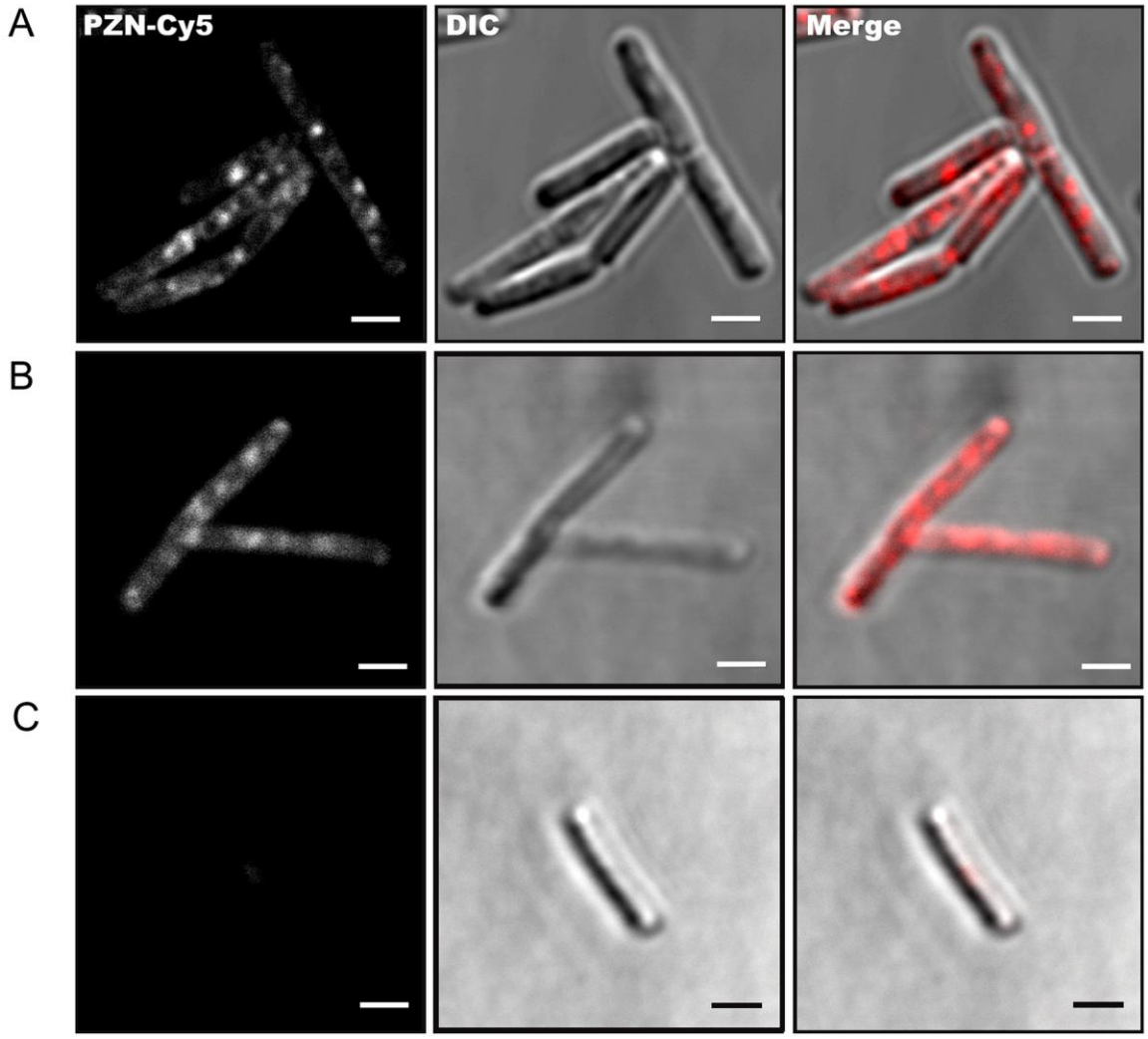

Figure 4.13 | PZN-Cy5 localizes to distinct foci on *B. anthracis*. (A) Representative fluorescence microscopy images are shown for the Cy5, DIC, and merged channels of *B. anthracis* Sterne treated with 0.1 μM PZN-Cy5 (0.05 × MIC) for 30 min. Competition experiments in a PZN-resistant *B. anthracis* strain (PR06, *vide infra*) show (B) robust labeling with 0.05 μM PZN-Cy5 in the absence of unlabeled PZN and (C) significantly decreased labeling when cells are pretreated with 1 μM PZN (0.016 × MIC, resistant strain PR06) for 20 min. Scale bars, 2 μm.

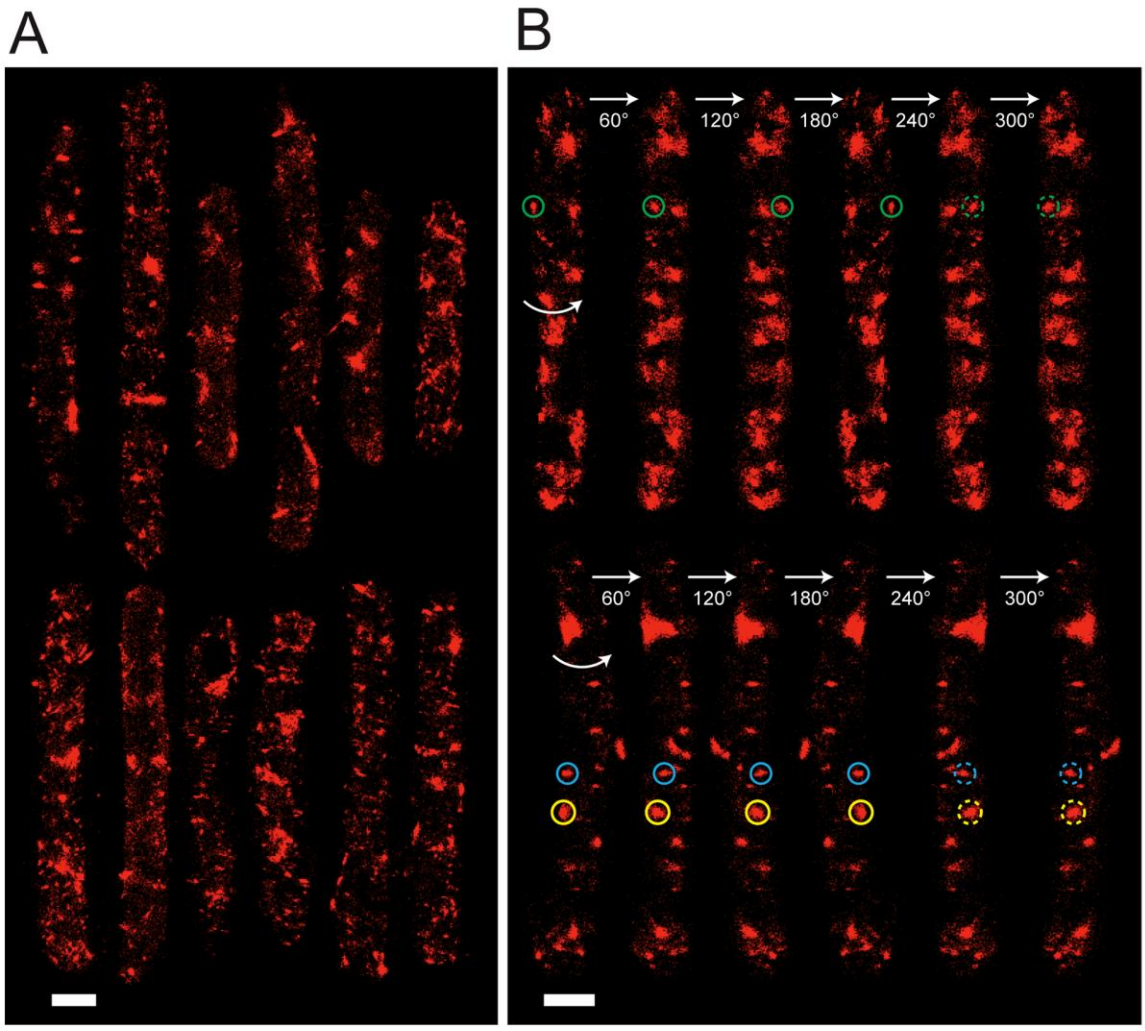

Figure 4.14 | STORM images of PZN-Cy5 labeled *B. anthracis*. (A) 3-D super-resolution images of 12 representative *B. anthracis* treated with PZN-Cy5. (B) Two representative cells rotated about the z-axis show distinct, non-septal localization of PZN-Cy5. Green, blue, and yellow circles mark three individual foci in each rotated view. Scale bars, 1 μm.

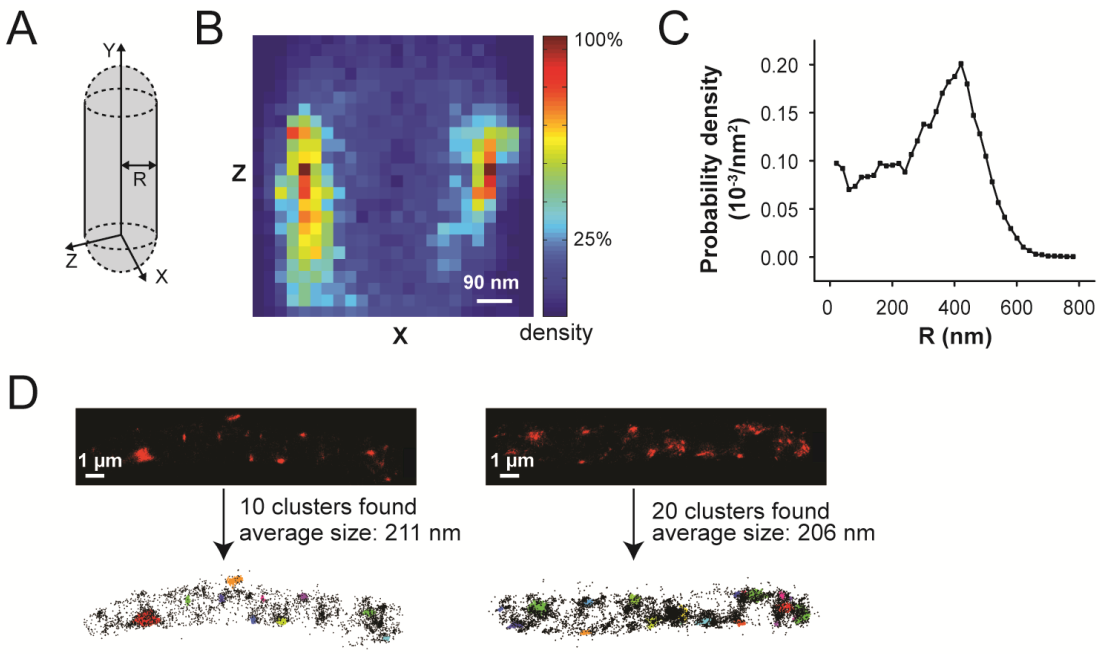

Figure 4.15 | Cluster analysis of *B. anthracis* treated with PZN-Cy5 and imaged by super-resolution microscopy. (A) Representation of cell alignment used in subsequent analyses. (B) PZN-Cy5 color density map of a representative cell projected onto the XZ plane. (C) Probability density of PZN-Cy5 increases as distance from the center of the cell (R) increases, reaching a maximum at the cell membrane. (D) Cluster analysis of two representative *B. anthracis* cells (top) shows identified clusters (bottom) used in subsequent size calculations.

A

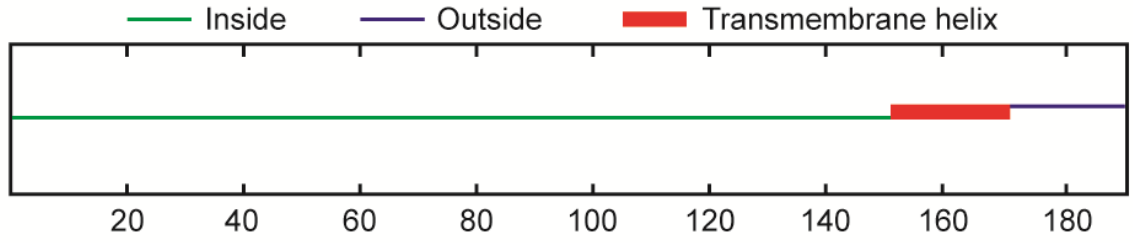

B

```
        10         20         30         40         50         60
MTANRIKAVA LSHFARYGYE GTSLANIAQE VGIKKPSIYA HFKGKEELYF ICLESALQKD

        70         80         90        100        110        120
LQSFTDDIEN FSNSSTEELL LQLLKGYAKR FGESEESMFW LRTSYFPPDA FREQIIEKAN

       130        140        150        160        170        180
AHIENVGKLL FPIFKQANEK SELHNIEVKD ALEAFLCLLD GLMVELLFAG LNRFETRLNA

       190
SWQVFWRGLS N
```

Figure 4.16 | Hydropathy plot of BAS4114 reveals a single transmembrane helix. (A) The amino acid sequence of BAS4114 was analyzed using SPOCTOPUS, which predicted a transmembrane domain from residues 151-171. (B) Corresponding amino acids for each predicted membrane association. Green, inside the membrane; Red, transmembrane; Blue, outside the membrane.

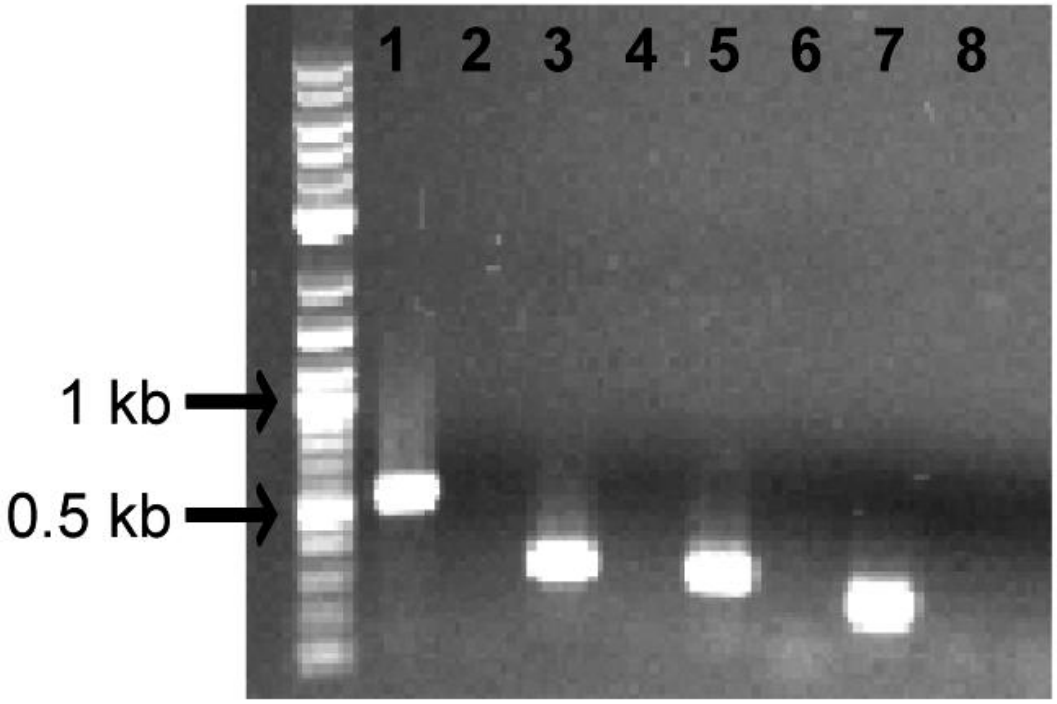

Figure 4.17 | Confirmation of *bas4114-4117* deletion in *B. anthracis* Sterne. Specific primers for each deleted gene were used to confirm their absence by PCR amplification. 1, *bas4114* in wild type Sterne (WT); 2, *bas4114* in deletion strain; 3, *bas4115* in WT; 4, *bas4115* in deletion strain; 5, *bas4116* in WT; 6, *bas4116* in deletion strain; 7, *bas4117* in WT; 8, *bas4117* in deletion strain.

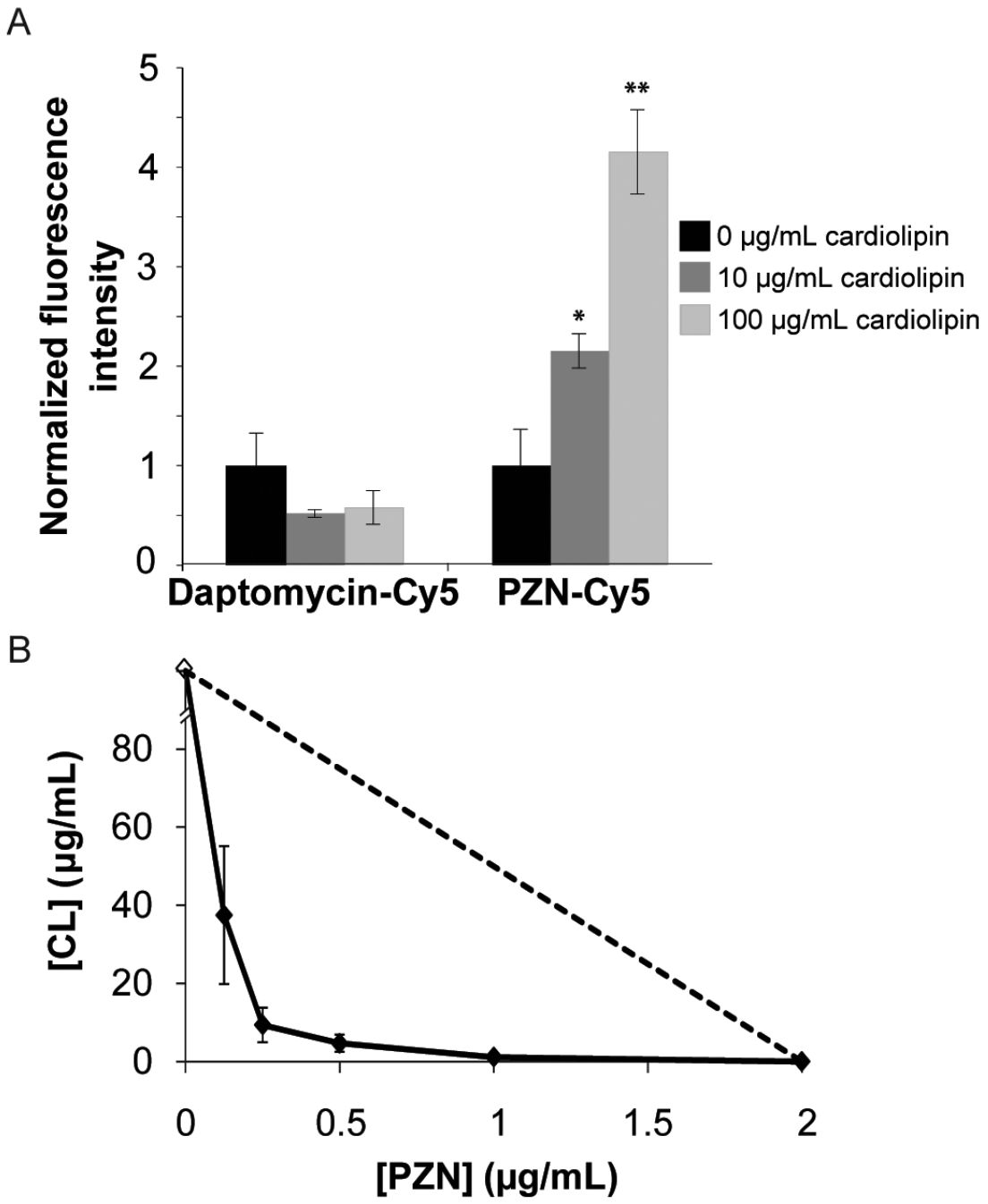

Figure 4.18 | Cardiolipin increases PZN-Cy5 interaction with bacterial cells. (A) Mean fluorescence intensities of *B. anthracis* cell populations treated with daptomycin-Cy5 or PZN-Cy5 in the presence or absence of exogenous CL were determined by flow cytometry and normalized to cells treated only with the Cy5-labeled compound and vehicle. Error is reported as standard deviation with n = 3. The PZN-Cy5 p-values are given relative to the 0 µg/mL control with * indicating <0.01 and ** indicating <0.001. The p-values for daptomycin-Cy5 were both >0.01. (B) Isobologram of the minimum inhibitory concentrations (µg/mL) of PZN and CL. Interactions taking place below the dotted line represent synergistic behavior.

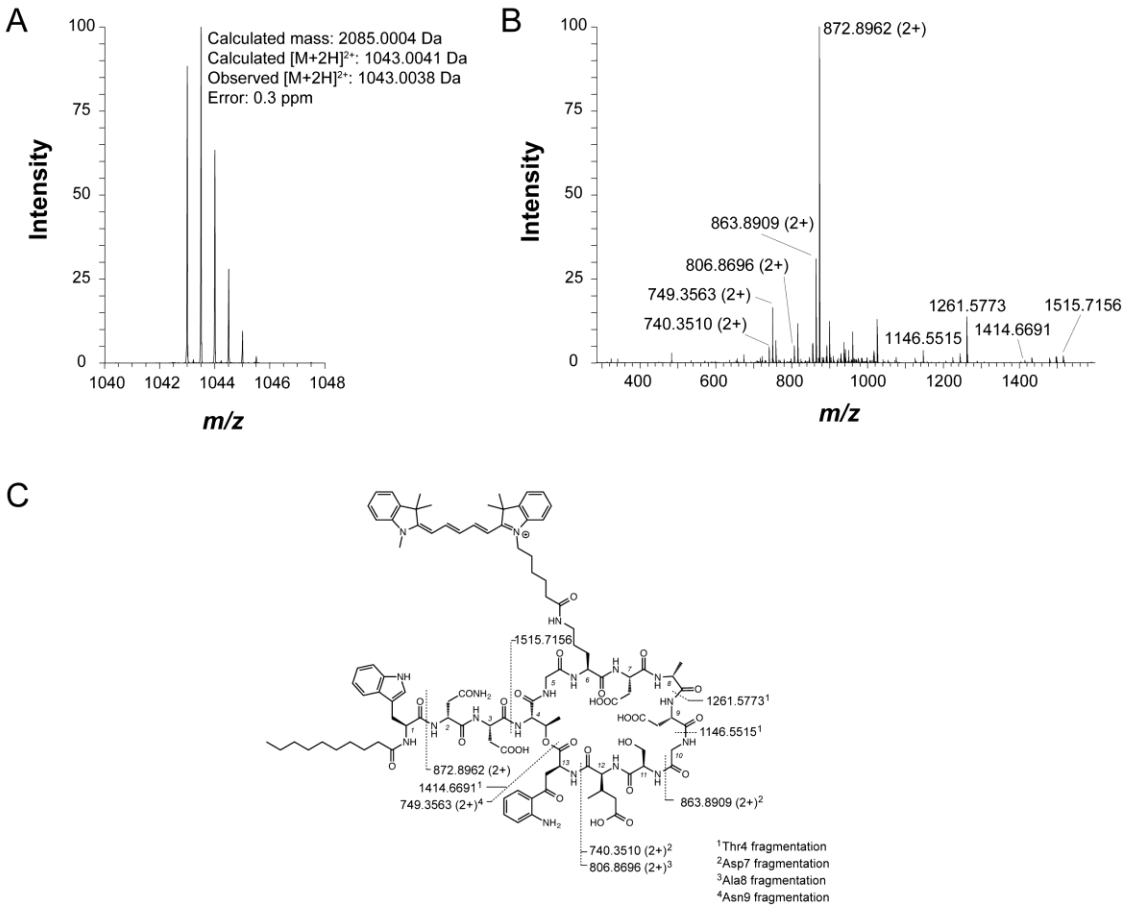

Figure 4.19 | Mass spectrometry characterization of daptomycin-Cy5. (A) Mass spectrum of the $[M+2H]^{2+}$ species by LTQ-FT-MS, which was used to calculate exact mass. (B) CID spectrum of the doubly charged ion acquired by LTQ-FT-MS. Labeled peaks correspond to identified fragments of daptomycin-Cy5, shown on the structure in panel (C).

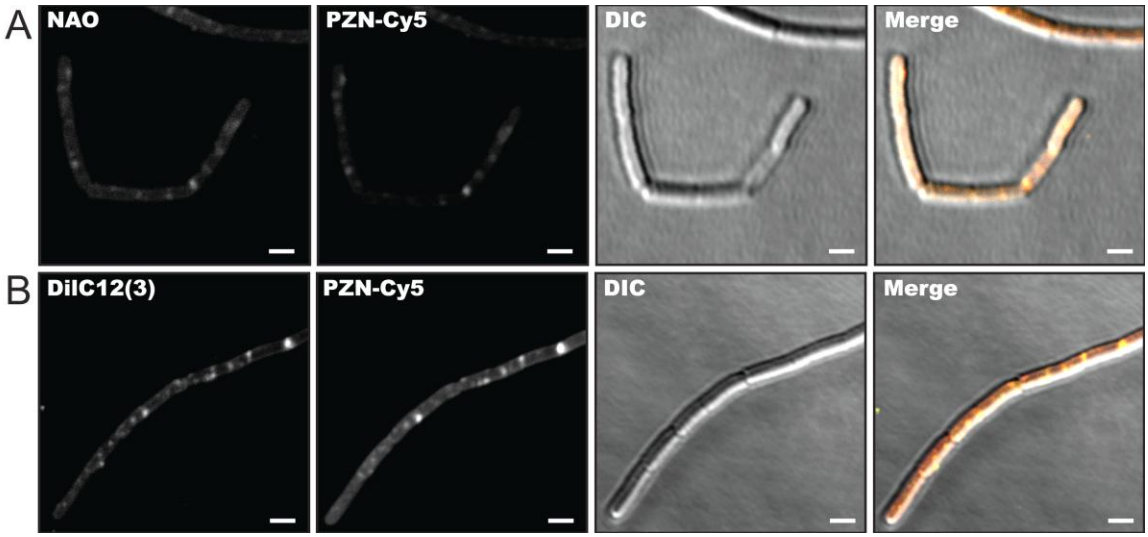

Figure 4.20 | PZN colocalizes with CL- and RIF-specific dyes. (A) From left to right, the channels for NAO, Cy5, DIC, and a merged image are shown to illustrate the co-localization of NAO (yellow) and PZN (red). (B) Same as panel A but with DilC12(3) replacing NAO. Scale bars, 2 μm.

4.8 Tables

Table 4.1 | Minimum inhibitory concentrations reveal the species specificity of plantazolicin (PZN)

Strain	MIC (μg/mL)	MIC (μM)	Source
***B. cereus* group**			
B. anthracis Sterne 34F2	1	0.75	S. Blanke (UIUC)
B. anthracis Sterne 7702	1	0.75	USDA
B. anthracis Sterne 7702 Δ*bas4114-4117*	1	0.75	This study
B. anthracis Sterne 7SBON30	1	0.75	(Davison *et al.*, 2005)
B. anthracis Sterne 7SBON40	1	0.75	(Davison *et al.*, 2005)
B. anthracis Sterne 7SDG30	1	0.75	(Davison *et al.*, 2005)
B. anthracis Sterne 7SBTR30	1	0.75	(Davison *et al.*, 2005)
B. anthracis Sterne 7SBONTO	1	0.75	(Davison *et al.*, 2005)
B. anthracis Sterne 7SBTRTO	1	0.75	(Davison *et al.*, 2005)
B. anthracis Sterne 7SBTO30	1	0.75	(Davison *et al.*, 2005)
B. anthracis BSL3 strains	2 – 16	1.5 – 12	USAMRIID
B. anthracis CDC 684	2	1.5	USAMRIID
B. anthracis Sterne 34F2 A0517-1	1	0.75	BEI
B. anthracis Sterne 34F2 A0517-2	2	1.5	BEI
B. anthracis Sterne 34F2 Δ*blsO*	1	0.75	(Anderson *et al.*, 2011)
B. anthracis Sterne 34F2 Δ*csaB*	1	0.75	(Kern *et al.*, 2010)
B. anthracis Sterne 34F2 Δ*sap*	1	0.75	(Nguyen-Mau *et al.*, 2012)
B. anthracis Sterne 34F2 Δ*eag*	1	0.75	(Nguyen-Mau *et al.*, 2012)
B. anthracis Sterne 34F2 Δanthrose	1	0.75	C. Turnbough (U. Alabama Birmingham)
B. anthracis Sterne 34F2 Δ*bclA*	1	0.75	(Tan and Turnbough, 2010)
B. anthracis Sterne BA850 (Δpetrobactin)	1	0.75	(Carlson *et al.*, 2010)
B. anthracis Sterne BA781	1	0.75	BEI
B. anthracis Weybridge	1	0.75	BEI
B. cereus 14579	>64	>48	USDA
B. cereus 541 (Δ*plcR*)	>64	>48	(Pomerantsev *et al.*, 2003)
B. cereus ATCC 7064	>64	>48	ATCC
B. cereus ATCC 13472	>64	>48	BGSC
B. *cereus* BAG4x2-1	>64	>48	BEI
B. *cereus* E33L	>64	>48	BEI

Table 4.1 (continued)

B. cereus G9241	8	6	BEI
B. cereus GP7	>64	>48	BGSC
B. cereus Rock3-44	64	48	NMRS
B. *cereus* VD014	>64	>48	BEI
B. *cereus* VD115	>64	>48	BEI
B. mycoides 96/3308	>64	>48	BGSC
B. samanii C1	>64	>48	BEI
B. thuringiensis Konkukian 97-27	>64	>48	BEI
B. thuringiensis israelensis ATCC 35646	>64	>48	BEI
B. thuringiensis subsp. *thuringiensis*	>64	>48	BGSC
Atypical gamma phage sensitivity			
B. cereus ATCC 4342	>64	>48	BEI
B. cereus CDC 32805	>64	>48	(Schuch and Fischetti, 2006)
B. cereus 2002013145	>64	>48	CDC
B. cereus 2002013146	>64	>48	CDC
B. cereus 2002013100	>64	>48	CDC
B. cereus 2000031002	>64	>48	CDC
Non *B. cereus* group			
B. methylotrophicus FZB42	>64	>48	BGSC
B. amyloliquefaciens B-14393T	>64	>48	BGSC
B. megaterium 899	32	24	BGSC
B. pumilus SAFR-032	>64	>48	BGSC
B. subtilis			
AKP4 (Δ*des*)	>64	>48	D. de Mendoza (U. Nacional de Rosario)
AKP21 (Δ*desRK*)	>64	>48	D. de Mendoza (U. Nacional de Rosario)
BSU-LIKE1 (Δ*liaIH*)	>64	>48	BGSC
HB0042	>64	>48	Personal Collection
HB0934 (Δ*liaGFSR*)	>64	>48	J. Helmann (Cornell)
HB5126 (Δ*liaIH*)	>64	>48	J. Helmann (Cornell)
str. 168	>64	>48	J. Wells (USCF)
Brevibacillus formosus SS 86-3	>64	>48	BGSC
Brevibacillus laterosporus ATCC 9141	>64	>48	BGSC
Neisseria meningititis serotype C	>64	>48	(Nassif *et al.*, 1991)

Table 4.1 (continued)

Neisseria sicca	>64	>48	ATCC
Staphylococcus aureus			
12608	>64	>48	P. Hergenrother (UIUC)
29213	64	48	P. Hergenrother (UIUC)
33591	64	48	P. Hergenrother (UIUC)
USA300	>64	>48	P. Hergenrother (UIUC)
Streptomyces coelicolor	>64	>48	USDA
Streptomyces lividans	>64	>48	USDA
Eukaryotic organisms			
Caenorhabditis elegans N2	>64	>48	CGC
Saccharomyces cerevisiae	>64	>48	H. Zhao (UIUC)
Talaromyces stipitatus	>64	>48	H. Zhao (UIUC)

[a]n ≥ 3 replicates

[b]Highlighted strains were tested for gamma phage susceptibility and are displayed in the main text

Table 4.2 | PZN is not antibacterial against *B. anthracis* endospores

[PZN] (μg/mL)	CFU/mL[a]
Vehicle	9.8E+08
0.5	4.3E+08
1	8.3E+08
2	6.8E+08
4	3.4E+08
8	6.5E+08
16	3.5E+08

[a]Colony forming units per mL of endospore suspension

Table 4.3 | γ phage sensitivity and PZN susceptibility of *Bacillus* strains

Strain	γ Phage Sensitivity[a]	PZN MIC[b]	Source[c]
B. anthracis Sterne 7702	+++	1	USDA
B. anthracis Sterne 34F2 A0517-1[d]	+++	2	BEI
B. cereus 2002013145	+++	>64	CDC[e]
B. cereus 2002013146	+++	>64	CDC[e]
B. cereus 2002013100	++	>64	CDC[e]
B. cereus 2000031002	+++	>64	CDC[e]
B. cereus ATCC 4342	+	>64	ATCC
B. cereus ATCC 7064	+	>64	ATCC
B. cereus CDC 32805	+	>64	(Schuch and Fischetti, 2006)
B. cereus G9241	-	8	BEI
B. megaterium 899	-	32	BGSC
B. mycoides 96/3308	-	>64	BGSC

[a] Plus signs indicate the level of phage sensitivity, with +++ representing the most sensitive
[b] MIC (minimum inhibitory concentration) as determined by microbroth dilution, units in μg/mL
[c] Abbreviations: USDA, United States Department of Agriculture; BEI, Biodefense and Emerging Infections Research Resources Repository; CDC, United States Centers for Disease Control and Prevention; ATCC, American Type Culture Collection; BGSC, Bacillus Genetic Stock Center
[d] LLNL A0517 was obtained from BEI as a mixture of two colony types. A0517_1 was confirmed to be devoid of pXO1 by PCR (Figure 4.2)
[e] Strains identified by multilocus sequence typing analysis (Hoffmaster *et al.*, 2006)

Table 4.4 | MICs of representative strains demonstrating PZN activity in various rich media

	MIC (μg/mL)		
Strain	LB[a]	MH	BHI
Bacillus anthracis Sterne	1	1	1
Bacillus cereus CDC32805	>64	>64	>64
Bacillus cereus ATCC 4242	>64	>64	>64
Bacillus sp. Al Hakam	>64	>64	>64
Bacillus methylotrophicus FZB42	>64	>64	>64
Bacillus subtilis strain 168	>64	>64	>64
Enterococcus faecium U503	>64	>64	>64
Listeria monocytogenes 4b	>64	>64	>64
Staphylococcus aureus ATCC 12608	>64	16	32
Staphylococcus aureus ATCC 29213	64	8	16
Staphylococcus aureus ATCC 33591	64	8	16
Staphylococcus aureus USA300	>64	>64	>64

[a]Luria-Bertani (LB), Mueller-Hinton (MH), Brain Heart Infusion (BHI)

Table 4.5 | Complete RNA-Seq analysis of differentially expressed *B. anthracis* genes after PZN treatment

Locus Tag	Gene	Description	Fold Change	q-value
BAS1222	*ywcJ*[a]	formate/nitrite transporter family protein	-7	3.19E-38
BAS0577	*lldp-1*	L-lactate permease	-7	2.14E-24
BAS4869	*ldh3*	L-lactate dehydrogenase	-6	6.40E-27
BAS0169		hypothetical protein	-6	1.30E-25
BAS4146		hypothetical protein	-5	3.66E-19
BAS4762	*ldh2*	L-lactate dehydrogenase	-4	1.19E-13
BAS1089	*yjzC*[a]	hypothetical protein	-4	5.38E-16
BAS1615	*yfmQ*[a]	hypothetical protein	-3	1.49E-05
BAS3917		hypothetical protein	-3	9.12E-04
BAS4690	*cydA-2*	cytochrome d ubiquinol oxidase subunit I	-3	4.40E-04
BAS0513	*bdbD*	hypothetical protein	-3	1.00E-03
BAS1942	*sdpI*[a]	hypothetical protein	2	5.98E-03
BAS3405		ahpC/TSA family protein	2	6.00E-03
BAS2363		hypothetical protein	2	1.27E-03
BAS2776	*yetG*[a]	hypothetical protein	2	9.17E-04
BAS1163		hypothetical protein	3	2.06E-03
BAS0730	*yfhC*[a]	nitroreductase family protein	3	6.85E-03
BAS4453		hypothetical protein	3	4.90E-04
BAS2568		TetR family transcriptional regulator	3	1.43E-03
BAS2566	*kynB*	hypothetical protein	3	2.83E-03
BAS0683	*yqgI*[a]	phosphate ABC transporter permease	3	7.44E-04
BAS4452		hypothetical protein	3	2.81E-05
BAS2565	*kynA*	tryptophan 2,3-dioxygenase family protein	3	3.85E-03
BAS3439	*hutG*[a]	formimidoylglutamase	3	1.17E-03
BAS3871		hypothetical protein	3	1.35E-05
BAS0214	*lagB*	invasion protein LagB	3	2.21E-04
BAS1691	*fabH2*	3-oxoacyl-ACP synthase	3	6.35E-04
BAS4502	*ytpI*[a]	hypothetical protein	3	2.71E-06
BAS1573		hypothetical protein	3	8.18E-03
BAS0849		hypothetical protein	3	1.49E-06
BAS1346	*liaF*[a]	hypothetical protein	3	1.77E-04
BAS0525	*yuaG*[a]	hypothetical protein	3	6.06E-04

Table 4.5 (continued)

BAS0610	*rocE*[a]	amino acid ABC transporter permease	3	1.77E-04
BAS4777	*sodC*	superoxide dismutase, Cu-Zn	3	6.63E-08
BAS0524	*yuaF*[a]	hypothetical protein	4	2.77E-07
BAS0848	*yhaR*[a]	enoyl-CoA hydratase	4	1.25E-07
BAS4173	*pstC*	phosphate ABC transporter permease	4	9.53E-06
BAS4172	*pstA*	phosphate ABC transporter permease	4	2.15E-07
BAS4171	*pstB*	phosphate transporter ATP-binding protein	4	7.63E-07
BAS1307	*ilvE1*	branched-chain amino acid aminotransferase	4	1.40E-08
BAS4560	*acsA*	acetyl-CoA synthetase	4	5.09E-06
BAS3772	*ylbP*[a]	hypothetical protein	4	2.05E-05
BAS0464	*rocR-1*	arginine utilization regulatory protein RocR	4	1.01E-09
BAS4877	*fadN*[a]	3-hydroxyacyl-CoA dehydrogenase	4	1.18E-09
BAS0624	*dppC*[a]	oligopeptide ABC transporter permease	4	7.90E-08
BAS4174	*phoX*	phosphate ABC transporter substrate-binding protein	4	1.87E-08
BAS5194	*fadF*[a]	ferredoxin, 4Fe-4S	4	1.32E-07
BAS1894	*dppE*[a]	oligopeptide ABC transporter substrate-binding protein	4	1.46E-08
BAS1070		hypothetical protein	4	1.73E-10
BAS4778		hypothetical protein	5	5.76E-14
BAS0681	*pstS*[a]	phosphate ABC transporter substrate-binding protein	5	1.12E-16
BAS4512		hypothetical protein	5	1.76E-24
BAS3440	*hutI*	imidazolonepropionase	5	3.49E-21
BAS2288		hypothetical protein	6	7.47E-08
BAS0625	*appB, oppB*[a]	oligopeptide ABC transporter permease	6	3.26E-20
BAS2146	*yokU*[a]	hypothetical protein	6	5.30E-39
BAS0626	*appF, oppF*[a]	oligopeptide ABC transporter ATP-binding protein	6	2.29E-19
BAS2145	*kamA*	L-lysine 2,3-aminomutase	7	4.12E-35
BAS3024		arsR family transcriptional regulator	7	1.17E-52
BAS2188	*mmgD*	citrate synthase 3	8	2.67E-54
BAS3441	*hutU*	urocanate hydratase	8	5.49E-50
BAS2649		hypothetical protein	9	5.16E-42
BAS2650		hypothetical protein	9	2.30E-45

Table 4.5 (continued)

BAS3442	*hutH*	histidine ammonia-lyase	10	9.17E-104
BAS0627	*appD*, *oppD*[a]	ABC transporter nucleotide-binding protein	11	1.62E-95
BAS2287	*yaaN*[a]	hypothetical protein	13	4.38E-93
BAS1521	*gerN*	germination protein gerN	28	0
BAS3456		hypothetical protein	40	0
BAS5200	*yvfU*, *desR*[a]	DNA-binding response regulator	49	0
BAS5201	*yvfT*, *desK*[a]	sensor histidine kinase	56	0
BAS5202	*yvfS*[a]	ABC transporter permease	130	0
BAS5203	*yvfR*[a]	ABC transporter ATP-binding protein	135	0
BAS1345	*liaH*[a]	PspA/IM30 family protein	1084	0
BAS1344	*liaI*[a]	membrane protein	1407	0

[a]Genes are annotated by sequence homology to the corresponding *Bacillus subtilis* gene
The q-value is an adjusted p-value, taking in to account the false discovery rate

Table 4.6 | RNA-Seq and qRT-PCR analysis of PZN-treated *Bacillus anthracis*

			Fold Change	
Locus Tag	**Gene**	**Description**	**RNA-Seq**	**qRT-PCR**[a]
BAS0577	*lldp-1*	L-lactate permease	-7	-7 ± 2
BAS4869	*ldh3*	L-lactate dehydrogenase	-6	-24 ± 14
BAS4762	*ldh2*	L-lactate dehydrogenase	-4	-3 ± 1
BAS3439	*hutG*	formimidoylglutamase	3	3 ± 1
BAS3440	*hutI*	imidazolonepropionase	5	4 ± 0
BAS3441	*hutU*	urocanate hydratase	8	3 ± 0
BAS3442	*hutH*	histidine ammonia-lyase	10	5 ± 2
BAS0627	*appD, oppD*[b]	ABC transporter nucleotide-binding protein	11	6 ± 3
BAS1521	*gerN*	germination protein	28	14 ± 9
BAS5200	*yvfU, desR*[b]	DNA-binding response regulator	49	37 ± 30
BAS5201	*yvfT, desK*[b]	sensor histidine kinase	56	94 ± 36
BAS1345	*liaH*[b]	PspA/IM30 family protein	1084	138 ± 10
BAS1344	*liaI*[b]	membrane protein	1407	352 ± 191

[a] Error is given as standard deviation with $n \geq 3$ replicates
[b] Gene annotations are derived from sequence homology to the given *B. subtilis* gene

Table 4.7 | Primers used in this study

Confirmation of LLNL A0517_1 pXO1 plasmid loss	
pXO1_0172 lef RT-r	GATGCGAAAGTAGTGCCAAAGA
pXO1_0172 lef RT-r	CCACAGCATGTCCAAATTCG
Confirmation of spontaneous mutants	
BamHI-BAS4114-f	AAAAGGATCCATGACAGCAAACCGCATTAAAG
NotI-BAS4114-r	AAAAGCGGCCGCTCAGTTTGAAAGGCCTCGC
Generation and Confirmation of the bas4114-bas4115 deletion strain	
G236Tet-up-vec-f	TGGAGCTCCACCGCGGTGGCAGGCGTTTGCTGATACAC
G236Tet-up-down-r	TAAAAAAGGACAGTTTCATCCCCTACCTACC
G236Tet-down-up-f	GGGGATGAAACTGTCCTTTTTTATATTCATTCAGAC
G236Tet-down-vec-r	TCGACCTGCAGCCAAGGACGCATCTGTCTTTGTTTCAGTG
TetR-f	GCAAACCGCATTAAAGCTGTAGC
TetR-r	CAGTTTGAAAGGCCTCGCC
SugE4115-f	GGCATGGATTTATGTAATCTTAGCTGG
SugE4115-r	GCCTCCTTCGCTTCTTTTTCTTC
SugE4116-f	GGCTTGGGTATTTTTAATTCTAGCTGG
SugE4116-r	CTTAATAGTTTTAAGCCAACAGCGCC
BAS4117-f	GTGGAAAGAAAAAGGGAAGCAACTG
BAS4117-r	GTTCAGAAGAACTGTCCTTTTTAAATAACTTATTCC
RT-qPCR	
Banth 16S qRT-f	CGGAATTATTGGGCGTAAAG
Banth 16S qRT-r	TCTCCCAGTTTCCAATGACC
BAS0577 lldp-1 qRT-f	TGGTTCACTATTCGCACCAC
BAS0577 lldp-1 qRT-r	TTTGCTATTGTGCCACCAAC
BAS0627 appD qRT-f	ACGAATTATCTGGCGGAATG
BAS0627 appD qRT-r	AGCCGTTGTTGGCTCATC
BAS1344 liaI qRT-f	GGAGCAGGAGTTGTGTACTGG
BAS1344 liaI qRT-r	GATGGACAAGCCGATTAAACC
BAS1345 liaH qRT-f	ATCAAAGCAAGCGCTTATCG
BAS1345 liaH qRT-r	TTCTAATCGAGTTACTTGCCCTTC
BAS1521 gerN qRT-f	ACGAATGACTGGATTTGATGC
BAS1521 gerN qRT-r	GAAAGTCCTGTTCCTGCAATG
BAS1659 CitB RR qRT-f	AACGACGTTCGATGATGATG
BAS1659 CitB RR qRT-r	TTATCGCATCACGAATACGC
BAS1660 Sensor HK qRT-f	TGAAAGCATTCGGATTACATTG
BAS1660 Sensor HK qRT-r	TCATGCTTACTGGCAAATTCC
BAS1661 ABC trans qRT-f	TGCGAAGATGAATATTGGTGTC
BAS1661 ABC trans qRT-r	ACCCGTACAGTCCAGCAAAG
BAS1662 ABC trans qRT-f	CGGTTGTAATGACGACGATG

Table 4.7 (continued)

BAS1662 ABC trans qRT-r	TAGGCGCAGCAATAAGGTG
BAS1663 ABC trans qRT-f	TATGGGAATGTAGGGCAAGG
BAS1663 ABC trans qRT-r	AGAAATTTCACCGTATCATTTGC
BAS1664 minor cls ClsB qRT-f	TGGCACAACAAACTTTACTTCG
BAS1664 minor cls ClsB qRT-r	AACGCCTTATTAACTTGCCCTAC
BAS1842 asbE qRT-f	GGGTATTTGCTTTCTGGTCTTG
BAS1842 asbE qRT-r	TTTCACGGAAGTATGCAAAGG
BAS1843 asbF qRT-f	CAGATCCAGTTGACAGCTTCC
BAS1843 asbF qRT-r	CGGTTCGAACACATGTAAATAATC
BAS3439 hutG qRT-f	TAACGGGCTTTGCAAACAG
BAS3439 hutG qRT-r	CATTTGACGGACCACCATC
BAS3440 hutI qRT-f	TGACCCGCATACTCATCTTG
BAS3440 hutI qRT-r	AAGAATACCTCCGCCTTGTTC
BAS3441 hutU qRT-f	ATTTGTTGGCTTGGTTACGG
BAS3441 hutU qRT-r	CACGACCGATAACGATTGG
BAS3442 hutH qRT-f	TGCGATGGTTGCTCTTACAG
BAS3442 hutH qRT-r	AAAGAACTCCTTGCGCTGTC
BAS4762 ldh2 qRT-f	AATCGTTCGCGGTATTATGG
BAS4762 ldh2 qRT-r	TGGTAGACCAGATTCTTTCCAAG
BAS4869 ldh3 qRT-f	AATCATGAACGTGCAGTTGG
BAS4869 ldh3 qRT-r	TTGCAGTCTTCATAGCTTCCTG
BAS5033 ftsX qRT-f	CGGAAAGACGTTTGAGTTATTTG
BAS5033 ftsX qRT-r	TCGCAATTGTTGCTGTATCTG
BAS5034 ABC ftsE qRT-f	TCTTGAAGATCGTGCAGACG
BAS5034 ABC ftsE qRT-r	ATCGGCAATTACGACTTTCG
BAS5200 desR qRT-f	TTGAAGTAATTGGGCAAGCTG
BAS5200 desR qRT-r	TCTAACCCGCTTTGAATTGG
BAS5201 desK qRT-f	GCAGTGACGAATGTTGTAAAGC
BAS5201 desK qRT-r	CCAATTCCGTTATCTTCTACCG
BAS5288 TetR reg qRT-f	AAGATGAGGAATTGCTTGTTACG
BAS5288 TetR reg qRT-r	CTTGTATAACCGGAATCCTTGG
BAS5289 transporter qRT-f	CGGAGCTCTTGTTGCCTTAC
BAS5289 transporter qRT-r	AAGCACGATTGCGTTTGTTAC

Table 4.8 | Minimum inhibitory concentrations (μM) of Me_2-Arg-Az_5 reveal a broader spectrum of activity than PZN

Strain	MIC (μM)[a]
Bacillus anthracis Sterne 7702	3
Bacillus anthracis PR06	3
Bacillus anthracis A0517-1	3
Bacillus cereus ATCC 4342	6
Bacillus megaterium 899	3
Bacillus subtilis 168	6
Escherichia coli DH5a	>48
Enterococcus faecium U503	48
Listeria monocytogenes 4b	>48
Neisseria sicca ATCC 29256	>48
Staphylococcus aureus USA300	3
Streptococcus pyogenes M1	48
Pseudomonas putida	>48

[a]Minimum inhibitory concentration, determined my microbroth dilution assay, measured in μM

Table 4.9 | Common differentially expressed genes after PZN and Me_2-Arg-Az_5 treatment

			Fold Change	
Locus Tag	**Gene**	**Description**	**PZN**	**Me_2-Arg-5Az**
BAS0169		hypothetical protein	-6	-4
BAS0513	*bdbD*	hypothetical protein	-3	-2
BAS0577	*lldp-1*	L-lactate permease	-7	-7
BAS1089		hypothetical protein	-4	-4
BAS1222	*ywcJ*	formate/nitrite transporter family protein	-7	-7
BAS1615		hypothetical protein	-3	-3
BAS3917		hypothetical protein	-3	-2
BAS4146		hypothetical protein	-5	-5
BAS4690	*cydA-2*	cytochrome d ubiquinol oxidase subunit I	-3	-2
BAS4762	*ldh2*	L-lactate dehydrogenase	-4	-4
BAS4869	*ldh3*	L-lactate dehydrogenase	-6	-4
BAS5200	*ycfU,desR*	DNA-binding response regulator	49	6
BAS5201	*yvfT, desK*	sensor histidine kinase	56	5
BAS5202	*yvfS*	ABC transporter permease	130	13
BAS5203	*yvfR*	ABC transporter ATP-binding protein	135	12

Table 4.10 | Complete RNA-Seq analysis of differentially expressed *B. anthracis* genes after Me_2-Arg-Az_5 treatment

Locus Tag	Gene	Description	Fold Change	qValue
BAS0577	*lldp-1*	L-lactate permease	-7	5.95E-90
BAS1222	*ywcJ*[a]	formate/nitrite transporter family protein	-7	1.30E-59
BAS4134		hypothetical protein	-7	1.61E-116
BAS4146		hypothetical protein	-5	6.09E-31
BAS4711		hypothetical protein	-5	3.53E-31
BAS0169		hypothetical protein	-4	9.57E-21
BAS1089	*yjzC*[a]	hypothetical protein	-4	2.76E-23
BAS1357	*hmp*	nitric oxide dioxygenase	-4	6.57E-12
BAS4762	*ldh2*	L-lactate dehydrogenase	-4	1.24E-16
BAS4869	*ldh3*	L-lactate dehydrogenase	-4	3.46E-17
BAS1023		hypothetical protein	-3	3.80E-06
BAS1349		hypothetical protein	-3	1.12E-08
BAS1615	*yfmQ*[a]	hypothetical protein	-3	1.28E-06
BAS4990	*cggR*	gapA transcriptional regulator CggR	-3	0.004179
BAS0070	*pabC*	4-amino-4-deoxychorismate lyase	-2	0.003344
BAS0513	*bdbD*	hypothetical protein	-2	8.87E-04
BAS0547	*maeN*[a]	citrate cation symporter family protein	-2	0.002003
BAS0566	*rapD, rapI*[a]	transcriptional regulator	-2	0.004179
BAS0631	*rbsR*	ribose operon repressor	-2	6.17E-05
BAS1024		hypothetical protein	-2	8.87E-04
BAS1185		hypothetical protein	-2	0.007387
BAS1273		ABC transporter permease	-2	8.71E-05
BAS1666	*gltT*[a]	proton/sodium-glutamate symport protein	-2	5.37E-04
BAS2706		hypothetical protein	-2	0.003549
BAS2707		ABC transporter ATP-binding protein	-2	8.05E-04
BAS3173		transcriptional regulator	-2	8.18E-07
BAS3917		hypothetical protein	-2	8.14E-04
BAS4414		succinate dehydrogenase, cytochrome b558 subunit	-2	0.003007
BAS4690	*cydA-2*	cytochrome d ubiquinol oxidase subunit I	-2	0.004179
BAS4922	*nupC*[a]	NupC family nucleoside transporter	-2	0.004085
BAS5002	*whiA*	hypothetical protein	-2	0.007026
BAS5316	*yycI*[a]	YycI protin	-2	7.74E-04
BAS0982	*fadR, yvdT*[a]	TetR family transcriptional regulator	3	8.50E-04
BAS4115	*sugE-1*	sugE protein	4	4.42E-10
BAS5201	*yvfT, desK*[a]	sensor histidine kinase	5	2.03E-21

Table 4.10 (continued)

BAS5200	*yvfU, desR*[a]	DNA-binding response regulator	6	4.21E-26
BAS0375	*yuxN, yfiR*[a]	TetR family transcriptional regulator	8	2.92E-37
BAS0902	*atpI*[a]	ATP synthase protein I	8	2.99E-46
BAS5203	*yvfR*[a]	ABC transporter ATP-binding protein	12	1.66E-119
BAS5202	*yvfS*[a]	ABC transporter permease	13	2.82E-151
BAS0376	*ykuC, yfiS*[a]	major facilitator family transporter protein	181	0

[a]Genes are annotated by sequence homology to the corresponding *Bacillus subtilis* gene
The q-value is an adjusted p-value, taking in to account the false discovery rate

Table 4.11 | *B. anthracis* Sterne mutations conferring PZN-resistance accumulate in *bas4114*, an AcrR family transcriptional regulator

Strain	*bas4114* Mutation	Consequence
Sterne	Wild type	D**ALEAFLCLLDGLMVELLFAGL**NRFETRLNASWQVFWRGLSN[a]
PR01[c]	457G→T	DAL*[b]
PR02	492^T	DALEAFLCLLDGLMV*
PR03	495^AG	DALEAFLCLLDGLMVESYYSQV*
PR04	504^C	DALEAFLCLLDGLMVELLFRRFKSL*
PR05	506^GC	DALEAFLCLLDGLMVELLFAQV*
PR06	507^ATTCGCA	DALEAFLCLLDGLMVELLFAIRRFKSL*

[a] Amino acids 150-191 of BAS4114. Bold residues represent the predicted transmembrane region, as defined by Spoctopus (Figure 4.16) (Viklund *et al.*, 2008)
[b] Asterisk (*) represents the termination of the protein sequence due to the nonsense mutation.
[c] MICs for the PZN-resistant (PR) mutants are ≥ 32 μg/mL PZN, compared to 1 μg/mL for the wild type.

Table 4.12 | Upregulation of *bas4114-4117* in PZN-resistant mutant, *B. anthracis* PR06

Gene	Annotation	Fold change
bas4114	*acrR* family transcriptional regulator	34
bas4115	*emrE* drug efflux pump	152
bas4116	*emrE* drug efflux pump	47
bas4117	hypothetical protein	62

Table 4.13 | MICs (μg/mL) of selected antibiotics against PZN-resistant mutant, *B. anthracis* PR06

Compound	***B. anthacis* Sterne**	***B. anthracis* PR06**
Plantazolicin	1	64
Tetracycline	0.125	0.125
Vancomycin	1	1
Triclosan	1	1
Nisin	2	2
Kanamycin	4	4
Cerulenin	4	8
Spectinomycin	8	4
Chloramphenicol	8	4
Daptomycin	8	8
Ethidium Bromide	16	16

Table 4.14 | PZN-resistant mutants of *B. anthracis* Sterne Δ*bas4114-4117*

Strain	Mutation	Gene	Amino Acid Consequence	MIC[a]
PR07	*bas5034* A425G	cell division ABC transporter, FtsE	G142E	8
PR08	*bas5034* G270T	cell division ABC transporter, FtsE	F90L	32
PR09-1	*bas1659* G190C	CitB RR[b]/luxR family transcriptional regulator	V64L	16
PR09-4	*bas1659* G190C	CitB RR[b]/luxR family transcriptional regulator	V64L	>64
	bas1662 A638G	ABC transporter permease	H213R	
PR10-4	*bas1659* C248T	CitB RR[b]/luxR family transcriptional regulator	T83M	64
	bas1663 C1127T	ABC transporter permease	A376V	
	bas1842 A43G	petrobactin biosynthesis *asbE*	S15G	

[a] MIC as determined by microbroth dilution, measured in μg/mL
[b] Response regulator

Table 4.15 | Effect of *B. anthracis* Sterne mutations and *B. subtilis* growth conditions on PZN susceptibility and cardiolipin content of bacterial membranes

Strain	MIC (μg/mL)	% CL[a]
B. anthracis Sterne 7702	1	4.6 ± 0.1
B. anthracis Sterne 7702 Δ*bas4114-4117*	1	3.6 ± 0.5
B. anthracis PR09-4	>64	6.1 ± 2.5
B. anthracis PR10-4	64	24.2 ± 1.6*
B. subtilis 168	>128	27.5 ± 2.7
B. subtilis 168[b]	32	37.0 ± 6.1

[a] Error is given as standard deviation with n = 3. P-values were compared to either a parental strain (Δ*bas4114-4117* for PR10-4) or the same strain grown in a normal osmolarity medium with * indicating <0.0001

[b] Luria-Bertani broth supplemented with 1.5 M NaCl

Table 4.16 | qRT-PCR of *cls* locus in evolved PZN-resistant mutants

	Fold change		
Gene	**PR09-1**	**PR09-4**	**PR10-4**
BAS1659	NS	NS	NS[a]
BAS1660	NS	NS	NS
BAS1661	21 ± 7	48 ± 26	NS
BAS1662	23 ± 13	NS	NS
BAS1663	24 ± 9	48 ± 26	NS
BAS1664 (*cls*)	39 ± 7	74 ± 26	NS
BAS1842 (*asbE*)	-	-	NS
BAS1843 (*asbF*)	-	-	NS

[a]NS not significant

4.9 References

1. (2006). Clinical and Laboratory Standards Institute. In Methods for Dilution Antimicrobial Susceptibility Tests for Bacteria that Grow Aerobically—Seventh Edition: Approved Standard (Wayne, PA, USA: CLSI).

2. Abshire, T.G., Brown, J.E., and Ezzell, J.W. (2005) Production and validation of the use of gamma phage for identification of *Bacillus anthracis*. *J Clin Microbiol*: **43**, 4780-4788.

3. Agaisse, H., Gominet, M., Okstad, O.A., Kolsto, A.B., and Lereclus, D. (1999) PlcR is a pleiotropic regulator of extracellular virulence factor gene expression in *Bacillus thuringiensis*. *Mol Microbiol*: **32**, 1043-1053.

4. Aguilar, P.S., Cronan, J.E., Jr., and de Mendoza, D. (1998) A *Bacillus subtilis* gene induced by cold shock encodes a membrane phospholipid desaturase. *J Bacteriol*: **180**, 2194-2200.

5. Anderson, V.J., Kern, J.W., McCool, J.W., Schneewind, O., and Missiakas, D. (2011) The SLH-domain protein BslO is a determinant of *Bacillus anthracis* chain length. *Mol Microbiol*: **81**, 192-205.

6. Arnison, P.G., Bibb, M.J., Bierbaum, G., Bowers, A.A., Bugni, T.S., Bulaj, G., Camarero, J.A., Campopiano, D.J., Challis, G.L., Clardy, J., *et al.* (2013) Ribosomally synthesized and post-translationally modified peptide natural products: overview and recommendations for a universal nomenclature. *Nat Prod Rep*: **30**, 108-160.

7. Banala, S., Ensle, P., and Sussmuth, R.D. (2013) Total synthesis of the ribosomally synthesized linear azole-containing peptide plantazolicin A from *Bacillus amyloliquefaciens*. *Angew Chem Int Ed Engl*: **52**, 9518-9523.

8. Barrett, T., Wilhite, S.E., Ledoux, P., Evangelista, C., Kim, I.F., Tomashevsky, M., Marshall, K.A., Phillippy, K.H., Sherman, P.M., Holko, M., *et al.* (2013) NCBI GEO: archive for functional genomics data sets--update. *Nucleic Acids Res*: **41**, D991-995.

9. Bates, M., Huang, B., Dempsey, G.T., and Zhuang, X. (2007) Multicolor super-resolution imaging with photo-switchable fluorescent probes. *Science*: **317**, 1749-1753.

10. Berenbaum, M.C. (1989) What is synergy? *Pharmacol Rev*: **41**, 93-141.

11. Bindman, N.A., and van der Donk, W.A. (2013) A general method for fluorescent labeling of the N-termini of lanthipeptides and its application to visualize their cellular localization. *J Am Chem Soc*: **135**, 10362-10371.

12. Brazas, M.D., and Hancock, R.E. (2005) Using microarray gene signatures to elucidate mechanisms of antibiotic action and resistance. *Drug Discov Today*: **10**, 1245-1252.

13. Brenner, S. (1974) The genetics of *Caenorhabditis elegans*. *Genetics*: **77**, 71-94.

14. Burdine, L., and Kodadek, T. (2004) Target identification in chemical genetics: the (often) missing link. *Chem Biol*: **11**, 593-597.

15. Burkett-Cadena, M., Kokalis-Burelle, N., Lawrence, K.S., van Santen, E., and Kloepper, J.W. (2008) Suppressiveness of root-knot nematodes mediated by rhizobacteria. *Biological Control*: **47**, 55-59.

16. Carlson, P.E., Jr., Dixon, S.D., Janes, B.K., Carr, K.A., Nusca, T.D., Anderson, E.C., Keene, S.E., Sherman, D.H., and Hanna, P.C. (2010) Genetic analysis of petrobactin transport in *Bacillus anthracis*. *Mol Microbiol*: **75**, 900-909.

17. Chen, X.H., Koumoutsi, A., Scholz, R., Eisenreich, A., Schneider, K., Heinemeyer, I., Morgenstern, B., Voss, B., Hess, W.R., Reva, O., *et al.* (2007) Comparative analysis of the complete genome sequence of the plant growth-promoting bacterium *Bacillus amyloliquefaciens* FZB42. *Nat Biotechnol*: **25**, 1007-1014.

18. Choudhury, B., Leoff, C., Saile, E., Wilkins, P., Quinn, C.P., Kannenberg, E.L., and Carlson, R.W. (2006) The structure of the major cell wall polysaccharide of *Bacillus anthracis* is species-specific. *J Biol Chem*: **281**, 27932-27941.

19. Cotsonas King, A., and Wu, L. (2009) Macromolecular synthesis and membrane perturbation assays for mechanisms of action studies of antimicrobial agents. *Curr Protoc Pharmacol*: **Chapter 13**, Unit 13A 17.

20. Cox, C.L., Doroghazi, J.R., and Mitchell, D.A. (2015) The genomic landscape of ribosomal peptides containing thiazole and oxazole heterocycles. *BMC Genomics*: **16**, 778.

21. Cybulski, R.J., Jr., Sanz, P., Alem, F., Stibitz, S., Bull, R.L., and O'Brien, A.D. (2009) Four superoxide dismutases contribute to *Bacillus anthracis* virulence and provide spores with redundant protection from oxidative stress. *Infect Immun*: **77**, 274-285.

22. Daszykowski, M., Walczak, B., and Massart, D.L. (2002) Looking for natural patterns in analytical data. 2. Tracing local density with OPTICS. *J Chem Inf Comput Sci*: **42**, 500-507.

23. Davison, S., Couture-Tosi, E., Candela, T., Mock, M., and Fouet, A. (2005) Identification of the *Bacillus anthracis* (gamma) phage receptor. *J Bacteriol*: **187**, 6742-6749.

24. de Man, P., Verhoeven, B.A., Verbrugh, H.A., Vos, M.C., and van den Anker, J.N. (2000) An antibiotic policy to prevent emergence of resistant bacilli. *Lancet*: **355**, 973-978.

25. Deane, C.D., Melby, J.O., Molohon, K.J., Susarrey, A.R., and Mitchell, D.A. (2013) Engineering unnatural variants of plantazolicin through codon reprogramming. *ACS Chem Biol*: **8**, 1998-2008.

26. Deng, W., Li, C., and Xie, J. (2013) The underling mechanism of bacterial TetR/AcrR family transcriptional repressors. *Cell Signal*: **25**, 1608-1613.

27. Emmons, S.W., Klass, M.R., and Hirsh, D. (1979) Analysis of the constancy of DNA sequences during development and evolution of the nematode *Caenorhabditis elegans*. *Proc Natl Acad Sci U S A*: **76**, 1333-1337.

28. Ezzell, J.W., Abshire, T.G., Little, S.F., Lidgerding, B.C., and Brown, C. (1990) Identification of *Bacillus anthracis* by using monoclonal antibody to cell wall galactose-N-acetylglucosamine polysaccharide. *J Clin Microbiol*: **28**, 223-231.

29. Fei, J., Singh, D., Zhang, Q., Park, S., Balasubramanian, D., Golding, I., Vanderpool, C.K., and Ha, T. (2015) RNA biochemistry. Determination of in vivo target search kinetics of regulatory noncoding RNA. *Science*: **347**, 1371-1374.

30. Friedman, L., Alder, J.D., and Silverman, J.A. (2006) Genetic changes that correlate with reduced susceptibility to daptomycin in *Staphylococcus aureus*. *Antimicrob Agents Chemother*: **50**, 2137-2145.

31. Ganguly, J., Low, L.Y., Kamal, N., Saile, E., Forsberg, L.S., Gutierrez-Sanchez, G., Hoffmaster, A.R., Liddington, R., Quinn, C.P., Carlson, R.W., *et al.* (2013) The secondary cell wall polysaccharide of *Bacillus anthracis* provides the specific binding ligand for the C-terminal cell wall-binding domain of two phage endolysins, PlyL and PlyG. *Glycobiology*: **23**, 820-832.

32. Goh, E.B., Yim, G., Tsui, W., McClure, J., Surette, M.G., and Davies, J. (2002) Transcriptional modulation of bacterial gene expression by subinhibitory concentrations of antibiotics. *Proc Natl Acad Sci U S A*: **99**, 17025-17030.

33. Hao, Y., Blair, P.M., Sharma, A., Mitchell, D.A., and Nair, S.K. (2015) Insights into methyltransferase specificity and bioactivity of derivatives of the antibiotic plantazolicin. *ACS Chem Biol*: **10**, 1209-1216.

34. Hoffmaster, A.R., Hill, K.K., Gee, J.E., Marston, C.K., De, B.K., Popovic, T., Sue, D., Wilkins, P.P., Avashia, S.B., Drumgoole, R., *et al.* (2006) Characterization of *Bacillus cereus* isolates associated with fatal pneumonias: strains are closely related to *Bacillus anthracis* and harbor *B. anthracis* virulence genes. *J Clin Microbiol*: **44**, 3352-3360.

35. Hoffmaster, A.R., Ravel, J., Rasko, D.A., Chapman, G.D., Chute, M.D., Marston, C.K., De, B.K., Sacchi, C.T., Fitzgerald, C., Mayer, L.W., *et al.* (2004) Identification of anthrax toxin genes in a *Bacillus cereus* associated with an illness resembling inhalation anthrax. *Proc Natl Acad Sci U S A*: **101**, 8449-8454.

36. Huang, B., Wang, W., Bates, M., and Zhuang, X. (2008) Three-dimensional super-resolution imaging by stochastic optical reconstruction microscopy. *Science*: **319**, 810-813.

37. Janes, B.K., and Stibitz, S. (2006) Routine markerless gene replacement in *Bacillus anthracis*. *Infect Immun*: **74**, 1949-1953.

38. Jensen, G.B., Hansen, B.M., Eilenberg, J., and Mahillon, J. (2003) The hidden lifestyles of *Bacillus cereus* and relatives. *Environ Microbiol*: **5**, 631-640.

39. Jordan, S., Hutchings, M.I., and Mascher, T. (2008) Cell envelope stress response in Gram-positive bacteria. *FEMS Microbiol Rev*: **32**, 107-146.

40. Kalyon, B., Helaly, S.E., Scholz, R., Nachtigall, J., Vater, J., Borriss, R., and Sussmuth, R.D. (2011) Plantazolicin A and B: structure elucidation of ribosomally synthesized thiazole/oxazole peptides from *Bacillus amyloliquefaciens* FZB42. *Org Lett*: **13**, 2996-2999.

41. Kan, S., Fornelos, N., Schuch, R., and Fischetti, V.A. (2013) Identification of a ligand on the Wip1 bacteriophage highly specific for a receptor on *Bacillus anthracis*. *J Bacteriol*: **195**, 4355-4364.

42. Kellogg, D.S., Jr., Peacock, W.L., Jr., Deacon, W.E., Brown, L., and Pirkle, D.I. (1963) *Neisseria gonorrhoeae*. I. Virulence genetically linked to clonal variation. *J Bacteriol*: **85**, 1274-1279.

43. Kern, J., Ryan, C., Faull, K., and Schneewind, O. (2010) *Bacillus anthracis* surface-layer proteins assemble by binding to the secondary cell wall polysaccharide in a manner that requires csaB and tagO. *J Mol Biol*: **401**, 757-775.

44. Kolsto, A.B., Tourasse, N.J., and Okstad, O.A. (2009) What sets *Bacillus anthracis* apart from other Bacillus species? *Annu Rev Microbiol*: **63**, 451-476.

45. Lee, J., Hao, Y., Blair, P.M., Melby, J.O., Agarwal, V., Burkhart, B.J., Nair, S.K., and Mitchell, D.A. (2013) Structural and functional insight into an unexpectedly selective N-methyltransferase involved in plantazolicin biosynthesis. *Proc Natl Acad Sci U S A*: **110**, 12954-12959.

46. Lee, J.Y., Janes, B.K., Passalacqua, K.D., Pfleger, B.F., Bergman, N.H., Liu, H., Hakansson, K., Somu, R.V., Aldrich, C.C., Cendrowski, S., *et al.* (2007) Biosynthetic analysis of the petrobactin siderophore pathway from *Bacillus anthracis*. *J Bacteriol*: **189**, 1698-1710.

47. Lee, S.W., Mitchell, D.A., Markley, A.L., Hensler, M.E., Gonzalez, D., Wohlrab, A., Dorrestein, P.C., Nizet, V., and Dixon, J.E. (2008) Discovery of a widely distributed toxin biosynthetic gene cluster. *Proc Natl Acad Sci U S A*: **105**, 5879-5884.

48. Li, X.Z., and Nikaido, H. (2009) Efflux-mediated drug resistance in bacteria: an update. *Drugs*: **69**, 1555-1623.

49. Li, Z., Hao, P., Li, L., Tan, C.Y., Cheng, X., Chen, G.Y., Sze, S.K., Shen, H.M., and Yao, S.Q. (2013) Design and synthesis of minimalist terminal alkyne-containing diazirine photo-crosslinkers and their incorporation into kinase inhibitors for cell- and tissue-based proteome profiling. *Angew Chem Int Ed Engl*: **52**, 8551-8556.

50. Liu, Z., Budiharjo, A., Wang, P., Shi, H., Fang, J., Borriss, R., Zhang, K., and Huang, X. (2013) The highly modified microcin peptide plantazolicin is associated with nematicidal activity of *Bacillus amyloliquefaciens* FZB42. *Appl Microbiol Biotechnol*: **97**, 10081-10090.

51. Lopez, C.S., Heras, H., Ruzal, S.M., Sanchez-Rivas, C., and Rivas, E.A. (1998) Variations of the envelope composition of *Bacillus subtilis* during growth in hyperosmotic medium. *Curr Microbiol*: **36**, 55-61.

52. Marston, C.K., Gee, J.E., Popovic, T., and Hoffmaster, A.R. (2006) Molecular approaches to identify and differentiate *Bacillus anthracis* from phenotypically similar Bacillus species isolates. *BMC Microbiol*: **6**, 22.

53. Martin, M., and de Mendoza, D. (2013) Regulation of *Bacillus subtilis* DesK thermosensor by lipids. *Biochem J*: **451**, 269-275.

54. Matsumoto, K., Kusaka, J., Nishibori, A., and Hara, H. (2006) Lipid domains in bacterial membranes. *Mol Microbiol*: **61**, 1110-1117.

55. McClure, R., Balasubramanian, D., Sun, Y., Bobrovskyy, M., Sumby, P., Genco, C.A., Vanderpool, C.K., and Tjaden, B. (2013) Computational analysis of bacterial RNA-Seq data. *Nucleic Acids Res*: **41**, e140.

56. Mesnage, S., Fontaine, T., Mignot, T., Delepierre, M., Mock, M., and Fouet, A. (2000) Bacterial SLH domain proteins are non-covalently anchored to the cell surface via a conserved mechanism involving wall polysaccharide pyruvylation. *EMBO J*: **19**, 4473-4484.

57. Mileykovskaya, E., and Dowhan, W. (2000) Visualization of phospholipid domains in *Escherichia coli* by using the cardiolipin-specific fluorescent dye 10-N-nonyl acridine orange. *J Bacteriol*: **182**, 1172-1175.

58. Mileykovskaya, E., and Dowhan, W. (2009) Cardiolipin membrane domains in prokaryotes and eukaryotes. *Biochim Biophys Acta*: **1788**, 2084-2091.

59. Molohon, K.J., Melby, J.O., Lee, J., Evans, B.S., Dunbar, K.L., Bumpus, S.B., Kelleher, N.L., and Mitchell, D.A. (2011) Structure determination and interception of biosynthetic intermediates for the plantazolicin class of highly discriminating antibiotics. *ACS Chem Biol*: **6**, 1307-1313.

60. Nassif, X., Puaoi, D., and So, M. (1991) Transposition of Tn1545-delta 3 in the pathogenic Neisseriae: a genetic tool for mutagenesis. *J Bacteriol*: **173**, 2147-2154.

61. Nguyen-Mau, S.M., Oh, S.Y., Kern, V.J., Missiakas, D.M., and Schneewind, O. (2012) Secretion genes as determinants of *Bacillus anthracis* chain length. *J Bacteriol*: **194**, 3841-3850.

62. Palmer, K.L., Daniel, A., Hardy, C., Silverman, J., and Gilmore, M.S. (2011) Genetic basis for daptomycin resistance in enterococci. *Antimicrob Agents Chemother*: **55**, 3345-3356.

63. Payne, D.J. (2008) Desperately seeking new antibiotics. *Science*: **321**, 1644-1645.

64. Peters, A.C., Thomas, L., and Wimpenny, J.W. (1991) Effects of salt concentration on bacterial growth on plates with gradients of pH and temperature. *FEMS Microbiol Lett*: **61**, 309-314.

65. Petit, J.M., Maftah, A., Ratinaud, M.H., and Julien, R. (1992) N-10-Nonyl acridine-orange interacts with cardiolipin and allows the quantification of this phospholipid in isolated mitochondria. *Eur J Biochem*: **209**, 267-273.

66. Pomerantsev, A.P., Kalnin, K.V., Osorio, M., and Leppla, S.H. (2003) Phosphatidylcholine-specific phospholipase C and sphingomyelinase activities in bacteria of the *Bacillus cereus* group. *Infect Immun*: **71**, 6591-6606.

67. Quinn, C.P., and Dancer, B.N. (1990) Transformation of vegetative cells of *Bacillus anthracis* with plasmid DNA. *J Gen Microbiol*: **136**, 1211-1215.

68. Rasko, D.A., Altherr, M.R., Han, C.S., and Ravel, J. (2005) Genomics of the *Bacillus cereus* group of organisms. *FEMS Microbiol Rev*: **29**, 303-329.

69. Romantsov, T., Guan, Z., and Wood, J.M. (2009) Cardiolipin and the osmotic stress responses of bacteria. *Biochim Biophys Acta*: **1788**, 2092-2100.

70. Ruhr, E., and Sahl, H.G. (1985) Mode of action of the peptide antibiotic nisin and influence on the membrane potential of whole cells and on cytoplasmic and artificial membrane vesicles. *Antimicrob Agents Chemother*: **27**, 841-845.

71. Rust, M.J., Bates, M., and Zhuang, X. (2006) Sub-diffraction-limit imaging by stochastic optical reconstruction microscopy (STORM). *Nat Methods*: **3**, 793-795.

72. Sahl, H.G., and Brandis, H. (1982) Mode of action of the staphylococcin-like peptide Pep 5 and culture conditions effecting its activity. *Zentralbl Bakteriol Mikrobiol Hyg A*: **252**, 166-175.

73. Schmittgen, T.D., and Livak, K.J. (2008) Analyzing real-time PCR data by the comparative C(T) method. *Nat Protoc*: **3**, 1101-1108.

74. Scholz, R., Molohon, K.J., Nachtigall, J., Vater, J., Markley, A.L., Sussmuth, R.D., Mitchell, D.A., and Borriss, R. (2011) Plantazolicin, a novel microcin B17/streptolysin S-like natural product from *Bacillus amyloliquefaciens* FZB42. *J Bacteriol*: **193**, 215-224.

75. Schuch, R., and Fischetti, V.A. (2006) Detailed genomic analysis of the Wbeta and gamma phages infecting *Bacillus anthracis*: implications for evolution of environmental fitness and antibiotic resistance. *J Bacteriol*: **188**, 3037-3051.

76. Schuch, R., Pelzek, A.J., Raz, A., Euler, C.W., Ryan, P.A., Winer, B.Y., Farnsworth, A., Bhaskaran, S.S., Stebbins, C.E., Xu, Y., *et al.* (2013) Use of a bacteriophage lysin to identify a novel target for antimicrobial development. *PLoS One*: **8**, e60754.

77. Sharma, A., Blair, P.M., and Mitchell, D.A. (2013) Synthesis of plantazolicin analogues enables dissection of ligand binding interactions of a highly selective methyltransferase. *Org Lett*: **15**, 5076-5079.

78. Shashikanth, N., Petrova, Y.I., Park, S., Chekan, J., Maiden, S., Spano, M., Ha, T., Gumbiner, B.M., and Leckband, D.E. (2015) Allosteric regulation of E-cadherin adhesion. *J Biol Chem*: **290**, 21749-21761.

79. Shaw, K.J., and Morrow, B.J. (2003) Transcriptional profiling and drug discovery. *Curr Opin Pharmacol*: **3**, 508-512.

80. Silver, L.L. (2011) Challenges of antibacterial discovery. *Clin Microbiol Rev*: **24**, 71-109.

81. Silverman, J.A., Perlmutter, N.G., and Shapiro, H.M. (2003) Correlation of daptomycin bactericidal activity and membrane depolarization in *Staphylococcus aureus*. *Antimicrob Agents Chemother*: **47**, 2538-2544.

82. Sterne, M., and Proom, H. (1957) Induction of motility and capsulation in *Bacillus anthracis*. *J Bacteriol*: **74**, 541-542.

83. Stojkovic, B., Torres, E.M., Prouty, A.M., Patel, H.K., Zhuang, L., Koehler, T.M., Ballard, J.D., and Blanke, S.R. (2008) High-throughput, single-cell analysis of macrophage interactions with fluorescently labeled *Bacillus anthracis* spores. *Appl Environ Microbiol*: **74**, 5201-5210.

84. Strahl, H., Burmann, F., and Hamoen, L.W. (2014) The actin homologue MreB organizes the bacterial cell membrane. *Nat Commun*: **5**, 3442.

85. Tan, L., and Turnbough, C.L., Jr. (2010) Sequence motifs and proteolytic cleavage of the collagen-like glycoprotein BclA required for its attachment to the exosporium of *Bacillus anthracis*. *J Bacteriol*: **192**, 1259-1268.

86. Tiyanont, K., Doan, T., Lazarus, M.B., Fang, X., Rudner, D.Z., and Walker, S. (2006) Imaging peptidoglycan biosynthesis in *Bacillus subtilis* with fluorescent antibiotics. *Proc Natl Acad Sci U S A*: **103**, 11033-11038.

87. Tourasse, N.J., and Kolsto, A.B. (2008) SuperCAT: a supertree database for combined and integrative multilocus sequence typing analysis of the *Bacillus cereus* group of bacteria (including *B. cereus*, *B. anthracis* and *B. thuringiensis*). *Nucleic Acids Res*: **36**, D461-468.

88. Unsay, J.D., Cosentino, K., Subburaj, Y., and Garcia-Saez, A.J. (2013) Cardiolipin effects on membrane structure and dynamics. *Langmuir*: **29**, 15878-15887.

89. Viklund, H., Bernsel, A., Skwark, M., and Elofsson, A. (2008) SPOCTOPUS: a combined predictor of signal peptides and membrane protein topology. *Bioinformatics*: **24**, 2928-2929.

90. Wang, Y.T., Oh, S.Y., Hendrickx, A.P., Lunderberg, J.M., and Schneewind, O. (2013) *Bacillus cereus* G9241 S-layer assembly contributes to the pathogenesis of anthrax-like disease in mice. *J Bacteriol*: **195**, 596-605.

91. Wecke, T., and Mascher, T. (2011) Antibiotic research in the age of omics: from expression profiles to interspecies communication. *J Antimicrob Chemother*: **66**, 2689-2704.

92. Wecke, T., Zuhlke, D., Mader, U., Jordan, S., Voigt, B., Pelzer, S., Labischinski, H., Homuth, G., Hecker, M., and Mascher, T. (2009) Daptomycin versus Friulimicin B: in-depth profiling of *Bacillus subtilis* cell envelope stress responses. *Antimicrob Agents Chemother*: **53**, 1619-1623.

93. Weidenmaier, C., and Peschel, A. (2008) Teichoic acids and related cell-wall glycopolymers in Gram-positive physiology and host interactions. *Nat Rev Microbiol*: **6**, 276-287.

94. Wilson, D.N., Harms, J.M., Nierhaus, K.H., Schlunzen, F., and Fucini, P. (2005) Species-specific antibiotic-ribosome interactions: implications for drug development. *Biol Chem*: **386**, 1239-1252.

95. Wilson, Z.E., Fenner, S., and Ley, S.V. (2015) Total syntheses of linear polythiazole/oxazole plantazolicin A and its biosynthetic precursor plantazolicin B. *Angew Chem Int Ed Engl*: **54**, 1284-1288.

96. Yang, D.C., Peters, N.T., Parzych, K.R., Uehara, T., Markovski, M., and Bernhardt, T.G. (2011) An ATP-binding cassette transporter-like complex governs cell-wall hydrolysis at the bacterial cytokinetic ring. *P Natl Acad Sci USA*: **108**, E1052-E1060.

97. Zhang, T., Muraih, J.K., Tishbi, N., Herskowitz, J., Victor, R.L., Silverman, J., Uwumarenogie, S., Taylor, S.D., Palmer, M., and Mintzer, E. (2014) Cardiolipin prevents membrane translocation and permeabilization by daptomycin. *J Biol Chem*: **289**, 11584-11591.

98. Zheng, J., Peng, D., Song, X., Ruan, L., Mahillon, J., and Sun, M. (2013) Differentiation of *Bacillus anthracis*, *B. cereus*, and *B. thuringiensis* on the basis of the csaB gene reflects host source. *Appl Environ Microbiol*: **79**, 3860-3863.

99. Ziegler, S., Pries, V., Hedberg, C., and Waldmann, H. (2013) Target identification for small bioactive molecules: finding the needle in the haystack. *Angew Chem Int Ed Engl*: **52**, 2744-2792.

APPENDIX A: PLANTAZOLICIN PUBLICATION WITH MINOR CONTRIBUTIONS

A.1 Engineering Unnatural Variants of Plantazolicin Through Codon Reprogramming

This chapter was preprinted with permission from (Deane *et al.*, 2013).

Deane, C.D., Melby, J.O., Molohon, K.J., Susarrey, A.R., and Mitchell, D.A. (2013) *ACS Chem Biol*: 8, 1998-2008. doi: 10.1021/cb4003392.

I constructed the fosmid library and isolated the clone used for PZN production.

ACS chemical biology

Articles

pubs.acs.org/acschemicalbiology

Engineering Unnatural Variants of Plantazolicin through Codon Reprogramming

Caitlin D. Deane,[†,‡] Joel O. Melby,[†,‡] Katie J. Molohon,[‡,§] Aziz R. Susarrey,[∥] and Douglas A. Mitchell[*,†,‡,§]

[†]Department of Chemistry, [‡]Institute for Genomic Biology, and [§]Department of Microbiology, [∥]School of Molecular and Cellular Biology, University of Illinois at Urbana−Champaign, Urbana, Illinois 61801, United States

Supporting Information

ABSTRACT: Plantazolicin (PZN) is a polyheterocyclic natural product derived from a ribosomal peptide that harbors remarkable antibiotic selectivity for the causative agent of anthrax, *Bacillus anthracis*. To simultaneously establish the structure−activity relationship of PZN and the substrate tolerance of the biosynthetic pathway, an *Escherichia coli* expression strain was engineered to heterologously produce PZN analogues. Variant PZN precursor genes were produced by site-directed mutagenesis and later screened by mass spectrometry to assess post-translational modification and export by *E. coli*. From a screen of 72 precursor peptides, 29 PZN variants were detected. This analogue collection provided insight into the selectivity of the post-translational modifying enzymes and established the boundaries of the natural biosynthetic pathway. Unlike other studied thiazole/oxazole-modified microcins, the biosynthetic machinery appeared to be finely tuned toward the production of PZN, such that the cognate enzymes did not process even other naturally occurring sequences from similar biosynthetic clusters. The modifying enzymes were exquisitely selective, installing heterocycles only at predefined positions within the precursor peptides while leaving neighboring residues unmodified. Nearly all substitutions at positions normally harboring heterocycles prevented maturation of a PZN variant, though some exceptions were successfully produced lacking a heterocycle at the penultimate residue. No variants containing additional heterocycles were detected, although several peptide sequences yielded multiple PZN variants as a result of varying oxidation states of select residues. Eleven PZN variants were produced in sufficient quantity to facilitate purification and assessment of their antibacterial activity, providing insight into the structure−activity relationship of PZN.

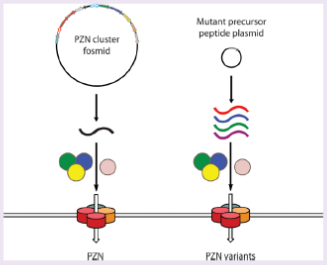

The clinical deployment of antibiotics revolutionized medical practice in the 20th century, but beginning in the late 1960s, the development of new classes of antibiotics slowed drastically while bacteria continued to acquire resistance.[1] Natural products have historically been the most valuable source of antibiotics and still today present a promising avenue to combat the growing problem of infections caused by antibiotic-resistant bacteria. Indeed, of the new antibacterial compounds approved by the FDA between 1981 and 2010, 66% were natural products or natural-product-derived.[2] In recent years, the increased ease of bacterial genome sequencing has facilitated the development of new strategies to tap into unexplored regions of natural product chemical space.[3] Natural product biosynthesis can potentially be "reprogrammed" to produce novel variants through genetic manipulation and/or supplying alternate substrates. Natural product engineering in modular biosynthetic pathways, such as polyketide synthases or nonribosomal peptide synthetases, remains difficult due to the complex nature of the multidomain megasynthases.[4−7] In contrast, the reprogramming of ribosomally synthesized and post-translationally modified peptides (RiPPs) is straightforward, as the natural product structure is directly encoded by the sequence of the precursor peptide gene.[8] Thus, site-directed mutagenesis leads to a predictable outcome in the resultant natural product, provided the modification enzymes tolerate the unnatural sequence.

Precursor peptide replacement *in vivo* has been used to study multiple RiPPs, most notably the lantibiotic nisin,[9−11] leading to the identification of multiple variants with increased activity. Similar approaches have also been applied to the study of other lanthipeptides, including lacticin 3147,[12,13] mersacidin,[14] lichenicidin,[15] and actagardine A.[16] This strategy has also garnered recent attention outside of the lanthipeptide family, where it has been successfully employed to engineer novel variants and explore the substrate requirements for the precursor peptides of several thiopeptides,[17−21] cyanobactins,[22] and microcin J25.[23]

The thiazole/oxazole-modified microcins (TOMMs)[8] comprise one RiPP subfamily characterized by thiazoline, (methyl)-oxazoline, and the corresponding 2-electron oxidized azoles, deriving from cysteines, serines, and threonines (Figure 1).[24] A

Received: May 14, 2013
Accepted: June 24, 2013
Published: June 24, 2013

dx.doi.org/10.1021/cb4003392 | ACS Chem. Biol. 2013, 8, 1998−2008

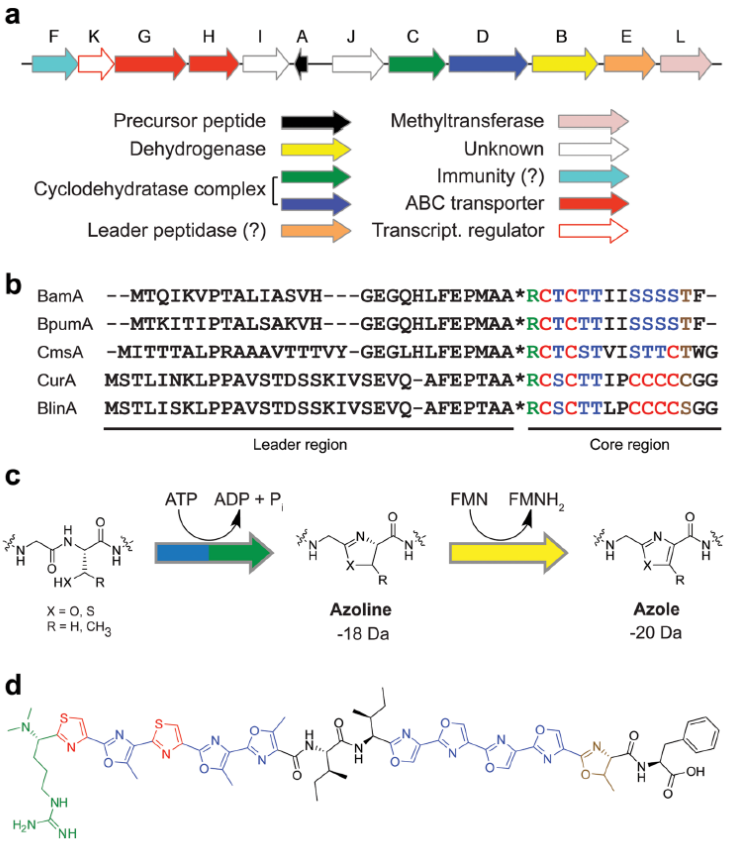

Figure 1. Genetics and enzymology of PZN biosynthesis. (a) The 10 kb PZN biosynthetic gene cluster from *Bacillus amyloliquefaciens* FZB42. (b) The precursor peptides for PZN and potential analogues from other species exhibit remarkable similarity. Bam, *B. amyloliquefaciens* FZB42; Bpum, *B. pumilus* ATCC 7061; Cms, *Clavibacter michiganensis* subsp. *sepedonicus*; Cur, *Corynebacterium urealyticum* DSM 7109; Blin, *Brevibacterium linens* BL2. Color-coding (predicted for Cms, Cur, and Blin): green, N^{α},N^{α}-dimethylarginine; red, thiazoles; blue, (methyl)oxazoles; brown, methyloxazoline; *, peptidase cleavage site. (c) Post-translational modification of cysteine, serine, and threonine residues in TOMM biosynthesis proceeds by cyclodehydration (mass loss of 18 Da) and subsequent oxidation (additional mass loss of 2 Da). (d) The chemical structure of PZN. Color-coding is identical to panel b.

trimeric enzymatic complex of a cyclodehydratase (C and D proteins) and a FMN-dependent dehydrogenase (B protein) catalyzes heterocycle formation and oxidation (Figure 1c).[24,25] Plantazolicin (PZN), a TOMM produced by the soil bacterium *Bacillus amyloliquefaciens* FZB42 displays a unique polyheterocyclic structure. After heterocycle formation, the unmodified N-terminal (leader peptide) region of the precursor peptide is proteolytically removed, likely by the putative peptidase (E protein) encoded in the gene cluster (Figure 1a).[26,27] Lastly, two methyl groups are installed onto the new N-terminus of the core peptide by an *S*-adenosylmethionine (SAM)-dependent methyltransferase (L protein) to yield the mature natural product (Figure 1d), which is then predicted to be exported by a dedicated transporter (G and H proteins), also within the gene cluster.[26,27]

PZN exhibits highly discriminating antibacterial activity against the causative agent of anthrax, *Bacillus anthracis*.[27] The spectrum of PZN activity excludes all Gram-negative strains and most Gram-positive strains tested thus far. Exploration within the closely related *B. cereus* subgroup revealed *B. anthracis* as the only strain significantly susceptible to PZN.[27] To date, similar biosynthetic gene clusters have been identified in four other bacterial species, indicating that these species have (or had at one time) the genetic capacity to produce PZN-like compounds, although only *B. pumilus* has been shown to do so during laboratory cultivation.[27] The precursor peptides in these species display a high degree of sequence similarity to the PZN precursor peptide (BamA), including many conserved residues in the core peptide (Figure 1b).[27] However, the role that these conserved residues play in

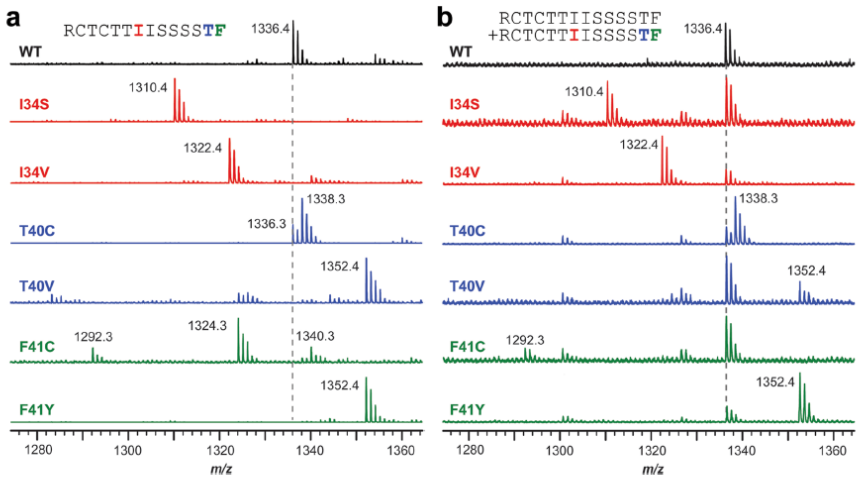

Figure 2. Representative MALDI mass spectra of PZN analogues. (a) Methanolic surface extracts from *E. coli* containing the PZN cluster Δ*bamA* fosmid plus BamA mutant plasmids. Color-coding: red, I34X mutants; blue, T40X mutants; green, F41X mutants. As indicated by the peak labels and the lack of *m*/*z* 1336 in each sample, production of PZN variants is only possible from plasmid-borne *mbp-bamA*. The *m*/*z* 1336 signal in the T40C spectrum corresponds to a variant containing a thiazole at position 40 (confirmation of structure given in Figure 4). The peaks at *m*/*z* 1324 and 1340 in the F41C spectrum correspond to oxidized C-terminal Cys (R-SO_xH, x = 2−3). Other labeled peaks correspond to PZN variants with wild-type-like modifications. (b) Same as panel a, but with the full PZN cluster fosmid plus BamA mutant plasmids. Wild-type PZN (*m*/*z* 1336) appears in every sample.

the post-translational modification of PZN and their importance in the bioactivity of the mature compound remained unknown. The current study sought to simultaneously address the structure−activity relationship of PZN and establish the substrate requirements for the biosynthetic pathway using heterologous expression of PZN analogues in *E. coli*.

RESULTS AND DISCUSSION

Heterologous Production of PZN. Although *B. amyloliquefaciens* FZB42 exhibits natural competency,[28] the inability to replicate plasmids, coupled with low transformation efficiency of integrative plasmids, necessitated the development of a heterologous system for facile expression and screening of PZN variants. Genomic DNA from the RS32 strain of *B. amyloliquefaciens*, in which the precursor peptide gene (*bamA*) is insertionally disrupted by a spectinomycin resistance cassette,[26] was digested and ligated into a DNA vector backbone to generate a fosmid library in *E. coli*. A fosmid bearing the Δ*bamA* PZN biosynthetic gene cluster (Supporting Figure S1) was identified through PCR screening of this library. The Δ*bamA* PZN cluster fosmid was under rhamnose-dependent copy control in *E. coli*,[29,30] while the PZN biosynthetic genes were under control of the native FZB42 promoters. To determine whether the fosmid-borne PZN biosynthetic enzymes were capable of modifying BamA supplied in *trans*, the PZN precursor peptide gene, *bamA*, was cloned into *E. coli* expression vector pBAD24 with an N-terminal fusion to maltose-binding protein (MBP) using standard methods (Supporting Table S1). Expression of *bamA* from this construct was under the control of the arabinose-inducible promoter, P_{ara}.[31]

Following growth in Luria−Bertani (LB) media supplemented with rhamnose and arabinose, PZN was obtained from the cell surface of the *E. coli* host by non-lytic methanolic extraction. Successful production and export of mature PZN was detected by high-performance liquid chromatography (HPLC) and matrix-assisted laser desorption ionization time-of-flight mass spectrometry (MALDI-MS) analysis (Supporting Figures S1 and S2), albeit at ∼5% of the 200−300 μg L^{-1} output from the native *B. amyloliquefaciens* producer.[27] It is plausible that the lower production level stems from an inefficient usage of *B. amyloliquefaciens* promoters by *E. coli*. *E. coli* cells containing the Δ*bamA* PZN fosmid only produced PZN when complemented with pBAD24-MBP-BamA after induction with rhamnose and arabinose (Supporting Figure S1). As short peptides have poor half-lives in *E. coli* when lacking a fusion partner,[32,33] inclusion of MBP was necessary for detection of PZN produced from plasmid-borne BamA. When the MBP tag was omitted, heterologous production of PZN was below the detection limit within the context of the crude cell surface extract, <20 pg (data not shown).

To provide an internal standard for evaluating the production level of PZN variants, a second fosmid was constructed bearing the PZN biosynthetic gene cluster from *B. amyloliquefaciens* FZB42 with the precursor peptide gene (*bamA*) intact. MALDI-MS and HPLC analysis of methanolic surface extracts from *E. coli* bearing this fosmid indicated production and export of mature PZN, even in the absence of the pBAD24-MBP-BamA construct (Supporting Figure S3).

Design and Evaluation of BamA Mutants. In order to assess the ability of the PZN post-translational pathway to accept alternate BamA substrates, nine residues in the core region of BamA were targeted for mutagenesis, based on the

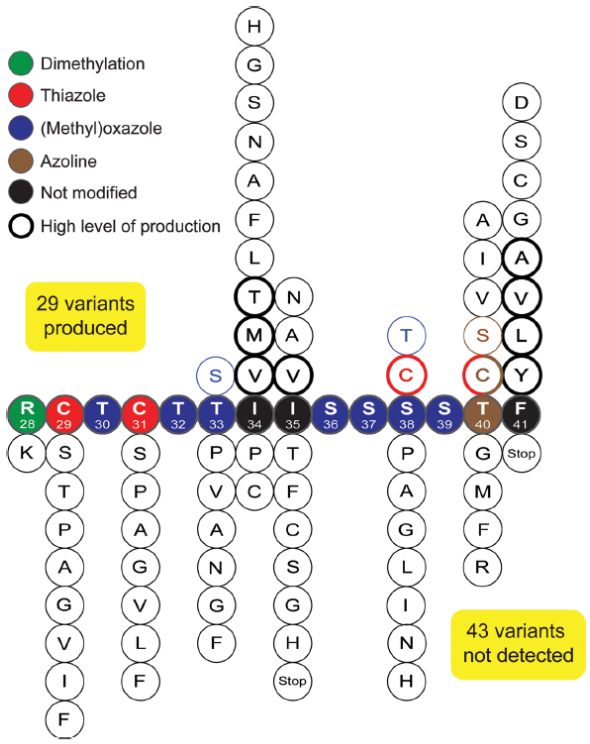

Figure 3. Summary of PZN variant production. PZN variants were heterologously expressed in *E. coli* prior to methanolic surface extraction and MALDI-MS analysis. Using this method, 29 point mutants of BamA were successfully converted to PZN variants (listed above core sequence), while 43 were not detected (listed below core sequence). Colored outlines indicate modifications to the altered residue as specified in the figure legend. Of the 29 analogues produced above the limit of detection (>20 pg in crude surface extracts), 10 were produced at levels greater than or equal to that of wild-type PZN (bold outlines), as assessed by relative peak heights during MALDI-MS analysis. The T40C variant produced two analogues, one with a thiazole at position 40 and the other with a thiazoline.

sequence similarity among the potential PZN producers (Figure 1b, Supporting Figure S4). This subset of the precursor peptide was selected in order to (i) include the most-conserved as well as the least-conserved residues, (ii) cover both heterocyclized and nonheterocyclized positions, and (iii) span the length of the precursor peptide core region. Rather than employ saturation mutagenesis, directed mutant panels were designed at eight of these positions (Supporting Figure S4). Each panel contained conservative and nonconservative mutations in order to sufficiently explore the available chemical space without generating an unnecessarily large number of mutants. Mutants were prepared by site-directed mutagenesis using primers with rationally chosen degenerate codons at select positions of pBAD24-MBP-BamA (Supporting Table S2). Following mutagenesis, polyclonal plasmid collections were transformed into competent *E. coli* cells bearing the complete PZN gene cluster fosmid. A medium-throughput method was employed to screen clones in groups of 20−40 for production of unnatural PZN analogues. Individual clones were cultured, PZN biosynthetic gene expression was induced with rhamnose and arabinose, and unnatural PZNs were isolated by non-lytic methanolic surface extraction, conditions that preclude isolation of intracellular contaminants. MALDI-MS was used to screen the surface extracts for unnatural PZN variants (Figure 2), and the positive clones were subjected to DNA sequencing (Figure 3). In addition, a selection of plasmids that did not produce a PZN variant were also sequenced in order to identify which precursor peptides were not processed by the post-translational modifying enzymes (Figure 3). The confirmed DNA sequence and the observed masses enabled deduction of the number and type of post-translational modifications for each variant (Figure 2). Using data from MALDI-MS analysis, comparison of the peak heights of wild-type PZN (fosmid-borne BamA, m/z 1336) and mutant PZN (plasmid-borne mutant BamA, variable mass) yielded a qualitative measure of production levels of the PZN variants (Figure 3). This preliminary assessment of production level enabled determination of which variants most warranted large-scale expression and purification, circumventing the time- and labor-intensive process of doing so with every variant.

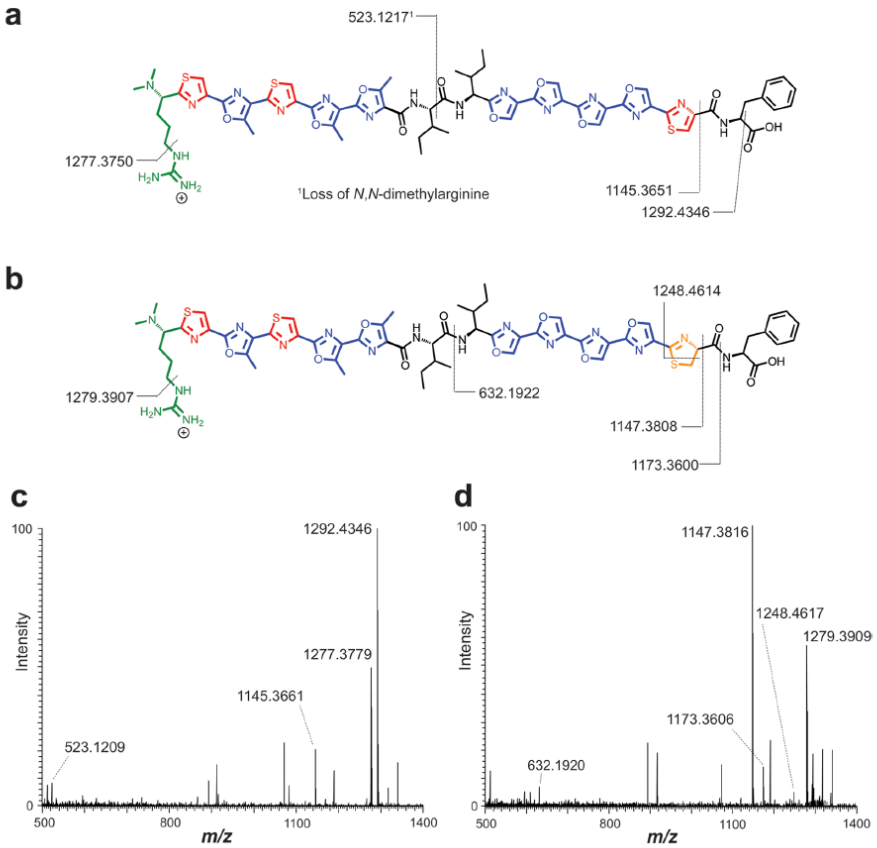

Figure 4. High resolution Fourier transform mass spectrometric (FTMS) analysis of PZN-T40C variants. (a) Structure, predicted fragments, and the calculated monoisotopic masses for PZN-T40C (deca-azole variant). One of the fragments was derived from multiple bond cleavages, denoted by the superscript. (b) Same as panel a, but for PZN-T40C (thiazoline variant). The thiazoline moiety is shown in orange. (c) Collision-induced dissociation of PZN-T40C (deca-azole variant, $C_{62}H_{65}N_{17}O_{12}S_3$, calcd m/z 1336.4239; exptl m/z 1336.4243, error 0.2 ppm) was consistent with the predicted structure. (d) Collision-induced dissociation of PZN-T40C (thiazoline variant, $C_{62}H_{67}N_{17}O_{12}S_3$, calcd m/z 1338.4395; exptl m/z 1338.4395, error 0.0 ppm) was consistent with the predicted structure, including localization of the thiazoline to position 40.

Assessment of the 72 mutants of BamA resulted in 29 clones that successfully produced and exported PZN variants within our detection limit (Figure 3). In this *in vivo* production system, a mutant precursor peptide must be successfully accepted as a substrate by multiple steps of the biosynthetic pathway (cyclodehydration, dehydrogenation, and leader peptidolysis), in addition to export, in order to yield a detectable product. Failure of any of these processes to accept an unnatural precursor peptide substrate led to an absence of detectable PZN variant. It is worth noting that such a result would not likely arise from failure at the methylation step of the biosynthetic pathway, as desmethylPZN can be successfully exported by *B. amyloliquefaciens*.[27] Of the 29 clones that successfully produced mature PZN variants, 26 had masses consistent with "wild-type-like" modifications: nine azole rings, one azoline ring, leader peptidolysis N-terminal to Arg28, and N-terminal dimethylation (Figure 1d). Three exceptions, PZN-T40A, -T40I, and -T40V, all produced MALDI-MS data consistent with the presence of one fewer heterocyclizable residue (nine azoles, no azolines) than wild-type PZN, as expected (Figure 3). Three other clones, I34M, T40C, and F41C, each yielded one or more modifications over "wild-type-like" processing, consistent with varying oxidation states at the mutated position (Figures 2a, 4 and 5; Supporting Figure S5).

Notably, the mutant *bamA* sequences differed by three nucleotides at most (out of 1394 bp, including MBP tag) and did not contain any rare *E. coli* codons.[34] Thus, the expression levels of the MBP-BamA peptides were expectedly comparable (Supporting Figure S6). The lack of detectable PZN variants for some mutants is attributed to the selectivity of the

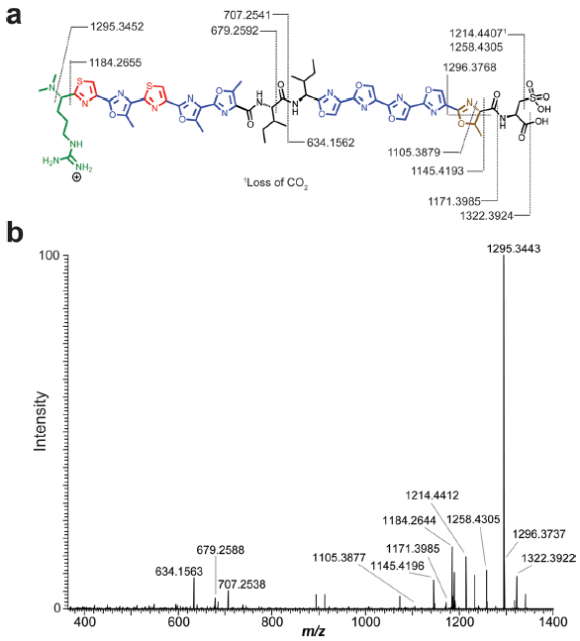

Figure 5. Fourier transform mass spectrometric (FTMS) analysis of PZN-F41C. (a) Structure, predicted fragments, and calculated monoisotopic masses for a sulfonic acid derivative of PZN-F41C. One of the fragments was derived from multiple bond cleavages, denoted by the superscript. (b) Collision-induced dissociation of PZN-F41C (sulfonic acid derivative, $C_{57}H_{65}N_{17}O_{16}S_3$, calcd m/z 1340.4036; exptl m/z 1340.4035, error 0.1 ppm) permitted localization of the sulfonic acid moiety to position 41.

biosynthetic pathway and not to poor expression of the precursor peptide. Ten of the 29 variants that were produced in the greatest quantity (Figure 3), as defined by ion intensity in MALDI-MS relative to that of the PZN internal standard (fosmid-borne *bamA*), were purified by HPLC (Supporting Figures S5, S7–S15). Subsequent tandem, high-resolution Fourier transform mass spectrometry (FTMS) data were consistent with the predicted structures (Figure 4; Supporting Figures S16–S24). Eight of the 10 PZN variants that were produced at "high" levels in *E. coli* harbored mutations at positions in PZN that do not receive side chain modifications: Ile34, Ile35, and Phe41 (Figure 3). This production level trend suggested that the biosynthetic pathway was more tolerant to variation at noncyclized positions relative to cyclized positions. The two remaining high production variants, PZN-S38C and -T40C (Figure 3), both replace a Ser/Thr with the heterocycle-competent Cys. In each case, the increased production level of the PZN variant was consistent with the increased nucleophilicity of the Cys side chain, which typically enhances the rate of cyclodehydration.[35−37]

Substrate Tolerance at Heterocyclized Positions. As the majority of analyzed mutant sequences failed to yield mature PZN variants, the PZN biosynthetic enzymes were less promiscuous *in vivo* than expected based on studies of other TOMMs.[17,35,37,38] Cys29 and Cys31, which are invariant throughout the PZN class (Figure 1b),[27] were critical for post-translational processing of BamA. No mutation at position 29 or 31 led to detectable PZN product formation *in vivo* (Figure 3). Even conservative mutations of Cys to Ser/Thr, or to the azol(in)e mimic Pro,[38] failed to produce mature analogues (Figure 3), demonstrating an unusual chemoselectivity for cysteine at these positions.[35−37,39] Multiple attempts to isolate intermediates in the post-translational cascade through utilization of the MBP tag via amylose affinity purification, coupled with MALDI-MS, were unsuccessful. For both accepted and unaccepted sequences, only the full-length unmodified BamA peptide could be detected in cell lysates. Identical results were obtained even when the arabinose concentration was lowered (serial dilutions to a final concentration of 3 μM) in an attempt to prevent any processed peptide signal from being overwhelmed by newly synthesized BamA.[31] This result implies that failure to cyclize a particular residue aborts downstream modification required for maturation and export, and that cyclodehydration is the first committed step in PZN maturation, but this hypothesis will require further confirmation.

In contrast to the invariant Cys at positions 29 and 31 (Figure 3), the PZN biosynthetic pathway tolerated conservative, heterocyclizable mutations at Thr33 and Ser38 but allowed more nonconservative mutations at Thr40 (Figure 3). Consistent with the variation at these positions in other PZN-like precursor peptides (Figure 1b), all other heterocyclizable residues substituted at these three positions resulted in full ("wild-type-like") maturation of the PZN analogue, including

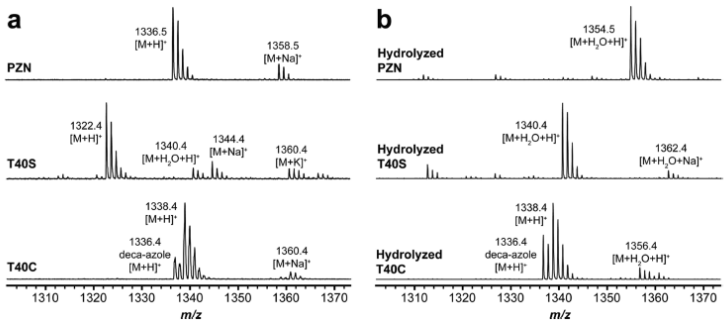

Figure 6. Hydrolytic stability of PZN analogues varied at Thr40. In naturally occurring PZN, Thr40 exists as a methyloxazoline. (a) MALDI-MS spectra from methanolic surface extracts of *E. coli* engineered to produced native PZN, -T40S, and -T40C. (b) Same as panel a, after treatment with 0.2% HCl for 4 h at 23 °C to induce hydrolysis. Under these conditions, the (methyl)oxazolines were virtually quantitatively hydrolyzed, whereas the T40C thiazoline was minimally hydrolyzed. The deca-azole variant contains a thiazole at position 40, which was unreactive toward hydrolysis.

cyclodehydration of the substituted residue (Figure 3). The absence of *β*-nucleophile-containing amino acids at these positions disrupts the contiguous polyheterocyclic structure of PZN. In the case of Thr33 and Ser38, we posit that this disruption prevents the formation of downstream heterocycles, as observed for other TOMM natural products.[37,40] However, the relative promiscuity of the cyclodehydratase was markedly increased at Thr40, as several noncyclizable, nonpolar residues (Ala, Val, Ile) were tolerated by the biosynthetic pathway, in addition to other heterocyclizable residues (Cys, Ser). The above-described intolerance toward mutations at Cys29 and Cys31, contrasted with the promiscuity at Thr40, suggests N- to C-terminal processing for PZN, which is the canonical direction of RiPP modification.[36,37,41] Alternatively, if position 40 is not the last position to be cyclodehydrated, other modifications of PZN certainly do not depend on position 40 being cyclized, unlike the case for positions 29 and 31.

In native PZN, Thr40 is converted to a methyloxazoline (Figure 1d) and is the only heterocycle to evade dehydrogenation.[27] Initial MALDI-MS results found that the PZN-T40S and -T40C variants each contained an azoline, presumably at position 40 (Figure 3). Given that thiazolines hydrolyze under mildly acidic conditions much more slowly than the corresponding (methyl)oxazolines,[42,43] we wondered if differential hydrolysis would be useful to rapidly assess the azoline content of natural products.[44] Upon exposing native PZN, -T40S, and -T40C to mild aqueous acid, only T40C was hydrolytically stable under the conditions employed (Figure 6). Intriguingly, when the T40C analogue was produced in the strain bearing the PZN Δ*bamA* fosmid, the absence of wild-type PZN (*m*/*z* 1336) permitted observation of a fully oxidized variant (deca-azole, *m*/*z* 1336), which was unreactive toward acid hydrolysis (Figure 6). FTMS/MS analysis confirmed the proposed structures (Figure 4).

Substrate Tolerance at Noncyclized Positions. As Thr40 could be substituted with noncyclizable residues, the substrate tolerance at naturally occurring noncyclizable residues was evaluated. Ile34 and Phe41 both lie on the C-terminal side of a contiguous polyazol(in)e moiety (Figure 1d), prompting the question of whether an additional heterocycle could be formed at these positions. While substitution with cyclizable residues was tolerated at these positions, the side chains did not undergo cyclodehydration (Figure 3), demonstrating that the PZN cyclodehydratase is remarkably regioselective. These structural assignments were supported by MS/MS data on the PZN-F41C and -I34T analogues (Figure 5, Supporting Figure S17). The free thiol of PZN-F41C was clearly susceptible to oxidation, as indicated by the MS-based detection of the sulfinic ($R\text{-}SO_2H$) and sulfonic ($R\text{-}SO_3H$) acid derivatives (Figures 2a and 5). Installation of a stop codon at position 41, however, failed to produce the expected PZN truncation (Figure 3), suggesting that the biosynthetic pathway required the presence of a C-terminal flanking residue for a cyclized position, as previously observed for other TOMMs.[37,39]

In the case of PZN-I34T, the newly installed Thr at position 34 could not be definitively proven to remain uncyclized, due to the difficulty of obtaining dissociation between heterocycles during MS/MS (Supporting Figure S17). However, the data were consistent with the presence of five fully oxidized heterocycles in the N-terminal half of the molecule, as seen in wild-type PZN.[27] Thus, if the substituted Thr was cyclized, it would require the omission of a normally installed heterocycle, which seems unlikely. Although the PZN biosynthetic enzymes could tolerate PZN-I34S/T, the pathway was unable to fully process PZN-I34C (Figure 3). It is possible that cyclodehydration of this newly installed Cys resulted in an intermediate that was incompatible with downstream processing. Unfortunately, all attempts to isolate potential biosynthetic intermediates of PZN-I34C resulted in the detection of only the full-length unmodified peptide (data not shown). Indirect support for the incompatibility of cyclization from PZN-I34C comes from variant -I34P, the only other assessed mutant at position 34 that did not produce PZN (Figure 3). As proline is known to mimic azol(in)e heterocycles, the intolerance toward PZN-I34P suggests the inability of the biosynthetic pathway to cope with the lack of conformational flexibility at this position.[37,38]

Among the four residues with unmodified side chains in the core sequence of wild-type BamA, the PZN biosynthetic pathway was least tolerant to mutation at Ile35 and Arg28 (Figure 3). Only conservative mutations were tolerated at Ile35: Ala, Val, and the sterically similar Asn (Figure 3). Many of the substitutions tolerated at Ile34 did not yield detectable

mature PZN analogues when probed at Ile35, including Gly, aromatic residues, and polar residues. This trend was consistent with the flanking residue requirements observed with other TOMM cyclodehydratases,[37,39] where the constraints for the residue in the −1 (N-terminal) position flanking a heterocycle are stricter than for the residue in the +1 (C-terminal) position. In PZN, with its two contiguous polyazol(in)e moieties, Ile35 occupies the −1 position for the C-terminal ring system, while Ile34 and Phe41 lie in +1 positions. By extension, Arg28 (N^{α},N^{α}-dimethylarginine in mature PZN) is in the −1 position for the N-terminal ring system (Figure 1d). The most conservative mutation possible, R28K, was not tolerated by the PZN biosynthetic pathway, and as such, did not garner further attention (Figure 3). Conceivably, the failure to process the R28K mutant was due to its proximity to the leader peptidase cleavage site, thus inhibiting leader peptide cleavage and export. Numerous attempts to detect intracellular PZN intermediates with intact leader peptides by affinity chromatography were unsuccessful. Postproteolysis, the methylation state of PZN should not affect export, as desmethylPZN was successfully exported in a Δ*bamL* strain of *B. amyloliquefaciens*.[26,27]

Pathway Tolerance for Variations in Substrate Length. In the continued interest of exploring the substrate tolerance of the PZN biosynthetic pathway, several BamA analogues were constructed to expand the PZN sequence by one residue in the middle of each polyazol(in)e moiety, between the two central Ile residues, and at the C-terminus (Supporting Figure S25, Supporting Table S2). Production of PZN variants based on these peptides was assessed as described above. BamA peptides expanded by an internal alanine residue were not processed (Supporting Figure S25). However, expansion of the peptide by a single residue at the C-terminus was tolerated in all cases tested, with the exception of proline (Supporting Figure S25). In addition to these expanded substrates, a contracted version of BamA was constructed by deletion of Ser38, potentially reducing the C-terminal polyazole system from five heterocycles to four. However, this substrate also eluded processing. Taken together with the failure to process substrates truncated at positions 35 and 41 (Figure 3), these data indicated that one or more of the PZN biosynthetic enzymes have precise length requirements as to the arrangement of heterocyclized residues within the BamA precursor peptide. In this regard, PZN biosynthesis stands in stark contrast to several other characterized TOMM biosynthetic pathways.[18,37,39]

Production of Other PZN-Class Natural Products. Although four other publicly available bacterial genomes encode PZN-like biosynthetic gene clusters (Figure 1), to date, only *Bacillus pumilus* has been shown to produce PZN during laboratory cultivation.[27] The amino acid sequences of the core peptides from *B. pumilus* ATCC 7061 and *B. amyloliquefaciens* FZB42 are identical (Figure 1b),[27] rendering it necessary to look to the other potential PZN producers in order to determine if *E. coli* could biosynthesize non-*Bacillus* PZN compounds. As substrate binding is mediated by the leader sequence,[38,45−47] the PZN biosynthetic enzymes from *B. amyloliquefaciens* were unlikely to accept significantly different leader peptides as substrates. Indeed, attempts to heterologously produce the *Clavibacter michiganensis* subsp. *sepedonicus* (Cms) encoded PZN (via pBAD24-MBP-CmsA) using the FZB42 biosynthetic pathway (fosmid-borne) proved unsuccessful. To circumvent the potential failure of leader peptide recognition during *E. coli* heterologous expression, precursor peptide chimeras were generated that consisted of the leader peptide sequence from the native producer (FZB42) and the core peptide sequence from other family members, yielding BamA-CmsA, BamA-CurA, and BamA-BlinA (Cur, *Corynebacterium urealyticum* DSM 7109; Blin, *Brevibacterium linens* BL2, Supporting Figure S26). Similar strategies employing precursor peptide chimeras have been previously used in other RiPP systems to enable the processing of unnatural core peptides.[37,38] Surprisingly, none of the products from the PZN chimeras were detected, although production of the unmodified peptides was verified by MALDI-MS (Supporting Figure S27). The inability to detect PZN-class natural products derived from the chimeric precursor peptides, despite their overall similarity to BamA/PZN, provided further evidence for the extraordinary specificity exhibited by the FZB42 biosynthetic pathway.

To shed further light on the inability of the chimeric peptides to produce PZN variants in *E. coli*, efforts were focused on the PZN cluster from *C. michiganensis*. This cluster bears the highest degree of sequence conservation to FZB42 (aside from *B. pumilus*) among (i) the precursor peptide (51/80; % identity/% similarity), (ii) the heterocycle-forming proteins (B: 57/87, C: 41/77, D: 57/76; % identity/% similarity), (iii) the other modifying enzymes (E: 16/55, L: 25/60), and (iv) the export apparatus (G: 33/71, H: 19/59).[27,48,49] In an effort to render the BamA-CmsA chimera more similar to BamA, two constructs were generated. These included the point mutant BamA-CmsA-S32T and truncation of the C-terminal Gly, BamA-CmsA-G42term (Supporting Figure S26). Unexpectedly, these altered BamA-CmsA sequences also failed to produce PZN analogues, indicating that neither of these positions was individually responsible for the failure of BamA-CmsA to be tolerated by the FZB42 pathway. The previously analyzed mutants BamA-I34V and -S38T both yielded mature PZN analogues (Figure 3), indicating that the Val34 or Thr38 residues found in CmsA (Supporting Figure S26) were also not responsible for processing failure. It is not obvious how the two residues in BamA-CmsA flanking Thr38 (i.e., Thr37 and Cys39) could pose an obstacle to post-translational modification. Trp41 also seems an unlikely problem, given that PZN variants at position Phe41 were successfully biosynthesized with a wide variety of amino acid replacements (Figure 3). Taken together, these data indicate that the failure of the PZN pathway to process the BamA-CmsA chimera was not due to a single residue difference in the precursor peptide, but instead a culmination of several amino acid changes.

Antibacterial Activity of PZN Analogues. Of the 29 PZN variants detected, 10 were produced in sufficient quantity (Figure 3) to permit assessment of their antibacterial activity against *B. anthracis* Sterne. These 10 analogues, as well as the wild-type BamA sequence, were expressed in conjunction with the PZN Δ*bamA* fosmid, extracted in methanol, and purified by HPLC (Supporting Figures S5, S7−S15), each yielding 3−5 μg of purified PZN analogue per 15 cm diameter plate of LB agar. The minimum inhibitory concentrations (MICs) of the purified PZN analogues were then determined by microbroth dilution assay against *B. anthracis* Sterne (Table 1). The activity of heterologously produced wild-type PZN was in good agreement with the published value for PZN from the native host.[27] The analogues exhibited a range of antibacterial potencies, although no analogues were observed to have increased potency against *B. anthracis*.

Table 1. Antibacterial activity of PZN analogues against *B. anthracis* Sterne

variant	MIC[a] (μg mL^{-1}) heterocycle at 40	Thr at 40
PZN	2	32[b]
I34M	32	>32
I34T	8	>32
I34V	8	>32
I35V	16	32
S38C	32	>32
T40C (thiazoline)	8	ND[c]
T40C (thiazole)	32	NA[d]
F41A	8	32
F41L	4	>32
F41V	16	32
F41Y	>32	>32

[a]MIC = minimum inhibitory concentration. [b]Reference 27. [c]ND = not determined. [d]NA = not applicable.

As expected, conservative mutations to the noncyclized Ile residues (I34V, I34T, I35V) resulted in relatively modest reductions (4- to 8-fold) in antibacterial potency (Table 1). In contrast, PZN-I34M, which lacks a β-methyl side chain substituent, resulted in a 16-fold reduction in potency, indicating that this region of the PZN structure does contribute to the anti-*B. anthracis* activity. Similarly, relatively conservative mutations to the C-terminal Phe (F41A, F41L, F41V) also led to modest reductions (2- to 8-fold) in potency. Surprisingly, a conservative mutation at this position, F41Y, abolished the antibacterial activity of PZN (Table 1). The similarly conservative S38C mutation (replaces an oxazole with a thiazole) also resulted in a 16-fold reduction in activity (Table 1). As these moieties are isosteric, the altered activity of the PZN analogue must arise from electronic effects.

Analysis of PZN-T40C yielded two analogues differing in heterocycle oxidation at the penultimate position (Figure 4). These species were separable by HPLC (Supporting Figure S11) and were tested for anti-*B. anthracis* activity. PZN-T40C(thiazoline) resulted in a 4-fold reduction in anti-*B. anthracis* potency, while the presence of the fully oxidized, "deca-azole" T40C(thiazole) resulted in a 16-fold reduction in activity (Table 1). These data indicate that the post-translational status of position 40 plays an important role in the activity of PZN. These results concur with the previously noted 16-fold loss of activity upon hydrolysis of the Thr40 methyloxazoline in native PZN (Table 1).[27] As expected, none of the oxazoline-containing PZN variants assayed in this study exhibited significant anti-*B. anthracis* activity (MIC <32 μg mL^{-1}) when hydrolyzed (Table 1). Analogues lacking a heterocycle at position 40 (PZN-T40A, -T40I, and -T40V; Figure 3) were not isolated in sufficient quantity (>10 μg) to facilitate purification and subsequent determination of anti-bacterial potency. However, based on the results for hydrolyzed PZN (reinstated Thr at position 40) and T40C, it is likely that these mutations would also severely reduce, if not abolish, activity. In accord with the observation that desmethylPZN had no measurable activity,[27] it is clear that multiple regions of PZN, including both N- and C-termini, as well as the internal Ile residues and the polyazole(in)e moieties, collectively contribute to the observed anti-*B. anthracis* activity.

In conclusion, we have developed a facile system for the heterologous expression of PZN in *E. coli*, which enabled the production of analogues from variant precursor peptides. Using this system, we have elucidated the scope of substrate tolerance in the PZN biosynthetic pathway and found it to be much less permissive than previously characterized RiPPs. From PZN analogues that were successfully produced, we have also provided significant insight into the structure–activity relationship for the PZN pharmacophore. This heterologous expression system has the potential to be applied to the study of any RiPP natural product by facilitating production of analogues in *E. coli*.

METHODS

Heterologous PZN Production. To heterologously produce PZN and analogues, *E. coli* cells containing a fosmid harboring the PZN biosynthetic gene cluster Δ*bamA* (Supporting Methods) were transformed with purified pBAD24-MBP-BamA or a variant thereof. Transformants were selected using Luria–Bertani (LB) agar supplemented with ampicillin (50 μg mL^{-1}) and chloramphenicol (12.5 μg mL^{-1}). Individual colonies were used to inoculate 10 mL cultures of LB broth supplemented with ampicillin (50 μg mL^{-1}) and chloramphenicol (12.5 μg mL^{-1}) in test tubes. Cultures were grown on a roller drum at 37 °C to an OD_{600} measurement of 0.6, at which point cells were harvested by centrifugation (4,000 × *g*) and resuspended in 1 mL of the LB supernatant. To induce production of PZN or analogues, 300 μL of cell suspension was spread on a 15 cm plate of LB agar supplemented with ampicillin (50 μg mL^{-1}), chloramphenicol (12.5 μg mL^{-1}), and rhamnose (10 mM) to increase copy number of the fosmid,[29] and arabinose (10 mM) to induce expression of MBP-BamA from the P_{ara} promoter of pBAD24. These cultures were grown at 30 °C for 40 h. Cells were harvested by resuspension in TE buffer (10 mM Tris, 1 mM EDTA, pH 8.0) and subsequent centrifugation (4,000 × *g*).

PZN Extraction. Crude PZN or analogues were obtained by a non-lytic, methanolic cell surface extraction, similar to methods described previously.[27] Briefly, cells were resuspended in MeOH (10 mL), agitated by vortex for 45 s, and equilibrated for 15 min at 22 °C. Cells were harvested by centrifugation (4,000 × *g*), and the MeOH supernatant was rotary evaporated to near dryness. The crude extract was resuspended in deionized water and lyophilized to dryness. Dried, crude extracts were resuspended in 500 μL of 80% (v/v) aqueous MeCN for purification by HPLC or in 500 μL of MeOH for analysis of crude extract by MALDI-MS.

Screening of Mutant Panels. To screen BamA mutant panels for production of PZN variants, purified polydonal plasmid libraries or individual plasmid sequences were used to transform chemically competent *E. coli* cells containing the entire PZN biosynthetic gene cluster (including *bamA*) on a fosmid, as described above. Individual colonies were used to inoculate 10 mL cultures of LB broth supplemented with ampicillin (50 μg mL^{-1}) and chloramphenicol (12.5 μg mL^{-1}) in test tubes. Cultures were grown on a roller drum at 37 °C to an OD_{600} of 0.6, at which point PZN production was induced by addition of rhamnose (10 mM) and arabinose (10 mM) to the liquid cultures. Following induction, cultures were grown with shaking at 30 °C for 24 h. Cells were harvested by centrifugation (4,000 × *g*), washed with TE buffer, and harvested again (8,000 × *g*). PZN variants were extracted analogously to the procedure described above using 1 mL of MeOH. Cells were harvested by centrifugation (8,000 × *g*), and the MeOH supernatant was evaporated in a speed-vac concentrator with minimal heating. Dry, crude extracts were resuspended in 10 μL of MeOH for analysis by MALDI-MS. Since the Quikchange site-directed mutagenesis method does not guarantee that all possible DNA sequences will be produced due to potential sequence biases, a sufficient number of clones were sequenced from each library to ensure 95% confidence in having detected all generated mutants, as calculated by $0.95 = 1 - (1 - f)^n$, where f = frequency of the least represented mutants and n = number of clones screened.[50]

Reverse Phase HPLC Purification. Crude PZN or analogues [suspended in 80% (v/v) aqueous MeCN] were reverse phase purified as described previously[27] using a Thermo BETASIL C18 column (250

mm × 10 mm; pore size 100 Å; particle size 5 μm) at a flow rate of 4 mL min^{-1}. A gradient of 65−95% MeOH with 0.1% (v/v) formic acid over 32 min was used. The fractions containing PZN or an analogue (as monitored by A_{266} and later verified by MALDI-MS) were collected into 20 mL borosilicate vials, and the solvent was removed *in vacuo*. Purified PZN analogues were quantified by A_{260} in DMSO solution.

Mass Spectrometry. MALDI-MS analysis used a Bruker Daltonics UltrafleXtreme MALDI-TOF/TOF instrument operating in reflector/positive mode using sinapic acid as the matrix. LC−MS analysis used an Agilent 1200 HPLC system coupled to a G1956B quadrupole mass spectrometer with an electrospray ionization (ESI) source. LC used a 2.1 mm × 150 mm Grace Vydac Denali C_{18} column (120 Å, 5 μm) with a gradient of 65−95% MeOH with 0.1% (v/v) formic acid over 25 min, with the analytes eluted directly into the MS.

HPLC-purified samples for high-resolution and tandem mass spectrometry were resuspended in 12 μL of 80% (v/v) MeCN with 1% (v/v) formic acid. An Advion Nanomate 100 directly infused the sample to a ThermoFisher Scientific LTQ-FT hybrid linear ion trap, operating at 11 T (calibrated weekly). The FTMS was operated using the following parameters: minimum target signal counts, 5000; resolution, 100,000; m/z range detected, dependent on target m/z; isolation width (MS/MS), 4−5 m/z; normalized collision energy (MS/MS), 35; activation q value (MS/MS), 0.4; activation time (MS/MS), 30 ms.

Antibacterial Activity Assay. Determination of MIC values for PZN analogues was performed as described previously[27] for *B. anthracis* Sterne with the only modification being that PZN analogues were added from DMSO solutions to a maximum final concentration of 32 μg mL^{-1} in bacterial cultures. Hydrolyzed samples were prepared by incubation of purified PZN analogues (suspended in MeOH) with 0.2% (w/v) HCl for 4 h at 23 °C, followed by removal of solvent in a speed-vac concentrator and subsequent resuspension in DMSO.

■ ASSOCIATED CONTENT

Supporting Information

Supporting methods, design of mutant panels, purification and mass spectrometric analysis of PZN variants, sequences of chimera peptides, and DNA sequences. This material is available free of charge via the Internet at http://pubs.acs.org.

■ AUTHOR INFORMATION

Corresponding Author

*E-mail: douglasm@illinois.edu.

Notes

The authors declare no competing financial interest.

■ ACKNOWLEDGMENTS

We are grateful to W. Metcalf and J. Cronan for the generous gifts of fosmid generation reagents and pBAD24, respectively. We also thank members of the Mitchell lab for the critical review of this manuscript. This work was supported in part by the National Institutes of Health (NIH, 1R01 GM097142 to D.A.M.), the NIH Director's New Innovator Award Program (DP2 OD008463 to D.A.M.), the Robert C. and Carolyn J. Springborn Endowment (to C.D.D.), and the Cell & Molecular Biology Training Grant (T32 GM007283 to K.J.M.). The Bruker UltrafleXtreme MALDI TOF/TOF mass spectrometer was purchased in part with a grant from the National Center for Research Resources, NIH (S10 RR027109 A).

■ REFERENCES

(1) Fischbach, M. A., and Walsh, C. T. (2009) Antibiotics for emerging pathogens. *Science 325*, 1089−1093.

(2) Newman, D. J., and Cragg, G. M. (2012) Natural products as sources of new drugs over the 30 years from 1981 to 2010. *J. Nat. Prod. 75*, 311−335.

(3) Challis, G. L. (2008) Genome mining for novel natural product discovery. *J. Med. Chem. 51*, 2618−2628.

(4) Kapur, S., Chen, A. Y., Cane, D. E., and Khosla, C. (2010) Molecular recognition between ketosynthase and acyl carrier protein domains of the 6-deoxyerythronolide B synthase. *Proc. Natl. Acad. Sci. U.S.A. 107*, 22066−22071.

(5) Kapur, S., Lowry, B., Yuzawa, S., Kenthirapalan, S., Chen, A. Y., Cane, D. E., and Khosla, C. (2012) Reprogramming a module of the 6-deoxyerythronolide B synthase for iterative chain elongation. *Proc. Natl. Acad. Sci. U.S.A. 109*, 4110−4115.

(6) Liu, T., Chiang, Y. M., Somoza, A. D., Oakley, B. R., and Wang, C. C. (2011) Engineering of an "unnatural" natural product by swapping polyketide synthase domains in Aspergillus nidulans. *J. Am. Chem. Soc. 133*, 13314−13316.

(7) Hughes, A. J., and Keatinge-Clay, A. (2011) Enzymatic extender unit generation for in vitro polyketide synthase reactions: structural and functional showcasing of Streptomyces coelicolor MatB. *Chem. Biol. 18*, 165−176.

(8) Arnison, P. G., Bibb, M. J., Bierbaum, G., Bowers, A. A., Bugni, T. S., Bulaj, G., Camarero, J. A., Campopiano, D. J., Challis, G. L., Clardy, J., Cotter, P. D., Craik, D. J., Dawson, M., Dittmann, E., Donadio, S., Dorrestein, P. C., Entian, K. D., Fischbach, M. A., Garavelli, J. S., Goransson, U., Gruber, C. W., Haft, D. H., Hemscheidt, T. K., Hertweck, C., Hill, C., Horswill, A. R., Jaspars, M., Kelly, W. L., Klinman, J. P., Kuipers, O. P., Link, A. J., Liu, W., Marahiel, M. A., Mitchell, D. A., Moll, G. N., Moore, B. S., Muller, R., Nair, S. K., Nes, I. F., Norris, G. E., Olivera, B. M., Onaka, H., Patchett, M. L., Piel, J., Reaney, M. J. T., Rebuffat, S., Ross, R. P., Sahl, H. G., Schmidt, E. W., Selsted, M. E., Severinov, K., Shen, B., Sivonen, K., Smith, L., Stein, T., Sussmuth, R. D., Tagg, J. R., Tang, G. L., Truman, A. W., Vederas, J. C., Walsh, C. T., Walton, J. D., Wenzel, S. C., Willey, J. M., and van der Donk, W. A. (2013) Ribosomally synthesized and post-translationally modified peptide natural products: overview and recommendations for a universal nomenclature. *Nat. Prod. Rep. 30*, 108−160.

(9) Piper, C., Hill, C., Cotter, P. D., and Ross, R. P. (2011) Bioengineering of a Nisin A-producing Lactococcus lactis to create isogenic strains producing the natural variants Nisin F, Q and Z. *Microb. Biotechnol. 4*, 375−382.

(10) Molloy, E. M., Field, D., Connor, P. M., Cotter, P. D., Hill, C., and Ross, R. P. (2013) Saturation mutagenesis of lysine 12 leads to the identification of derivatives of nisin a with enhanced antimicrobial activity. *PloS One 8*, e58530.

(11) Molloy, E. M., Ross, R. P., and Hill, C. (2012) 'Bac' to the future: bioengineering lantibiotics for designer purposes. *Biochem. Soc. Trans. 40*, 1492−1497.

(12) Cotter, P. D., Deegan, L. H., Lawton, E. M., Draper, L. A., O'Connor, P. M., Hill, C., and Ross, R. P. (2006) Complete alanine scanning of the two-component lantibiotic lacticin 3147: generating a blueprint for rational drug design. *Mol. Microbiol. 62*, 735−747.

(13) Field, D., Molloy, E. M., Iancu, C., Draper, L. A., O' Connor, P. M., Cotter, P. D., Hill, C., and Ross, R. P. (2013) Saturation mutagenesis of selected residues of the alpha-peptide of the lantibiotic lacticin 3147 yields a derivative with enhanced antimicrobial activity. *Microb. Biotechnol*, DOI: 10.1111/1751-7915.12041.

(14) Appleyard, A. N., Choi, S., Read, D. M., Lightfoot, A., Boakes, S., Hoffmann, A., Chopra, I., Bierbaum, G., Rudd, B. A., Dawson, M. J., and Cortes, J. (2009) Dissecting structural and functional diversity of the lantibiotic mersacidin. *Chem. Biol. 16*, 490−498.

(15) Caetano, T., Krawczyk, J. M., Mosker, E., Sussmuth, R. D., and Mendo, S. (2011) Heterologous expression, biosynthesis, and mutagenesis of type II lantibiotics from Bacillus licheniformis in Escherichia coli. *Chem. Biol. 18*, 90−100.

(16) Boakes, S., Ayala, T., Herman, M., Appleyard, A. N., Dawson, M. J., and Cortes, J. (2012) Generation of an actagardine A variant library through saturation mutagenesis. *Appl. Microbiol. Biotechnol. 95*, 1509−1517.

(17) Bowers, A. A., Acker, M. G., Koglin, A., and Walsh, C. T. (2010) Manipulation of thiocillin variants by prepeptide gene replacement: structure, conformation, and activity of heterocycle substitution mutants. *J. Am. Chem. Soc. 132*, 7519−7527.
(18) Bowers, A. A., Acker, M. G., Young, T. S., and Walsh, C. T. (2012) Generation of thiocillin ring size variants by prepeptide gene replacement and in vivo processing by Bacillus cereus. *J. Am. Chem. Soc. 134*, 10313−10316.
(19) Li, C., Zhang, F., and Kelly, W. L. (2011) Heterologous production of thiostrepton A and biosynthetic engineering of thiostrepton analogs. *Mol. Biosyst. 7*, 82−90.
(20) Li, C., Zhang, F., and Kelly, W. L. (2012) Mutagenesis of the thiostrepton precursor peptide at Thr7 impacts both biosynthesis and function. *Chem. Commun. 48*, 558−560.
(21) Young, T. S., Dorrestein, P. C., and Walsh, C. T. (2012) Codon randomization for rapid exploration of chemical space in thiopeptide antibiotic variants. *Chem. Biol. 19*, 1600−1610.
(22) Tianero, M. D., Donia, M. S., Young, T. S., Schultz, P. G., and Schmidt, E. W. (2012) Ribosomal route to small-molecule diversity. *J. Am. Chem. Soc. 134*, 418−425.
(23) Pan, S. J., and Link, A. J. (2011) Sequence diversity in the lasso peptide framework: discovery of functional microcin J25 variants with multiple amino acid substitutions. *J. Am. Chem. Soc. 133*, 5016−5023.
(24) Lee, S. W., Mitchell, D. A., Markley, A. L., Hensler, M. E., Gonzalez, D., Wohlrab, A., Dorrestein, P. C., Nizet, V., and Dixon, J. E. (2008) Discovery of a widely distributed toxin biosynthetic gene cluster. *Proc. Natl. Acad. Sci. U.S.A. 105*, 5879−5884.
(25) Dunbar, K. L., Melby, J. O., and Mitchell, D. A. (2012) YcaO domains use ATP to activate amide backbones during peptide cyclodehydrations. *Nat. Chem. Biol. 8*, 569−575.
(26) Scholz, R., Molohon, K. J., Nachtigall, J., Vater, J., Markley, A. L., Sussmuth, R. D., Mitchell, D. A., and Borriss, R. (2011) Plantazolicin, a novel microcin B17/streptolysin S-like natural product from Bacillus amyloliquefaciens FZB42. *J. Bacteriol. 193*, 215−224.
(27) Molohon, K. J., Melby, J. O., Lee, J., Evans, B. S., Dunbar, K. L., Bumpus, S. B., Kelleher, N. L., and Mitchell, D. A. (2011) Structure determination and interception of biosynthetic intermediates for the plantazolicin class of highly discriminating antibiotics. *ACS Chem. Biol. 6*, 1307−1313.
(28) Idris, E. E., Iglesias, D. J., Talon, M., and Borriss, R. (2007) Tryptophan-dependent production of indole-3-acetic acid (IAA) affects level of plant growth promotion by Bacillus amyloliquefaciens FZB42. *Mol. Plant-Microbe Interact. 20*, 619−626.
(29) Eliot, A. C., Griffin, B. M., Thomas, P. M., Johannes, T. W., Kelleher, N. L., Zhao, H., and Metcalf, W. W. (2008) Cloning, expression, and biochemical characterization of Streptomyces rubellomurinus genes required for biosynthesis of antimalarial compound FR900098. *Chem. Biol. 15*, 765−770.
(30) Bates, P. F., and Swift, R. A. (1983) Double cos site vectors: simplified cosmid cloning. *Gene 26*, 137−146.
(31) Guzman, L. M., Belin, D., Carson, M. J., and Beckwith, J. (1995) Tight regulation, modulation, and high-level expression by vectors containing the arabinose PBAD promoter. *J. Bacteriol. 177*, 4121−4130.
(32) Kuliopulos, A., and Walsh, C. T. (1994) Production, purification, and cleavage of tandem repeats of recombinant peptides. *J. Am. Chem. Soc. 116*, 4599−4607.
(33) Kapust, R. B., Routzahn, K. M., and Waugh, D. S. (2002) Processive degradation of nascent polypeptides, triggered by tandem AGA codons, limits the accumulation of recombinant tobacco etch virus protease in Escherichia coli BL21(DE3). *Protein Expression Purif. 24*, 61−70.
(34) Bouallag, N., Gaillard, C., Marechal, V., and Strauss, F. (2009) Expression of Epstein-Barr virus EBNA1 protein in Escherichia coli: purification under nondenaturing conditions and use in DNA-binding studies. *Protein Expression Purif. 67*, 35−40.
(35) Belshaw, P. J., Roy, R. S., Kelleher, N. L., and Walsh, C. T. (1998) Kinetics and regioselectivity of peptide-to-heterocycle conversions by microcin B17 synthetase. *Chem. Biol. 5*, 373−384.
(36) Kelleher, N. L., Hendrickson, C. L., and Walsh, C. T. (1999) Posttranslational heterocyclization of cysteine and serine residues in the antibiotic microcin B17: distributivity and directionality. *Biochemistry 38*, 15623−15630.
(37) Melby, J. O., Dunbar, K. L., Trinh, N. Q., and Mitchell, D. A. (2012) Selectivity, directionality, and promiscuity in peptide processing from a Bacillus sp. Al Hakam cyclodehydratase. *J. Am. Chem. Soc. 134*, 5309−5316.
(38) Mitchell, D. A., Lee, S. W., Pence, M. A., Markley, A. L., Limm, J. D., Nizet, V., and Dixon, J. E. (2009) Structural and functional dissection of the heterocyclic peptide cytotoxin streptolysin S. *J. Biol. Chem. 284*, 13004−13012.
(39) Sinha Roy, R., Belshaw, P. J., and Walsh, C. T. (1998) Mutational analysis of posttranslational heterocycle biosynthesis in the gyrase inhibitor microcin B17: distance dependence from propeptide and tolerance for substitution in a GSCG cyclizable sequence. *Biochemistry 37*, 4125−4136.
(40) Roy, R. S., Allen, O., and Walsh, C. T. (1999) Expressed protein ligation to probe regiospecificity of heterocyclization in the peptide antibiotic microcin B17. *Chem. Biol. 6*, 789−799.
(41) Lee, M. V., Ihnken, L. A., You, Y. O., McClerren, A. L., van der Donk, W. A., and Kelleher, N. L. (2009) Distributive and directional behavior of lantibiotic synthetases revealed by high-resolution tandem mass spectrometry. *J. Am. Chem. Soc. 131*, 12258−12264.
(42) Martin, R. B., and Parcell, A. (1961) Hydrolysis of 2-methyl-delta-oxazoline - an intramolecular O-N-acetyl transfer reaction. *J. Am. Chem. Soc. 83*, 4835−4838.
(43) Martin, R. B., Hedrick, R. L, and Parcell, A. (1964) Thiazoline + oxazoline hydrolyses + sulfur-nitrogen + oxygen-nitrogen acyl transfer reactions. *J. Org. Chem. 29*, 3197−3206.
(44) Dunbar, K. L., and Mitchell, D. A. (2013) Insights into the mechanism of peptide cyclodehydrations achieved through the chemoenzymatic generation of amide derivatives. *J. Am. Chem. Soc. 135*, 8692−8701.
(45) Roy, R. S., Kim, S., Baleja, J. D., and Walsh, C. T. (1998) Role of the microcin B17 propeptide in substrate recognition: solution structure and mutational analysis of McbA1−26. *Chem. Biol. 5*, 217−228.
(46) Madison, L. L., Vivas, E. I., Li, Y. M., Walsh, C. T., and Kolter, R. (1997) The leader peptide is essential for the post-translational modification of the DNA-gyrase inhibitor microcin B17. *Mol. Microbiol. 23*, 161−168.
(47) Oman, T. J., and van der Donk, W. A. (2010) Follow the leader: the use of leader peptides to guide natural product biosynthesis. *Nat. Chem. Biol. 6*, 9−18.
(48) Bentley, S. D., Corton, C., Brown, S. E., Barron, A., Clark, L., Doggett, J., Harris, B., Ormond, D., Quail, M. A., May, G., Francis, D., Knudson, D., Parkhill, J., and Ishimaru, C. A. (2008) Genome of the actinomycete plant pathogen Clavibacter michiganensis subsp. sepedonicus suggests recent niche adaptation. *J. Bacteriol. 190*, 2150−2160.
(49) Chen, X. H., Koumoutsi, A., Scholz, R., Eisenreich, A., Schneider, K., Heinemeyer, I., Morgenstern, B., Voss, B., Hess, W. R., Reva, O., Junge, H., Voigt, B., Jungblut, P. R., Vater, J., Sussmuth, R., Liesegang, H., Strittmatter, A., Gottschalk, G., and Borriss, R. (2007) Comparative analysis of the complete genome sequence of the plant growth-promoting bacterium Bacillus amyloliquefaciens FZB42. *Nat. Biotechnol. 25*, 1007−1014.
(50) Jeltsch, A., and Lanio, T. (2002) Site-directed mutagenesis by polymerase chain reaction. *Methods Mol. Biol. 182*, 85−94.

A.2 References

1. Deane, C.D., Melby, J.O., Molohon, K.J., Susarrey, A.R., and Mitchell, D.A. (2013) Engineering unnatural variants of plantazolicin through codon reprogramming. *ACS Chem Biol*: **8**, 1998-2008.

APPENDIX B: OTHER PUBLICATIONS WITH MINOR CONTRIBUTIONS

B.1 HIV-1 Integrase Inhibitor-Inspired Antibacterials Targeting Isoprenoid Biosynthesis

This chapter was reprinted with permission (Zhang *et al.*, 2012).

Zhang, Y., Fu-Yang, L., Li, K., Zhu, W., Liu, Y.L., Cao, R., Pang, R., Lee, E., Axelson, J., Hensler, M., Wang, K., Molohon, K.J., Wang, Y., Mitchell, D.A., Nizet, V., and Oldfield, E. (2012) *ACS Med Chem Lett*: 3, 402-406. doi: 10.1021/ml300038t.

I conducted the assays generating the minimum inhibitory concentrations for the compounds in this manuscript.

ACS Medicinal Chemistry Letters

Letter

pubs.acs.org/acsmedchemlett

HIV-1 Integrase Inhibitor-Inspired Antibacterials Targeting Isoprenoid Biosynthesis

Yonghui Zhang,[*,†,‡] Fu-Yang Lin,[§,○] Kai Li,[‡,○] Wei Zhu,[§] Yi-Liang Liu,[§] Rong Cao,[‡] Ran Pang,[∥] Eunhae Lee,[∥] Jordan Axelson,[‡] Mary Hensler,[▽] Ke Wang,[‡] Katie J. Molohon,[⊥] Yang Wang,[‡] Douglas A. Mitchell,[‡,⊥,#] Victor Nizet,[▽] and Eric Oldfield[*,‡,§]

[†]PrenylX Research Institute, Zhangjiagang, 215600, People's Republic of China

[‡]Department of Chemistry, [§]Center for Biophysics & Computational Biology, [∥]School of Molecular and Cellular Biology, [⊥]Department of Microbiology, and [#]Institute for Genomic Biology, University of Illinois at Urbana−Champaign, Urbana, Illinois 61801, United States

[▽]Department of Pediatrics and Skaggs School of Pharmacy and Pharmaceutical Sciences, University of California, San Diego, La Jolla, California 92093, United States

Supporting Information

ABSTRACT: We report the discovery of antibacterial leads, keto- and diketo-acids, targeting two prenyl transferases: undecaprenyl diphosphate synthase (UPPS) and dehydrosqualene synthase (CrtM). The leads were suggested by the observation that keto- and diketo-acids bind to the active site Mg^{2+}/Asp domain in HIV-1 integrase, and similar domains are present in prenyl transferases. We report the X-ray crystallographic structures of one diketo-acid and one keto-acid bound to CrtM, which supports the Mg^{2+} binding hypothesis, together with the X-ray structure of one diketo-acid bound to UPPS. In all cases, the inhibitors bind to a farnesyl diphosphate substrate-binding site. Compound 45 had cell growth inhibition MIC_{90} values of ∼250−500 ng/mL against *Staphylococcus aureus*, 500 ng/mL against *Bacillus anthracis*, 4 μg/mL against *Listeria monocytogenes* and *Enterococcus faecium*, and 1 μg/mL against *Streptococcus pyogenes* M1 but very little activity against *Escherichia coli* (DH5α, K12) or human cell lines.

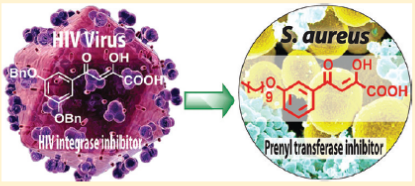

KEYWORDS: *antibacterials, isoprenoid biosynthesis, HIV integrase, undecaprenyl diphosphate synthase, dehydrosqualene synthase*

There is currently an urgent need for new types of antibacterials exhibiting novel modes of action, due to the rapid rise in drug resistance,[1] and isoprenoid biosynthesis[2,3] is one attractive target. For example, cell wall biosynthesis can be inhibited by targeting farnesyl diphosphate synthase (FPPS) or undecaprenyl diphosphate synthase (UPPS), involved in lipid I biosynthesis (Figure 1). In addition, in *Staphylococcus aureus*, the formation of the virulence factor staphyloxanthin[4] can be blocked by inhibiting dehydrosqualene synthase (CrtM), resulting in a lowering of the antioxidant shield to host derived reactive oxygen species (ROS)[5] (Figure 1). The bisphosphonate class of drugs such as zoledronate (1, Chart 1) are potent, low nanomolar inhibitors of FPPS, but 1 has little antibacterial activity (presumably due to lack of cell penetration), although more lipophilic bisphosphonates such as 2 (BPH-210, Chart 1) have modest activity (IC_{50} ∼ 30 μM) against *Escherichia coli*.[6] More lipophilic bisphosphonates also potently target UPPS,[7] as well as CrtM,[5] but again, they have essentially no activity in bacteria. Replacing one phosphonate group by a sulfonate to form a phosphonosulfonate results, however, in potent CrtM inhibitors (e.g., 3, BPH-652, Chart 1, IC_{50} ∼ 7.9 μM, K_i ∼ 80 nM) that also blocks carotenoid pigment formation in cells (IC_{50} ∼ 110 nM).[8] In addition, there has recently been interest in developing phosphorus-free prenyl transferase inhibitors, which might have even more druglike properties. For example, Jahnke et al. reported a series of FPPS inhibitors, dicarboxylic acids, that bound to a novel, allosteric site.[9] In addition, other species such as tetramic acid UPPS inhibitors have been described (e.g., 4, Chart 1),[10] but to date, their X-ray structures have not been reported, although an allosteric model has been proposed.[11]

A key component of the active site of most prenyl transferases is a Mg^{2+}/Asp motif that interacts with a substrate's diphosphate group. We reasoned that HIV-1 integrase (IN) inhibitors[12] might provide clues for new prenyl transferase inhibitors, since IN contains a similar Asp/Mg^{2+} motif[13] and IN inhibitors such as 5 (L-708,906, Chart 1)[14] and 6 (elvitegravir, Chart 1),[15] diketo-acids and keto-acids, respectively, are thought to bind at or near the Mg^{2+}/Asp motif in the IN active site.[16,17] In addition, many other IN inhibitors like raltegravir, dolutegravir, MK2048, etc. (structures not shown) have been found to bind Mg^{2+}.[17−19]

Received: February 12, 2012
Accepted: April 3, 2012
Published: April 3, 2012

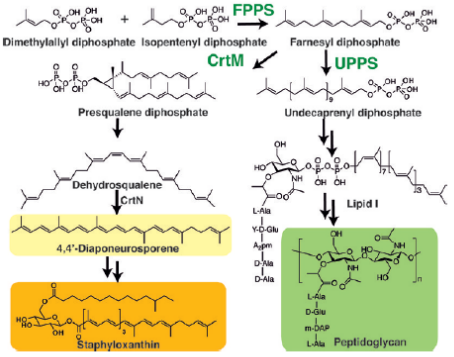

Figure 1. Biosynthetic reactions catalyzed by CrtM and UPPS, with the end products of the pathways shown.

We thus made a small screening library (38 compounds) of IN inhibitor-inspired molecules and their structures, and inhibition of *S. aureus* CrtM, *E. coli* UPPS, and *S. aureus* UPPS are shown in Figure S1 in the Supporting Information. Most compounds were amide-diketo acids (**7**−**40**, class I, Figure S1 in the Supporting Information) and were conveniently prepared from the synthon (*Z*)-2,2-dimethyl-5-carboxymethylene-1,3-dioxolan-4-one[20] by amine coupling. Among these compounds, **7** (Chart 1) inhibited CrtM with $IC_{50} \sim 24\ \mu M$, $K_i \sim 250$ nM (for comparison, K_i of 3 ∼ 70 nM[8]) and blocked staphyloxanthin pigment formation (IC_{50} = 4 μM). Inhibitors of class II were keto-acids, dihydropyridone-3-carboxylates, and were based on **6** (Elvitegravir) and dihydroquinoline-3-carboxylic acid IN inhibitors,[21] which again are thought to bind via their carboxyl and carbonyl oxygens to Mg^{2+}/Asp.[22] We made two analogues, **41** and **42** (Chart 1), with alkoxy-aryl tails to mimic the substrate farnesyl diphosphate (FPP). The longer chain species **42** had no activity, but the shorter chain species **41** had a CrtM IC_{50}= 45 μM, K_i = 450 nM, and a loss of pigmentation IC_{50} = 33 μM.

To see how these inhibitors bound to CrtM, we carried out cocrystallization and soaking experiments with **7** (class I) and **41** (class II) and obtained crystals (by soaking) that diffracted to 2.3 and 1.9 Å, respectively. Full X-ray crystallographic data and structure refinement details are given in the Supporting Information, Table S1. Electron density results for **7** are shown in Figure 2a and indicate the presence of **7** in addition to one molecule of farnesyl monophosphate (FMP) that copurified with the protein. The identity of FMP was further confirmed by LC-MS (Supporting Information, Figure S2) and the electron density results (Figure 2a). The diphenyl ether fragment in **7** (cyan) binds into the CrtM S1 site[23] and is shown in Figure 2b superimposed on one of the *S-thiolo*-farnesyl diphosphate (FSPP) inhibitors (in yellow, green) whose structures were reported previously.[5] This binding mode is similar to that seen with the phosphonosulfonate **3** (Figure 2c), with the diketo-acid headgroup interacting with two of the three Mg^{2+} ($Mg^{2+}_{B,C}$) seen in the CrtM-FSPP structure (Figure 2d). The farnesyl side chain in FMP bound to the S2 site and had a 0.8 Å rmsd from the S2 FSPP reported previously.[5] With **41**, the ligand electron density is again well-defined (Figure 3a), and the crystallographic results show that the side chain binds in S2, similar to the farnesyl side chain in the FSPP structures (Figure 3b), as well as the phosphonoacetamide analogue of **7** (**43**, BPH-830,[24] Figure 3c). There are three Mg^{2+} in the X-ray structure. However, these are not the Mg^{2+}_{ABC} seen in most prenyl transferases[25] but rather Mg^{2+}_{BCD}. That is, there is a new Mg^{2+} binding site, Mg^{2+}_{D}. The dihydropyridone side chain interacts with Mg^{2+}_{CD} but, surprisingly, via the two ring oxygens, not the carboxylate (Figure 3d), which interacts with two water molecules (Supporting Information, Figure S3). These inhibition and structural results for **7** and **41** clearly support the Mg^{2+} binding hypothesis, at least for CrtM.

CrtM is a so-called head-to-head prenyl transferase so we next sought to see if any of the molecules synthesized might also inhibit the head-to-tail prenyl transferase FPPS or the *cis*-prenyl transferase, UPPS. There was no activity against FPPS (probably due to the lack of a positively charged feature that mimics the carbocation involved in FPP biosynthesis), but most of the amide-diketo acids (class I) were potent UPPS inhibitors

Chart 1. Chemical Structures of Selected Compounds and the Inhibition of CrtM, *E. coli* UPPS, and *S. aureus* UPPS by 7−9, 41, 42, 44, and 45

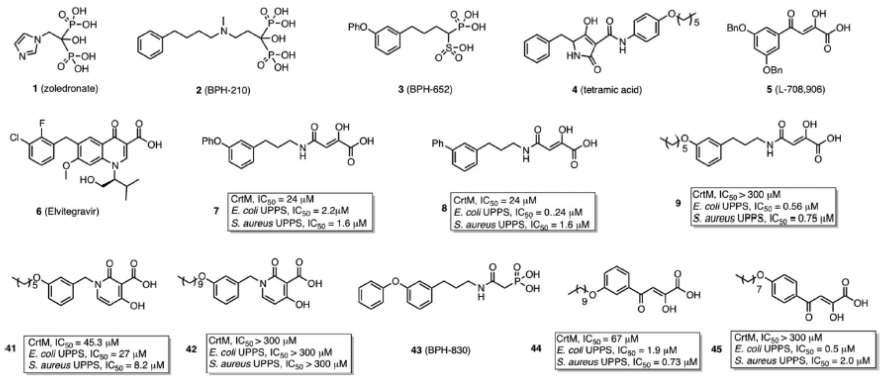

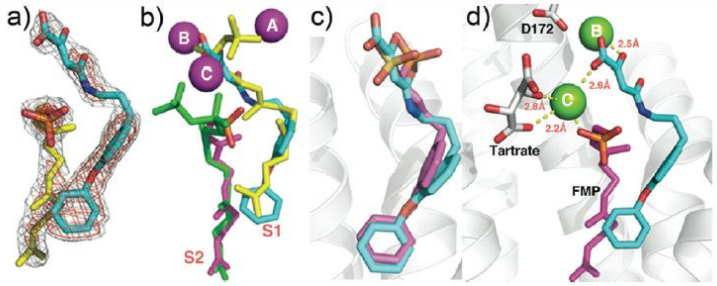

Figure 2. CrtM crystallographic structures. (a) Compound 7 (cyan) plus FMP (yellow) electron density, bound to CrtM. (b) Compound 7 (cyan) bound to CrtM, superimposed on two FSPP molecules (yellow, green; PDB ID code 2ZCP). Also shown is the FMP (magenta) that cocrystallized. The Mg^{2+} are from the FSPP structure. (c) Comparison between 7 (cyan) and 3 (magenta, PDB ID code 2ZCQ) bound to CrtM. Both diphenyl ether side chains bind in S1. (d) Interactions between 7 (cyan), FMP (magenta), and Mg^{2+} in CrtM.

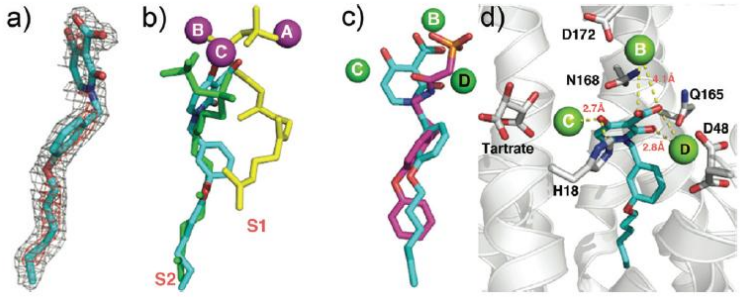

Figure 3. CrtM crystallographic structures. (a) Electron density of **41** bound to CrtM. (b) Structure of **41** (cyan) bound to CrtM shown superimposed on two FSPP molecules (yellow, green). (c) Comparison between **41** (cyan) and the phosphonoacetamide analog of 7 (compound **43**, BPH-830)[24] (magenta) bound to CrtM (PDB ID code 2ZY1). (d) Interactions between **41** (cyan) and Mg^{2+} in CrtM.

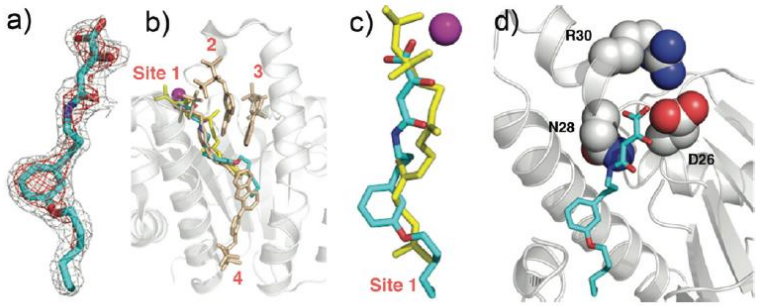

Figure 4. UPPS crystallographic structures. (a) Electron density of **9** bound to UPPS. (b) Structure of **9** (cyan) bound to UPPS, superimposed on FSPP/Mg^{2+} (from PDB ID code 1X06) and four bisphosphonate inhibitors (PDB ID code 2E98). (c) Superposition of **9** (cyan) on FSPP (yellow) in site 1 in UPPS. The Mg^{2+} is from the FSPP structure. (d) The diketo-acid headgroup of **9** binds into the active site of UPPS and interacts with D26 and N28.

with the most active one (**8**) having an $IC_{50} \sim 240$ nM and $K_i \sim 120$ nM, comparable to the most active bisphosphonate UPPS inhibitor BPH-629 ($IC_{50} \sim 300$ nM for *E. coli* UPPS).[7] There are four different ligand-binding sites in UPPS (designated 1−4 in ref 7) found with bisphosphonate inhibitors. This is not unexpected since the UPPS product, undecaprenyl diphosphate (UPP), contains 55-carbon atoms and is thus much larger than the (C_{15}) FPP substrate. In principle, then, novel inhibitors might occupy multiple binding sites.

Cocrystallization of *E. coli* UPPS with **9** (IC_{50} = 560 nM) produced well-formed crystals with *E. coli* UPPS, and the

electron density was well resolved (Figure 4a). As can be seen in Figure 4b, 9 binds to site 1,[7] the FPP binding site, and as can be seen in Figure 4c, 9 (in cyan) closely maps the FPP backbone structure (in yellow) with the diketo-acid fragment being located close to two of the three most essential residues in UPPS, D26 and N28 (Figure 4d). We found no evidence for the presence of Mg^{2+}, but this observation is not entirely unexpected since even with the five *E. coli* UPPS X-ray structures with strong Mg^{2+} chelators, bisphosphonates (PDB ID codes 2E98, 2E99, 2E9A, 2E9C, and 2E9D),[7] Mg^{2+} was not observed.

The amide-diketo acids were not growth suppressive toward *S. aureus* or *E. coli*, perhaps due to the instability of the amide bond inside the cells or a lack of cell permeability. However, 44 and 45 (aryldiketo acids, class III) had good activity against *S. aureus* UPPS (44, IC_{50} = 0.73 μM, K_i = 230 nM; 45, IC_{50} = 2.0 μM, K_i = 670 nM), and both were active against the USA300 (MRSA) strain of *S. aureus* with MIC_{90} values of 500 (44) and 250−500 ng/mL (45). There was no appreciable activity against the Gram-negative *E. coli*; however, there was promising activity against other Gram-positives: ∼ 500 ng/mL against *Bacillus anthracis* str. Sterne, ∼ 4 μg/mL against *Listeria monocytogenes* and *Enterococcus faecium* U503, and ∼1 μg/mL for *Streptococcus pyogenes* M1. While the precise mechanism of action of these compounds in each cell remains to be determined, UPPS inhibition is a likely candidate. In addition, we found low toxicity against a human cell line (MCF-7; IC_{50} ∼ 30 μM), consistent with poor FPPS inhibition.

These results are important for several reasons. First, we tested the hypothesis that keto- and diketo-acids might inhibit prenyl transferase enzymes, based on the presence of Mg^{2+}/Asp motifs in their active sites—an "integrase inhibitor-inspired" approach. The best CrtM inhibitors had K_i ∼ 250 nM and were active in blocking staphyloxanthin biosynthesis in *S. aureus*, and we solved two structures of lead compounds bound to CrtM. In both, the inhibitor head groups bound to Mg^{2+}, while the side chains bound to one or the other of the two FPP side chain binding sites. Second, we tested this small library for FPPS and UPPS inhibition. There was no FPPS inhibition, but the most potent UPPS inhibitor had an IC_{50} = 240 nM, and we determined the structure of one such lead bound to *E. coli* UPPS—the first UPPS X-ray structure reported for a nonbisphosphonate inhibitor. We also found low toxicity and promising activity against a subset of Gram-positive bacteria with MIC_{90} values as low as 250−500 ng/mL against USA300 *S. aureus* and 500 ng/mL against *Bacillus anthracis* str. Sterne and low activity against *E. coli* and a human cell line. Overall, these results indicate that integrase-inspired inhibitors may be engineered into drug leads that target isoprenoid biosynthesis.

■ ASSOCIATED CONTENT

Supporting Information

X-ray study, synthesis, and characterization of the screening library compounds. This material is available free of charge via the Internet at http://pubs.acs.org.

■ AUTHOR INFORMATION

Corresponding Author

*E-mail: yhzhang30@yahoo.com (Y.Z.) or eo@chad.scs.uiuc.edu (E.O.).

Author Contributions

○These authors contributed equally.

Funding

This work was supported by the U.S. Public Health Service (NIH Grant 5R01AI074233-16 to E.O.) and the NIH Director's New Innovator Award Program (DP2 OD008463 to D.A.M.). K.J.M. was supported in part by a NIH Cellular and Molecular Biology Training Grant (T32 GM007283). The Advanced Photon Source was supported by Department of Energy Contract DE-AC02-06CH11357. The Life Science Collaborative Access Team Sector 21 was supported by the Michigan Economic Development Corporation and Michigan Technology Tri-Corridor (Grant 085P000817).

Notes

The authors declare no competing financial interest.

■ ACKNOWLEDGMENTS

We thank Andrew H.-J. Wang of the Institute of Biological Chemistry, Academia Sinica (Taipei, Taiwan), for providing *E. coli* UPPS plasmids and *S. aureus* CrtM plasmids.

■ ABBREVIATIONS

CrtM, dehydrosqualene synthase; UPPS, undecaprenyl diphosphate synthase; FPPS, farnesyl diphosphate synthase; FPP, farnesyl diphosphate; FMP, farnesyl monophosphate; FSPP, *S-thiolo*-farnesyl diphosphate; IN, HIV-1 integrase

■ REFERENCES

(1) Walsh, C. T.; Fischbach, M. A. Repurposing libraries of eukaryotic protein kinase inhibitors for antibiotic discovery. *Proc. Natl. Acad. Sci. U.S.A.* **2009**, *106*, 1689−1690.

(2) Oldfield, E. Targeting isoprenoid biosynthesis for drug discovery: Bench to bedside. *Acc. Chem. Res.* **2010**, *43*, 1216−1226.

(3) Oldfield, E.; Lin, F. Y. Terpene biosynthesis: Modularity rules. *Angew. Chem., Int. Ed. Engl.* **2012**, *51*, 1124−1137.

(4) Liu, G. Y.; Essex, A.; Buchanan, J. T.; Datta, V.; Hoffman, H. M.; Bastian, J. F.; Fierer, J.; Nizet, V. *Staphylococcus aureus* golden pigment impairs neutrophil killing and promotes virulence through its antioxidant activity. *J. Exp. Med.* **2005**, *202*, 209−215.

(5) Liu, C. I.; Liu, G. Y.; Song, Y.; Yin, F.; Hensler, M. E.; Jeng, W. Y.; Nizet, V.; Wang, A. H.; Oldfield, E. A cholesterol biosynthesis inhibitor blocks *Staphylococcus aureus* virulence. *Science* **2008**, *319*, 1391−1394.

(6) Leon, A.; Liu, L.; Yang, Y.; Hudock, M. P.; Hall, P.; Yin, F.; Studer, D.; Puan, K. J.; Morita, C. T.; Oldfield, E. Isoprenoid biosynthesis as a drug target: Bisphosphonate inhibition of *Escherichia coli* K12 growth and synergistic effects of fosmidomycin. *J. Med. Chem.* **2006**, *49*, 7331−7341.

(7) Guo, R. T.; Cao, R.; Liang, P. H.; Ko, T. P.; Chang, T. H.; Hudock, M. P.; Jeng, W. Y.; Chen, C. K.; Zhang, Y.; Song, Y.; Kuo, C. J.; Yin, F.; Oldfield, E.; Wang, A. H. Bisphosphonates target multiple sites in both *cis*- and *trans*-prenyltransferases. *Proc. Natl. Acad. Sci. U.S.A.* **2007**, *104*, 10022−10027.

(8) Song, Y.; Lin, F. Y.; Yin, F.; Hensler, M.; Rodrigues Poveda, C. A.; Mukkamala, D.; Cao, R.; Wang, H.; Morita, C. T.; Gonzalez Pacanowska, D.; Nizet, V.; Oldfield, E. Phosphonosulfonates are potent, selective inhibitors of dehydrosqualene synthase and staphyloxanthin biosynthesis in *Staphylococcus aureus*. *J. Med. Chem.* **2009**, *52*, 976−988.

(9) Jahnke, W.; Rondeau, J. M.; Cotesta, S.; Marzinzik, A.; Pelle, X.; Geiser, M.; Strauss, A.; Gotte, M.; Bitsch, F.; Hemmig, R.; Henry, C.; Lehmann, S.; Glickman, J. F.; Roddy, T. P.; Stout, S. J.; Green, J. R. Allosteric non-bisphosphonate FPPS inhibitors identified by fragment-based discovery. *Nat. Chem. Biol.* **2010**, *6*, 660−666.

(10) Peukert, S.; Sun, Y.; Zhang, R.; Hurley, B.; Sabio, M.; Shen, X.; Gray, C.; Dzink-Fox, J.; Tao, J.; Cebula, R.; Wattanasin, S. Design and structure-activity relationships of potent and selective inhibitors of undecaprenyl pyrophosphate synthase (UPPS): Tetramic, tetronic

acids and dihydropyridin-2-ones. *Bioorg. Med. Chem. Lett.* **2008**, *18*, 1840−1884.
(11) Lee, L. V.; Granda, B.; Dean, K.; Tao, J.; Liu, E.; Zhang, R.; Peukert, S.; Wattanasin, S.; Xie, X.; Ryder, N. S.; Tommasi, R.; Deng, G. Biophysical investigation of the mode of inhibition of tetramic acids, the allosteric inhibitors of undecaprenyl pyrophosphate synthase. *Biochemistry* **2010**, *49*, 5366−5376.
(12) For a review, see Neamati, N. *HIV-1 Integrase: Mechanism and Inhibitor Design*; John Willey & Sons Inc.: Hoboken, NJ, 2011.
(13) Goldgur, Y.; Dyda, F.; Hickman, A. B.; Jenkins, T. M.; Craigie, R.; Davies, D. R. Three new structures of the core domain of HIV-1 integrase: an active site that binds magnesium. *Proc. Natl. Acad. Sci. U.S.A.* **1998**, *95*, 9150−9154.
(14) Hazuda, D. J.; Felock, P.; Witmer, M.; Wolfe, A.; Stillmock, K.; Grobler, J. A.; Espeseth, A.; Gabryelski, L.; Schleif, W.; Blau, C.; Miller, M. D. Inhibitors of strand transfer that prevent integration and inhibit HIV-1 replication in cells. *Science* **2000**, *287*, 646−650.
(15) Sato, M.; Kawakami, H.; Motomura, T.; Aramaki, H.; Matsuda, T.; Yamashita, M.; Ito, Y.; Matsuzaki, Y.; Yamataka, K.; Ikeda, S.; Shinkai, H. Quinolone carboxylic acids as a novel monoketo acid class of human immunodeficiency virus type 1 integrase inhibitors. *J. Med. Chem.* **2009**, *52*, 4869−4882.
(16) Grobler, J. A.; Stillmock, K.; Hu, B.; Witmer, M.; Felock, P.; Espeseth, A. S.; Wolfe, A.; Egbertson, M.; Bourgeois, M.; Melamed, J.; Wai, J. S.; Young, S.; Vacca, J.; Hazuda, D. J. Diketo acid inhibitor mechanism and HIV-1 integrase: Implications for metal binding in the active site of phosphotransferase enzymes. *Proc. Natl. Acad. Sci. U.S.A.* **2002**, *99*, 6661−6666.
(17) Hare, S.; Gupta, S. S.; Valkov, E.; Engelman, A.; Cherepanov, P. Retroviral intasome assembly and inhibition of DNA strand transfer. *Nature* **2010**, *464*, 232−236.
(18) Hare, S.; Smith, S. J.; Métifiot, M.; Jaxa-Chamiec, A.; Pommier, Y.; Hughes, S.; Cherepanov, P. Structural and functional analyses of the second-generation integrase strand transfer inhibitor dolutegravir (S/GSK 1349572). *Mol. Pharmacol.* **2011**, *80*, 565−572.
(19) Hare, S.; Vos, A. M.; Clayton, R. F.; Thuring, J. W.; Cummings, M. D.; Cherepanov, P. Molecular mechanisms of retroviral integrase inhibition and the evolution of viral resistance. *Proc. Natl. Acad. Sci. U.S.A.* **2010**, *107*, 20057−20062.
(20) Zhu, K.; Simpson, J. H.; Delaney, E. J.; Nugent, W. A. Synthesis of *Z*-5-carboxymethylene-1,3-dioxolan-4-ones: A better way. *J. Org. Chem.* **2007**, *72*, 3949−3951.
(21) Sechi, M.; Rizzi, G.; Bacchi, A.; Carcelli, M.; Rogolino, D.; Pala, N.; Sanchez, T. W.; Taheri, L.; Dayam, R.; Neamati, N. Design and synthesis of novel dihydroquinoline-3-carboxylic acids as HIV-1 integrase inhibitors. *Bioorg. Med. Chem.* **2009**, *17*, 2925−2935.
(22) Vandurm, P.; Cauvin, C.; Guiguen, A.; Georges, B.; Le Van, K.; Martinelli, V.; Cardona, C.; Mbemba, G.; Mouscadet, J. F.; Hevesi, L.; Van Lint, C.; Wouters, J. Structural and theoretical studies of [6-bromo-1-(4-fluorophenylmethyl)-4(1H)-quinolinon-3-yl)]-4-hydroxy-2-oxo- 3-butenoic acid as HIV-1 integrase inhibitor. *Bioorg. Med. Chem. Lett.* **2009**, *19*, 4806−4809.
(23) Lin, F. Y.; Liu, C. I.; Liu, Y. L.; Zhang, Y.; Wang, K.; Jeng, W. Y.; Ko, T. P.; Cao, R.; Wang, A. H.; Oldfield, E. Mechanism of action and inhibition of dehydrosqualene synthase. *Proc. Natl. Acad. Sci. U.S.A.* **2010**, *107*, 21337−21342.
(24) Song, Y.; Liu, C. I.; Lin, F. Y.; No, J. H.; Hensler, M.; Liu, Y. L.; Jeng, W. Y.; Low, J.; Liu, G. Y.; Nizet, V.; Wang, A. H.; Oldfield, E. Inhibition of staphyloxanthin virulence factor biosynthesis in *Staphylococcus aureus*: In vitro, in vivo, and crystallographic results. *J. Med. Chem.* **2009**, *52*, 3869−3880.
(25) Aaron, J. A.; Christianson, D. W. Trinuclear Metal Clusters in Catalysis by Terpenoid Synthases. *Pure Appl. Chem.* **2010**, *82*, 1585−1597.

B.2 Antibacterial Drug Leads Targeting Isoprenoid Biosynthesis

This chapter was reprinted with permission (Zhu *et al*., 2013).

Zhu W, Zhang Y, Sinko W, Hensler ME, Olson J, Molohon KJ, Lindert S, Cao R, Li K, Wang K, Wang Y, Liu YL, Sankovsky A, de Oliveira CA, Mitchell DA, Nizet V, McCammon JA, Oldfield E. (2013) *Proc Natl Acad Sci U S A*: 110, 123-128. doi: 10.1073/pnas.1219899110.

I obtained the minimum inhibitory concentrations of the compounds in this manuscript, as well as reported the synergistic activity of cpd **17** with methicillin (Figure 7A).

Antibacterial drug leads targeting isoprenoid biosynthesis

Wei Zhu[a,1], Yonghui Zhang[b,1,2], William Sinko[c,d,1], Mary E. Hensler[e], Joshua Olson[e], Katie J. Molohon[f], Steffen Lindert[c], Rong Cao[a], Kai Li[b], Ke Wang[b], Yang Wang[b], Yi-Liang Liu[a], Anna Sankovsky[b], César Augusto F. de Oliveira[c,g], Douglas A. Mitchell[b,f,h], Victor Nizet[e], J. Andrew McCammon[c,d,g,i,2], and Eric Oldfield[a,b,2]

[a]Center for Biophysics and Computational Biology and [b]Department of Chemistry, University of Illinois, Urbana, IL 61801; [c]Department of Pharmacology, [d]Biomedical Sciences Program, and [e]Department of Pediatrics and Skaggs School of Pharmacy and Pharmaceutical Sciences, University of California at San Diego, La Jolla, CA 92093; [f]Department of Microbiology, University of Illinois, Urbana, IL 61801; [g]Department of Chemistry and Biochemistry, University of California at San Diego, La Jolla, CA 92093; [h]Institute for Genomic Biology, University of Illinois, Urbana, IL 61801; and [i]Howard Hughes Medical Institute, University of California at San Diego, La Jolla, CA 92093

Contributed by J. Andrew McCammon, November 16, 2012 (sent for review October 2, 2012)

With the rise in resistance to antibiotics such as methicillin, there is a need for new drugs. We report here the discovery and X-ray crystallographic structures of 10 chemically diverse compounds (benzoic, diketo, and phosphonic acids, as well as a bisamidine and a bisamine) that inhibit bacterial undecaprenyl diphosphate synthase, an essential enzyme involved in cell wall biosynthesis. The inhibitors bind to one or more of the four undecaprenyl diphosphate synthase inhibitor binding sites identified previously, with the most active leads binding to site 4, outside the catalytic center. The most potent leads are active against *Staphylococcus aureus* [minimal inhibitory concentration (MIC_{90} ~0.25 μg/mL], and one potently synergizes with methicillin (fractional inhibitory concentration index = 0.25) and is protective in a mouse infection model. These results provide numerous leads for antibacterial development and open up the possibility of restoring sensitivity to drugs such as methicillin, using combination therapies.

drug discovery | *in silico* high-throughput screening | peptidoglycan | protein structure

Targeting isoprenoid biosynthesis is a potentially important route for antibiotic discovery because isoprenoids are involved in the very early steps of bacterial cell-wall biosynthesis—the condensation of dimethylallyl diphosphate (DMAPP, **1**) with two molecules of isopentenyl diphosphate (IPP, **2**) to form farnesyl diphosphate (FPP, **3**), catalyzed by the enzyme farnesyl diphosphate synthase (FPPS), followed by the addition of eight more IPP molecules to form undecaprenyl diphosphate (UPP, **4**) (1, 2) (Fig. 1). Formation of **4** is catalyzed by the enzyme undecaprenyl diphosphate synthase (UPPS), and several UPPS inhibitors have been reported (3–10). UPP is then hydrolyzed to the monophosphate, which is next converted to lipid I and lipid II, leading to formation of cell wall peptidoglycan (Fig. 1) (11, 12). Antibiotics such as methicillin and vancomycin act in the latter stages of peptidoglycan formation, again as shown in Fig. 1. Here, we focus on the development of UPPS inhibitors because UPPS is an essential protein not produced by humans (13). UPPS inhibitors are predicted to synergize with the more-conventional cell-wall biosynthesis inhibitors, potentially reducing the toxicity of drugs such as vancomycin (by decreasing dosage), or restoring drug sensitivity [e.g., with methicillin-resistant *Staphylococcus aureus* (MRSA)]. The UPPS structure is unusual in that there are four known ligand binding sites (5), opening up the possibility of designing a diverse range of inhibitors.

Results and Discussion

UPPS Inhibitors. In previous work, we and others reported the discovery of several UPPS inhibitors, including bisphosphonates such as BPH-629 (**5**) (5), tetramic acids such as **6** (6), as well as diketoacids such as **7** (10) and benzoic acids such as **8** (9) (Fig. 2). Based on *in silico* high-throughput screening (9) and hit development (Fig. S1), we produced a small series of benzoic (**9**–**12**), phosphonic (**13**), and diketoacids (**14**, **15**) that had activity against UPPS (Fig. 2). In addition to these anionic species, we discovered several potent cationic inhibitors (**16**–**18**); this was unexpected from both a computational and experimental standpoint because these compounds do not mimic the (anionic) FPP substrate, and the UPPS mechanism is not thought to involve carbocation intermediates (14). We thus sought to determine how these inhibitors bind to their UPPS target, by obtaining crystal structures of **8**–**16** and **18** bound to *Escherichia coli* UPPS.

Four Inhibitor Binding Sites in UPPS. UPPS functions by sequentially adding IPP to an allylic substrate, initially FPP (15). It might reasonably be expected, then, that anionic inhibitors with lipophilic side-chains would bind to the FPP substrate site, as shown in Fig. 3*A*, yellow (PDB ID code 1X06). However, in a second structure (PDB ID code 1V7U), two FPP molecules bind, one in the substrate site and the other in a second site at the "bottom" of the protein (Fig. 3*A*, green). Moreover, with the bisphosphonate inhibitor **5**, there are actually four binding sites (sites 1–4) (5) that can be occupied (Fig. 3*B*, cyan; PDB ID code 2E98) in which the side chains in each of the four inhibitor molecules occupy the large hydrophobic center of the protein that normally accommodates the C_{55} side chain in the UPP product. With the two less-active benzoic acid inhibitors, **8** and **9**, we find that only site 3 (Fig. 3*C*; PDB ID code 3SGT) or sites 1, 2, and 3 are occupied (Fig. 3*D*; PDB ID code 3SGV), but the activity of both of these inhibitors is weak (**8**, *E. coli* UPPS, IC_{50} = 150 μM; *S. aureus* UPPS, 170 μM; **9**, *E. coli* UPPS, IC_{50} = 35 μM, *S. aureus* UPPS, 72 μM; Table S1). Full data acquisition and structure refinement details are in Table S2, and electron densities (2Fo-Fc and simulated-annealing Fo-Fc omit maps) are in Fig. S2 *A* and *B*. So, with these two benzoic acid inhibitors, binding to sites 1, 2, or 3 correlates only to weak UPPS inhibition.

Potent Benzoic Acid Inhibitors Bind to Site 4. We next determined the structures of the three potent benzoic acid inhibitors (10–12) (Fig. 2) bound to UPPS (Fig. 4 *A*–*C*). Each of these molecules contains a long hydrophobic side-chain and, on average,

Author contributions: W.Z., Y.Z., J.A.M., and E.O. designed research; W.Z., Y.Z., W.S., M.E.H., J.O., K.J.M., S.L., R.C., K.L., K.W., Y.W., Y.-L.L., A.S., C.A.F.d.O., D.A.M., V.N., J.A.M., and E.O. performed research; and E.O. wrote the paper.

The authors declare no conflict of interest.

Data deposition: Crystallography, atomic coordinates, and structure factors have been deposited in the Protein Data Bank, www.pdb.org (PDB ID codes 3SGT, 3SGV, 3SGX, 3SH0, 4H2O, 4H38, 4H3C, 4H3A, 4H2J, 4H2M, and 4H8E).

[1]W.Z., Y.Z., and W.S. contributed equally to this work.

[2]To whom correspondence may be addressed. E-mail: eo@chad.scs.uiuc.edu, yhzhang@illinois.edu, or jmccammon@ucsd.edu.

This article contains supporting information online at www.pnas.org/lookup/suppl/doi:10.1073/pnas.1219899110/-/DCSupplemental.

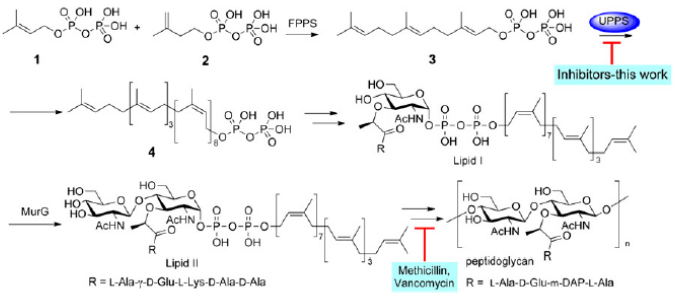

Fig. 1. Schematic outline of cell wall biosynthesis (in most bacteria) showing involvement of isoprenoid biosynthesis in the early stages of peptidoglycan formation.

the IC_{50} values against both *E. coli* and *S. aureus* UPPS are ~3 μM (Table S1). What is notable about these X-ray structures is that in each case, site 4 is occupied, together with either sites 1, 2, or 3. Full data acquisition and structure refinement details are in Table S2, and electron densities are in Fig. S2 *A* and *B*. In addition, we found that the aryl phosphonate inhibitor **13** also occupied two sites (Fig. 4*D*). However, there are two chains in one asymmetric unit, and site occupancies in the two chains are variable: the lower site-occupancy chains are shown in Fig. S2*C*. These four structures suggest that good UPPS inhibition correlates with occupancy of site 4.

Diketoacids, a Bisamidine and a Bisamine also Target Site 4. In previous work (10), we found that the diketoacid **15** had potent cell-growth inhibition activity with the following minimal inhibitory concentration $(MIC)_{90}$ values: 0.25–0.5 μg/mL against *S. aureus*; 0.5 μg/mL against *Bacillus anthracis*; 4 μg/mL against *Listeria monocytogenes* and *Enterococcus faecium*; and 1 μg/mL against *Streptococcus pyogenes*, but little toxicity toward human cell lines (>20 μM). We therefore determined the structure of **15** and a second diketoacid (**14**), bound to UPPS. As seen in Fig. 5 *A* and *B*, both diketoacids bind to site 4, with **14** also binding to site 3. The observation that **15** binds only to site 4 is of interest because this inhibitor has very good antibiotic activity (10). Plus, the occupation of site 4 in both structures is consistent with the results for the other potent anionic inhibitors (Fig. 4).

A surprising result from the *in silico* screening work (Fig. S1) was that bisamidines such as **16** had modest activity against UPPS. Moreover, the biphenyl bisamidine **17** showed potent activity against UPPS (IC_{50} = 0.1 μM) as well as a MIC_{90} of 0.25 μg/mL against *S. aureus* (USA300, MRSA strain). We also found that another dicationic species **18** was a UPPS inhibitor active against *S. aureus* (Table S1). We were unable to obtain the structure of **17** bound to UPPS, but we did obtain structures of **16** and **18** bound to UPPS.

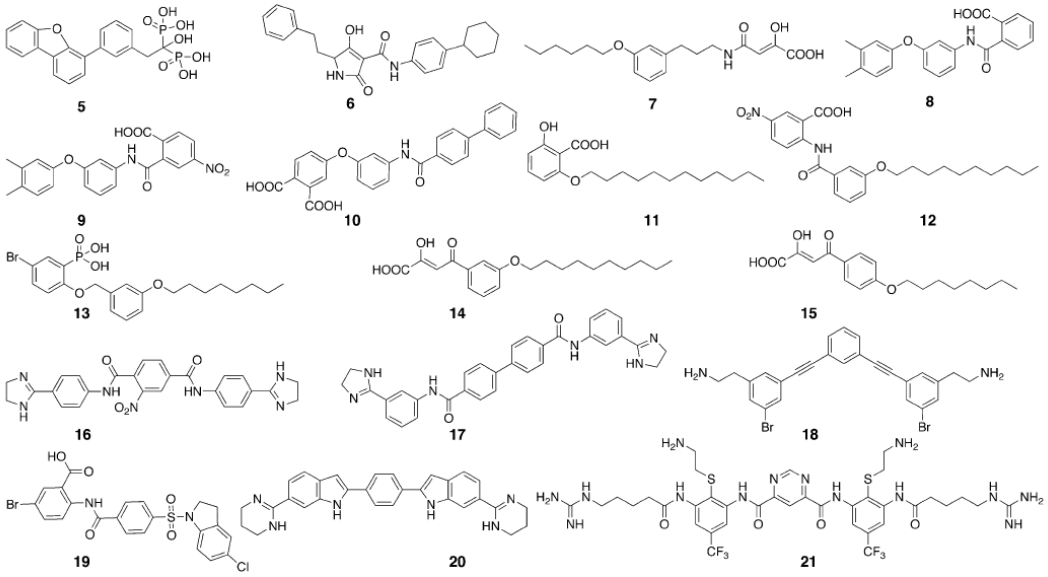

Fig. 2. Chemical structures of UPPS inhibitors and drug leads of interest.

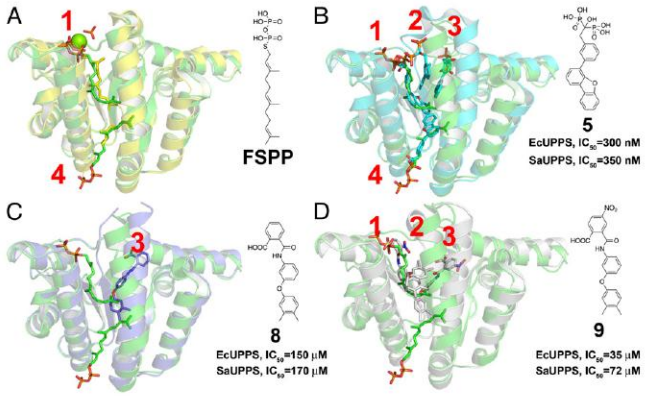

Fig. 3. X-ray structures of *E. coli* UPPS showing substrate and inhibitor binding sites. (*A*) FSPP (yellow) binds to site 1 (PDB ID code 1X06) and FPP (green) binds to sites 1 and 4 (PDB ID code 1V7U). (*B*) A bisphosphonate (**5**) binds to sites 1–4 (PDB ID code 2E98). (*C*) Benzoic acid inhibitor **8** binds to site 3 (cyan, PDB ID code 3SGT), superimposed on FPP-bound structure (green, PDB ID code 1V7U). (*D*) Benzoic acid inhibitor **9** binds to sites 1–3 (cyan, PDB ID code 3SGV), superimposed on FPP-bound structure (green, PDB ID code 1V7U). The large red numbers indicate sites 1–4.

With these two cationic inhibitors, rather than two individual molecules binding, we observe that a single molecule binds, with its polar, cationic groups located at or near the protein's surface, whereas the hydrophobic "spacer" is buried inside the protein's hydrophobic interior, (Fig. 5 *C* and *D*; PDB ID codes 4H2J and 4H2M). Though we did not succeed in crystallizing the most potent lead **17**, a similar "polar-hydrophobic-polar" binding arrangement in which the biphenyl group is buried seems very likely for this species also, and is supported by the results of computational docking, as shown in Fig. S2*D*.

Comparison of *E. coli* and *S. aureus* UPPS Structures and Their Inhibition. In this work, we determined the activity of each inhibitor against both *E. coli* UPPS and *S. aureus* UPPS, finding that there is a very good correlation ($R^2 = 0.8$) between the 14 sets of pIC_{50} ($= -\log_{10}IC_{50}$) values (Table S1; Fig. S3*A*); this is not unexpected because 18 of the top 20 residues in a SCORECONS (16) analysis of *E. coli* UPPS are present in *S. aureus* UPPS and most other bacterial UPPSs (Table S3). We were not able to determine the X-ray structures of any inhibitor bound to *S. aureus* UPPS, but we did determine the structure of the protein with a bound FPP (PDB ID code 4H8E; full data acquisition and structure refinement details are in Table S4). *S. aureus* UPPS cocrystallized with FPP in site 1, together with a SO_4^{2-} in the IPP binding site, as reported in a patent application (17). A superposition of the *S. aureus* and *E. coli* proteins is shown in Fig. S3*B*, where we find a Cα rmsd of 0.91 Å over 202 residues, indicating that both structures are very similar [in the presence of FPP/FSPP (*S-thiolo*-FPP) and either IPP or SO_4^{2-}], consistent with the pIC_{50} correlation.

Relationship to Other Inhibitors: Is UPPS a Missing Link? The structures of several of the UPPS inhibitors described here are similar to (and with **18**, the same as) those being developed as antiinfective drug leads but whose mechanisms of action are not clear. For example, the chemical structures of the benzoic acid inhibitors are similar to those of anthranilic (*ortho*-aminobenzoic) acids reported by Larsen et al. (18) and Mott et al. (19) having activity against *S. aureus*. The molecular mechanism of action of these inhibitors was initially thought to involve inhibition of translation/termination, but in later work this inhibition was not found to correlate with cell growth inhibition, and a new target (SA1575, of unknown function), as well as inhibition of cell wall biosynthesis, was reported. We find that

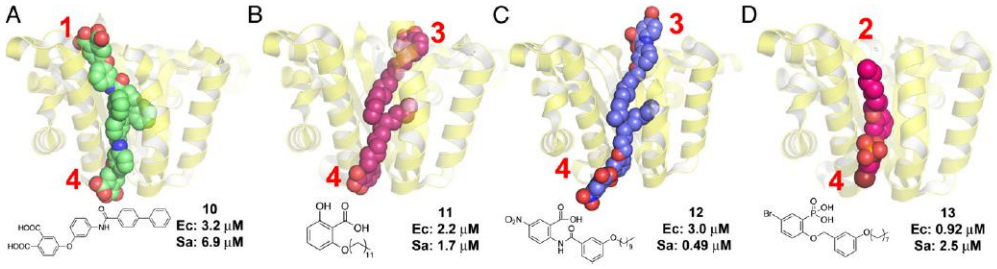

Fig. 4. Crystal structures of the more potent benzoic acids and a phosphonate inhibitor. (*A*) **10** (PDB ID code 3SGX). (*B*) **11** (PDB ID code 3SH0). (*C*) **12** (PDB ID code 4H2O). (*D*) **13** (PDB ID code 4H38). In each case, site 4 is occupied, together with either site 1, 2, or 3, indicating the likely importance of site 4 binding for good activity. The values shown are the IC_{50}s for *E. coli* UPPS inhibition (Ec) or *S. aureus* UPPS inhibition (Sa).

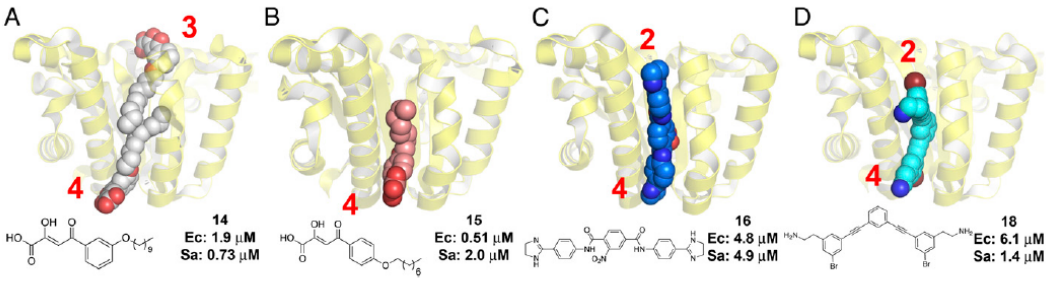

Fig. 5. Crystal structures of diketo acids and two dicationic inhibitors bound to *E. coli* UPPS. (*A*) **14** (PDB ID code 4H3C). (*B*) **15** (PDB ID code 4H3A). (*C*) **16** (PDB ID code 4H2J). (*D*) **18** (PDB ID code 4H2M). The common feature in each case is binding to site 4. The values shown are the IC_{50}s for *E. coli* UPPS inhibition (Ec) or *S. aureus* UPPS inhibition (Sa).

a pharmacophore model (Fig. 6*A*) of seven potent benzoic acid UPPS inhibitors we synthesized (Fig. S4*A*) is very similar to that obtained for *S. aureus* cell growth inhibition (Fig. 6*B*) using five structures reported by Larsen et al. (Fig. S4*B*), making UPPS inhibition one likely mechanism for these inhibitors—in particular because they are already known to inhibit cell wall biosynthesis. In addition, we found that the lead **19** reported by Larsen et al. (18) is a ~1 to 2 μM UPPS inhibitor (Table S1), consistent with a role in *S. aureus* growth inhibition.

In addition to the benzoic/anthranilic acids, there is also interest in the mechanisms of action of bisamidines, such as **20** (20, 21), as well as of other cationic species, such as **21** (22), and it has been proposed that these and related compounds could bind to the minor groove of DNA (20), or that they could alter lipid bilayer structure (23–25), as illustrated schematically in Fig. 6 *C* and *D*. Based on our crystallographic (Fig. 5 *C* and *D*) as well as enzyme inhibition results, it is clear, however, that in addition to these binding modes, polar-hydrophobic-polar inhibitors (such as **17** or **18**) can also bind to proteins, as shown in the cartoon in Fig. 6*E*, with their polar headgroups located near polar protein residues (or at the protein/water interface), whereas their hydrophobic centers are buried inside the protein target (Fig. 5 *C* and *D*).

Notably, as with the benzoic acids, bisamidines such as **20** can inhibit cell wall biosynthesis, and with **20** we find quite potent (470 nM) UPPS inhibition.* The ability to inhibit UPPS in addition to, e.g., DNA and lipid membrane targeting likely contribute to the potent activity of these compounds and, in some cases, the lack of resistance observed experimentally. In addition, it is also possible that other prenyltransferases, such as FPPS, may in some cases be targeted.

Synergy and in Vivo Results. The UPPS inhibition results suggested to us the possibility of synergistic activity with downstream cell-wall biosynthesis inhibitors, such as methicillin (Fig. 1); this is indeed the case, as shown in Fig. 7*A* in which we present the isobologram (26) for **17** + methicillin against a USA300 strain of MRSA. We observe a potent synergistic interaction with a fractional inhibitory concentration index (FICI), defined as

$$\mathrm{FICI} = \mathrm{FIC_A} + \mathrm{FIC_B} = \mathrm{MIC_{90}(AB)/MIC_{90}(A)} + \mathrm{MIC_{90}(BA)/MIC_{90}(B)},$$

where, $\mathrm{FIC_A}$, $\mathrm{FIC_B}$ are the fractional inhibitory concentrations of drugs A and B, and $\mathrm{MIC_{90}}$ (AB), $\mathrm{MIC_{90}}$ (BA) are the $\mathrm{MIC_{90}}$ values of the most effective combination of A or B in the presence of B or A (27, 28). Using this method, FICI values <0.5 represent synergism; >0.5 and <1.0 represent additivity; >1 and <2 represent an indifferent effect; and ≥2 represents drug antagonism (29). An FICI = 0.25 thus represents strong synergism, opening up the probability of restoring drug sensitivity in drug-resistant strains. However, are such compounds active in in vivo models of infection?

In previous work, it has been found that, e.g., benzoic acids (such as **19**) as well as tetramic acids (such as **6**) have potent activity against bacteria; however, there have been no previous

*Opperman TJ, et al. Poster Session, 50th Interscience Conference on Antimicrobial Agents and Chemotherapy, September 12–15, 2010, Boston.

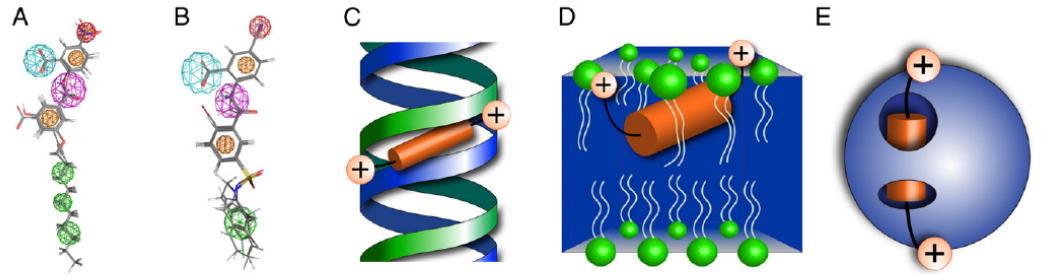

Fig. 6. UPPS as a missing link. Models and cartoons. (*A*) Pharmacophore model for UPPS inhibition by benzoic acids. (*B*) Pharmacophore model for *S. aureus* growth inhibition by benzoic acids. Common features are benzoic acid carboxylates (cyan) with electron-withdrawing *meta* substituents (red); an x–y spacer (dark pink); two aromatic features (orange); and more-distal hydrophobic features (green). (*C*) Cationic-hydrophobic-cationic inhibitor binding to DNA. (*D*) Cationic-hydrophobic-cationic inhibitor binding to anionic lipids in a membrane. (*E*) Cationic-hydrophobic-cationic inhibitor binding to a protein.

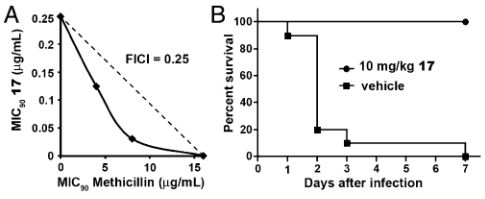

Fig. 7. In vitro synergy and in vivo results with **17**. (*A*) Isobologram for **17** + methicillin inhibition of *S. aureus* (USA300) cell growth. FICI = 0.25. (*B*) Activity of **17** in a mouse model of *S. aureus* (USA200) infection. Shown is one representative experiment repeated twice (n = 10 mice per group per experiment). No mice in the group treated once daily with 10 mg/kg of **17** (three doses total) died during either experiment.

reports of in vivo activity, due perhaps to strong binding to plasma proteins. Because **17** had potent activity against UPPS (110 nM), we tested it in a mouse model of infection using the USA200 Sanger 252 (MRSA) strain of *S. aureus*. As can be seen in Fig. 7*B*, mice treated postinfection only with vehicle control all died, whereas mice treated with **17** (20/20 total, pooled results of two experiments) survived with no apparent adverse reactions.

Computational Results: FTMap, Principal Component, and Receiver Operating Characteristic/Area Under the Curve Analyses. The results described above represent the discovery of a series of UPPS inhibitors—drug leads—some of which have potent activity in cells and a mouse infection model. From a structural perspective, the most surprising result was that the most potent inhibitors all bound to site 4, not the substrate site, site 1. In previous work on bisphosphonate UPPS inhibitors (5) we found that a wide range of bisphosphonates bound to site 1, and that enzyme inhibition and site 1 docking scores were highly correlated (5). However, with all of the nonbisphosphonate inhibitors described here, we find that binding to site 4 is the common structural denominator for ligands with high affinity. Other sites are also often occupied, with either two molecules binding, or one inhibitor spanning two sites (sites 4 and 2, with the dicationic species).

Site 4 is quite removed from the most-flexible loop region (residues 72–82) of the active site, suggesting that there may be fewer entropic costs due to constraining this loop, associated with inhibitor binding to site 4, rather than to sites 1–3, where the ligand directly contacts and restrains the loop. Site 4 is also predicted to be druggable when using the solvent-mapping program FTMap (30), as shown in Fig. 8*A*, again supporting the idea that inhibitors that bind to site 4 will be good drug leads. With the nonbisphosphonate inhibitors, we also see that the global structures are quite similar to apo UPPS (Fig. 8*B*, red), using principal component analysis (31). The bisphosphonate inhibitors (blue) and substrate (yellow)-bound structures are altered to a greater extent from the apo form than are the nonbisphosphonate structures (red), which suggests less induced-fit occurs on binding, which again will reduce any energetic costs associated with protein conformational changes upon binding.

Finally, because many of these inhibitors were the result of virtual screening, we assessed the predictive nature of each structure using a receiver operating characteristic/area under the curve (ROC/AUC) approach (32) with a 112-compound screening dataset (Fig. S5). Enrichment results are shown in Fig. 8*C* and Fig. S6. Good results (AUC = 0.768) are obtained when using the "open" structure containing **5** bound to sites 1–4, but the best result is obtained using the **15** structure (PDB ID code 4H3A), an "ajar" (Fig. 8*B*) or partially closed structure in which only site 4 is occupied (Fig. 8*C*, bottom), where AUC = 0.802. Taken together, these results strongly support the importance of developing compounds that bind to site 4 as UPPS inhibitor drug leads, and that computational models based on these structures can significantly enrich the hit rate.

Conclusions

The results we have described herein are of interest for several reasons. First, we obtained the X-ray structures of 10 UPPS inhibitors covering a diverse range of structures: benzoic acids, diketoacids, an aryl phosphonate, a bisamidine, and a bisamine. The surprising result was that both cationic as well as anionic compounds were inhibitors, the cationic species having an unusual polar-hydrophobic-polar structural motif. Second, we find evidence that occupancy of site 4 (not the FPP substrate site, site 1) correlates with the potent activity of these inhibitors, and that site 4 is predicted to be druggable. Third, we find that the cationic

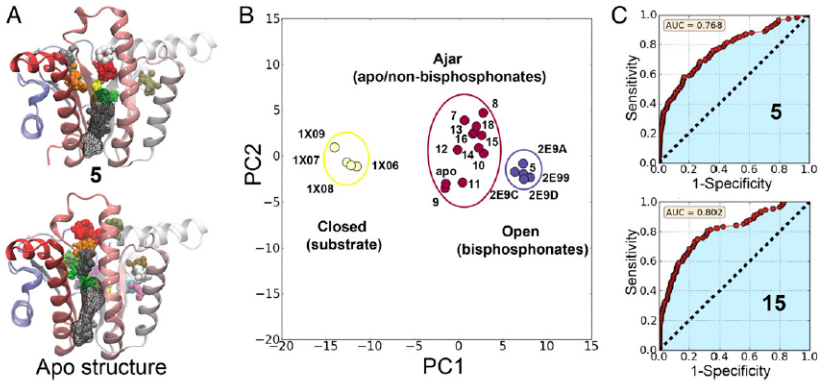

Fig. 8. Computational analysis of UPPS structural results. (*A*) FTMap computational solvent mapping of UPPS structures (PDB ID codes 2E98 and 3QAS) suggest that site 4 is druggable in either inhibitor-bound complexes or unbound. UPPS is represented as a cartoon; small probes are colored spheres; black wireframe outlines site 4. (*B*) Principal component analysis of *E. coli* UPPS structures. Substrate-bound structures (yellow) are closed (33); bisphosphonates (blue) are open (33); the apo and nonbisphosphonate structures (red) are all ajar (slightly open). (*C*) ROC/AUC analysis of most-predictive UPPS structures in terms of initial enrichment for actives under 100 μM (Fig. S6).

(bisamidine and a bisamine) inhibitors span both sites 2 and 4, with their polar groups at or near the protein/water interface, whereas their hydrophobic domains are buried. This result is of particular importance because this motif is very similar to that proposed to be important for DNA and lipid membrane binding with structurally related inhibitors, leading to the idea that such compounds may have multiple targets (including UPPS), thereby increasing potency. We also find that a closely related biphenyl analog (**17**) inhibits UPPS at ~100 nM levels, has a MIC_{90} of 0.25 μg/mL, and strongly synergistic activity (FICI = 0.25) with methicillin in an MRSA strain otherwise resistant to the antibiotic. In addition, this compound shows clear therapeutic activity in a mouse model of infection. Finally, we propose that anthranilic acids, known to be potent inhibitors of *S. aureus* growth that target cell-wall biosynthesis, also target bacterial UPPS. Taken together, these results open up additional routes to anti-infective therapies targeting bacterial isoprenoid biosynthesis, and suggest that in some cases drug leads that have been proposed to target DNA and lipid membrane structure may also target bacterial cell-wall biosynthesis via UPPS inhibition.

Methods

E. coli UPPS and *S. aureus* UPPS were expressed and purified as described previously (9). UPPS inhibition assays were carried out as described previously (5). UPPS/inhibitor crystals were obtained via soaking as described previously (5). Structure determinations and refinements were carried out basically as described previously (5), with full details given in *SI Methods*. For the 11 structures reported, the resolution was on average 1.88 Å (±0.29 Å), and R_{free} was on average 24.6% (±3.9%). Full synthesis and characterization details for all compounds investigated crystallographically are provided in *SI Methods*. In vivo experiments used female BALB/c mice infected intraperitoneally with *S. aureus* (USA200), as described in detail in *SI Methods*. Bacterial cell-growth inhibition assays were carried out as described previously (10). The care and experimental manipulation of our mice were reviewed and approved by the Institutional Animal Care and Use Committee at the University of California at San Diego.

ACKNOWLEDGMENTS. We thank Yigui Gao from the University of Illinois Macromolecular Crystallization Laboratory for providing crystallization facilities, and F. Guerra for help with the graphics. Use of the Advanced Photon Source was supported by the US Department of Energy, Office of Science, Office of Basic Energy Sciences, under Contract DE-AC02-06CH11357. Use of the Life Science Collaborative Access Team Sector 21 was supported by the Michigan Economic Development Corporation and Michigan Technology Tri-Corridor Grant 085P1000817. Funding for this work was provided by US Public Health Services National Institutes of Health (NIH) Grants AI074233, GM65307, and CA158191. Work at the University of California at San Diego was supported by Molecular Biophysics Training Grant GM08326; NIH Grants GM31749 and HD071600; National Science Foundation Grant MCB-1020765; the National Biomedical Computation Resource, the Center for Theoretical Biological Physics, and the Howard Hughes Medical Institute.

1. Oldfield E (2010) Targeting isoprenoid biosynthesis for drug discovery: Bench to bedside. *Acc Chem Res* 43(9):1216–1226.
2. Oldfield E, Lin FY (2012) Terpene biosynthesis: Modularity rules. *Angew Chem Int Ed Engl* 51(5):1124–1137.
3. Scholte AA, Eubanks LM, Poulter CD, Vederas JC (2004) Synthesis and biological activity of isopentenyl diphosphate analogues. *Bioorg Med Chem* 12(4):763–770.
4. Guo RT, et al. (2005) Crystal structures of undecaprenyl pyrophosphate synthase in complex with magnesium, isopentenyl pyrophosphate, and farnesyl thiopyrophosphate: Roles of the metal ion and conserved residues in catalysis. *J Biol Chem* 280(21):20762–20774.
5. Guo RT, et al. (2007) Bisphosphonates target multiple sites in both *cis*- and *trans*-prenyltransferases. *Proc Natl Acad Sci USA* 104(24):10022–10027.
6. Peukert S, et al. (2008) Design and structure-activity relationships of potent and selective inhibitors of undecaprenyl pyrophosphate synthase (UPPS): Tetramic, tetronic acids and dihydropyridin-2-ones. *Bioorg Med Chem Lett* 18(6):1840–1844.
7. Fujikura K, Maki Y, Ohya N, Satoh M, Koyama T (2008) Kinetic studies of *Micrococcus luteus* B-P 26 undecaprenyl diphosphate synthase reaction using 3-desmethyl allylic substrate analogs. *Biosci Biotechnol Biochem* 72(3):851–855.
8. Kuo CJ, et al. (2008) Structure-based inhibitors exhibit differential activities against *Helicobacter pylori* and *Escherichia coli* undecaprenyl pyrophosphate synthases. *J Biomed Biotechnol* 2008:841312.
9. Durrant JD, et al. (2011) Non-bisphosphonate inhibitors of isoprenoid biosynthesis identified via computer-aided drug design. *Chem Biol Drug Des* 78(3):323–332.
10. Zhang Y, et al. (2012) HIV-1 integrase inhibitor-inspired antibacterials targeting isoprenoid biosynthesis. *ACS Med Chem Lett* 3(5):402–406.
11. van Heijenoort J (2007) Lipid intermediates in the biosynthesis of bacterial peptidoglycan. *Microbiol Mol Biol Rev* 71(4):620–635.
12. Hao H, Cheng G, Dai M, Wu Q, Yuan Z (2012) Inhibitors targeting on cell wall biosynthesis pathway of MRSA. *Mol Biosyst* 8(11):2828–2838.
13. Apfel CM, Takács B, Fountoulakis M, Stieger M, Keck W (1999) Use of genomics to identify bacterial undecaprenyl pyrophosphate synthetase: Cloning, expression, and characterization of the essential uppS gene. *J Bacteriol* 181(2):483–492.
14. Lu YP, Liu HG, Liang PH (2009) Different reaction mechanisms for *cis*- and *trans*-prenyltransferases. *Biochem Biophys Res Commun* 379(2):351–355.
15. Lu YP, Liu HG, Teng KH, Liang PH (2010) Mechanism of *cis*-prenyltransferase reaction probed by substrate analogues. *Biochem Biophys Res Commun* 400(4):758–762.
16. Valdar WSJ (2002) Scoring residue conservation. *Proteins* 48(2):227–241.
17. Ammirati M, Pandit J (2002) Crystal structure of *Staphylococcus* undecaprenyl pyrophosphate synthase and uses thereof. US Patent Application No. 10/688,167.
18. Larsen SD, et al. (2006) Discovery and initial development of a novel class of antibacterials: Inhibitors of *Staphylococcus aureus* transcription/translation. *Bioorg Med Chem Lett* 16(24):6173–6177.
19. Mott JE, et al. (2008) Resistance mapping and mode of action of a novel class of antibacterial anthranilic acids: Evidence for disruption of cell wall biosynthesis. *J Antimicrob Chemother* 62(4):720–729.
20. Panchal RG, et al. (2009) Novel broad-spectrum bis-(imidazolinylindole) derivatives with potent antibacterial activities against antibiotic-resistant strains. *Antimicrob Agents Chemother* 53(10):4283–4291.
21. Butler MM, et al. (2010) Comparative in vitro activity profiles of novel bis-indole antibacterials against gram-positive and gram-negative clinical isolates. *Antimicrob Agents Chemother* 54(9):3974–3977.
22. Tew GN, Scott RW, Klein ML, Degrado WF (2010) De novo design of antimicrobial polymers, foldamers, and small molecules: From discovery to practical applications. *Acc Chem Res* 43(1):30–39.
23. Som A, Tew GN (2008) Influence of lipid composition on membrane activity of antimicrobial phenylene ethynylene oligomers. *J Phys Chem B* 112(11):3495–3502.
24. Su Y, DeGrado WF, Hong M (2010) Orientation, dynamics, and lipid interaction of an antimicrobial arylamide investigated by 19F and 31P solid-state NMR spectroscopy. *J Am Chem Soc* 132(26):9197–9205.
25. Yang L, et al. (2008) Mechanism of a prototypical synthetic membrane-active antimicrobial: Efficient hole-punching via interaction with negative intrinsic curvature lipids. *Proc Natl Acad Sci USA* 105(52):20595–20600.
26. Berenbaum MC (1989) What is synergy? *Pharmacol Rev* 41(2):93–141.
27. Eliopoulos GM, Moellering RC (1998) Antimicrobial combinations. *Antibiotics in Laboratory Medicine*, ed Lorian V (Williams & Wilkins, Baltimore), 4th Ed, pp 330–396.
28. Singh PK, Tack BF, McCray PB, Jr., Welsh MJ (2000) Synergistic and additive killing by antimicrobial factors found in human airway surface liquid. *Am J Physiol Lung Cell Mol Physiol* 279(5):L799–L805.
29. European Committee for Antimicrobial Susceptibility Testing (EUCAST) of the European Society of Clinical Microbiology and Infectious Dieases (ESCMID) (2000) EUCAST Definitive Document E.Def 1.2, May 2000: Terminology relating to methods for the determination of susceptibility of bacteria to antimicrobial agents. *Clin Microbiol Infect* 6(9):503–508.
30. Ngan CH, et al. (2012) FTMap: Extended protein mapping with user-selected probe molecules. *Nucleic Acids Res* 40(Web Server issue):W271–W275.
31. Grant BJ, Rodrigues APC, ElSawy KM, McCammon JA, Caves LSD (2006) Bio3d: An R package for the comparative analysis of protein structures. *Bioinformatics* 22(21):2695–2696.
32. Lee HS, et al. (2008) Optimization of high throughput virtual screening by combining shape-matching and docking methods. *J Chem Inf Model* 48(3):489–497.
33. Teng KH, Liang PH (2012) Structures, mechanisms and inhibitors of undecaprenyl diphosphate synthase: A *cis*-prenyltransferase for bacterial peptidoglycan biosynthesis. *Bioorg Chem* 43:51–57.

B.3 Multitarget Drug Discovery for Tuberculosis and Other Infectious Diseases

This chapter was reprinted with permission (Li *et al.*, 2014).

Li, K., Schurig-Briccio, L.A., Feng, X., Upadhyay, A., Pujari, V., Lechartier, B., Fontes, F.L., Yang, H., Rao, G., Zhu, W., Gulati, A., No, J.H., Cintra, G., Bogue, S., Liu, Y.L, Molohon, K.J., Orlean, P., Mitchell, D.A., Freitas-Junior, L., Ren, F., Sun, H., Jiang, T., Li, Y., Guo, R.T, Cole, S.T., Gennis, R.B., Crick, D.C., and Oldfield, E. (2014) *J. Med. Chem*: 57, 3126-3139. doi: 10.1021/jm500131s.

I obtained the minimum inhibitory concentrations of the compounds against methicillin resistant

Staphylococcus aureus USA300 (Table 1).

Journal of Medicinal Chemistry

Article

pubs.acs.org/jmc

Multitarget Drug Discovery for Tuberculosis and Other Infectious Diseases

Kai Li,[†,&] Lici A. Schurig-Briccio,[‡,&] Xinxin Feng,[†,&] Ashutosh Upadhyay,[§] Venugopal Pujari,[§] Benoit Lechartier,[∥] Fabio L. Fontes,[§] Hongliang Yang,[§] Guodong Rao,[†] Wei Zhu,[⊥] Anmol Gulati,[†] Joo Hwan No,[¶] Giovana Cintra,[¶] Shannon Bogue,[‡] Yi-Liang Liu,[⊥] Katie Molohon,[□] Peter Orlean,[□] Douglas A. Mitchell,[†,□,▽] Lucio Freitas-Junior,[¶] Feifei Ren,[#] Hong Sun,[#] Tong Jiang,[#] Yujie Li,[#] Rey-Ting Guo,[#] Stewart T. Cole,[∥] Robert B. Gennis,[†,‡] Dean C. Crick,[§] and Eric Oldfield[*,†,⊥]

[†]Department of Chemistry, University of Illinois at Urbana−Champaign, 600 South Mathews Avenue, Urbana, Illinois 61801, United States

[‡]Department of Biochemistry, University of Illinois at Urbana−Champaign, 600 South Mathews Avenue, Urbana, Illinois 61801, United States

[§]Department of Microbiology, Immunology and Pathology, Colorado State University, 200 West Lake Street, Fort Collins, Colorado 80523, United States

[∥]Global Health Institute, École Polytechnique Fédérale de Lausanne, Lausanne, Switzerland

[⊥]Center for Biophysics and Computational Biology, University of Illinois at Urbana−Champaign, 607 South Mathews Avenue, Urbana, Illinois 61801, United States

[¶]Institut Pasteur Korea, Sampyeong-dong 696, Bundang-gu, Seongnam-si, Gyeonggi-do, Korea

[□]Department of Microbiology, University of Illinois at Urbana−Champaign, 601 South Goodwin Avenue, Urbana, Illinois 61801, United States

[▽]Institute for Genomic Biology, University of Illinois at Urbana−Champaign, 1206 West Gregory Drive, Urbana, Illinois 61801, United States

[#]Industrial Enzymes National Engineering Laboratory, Tianjin Institute of Industrial Biotechnology, Chinese Academy of Sciences, Tianjin 300308, China

Supporting Information

ABSTRACT: We report the discovery of a series of new drug leads that have potent activity against *Mycobacterium tuberculosis* as well as against other bacteria, fungi, and a malaria parasite. The compounds are analogues of the new tuberculosis (TB) drug SQ109 (**1**), which has been reported to act by inhibiting a transporter called MmpL3, involved in cell wall biosynthesis. We show that **1** and the new compounds also target enzymes involved in menaquinone biosynthesis and electron transport, inhibiting respiration and ATP biosynthesis, and are uncouplers, collapsing the pH gradient and membrane potential used to power transporters. The result of such multitarget inhibition is potent inhibition of TB cell growth, as well as very low rates of spontaneous drug resistance. Several targets are absent in humans but are present in other bacteria, as well as in malaria parasites, whose growth is also inhibited.

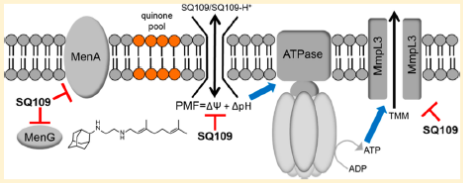

INTRODUCTION

Antibiotic resistance is a public health problem that, arguably, has the potential to destroy the efficacy of all antibiotics in the next 10−20 years.[1,2] There is, therefore, an urgent need for new drugs, especially ones that might be more "resistance-resistant". One possible approach to achieving this goal is to move away from targeting the direct killing of pathogens to inhibiting their virulence, because this might lead to a decreased "life or death" pressure on the organism to develop resistance.[3] A second approach would be to develop more drugs that target pathogen cell membranes. An example of this type of drug would be the antifungal amphotericin,[4] which functions by binding to ergosterol (which is not present in human cell membranes). A third and well-known approach is to employ combination therapies,[5] although the problems associated with finding two new drugs active against two new targets are clearly significant. A fourth approach is to use "multitargeting" or "polypharma-

Received: January 24, 2014
Published: February 25, 2014

cology" in which a single drug has more than one target.[6,7] This could involve "series inhibition", in which targets would be in the same metabolic pathway (Figure 1, left), "parallel inhibition", in which the targets would be unrelated but an inhibitor might mimic a common substrate or would affect, for example, a membrane function (Figure 1, middle), or "network inhibition", in which many targets in series and/or in parallel could be involved (Figure 1, right). While challenging, many drugs that have been effective in monotherapy do in fact have multiple targets[6] while single-target drugs (many of which are used in treating tuberculosis) are often only effective in combination therapies.

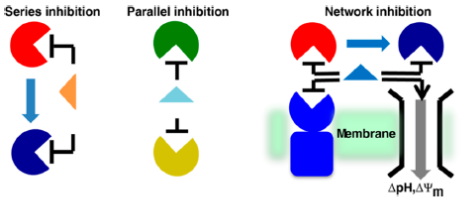

Figure 1. Series (in the same metabolic pathway), parallel (unrelated pathways or DNA/membrane targets), or network (series and parallel target) inhibition.

In this work, we consider the mechanism(s) of action of the new antituberculosis drug **1** (Chart 1), currently in phase II clinical trials.[8] This drug candidate appeared of interest because it contains a C_{10} isoprenoid (geranyl) side chain together with a strongly basic (ethylenediamine) fragment, a likely cationic center, suggesting that it might act as a carbocation isostere for a transition state/reactive intermediate in isoprenoid biosynthesis[9] and, as with other inhibitors of isoprenoid biosynthesis, it might be involved in multitargeting.[10] **1** was developed in a synthesis/screening program[11] in which ~64 000 ethylenediamine analogues of the antituberculosis drug ethambutol (**2**) were synthesized. **1** was ~4× more active than any of the other leads developed, having a minimum inhibitory concentration (MIC) of ~0.7−1.56 μM against *M. tuberculosis* (H37Rv, Erdman, and drug-resistant strains), and insights into its mode of action recently became available when the target of SQ109 was proposed[12] to be MmpL3, a trehalose monomycolate (TMM) transporter, an essential membrane protein that transports TMM into the cell envelope. This conclusion was based on the observation that several *M. tuberculosis* mutants produced via serial passage with several **1**-like inhibitors had mutations in the *mmpL3* gene and cross-resistance to **1**, although these latter effects were rather small.[12] More intriguingly, no spontaneous resistant mutants were obtained when using **1**, suggesting the possibility of multiple targets.[12,13] That idea is supported by the observation that **1** also has activity against other bacteria, e.g., *Helicobacter pylori*[14] as well as against the yeast *Candida albicans*,[15] neither of which possess the *mmpL3* gene, suggesting again that other **1** targets are harbored by these organisms and, potentially, by *M. tuberculosis*.

In this work, we synthesized a series of analogues of **1** in which we varied the adamantane headgroup and the ethylenediamine linker (varying the possible charge centers), Chart 1. All compounds were screened against a panel of bacteria (*M. tuberculosis*, *M. smegmatis*, *Escherichia coli*, *Staphylococcus aureus*, and *Bacillus subtilis*), two yeasts (*Saccharomyces cerevisiae* and *Candida albicans*), a malaria parasite (*Plasmodium falciparum*), and a human cell line (MCF-7), to establish antibacterial, antifungal and antimalarial structure−activity relationships and to assess mammalian cell toxicity. In addition, we investigated a subset of compounds for activity against a series of putative targets, isoprenoid biosynthesis enzymes, in addition to investigating the effects of these compounds on respiration, ATP synthesis, and the proton motive force (PMF).

RESULTS AND DISCUSSION

Only One Cationic Center Is Needed for Potent Activity in Mycobacteria. To investigate which features contribute to the activity of **1** against a broad range of organisms, we synthesized **1** and the 11 analogues (**3**−**13**) shown in Chart 1 in which the ethylenediamine linker was replaced by ethanolamine, choline, propanolamine, ethylene glycol, or glycolic amide moieties (providing linkers with potentially 0, 1, or 2 positive charges), as well several "head group" analogues in which the adamantyl group was varied. The geranyl "side chain" was kept constant. Full synthesis and characterization details are given in the Supporting Information. As expected, **1** had potent activity against *M. tuberculosis* with an MIC of ~0.1−0.2 μg/mL (Table 1). Interestingly, the *N*-geranyl ethanolamines **3** and **13** were more potent (MIC values as low as 0.02−0.05 μg/mL), indicating that the presence of two nitrogens was not essential for activity. The *O*-geranyl ethanolamine derivative (**4**) had activity similar to that of **1** (~0.2 μg/mL), Table 1. With the *N*-geranyl ethanolamines (**3**, **13**), activity was about 30-fold higher than with ethambutol (**2**). The ethylene glycol (**5**) was far less active (50 μg/mL), as was the glycolic amide **9** (12 μg/mL). Thus, the most active compounds all contain one strongly basic nitrogen in the linker region, with most activity being found with the two *N*-geranyl

Chart 1. Structures of Compounds Investigated

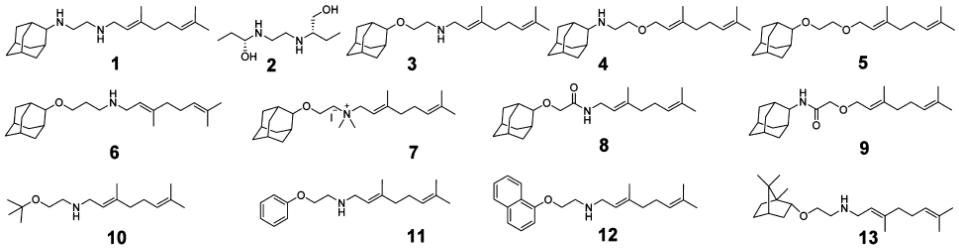

dx.doi.org/10.1021/jm500131s | J. Med. Chem. 2014, 57, 3126−3139

Table 1. Inhibition by 1 and Analogues of *M. tuberculosis* (Mt), *M. smegmatis* (Ms), *S. aureus* (Sa), *B. subtilis* (Bs), *E. coli* (Ec), *S. cerevisiae* (Sc), *C. albicans* (Ca), *P. falciparum* (Pf), and Human (MCF-7) Cell Growth

	Mt[a]	Ms[a]	Sa[a]	Bs[b]	Ec[b]	Sc[b]	Ca[b]	Pf[b]	MCF-7[b]
1	0.1−0.2 (0.3−0.6)	3.1(9.4)	>120(364)	7.6(23)	2.8(8.5)	1.1(3.3)	3.3(10)	1.0(3.0)	6.0(18)
2	2(9.8)[c]	1(4.9)[d]	–	–	–	–	–	–	–
3	0.02−0.05 (0.06−0.15)	1.6(4.8)	8(24)	16(48)	2.8(8.5)	1.8(5.4)	12(36)	0.79(2.4)	10(30)
4	0.19(0.57)	6.2(19)	>120(362)	>66(199)	4.3(13)	>33(100)	>66(199)	0.93(2.8)	112(338)
5	50(150)	>50(150)	>64(193)	>66(199)	>332(1000)	>332(1000)	>66(198)	7.9(24)	73(220)
6	1.6(4.6)	6.2(18)	8(23)	3.0(8.7)	2.3(6.7)	2.7(7.8)	6.5(19)	0.83(2.4)	3.4(9.8)
7	0.78(1.6)	12(24)	8(16)	4.2(8.6)	37(76)	15(31)	18(37)	0.08(0.16)	3.2(6.5)
8	0.78(2.2)	6.2(18)	>120(345)	>69(200)	>345(1000)	>69(200)	>69(200)	6.2(18)	12(35)
9	12(34)	25(72)	>120(348)	17(49)	>345(1000)	>69(200)	>69(200)	3.8(11)	9.3(27)
10	6.2(24)	50(198)	>16(63)	>50(198)	>126(498)	44(174)	>50(198)	3.2(13)	45(178)
11	6.2(23)	12(44)	32(117)	17(62)	60(220)	3.0(11)	20(74)	14(51)	6.3(23)
12	6.2(19)	12(37)	8(25)	2.4(7.4)	15(46)	3.7(11)	12(37)	>100(309)	7.1(22)
13	0.05(0.15)	1.6(4.8)	8(24)	1.8(5.4)	12(36)	0.89(2.7)	6.3(19)	2.0(6.0)	1.3(3.9)

[a]MIC, μg/mL, values in parentheses are in μM. [b]IC_{50}, μg/mL, values in parentheses are in μM. [c]Reference 16. [d]Reference 17.

ethanolamines 3 and 13 (Table 1), with 3 being ∼4−5 times more active than that of 1.

We then tested all 12 compounds against *M. smegmatis*. The results (Table 1) show that overall activity against *M. smegmatis* is less than that observed against *M. tuberculosis*, as can also be seen in the "heat map" shown in Figure 2A. There is, however, a very high correlation coefficient (R^2 = 0.9, Figure 2B) between the pIC_{50} (= $-\log_{10}$ IC_{50}) values for *M. tuberculosis* and *M. smegmatis*, indicating a similar mechanism of action, leading to our use of *M. smegmatis* in several mechanism of action studies, as described below.

The Cationic Inhibitors Exhibit Broad Antibacterial, Antifungal, and Antimalarial Activity. All 12 compounds (1, 3−13) were then tested against three other bacteria: *S. aureus*, *B. subtilis*, and *E. coli*, Table 1. With *S. aureus* (the methicillin-resistant *S. aureus* (MRSA) USA300 strain), 1 itself had little activity; however, the *N*-geranyl ethanolamines 3, 12, 13 and the *N*-geranyl propanolamine 6 all had MIC values of ∼8 μg/mL, while the other analogues were much less active (MIC > 32 μg/mL). A similar pattern of activity was seen against *B. subtilis*, with the three ethanolamines (6, 12, 13) exhibiting the highest levels of activity. In addition, unlike with *S. aureus*, 1 itself had activity (7.6 μg/mL, Table 1). With *E. coli*, 1, the *N*-geranyl ethanolamine (3) and the *N*-geranyl propanolamine (6) were all quite active, with IC_{50} values of ∼2−3 μg/mL, Table 1. Moreover, there was a modest correlation (R^2 = 0.5) between the *M. tuberculosis* (or *M. smegmatis*) pMIC values and those found with *E. coli*, Figure 2B. These results again indicate that at least one basic amine, most likely a cationic center, is required for best activity; plus, there must be a target or targets other than MmpL3 in *E. coli* because the *mmpL3* gene is absent in this organism. Bioinformatics searches did locate uncharacterized *mmpL3*-like genes in *S. aureus* and *B. subtilis*, but it remains to be seen if the corresponding proteins are targeted by our compounds.

We next tested all 12 compounds (1, 3−13) for activity against *S. cerevisiae* and *C. albicans*. As can be seen in Table 1 and Figure 2A, 1 and the ethanolamines 3, 6, 11, and 13 had activity in the 1−3 μg/mL range, with 1 and 13 being the most potent, having an IC_{50} ∼ 1 μg/mL. With *C. albicans*, 1 was most active, followed by the ethanolamines 3 and 13. Not unexpectedly, there was a high correlation between the pIC_{50} values seen between *S. cerevisiae* and *C. albicans* (R^2 = 0.8; Table 1 and Figure 2B). A modest correlation between the pIC_{50} values for the yeasts and *E. coli* or *B. subtilis* is also apparent (R = 0.6−0.7, Figure 2B), suggesting the possibility of target conservation between fungi and bacteria. Because a recognizable *mmpL3* gene is absent in the fungi, these results again indicate an alternate target or targets. These results also lead to the idea that there could be additional targets in *M. tuberculosis*, which would help explain the very low MIC values observed and the inability to induce resistance via serial passage, as noted by Tahlan et al.,[12] although multiple-targeting does not necessarily guarantee improved potency. The results with the bacteria and fungi then suggested the possibility that the growth of other organisms (protozoa) might also be inhibited by 1 or its analogues.

To evaluate antiprotozoal activity we screened all 12 compounds (1, 3−13) against the intraerythrocytic form of the malaria parasite, *Plasmodium falciparum*. As can be seen in Table 1, 1 had a ∼1 μg/mL activity against *P. falciparum*, and the three ethanolamines (3, 4, and 6) also had good activity. As viewed on the heat map (Figure 2A), inhibition of *M. tuberculosis* cell growth is strongest but is followed by *P. falciparum* (in the intraerythrocytic assay) and in each case where there is activity against *P. falciparum* (2, 3, 4, 6, 7), the inhibitors (Chart 1) are expected to carry a +1 charge, as with the best *M. tuberculosis* growth inhibitors. When compared to growth inhibition results with a human cell line (MCF-7; Table 1), we see that activity against the human cells is much weaker than against *P. falciparum* and, of course, against *M. tuberculosis*. We calculate a therapeutic index (TI), defined as:

$$\mathrm{TI} = \frac{IC_{50}(\text{human cell line})}{IC_{50}(\text{pathogen})}$$

of ∼18 for 1 against *P. falciparum* and ∼40 for 3, while for *M. tuberculosis* we find TI = 120 (1) and TI = 900 (3), suggesting that these and related analogues may also be promising *P. falciparum* drug leads. Because the human cell growth assays are carried out in the presence of 10% fetal bovine serum (FBS), we tested three of the most active compounds (1, 3, 13) against *E. coli* in the presence or absence of 10% FBS. There was only a 1.6 ± 0.07× increase in the IC_{50}, meaning that, as expected, serum binding is small and quite similar for each of these compounds. We next sought to explore what the additional targets for these compounds might be in cells that lack MmpL3.

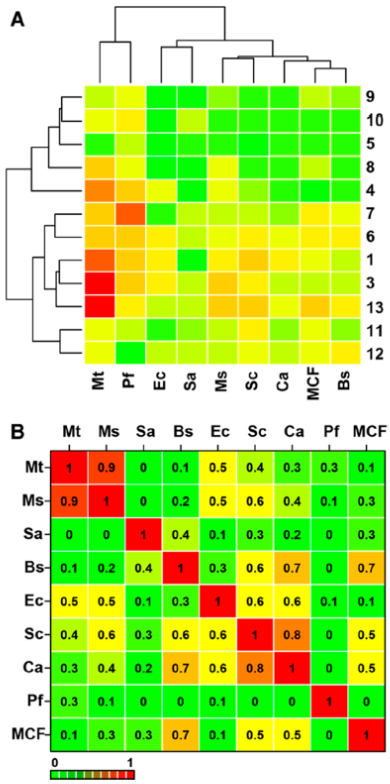

Figure 2. Inhibition of cell growth for *M. tuberculosis* (Mt), *M. smegmatis* (Ms), *S. aureus* (Sa), *B. subtilis* (Bs), *E. coli* (Ec), *S. cerevisiae* (Sc), *C. albicans* (Ca), *P. falciparum* (Pf), and a human cell line (MCF-7) by **1**, **3**–**13**. (A) Heat map. Red = strong inhibition; yellow = moderate inhibition; green = weak/no inhibition. (B) Correlation *R* values for cell growth inhibition pIC_{50} (= $-\log_{10}$ IC_{50}, μM) or pMIC = ($-\log_{10}$ MIC, μM) between all systems investigated.

Possible Protein Targets for SQ109 and Its Analogues. The general patterns of activity seen with the compounds described above have some similarities across the diverse organisms investigated in that at least one cationic center, or perhaps more importantly a protonatable nitrogen, is required for activity. In *M. tuberculosis*, **1** is thought to act by inhibiting MmpL3, a TMM transporter,[12] although as noted by Tahlan et al., other targets could also be involved. This seems quite likely because in most cases these other organisms lack *mmpL3* or a clearly identifiable orthologue, and do not utilize TMM, as is also the case with *H. pylori*.[14] Given that protonated geranylamines might be good isosteres for transition states or reactive intermediates in enzymes involved in isoprenoid biosynthesis (Scheme 1), we investigated if **1** could inhibit any of the following enzymes: *M. tuberculosis cis*-farnesyl diphosphate synthase (Rv1086); *M. tuberculosis cis*-decaprenyl diphosphate synthase (Rv2361); *P. vivax* geranylgeranyl diphosphate synthase (GGPPS); *S. aureus* and *E. coli* undecaprenyl diphosphate synthases (UPPSs), *S. aureus* farnesyl diphosphate synthase (FPPS), and human GGPPS. In essentially all cases, IC_{50} values were $\geq$50 μM. The exception was human GGPPS, which was inhibited by **1** (the only compound with two basic groups) with a 4.5 μM IC_{50}. These enzymes are all so-called *cis* or *trans*-"head-to-tail" prenyltransferases[18] and the presence of the two (as opposed to one) hydrophobic domains (in addition to the cationic center) might not be required for enzyme inhibition. There are, however, other prenyl transferases that might be targeted in which two hydrophobic domains, together with a carbocation center, would better mimic transition states/reactive intermediates. These would include the so-called "head-to-head" prenyl transferases, as well as some of the enzymes involved in quinone biosynthesis. There are demonstrated or putative head-to-head prenyl transferases in *M. tuberculosis* (Rv3397c), *M. smegmatis*, (Mycsm_04912), *S. aureus* (CrtM), *B. subtilis* (YisP), *S. cerevisiae* (squalene synthase, SQS), and *C. albicans* (SQS) and in humans (SQS), but no homologous proteins can be found by standard BLAST searches in *P. falciparum*. The products (where known) of these enzymes vary, and not all are essential for survival in vitro. Nevertheless, we tested a subset of compounds (**1**, **3**, **4**) for activity against either SaCrtM or human SQS, finding only weak activity (~100 μM) in all cases. These results support the notion that the head-to-head prenyl transferases are unlikely cell growth inhibition targets of our compounds in these organisms.

The other obvious candidates are the enzymes involved in quinone biosynthesis (Scheme 2) or quinone utilization. We thus next investigated the two quinone biosynthesis enzymes, MenA and MenG, both of which are likely to utilize cationic transition states/reactive intermediates during catalysis. MenA (EC 2.5.1.74, 1,4-dihydroxy-2-naphthoate polyprenyl transferase) catalyzes the isoprenylation of 1,4-dihydroxy-2-naphthoic acid by long chain isoprenoid diphosphates,[19] Scheme 2, and MenA is of interest as an *M. tuberculosis* drug target.[20−22] In an initial set of experiments we tested three potent *M. tuberculosis* and *M. smegmatis* growth inhibitors (**1**, **3**, and **13**) in the *M. smegmatis* MenA (MsMenA) membrane fragment inhibition assay described previously,[20−22] finding IC_{50} values of ~6 μM (Table 2). Typical dose−response curves are shown in Figure S1A, Supporting Information. While this assay revealed only modest activity, the observation that MenA activity was in fact inhibited by the three most potent inhibitors is a potentially important one because this inhibition might be expected to inhibit electron transfer/ATP synthesis, of particular importance in nonreplicating/persister cells,[22] and to contribute to cell growth inhibition beyond that seen with MmpL3 inhibition alone. What was also of interest was that **1** had similar activity (IC_{50} = 9 μM, in the same assay as used here[22]) against MenA to that we reported previously with Ro 48-8071, a lipophilic amine that decreases menaquinone biosynthesis and blocks *M. tuberculosis* as well as *M. smegmatis* cell growth. These growth inhibition effects with Ro 48-8071 (as well as the inhibition of respiration) were reported previously to be reversed in both organisms by addition of 400 μM menaquinone-4 (MK-4) or phylloquinone to the medium.[22]

A second possible target is MenG (EC 2.1.1.163, 2-polyprenyl-1,4-naphthoquinone methyltransferase) which carries out the *S*-adenosylmethionine (SAM)-dependent methylation of demethylmenaquinone (the product of the MenA

Scheme 1. Several Reactions of Interest in Isoprenoid Biosynthesis in the Systems Investigated in This Study[a]

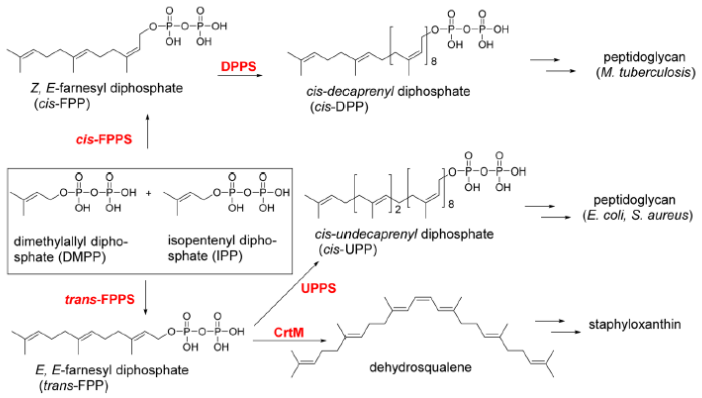

[a]The enzymes in red were tested for inhibition by **1**. *cis*-FPPS and *trans*-FPPS, UPPS, and DPPS are not inhibited by **1** but CrtM is, and CrtM-**1** structures have been reported (PDB ID 4EA1, 4EA2) and serve as models for MenA inhibition.

Scheme 2. Menaquinone Biosynthesis of MK-3[a]

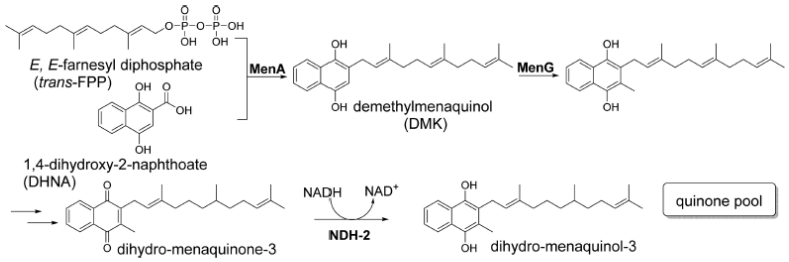

[a]MK-8,9 are the abundant species in cells. MenA forms demethylmenaquinol (DMK), which spontaneously oxidizes to demethylmenaquinone. DMK is the substrate of MenG.

reaction). As with MenA, the MenG reaction is inhibited by **1** and the potent ethanolamine analogues **3**, **13** (Table 2, and Figure S1B,C, Supporting Information), with IC_{50} in the 6−13 μM range. Unlike the C-alkylations with prenyl diphosphates, the MenG reaction uses SAM (as a C_1 source), and Mg^{2+} is not required. With **1** binding to MenG, the cationic center in the inhibitor might mimic a cationic transition state/reactive intermediate, although another possibility is that the cationic center simply mimics the SAM *S*-methyl sulfonium group. Thus, both MenA and MenG are inhibited in vitro by **1** and its analogues, which can be expected to supplement MmpL3-based inhibition in the mycobacteria, as well as provide alternative targets in some of the organisms that lack the *mmpL3* gene. Moreover, inhibition of two sequential targets (series inhibition) in a biosynthetic pathway can often be quite effective because the product of the first reaction is the substrate for the second reaction.[23]

We next used an expressed *E. coli* MenA (hereafter EcMenA) detergent-based assay to obtain inhibition data for all 12 inhibitors, Table 2, and Figure S2, Supporting Information. Interestingly, the most potent inhibitor was **3** (IC_{50} = 400 nM), and **3** was also the most potent inhibitor of *M. tuberculosis* cell growth (and, within experimental error, of *E. coli* cell growth, Table 1). We additionally found that there was a moderate correlation between *E. coli* cell growth inhibition and EcMenA inhibition with an R^2 = 0.43 (using $pIC_{50} = -\log_{10} IC_{50}$, both values in μM) values, suggesting that MenA inhibition may be involved in cell growth inhibition. As described below, the experimental vs predicted *E. coli* cell growth inhibition correlation increased to R^2 = 0.77 with the incorporation of a second experimental parameter, ΔpH collapse.

The structure of MenA is not known, but it is predicted to be a transmembrane protein containing about nine α-helices, as shown in Figure 3A.[24] Using modern structure prediction programs such as Phyre2[25] that are secondary-structure based, MenA is predicted (Figure 3B) to adopt basically all the same α-helical folds as found in farnesyl diphosphate synthase and CrtM (the *S. aureus* dehydrosqualene synthase) but where one N- and two C-terminal helices (transmembrane helices 1, 8, and 9 in Figure 3A) are not modeled, Figure 3B. A total of 198 residues (68%) are, however, modeled at a predicted >90% accuracy, and the predicted structure has the closest similarity to the crystal structure of farnesyl diphosphate synthase from *Methylococcus capsulatus* (PDB ID 3TS7), although remarkably

Table 2. Enzyme, Respiration, and PMF (ΔpH, Δψ) Inhibition Results

	Mycobacterium smegmatis				*Escherichia coli*	
entry	MenA[a]	MenG[a]	respiration[b]	Δψ collapse[c]	MenA[d]	ΔpH collapse[e]
1	4.8	13	58	55	3.3	0.8
3	4	15	0.5	31	0.4	0.8
4	N.D.	N.D.	36	78	1.8	1.0
5	N.D.	N.D.	600	150	4.2	15
6	N.D.	N.D.	4.8	50	1.9	1.1
7	N.D.	N.D.	0.5	51	1.0	18
8	N.D.	N.D.	330	150	5.8	12
9	N.D.	N.D.	280	150	16	7.4
10	N.D.	N.D.	9500.0	150	4.6	4.7
11	N.D.	N.D.	2500.0	150	4.6	6.7
12	N.D.	N.D.	140.0	130	3.3	7.1
13	8	5.7	0.3	44	3.2	0.8

[a] IC_{50} in μM, *M. smegmatis* membrane fraction (Figure S1, Supporting Information). [b] IC_{50} in μM, from methylene blue reduction assay (Figure S3, Supporting Information). [c] IC_{50} in μM, from DisC3(5) assay (Figure S7, Supporting Information). [d] IC_{50} in μM, expressed *E. coli* MenA (Figure S2, Supporting Information). [e] IC_{50} in μM, measured with *E. coli* IMVs (Figures S4 and S5, Supporting Information). N.D.: not determined

there is only a 10% residue identity. The first and second aspartate-rich motifs essential for Mg^{2+} binding and catalysis in FPPS and CrtM are located in very similar regions in the MtMenA model, as shown in the superposition with CrtM in Figure 3C (orange spheres = conserved Asps in EcMenA model; blue spheres = Asp-rich motif in CrtM). This then suggests, based on the **1**–CrtM X-ray structure,[26] the binding sites for **1** (pink) shown in Figure 3C. The two Asp-rich domains in MenA are also highly conserved, as shown by a SCORECONS[27] analysis (Table S1, Supporting Information). Although only a computational prediction, it is of interest that the highest scoring Phyre2 prediction is found with a prenyl transferase enzyme that is known to utilize a carbocation mechanism, consistent with the experimental observation that only cationic species inhibit MenA.

Menaquinone Rescue Experiments. We next measured the activity of **1** against both actively growing (*M. tuberculosis* H37Rv) and nonreplicating (streptomycin-starved *M. tuberculosis* 18b)[28] mycobacteria, using a resazurin microplate reduction assay (REMA; Figure 4). **1** had a MIC of 0.15 μg/mL against actively replicating H37Rv in this assay, as expected. It also displayed activity against the nonreplicating streptomycin-starved 18b strain (where MmpL3/TMM transport is presumably not involved because there is no cell growth), and the effects of **1** on both strains were affected by MK-4 addition (Figure 4). In the H37Rv aerobic assay, the MIC shifted from 0.15 μg/mL in the absence of MK-4 (Figure 4A) to ~1 μg/mL when the medium was supplemented with 1 mM menaquinone, consistent with a role for **1** in inhibiting quinone biosynthesis and/or electron transport. As noted above, a remarkably similar effect was seen previously with Ro 48-8071, another lipophilic amine, at 400 μM MK-4,[22] for both *M. tuberculosis* and *M. smegmatis*. The effect of **1** against nonreplicating (streptomycin-starved 18b) bacteria, as seen by REMA as a decrease in fluorescence (lack of resazurin reduction to the highly fluorescent red resorufin) above a **1** concentration of 1 μg/mL was also blocked by MK-4 addition (Figure 4B). The activity of **1** against nonreplicating (streptomycin-starved 18b) cells was confirmed by plating and counting CFU after 7 days of drug exposure (Figure 4C) with normal 7H9 medium or with 7H9 medium containing 1 mM MK-4. As can be seen in Figure 4C, **1** at 1 μg/mL had essentially no effect on (nonreplicating) bacterial activity in the presence of MK-4 and only a small effect in the absence of MK-4. However, at 10 μg/mL **1**, while there was again a small effect on activity in the presence of MK-4, cell activity in the absence of MK-4 was reduced by ~4 log units, consistent with a role for **1** in blocking respiration and hence ATP synthesis.

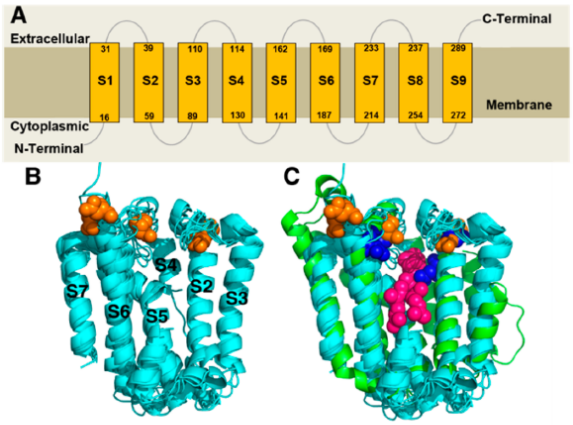

Figure 3. (A) Transmembrane helices predictions for MtMenA. (B) Transmembrane helices in Phyre2 model of MtMenA (helices S1, S8, and S9 from A are not modeled). Orange: Asp-rich motifs. (C) MenA model (cyan) and CrtM (green, PDB: 4EA1, N- and C-terminal helices are removed). Blue: Asp-rich motifs in CrtM. CrtM structure contains SQ109 (two conformers), shown as magenta spheres.

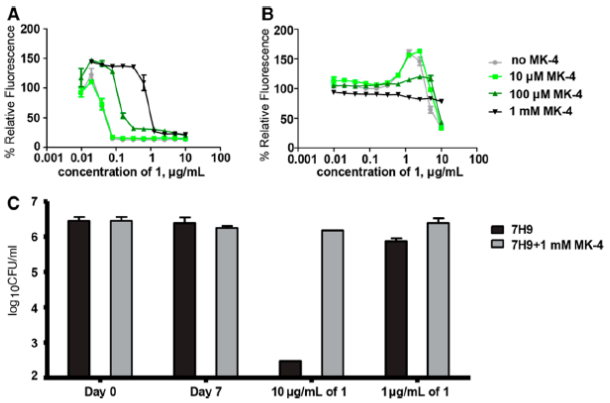

Figure 4. Menaquinone rescue experiments. (A) Aerobic *M. tuberculosis* H37Rv growth inhibition in the presence of increasing MK-4 concentrations, measured by REMA. (B) As in A but with nonreplicating *M. tuberculosis* 18b. (C) *M. tuberculosis* 18b cells were plated after 7 days of drug exposure with (gray) or without (black) MK-4. Colony forming unit counts were assessed after one month of incubation. Concentrations are in μg/mL.

Respiration, TMM, and the PMF. The results described above show that **1** has activity against not only the two mycobacteria (*M. tuberculosis* and *M. smegmatis*) but also a range of other bacteria, fungi, and a protozoan, each of which lack a bioinformatically recognizable *mmpL3* gene. In *M. tuberculosis* and *M. smegmatis*, inhibition of MenA/MenG would inhibit respiration, resulting in a decrease in ATP biosynthesis. This could help explain how **1** increases the level of TMM given that MmpL3 is a TMM transporter of the RND family of efflux pumps, many of which are powered by the PMF. Restated, **1** might exhibit an indirect action upon the TMM transporter by removing its "power source" (the proton motive force), in addition to directly binding to, and inhibiting, the transporter. This indirect action could be accomplished in one of two ways: (1) blocking respiration (by depletion of menaquinone by inhibition of MenA or MenG or by directly inhibiting a component of the electron transport chain); (2) a direct effect on the PMF ($\Delta\psi$ + ΔpH, where $\Delta\psi$ is the membrane potential and ΔpH, the pH gradient). The possibility of the involvement of the PMF is suggested from the results of a number of studies in which lipophilic bases (e.g., amiodarone, local anesthetics, and NSAIDS[29−31]) can act as uncouplers. In addition, there could also be multidrug targeting affecting MmpL3 (or efflux pumps[32]), MenA, MenG, and the PMF, which would be expected to produce potent inhibition of cell growth/respiration/ATP synthesis, as well as a low rate of resistance.

Respiration and Electron Transport. In earlier work,[21,22] we showed that several MenA inhibitors, analogues of Ro 48-8071, blocked respiration in *M. tuberculosis* and *M. smegmatis* (as evidenced by inhibiting the reduction of methylene blue), that there was a correlation between cell growth inhibition and respiration inhibition,[22] and that the effects of the inhibitors could (at least in part) be reversed by adding MK-4 at the 400 μM level. We thus next tested all compounds for their effects on methylene blue reduction, in *M. smegmatis* (Figure S3, Supporting Information), finding that there was a moderate correlation between pMIC (= $-\log_{10}$ MIC, MIC in μM) for cell growth inhibition and the pIC_{50} (= $-\log_{10}$ IC_{50}, IC_{50} in μM) for inhibition of whole cell respiration inhibition (R^2 = 0.55) for all 12 compounds (Tables 1 and 2).

These results suggest the possibility of a direct effect on electron transport (because the effects observed are rapid: tens of minutes), blocking respiration, consistent with the MK-4 rescue experiments. The nature of the target or targets involved are beyond the scope of this current study, but we did carry out preliminary experiments with **1** against a series of dehydrogenases by monitoring the reduction of the artificial electron acceptor MTT (3-(4,5-dimethyl-2-thiazolyl)-2,5-diphenyl-2*H*-tetrazolium bromide). We used an *M. smegmatis* membrane preparation and a variety of substrates including NADH (measuring both Complex I and alternative NADH dehydrogenases, NDH-2), deamino-NADH (measuring Complex I activity but not NDH-2), succinate (measuring succinate dehydrogenase), malate (measuring quinone-dependent malate dehydrogenase), and lactate (measuring lactate dehydrogenase). IC_{50} values for **1** were in general ~30 μg/mL, the exception being malate dehydrogenase (IC_{50} = 10 μg/mL), results that suggest that more than one-electron-transfer protein may be involved, in cells, with the inhibitors mimicking quinone substrates.

Uncoupler Effects in Membrane Vesicles and in Cells. The results presented above show that **1** and its analogues inhibit MenA, MenG, electron transfer proteins, and respiration and that MK-4 can rescue cell growth or activity, the relatively high IC_{50}s for enzyme inhibition/respiration (when compared to cell growth inhibition) being suggestive of multiple targeting. What is of particular interest about all of the results described above is that they seem to point in one direction: respiration, offering a possible explanation for the previous observation that TMM accumulates (with **1**), in *M. tuberculosis*, due to MmpL3 inhibition. This MmpL3 inhibition could be due to direct binding or a more indirect effect on the PMF/ATP synthesis.

To test the hypothesis that **1** and its analogues might collapse the PMF, we first used *E. coli* inverted membrane vesicles (IMVs), essentially as described by Haagsma.[33] The results

obtained with SF6847, one of the most potent uncouplers known, are shown in Figure 5A and indicate a very rapid

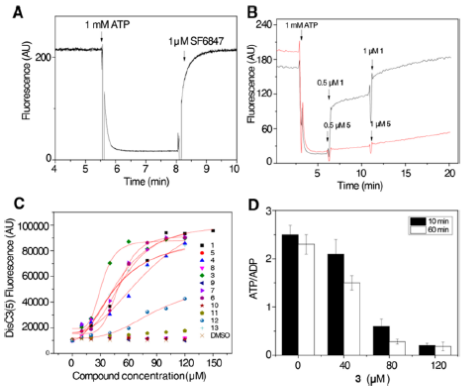

Figure 5. (A) ΔpH collapse in *E. coli* IMVs by a known uncoupler SF6847. (B) ΔpH collapse in *E. coli* IMVs by **1** and **5**. (C) Effects of **1** and analogues on Δψ in *M. smegmatis* cells. (D) Effects of **3** on ATP biosynthesis of effect in *M. smegmatis* cells.

(seconds) collapse in ΔpH, as reported by Haagsma et al.[33] The same effect was seen with **1** and analogues that have potent activity in cell growth inhibition, while inactive (diether/amide) analogues (e.g., **5**) had no effect, Figure 5B, Figures S4 and S5, Supporting Information. Similar results were obtained with both *E. coli* and *M. smegmatis* vesicles. The effects on the collapse in ΔpH were seen in vesicles in which the pH gradient was driven by either ATP hydrolysis or by electron transport in the presence of succinate or NADH. Using Oxonol VI as a probe, we also found that Δψ in *E. coli* IMVs (positive inside) was collapsed (Figure S6A) by the same compounds, and there was a correlation between the collapse of the membrane potential and the collapse in ΔpH (using ACMA fluorescence; Table 2; R^2 = 0.79, Figure S6B, Supporting Information). This is consistent with these lipophilic cations acting as protonophores, carrying protons across the membrane lipid bilayer, with only compounds containing a basic nitrogen supporting the uncoupling activity.

We found similar PMF effects in intact *M. smegmatis* cells in which there was a collapse in Δψ (positive outside), as measured by using DisC3(5) fluorescence, Figure S7, Supporting Information. Addition of **1** or the potent analogues to *M. smegmatis* cells resulted in an immediate increase in DisC3(5) fluorescence, indicating a collapse of Δψ. As can be seen in Figure S7B, Supporting Information, **1** collapses the membrane potential in a dose-dependent manner with an "EC_{50}" of ∼20 μg/mL. The EC_{50} for one of the most potent cell growth inhibitors **13** was ∼15 μg/mL.

In addition to these investigations of Δψ collapse in intact cells, we investigated ΔpH collapse in intact *M. smegmatis* cells, using ^{31}P NMR spectroscopy. Phosphorus NMR chemical shifts are sensitive indicators of local pH values.[34] As can be seen in Figure S8A, Supporting Information, the ^{31}P NMR chemical shift of phosphate inside *M. smegmatis* is ∼0.35 ppm downfield from external P_i, and from these chemical shifts, the internal and external pH values can be determined: results are shown in Figure S8B, Supporting Information. There is a ΔpH = 0.26 (inside more basic) in wild type *M. smegmatis* cells, but this pH gradient is collapsed by the uncoupler CCCP (*m*-chlorophenylcarbonyl cyanide phenylhydrazone), by the antiporter nigericin, and by **1** and **13**, while as expected, the K^+ ionophore valinomycin has no effect. The effects of **1** and the other potent analogue thus leads to collapse of Δψ as well as ΔpH in both inverted vesicles and in whole cells. This collapse in the PMF, in cells, can be expected to result in an inhibition of ATP synthesis, as is indeed found experimentally (Figure 5D) with the potent lead, **3**. In addition, the collapse of the proton motive force is expected to inhibit activity of the MmpL3/TMM transporter.

Quantitative Models for Cell Growth Inhibition. Any quantitative analysis of cell growth inhibition based on enzyme inhibition or another property (e.g., ΔpH collapse) is of course challenging, but it should be possible to use the multidescriptor approach described previously[35] with, in this case, no purely mathematical descriptors being required. We thus use eq 1:

$$pIC_{50}(\text{cell}) = a \times pIC_{50}(A) + b \times pIC_{50}(B) + c \qquad (1)$$

where $pIC_{50}(A)$ is $-\log_{10}$ (IC_{50}, A) for enzyme or property A (such as MenA inhibition), and B is a second property, e.g., ΔpH collapse. We show by way of examples in Figures 6A,B, three-dimensional plots for *E. coli* cell growth inhibition: log IC_{50} = *f* (MenA, ΔpH), and for *M. smegmatis*: log MIC = *f* (respiration, Δψ), where we find correlation coefficients of R^2 =

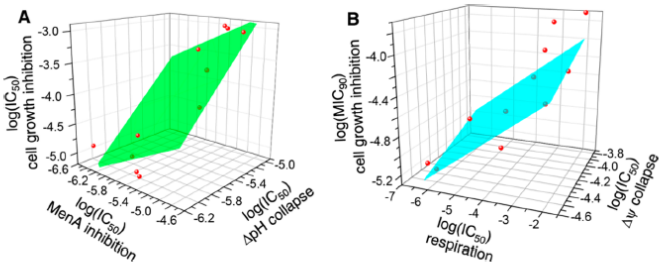

Figure 6. Experimental (red circles) and computed (colored plane) results for cell growth inhibition based on eq 1. (A) *E. coli* cell growth inhibition predicted using MenA, ΔpH collapse (IC_{50}s in μM, R^2 for the model = 0.77). (B) *M. smegmatis* growth inhibition using respiration (methylene blue assay) and Δψ collapse (MIC and IC_{50}s in μM, R^2 for the model = 0.64).

0.82 (*E. coli*) and R^2 = 0.72 (*M. smegmatis*) values for the experimental-versus-predicted cell growth inhibition results. In previous work we investigated correlations between cell and enzyme activity (pIC_{50}) assays in 10 diverse systems finding[35] on average an R^2 = 0.32 for the 10 cell/enzyme correlations, similar to the R^2 = 0.43 we find for the MenA alone/*E. coli* cell growth inhibition correlation. Incorporation of the second parameter (the percentage of ΔpH collapse) increases the R^2 to 0.77, suggesting the importance of multitargeting, in *E. coli*. The correlation is worse for *M. smegmatis* due, perhaps, to the omission of an MmpL3 term, expected to be particularly important in the mycobacteria.

Are There Other MenA-like Targets? The results presented above show that *E. coli* MenA is inhibited by **1** and its analogues and that there is a correlation between MenA inhibition and cell growth inhibition (in *M. smegmatis*), suggesting that diverse MenAs may be inhibited by these compounds. However, this result is perhaps surprising in that in *E. coli*, MenA is not an essential gene for aerobic growth because UbiA can be used in aerobic respiration. One possibility is that EcUbiA might also be inhibited by **1** (and its analogues). While we have not yet investigated this experimentally, what we have found is that MtMenA, EcMenA, and EcUbiA are all predicted (using the Phyre2 program) to have an FPPS/GGPPS-like structure.

In all three cases the structures are predicted to contain a central FPPS/GPPS-like catalytic domain (comprising ~2/3 of the overall amino acid sequence) that has close similarity to the same two (soluble) prenyl synthases: *Methylococcus capulatus* FPPS and *Lactobacillus brevis* GGPPS. Predicted sequence identity investigations have shown that MenA and UbiA have moderate homology,[36,37] but correlations with FPPS and GGPPS were not made in those studies because the actual sequence identities are very low, about 10−16%. However, secondary-structure-based algorithms do permit accurate structure predictions, even when residue identities are low.

These previous bioinformatics studies also demonstrated that another class of proteins, protoporphyrin IX farnesyl transferases (e.g., heme o synthase), have significant sequence homology to the MenA/UbiA proteins, and all three classes of proteins are Mg^{2+}-dependent prenyl transferases. Once again, the structure of heme o synthase is not known but is predicted to be another nine-helix transmembrane protein with a central FPPS/GGPPS-like core, suggesting that MenA, UbiA, and protoporphyrin IX farnesyl transferases are all likely to be inhibited by **1** and related systems.

MmpL3 and MmpL11 as Targets. MmpL3 is thought to be a target for **1** (and other diverse inhibitors[12,13,38,39]), blocking TMM transport. It has also been shown that MmpL3 together with a related protein, MmpL11, is associated with heme uptake.[40,41] The X-ray structures of MmpL3 and MmpL11 have not been reported. However, both are membrane proteins and are predicted to have 11−12 transmembrane helices.[24] Using the Phyre2 program,[25] we find with MmpL3 that 653 residues (69% coverage) are predicted with 100% confidence to have the structure shown in Figure 7A and with MmpL11, 642 residues (66% coverage) are predicted with 100% confidence to have the structure shown in Figure 7B. Both structures are very similar to those found in cation efflux pumps such as CusA (PDB ID 3ko7) and multidrug efflux pumps such as the acriflavin resistance protein B (AcrB; PDB ID 1oy8), although the C-terminus (~1/3 of the total protein) is not modeled in either MmpL3 or MmpL11.

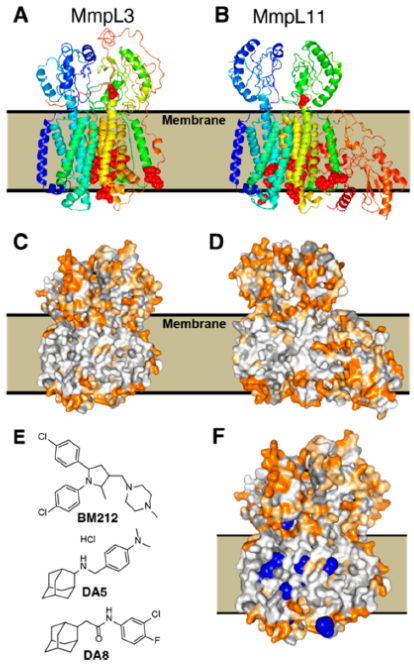

Figure 7. Molecular models for MmpL3, MmpL11. (A) Phyre2 structure predictions for MmpL3. (B) Phyre2 structure predictions for MmpL11. (C) Phyre2 predictions showing hydrophobic residues (white/gray) and their proposed relation to the membrane for MmpL3. (D) Phyre2 predictions showing hydrophobic residues (white/gray) and their proposed relation to the membrane for MmpL11. (E) Structure of representative *M. tuberculosis* growth inhibitors that are thought to target MmpL3 and (F) sites of resistance mutations (blue spheres) in MmpL3.

The transmembrane hydrophobic domains are shown in Figure 7C,D (in white/light orange). **1** as well as several other inhibitors[12,13] (Figure 7E) has been proposed to target MmpL3 (detected by sequencing mutants that arose under drug pressure), but the sites of these mutations, shown as blue spheres in Figure 7F, are spread throughout the protein, suggesting, perhaps, multisite targeting of MmpL3/11 as an additional basis for the lack of resistant mutations with **1**. Overall, however, the effects of **1** on the PMF and respiration, the menaquinone-reversal experiments, activity against diverse organisms as well as the ability to make generally good predictions of cell activity without MmpL3 inhibition data suggests that MmpL3 may not be the primary target for **1**, in *M. tuberculosis*. In addition, of course, other targets may exist.

A Multitarget Model for Antiinfective Activity. We show in Figure 8 a summary of the proposed sites of action for **1** and its analogues in *M. tuberculosis* and in *M. smegmatis*. Some of these targets are also present in the other pathogens investigated but not in human cells. In addition to its previously proposed role in targeting MmpL3, **1** and its analogues also inhibit MenA and MenG and, as described above, the inhibition

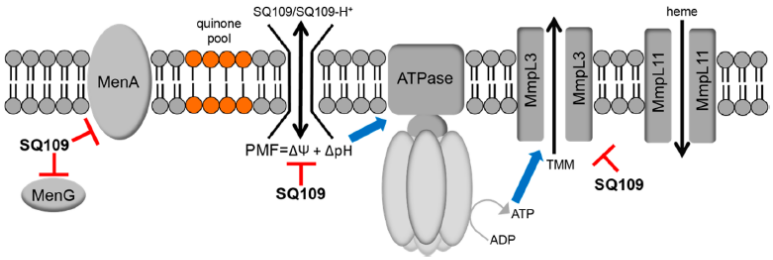

Figure 8. Proposed sites of action of SQ109 and its analogues. MenA, MenG targeting can affect respiration/electron transfer; PMF (ΔpH, Δψ) collapse leads to decreased ATP biosynthesis, reduction in PMF/ATP-powered transporters (e.g., MmpL3), increased TMM accumulation, and decreased cell wall biosynthesis.

of *M. tuberculosis* cell growth or activity is rescued by MK-4. We also find that the PMF is inhibited by the most active compounds, which act as protonophores/uncouplers. This results in a decrease in ATP synthesis and, we propose, decreased activity of MmpL3/11, helping explain the accumulation[12] of TMM (with **1**).

This multiple-targeting is perhaps best thought of as involving network inhibition in which both series and parallel paths are involved (Figure 1C) because at least in the mycobacteria, MenA, MenG, electron transport, ΔpH, Δψ, and MmpL3 (and presumably other pumps dependent on the PMF) can all be affected. There are, of course, likely to be differences in the mechanisms of action of different inhibitors in different organisms (and in the same organisms under different growth conditions), although effects on the PMF are expected to be quite common because they are based on more "physical" properties, rather than purely enzyme inhibition. The uncoupling effects we observe could also help explain the growth inhibition seen in human cell lines, as could inhibition of the human MenA, UbiA, and MenG/UbiE orthologues: UbiAD1, CoQ2, and CoQ3.

Also of interest are the likely differences in time scales (and concentrations) for the different reactions involved. The effects on the collapse in Δψ and ΔpH are very rapid-on the seconds to minutes time scale and are observed (in vesicle experiments) at low μM concentrations, for the most active species. The effects on respiration as determined by methylene blue reduction (in intact cells) are also rapid, typically observable in minutes, and may reflect the time required for inhibitors to enter the cell and accumulate (because they could also be actively pumped out). Little is known about the rate of menaquinone turnover, but it is likely that several cell divisions are required for a large reduction in menaquinone levels, so while MenA/MenG inhibition may be rapid, the effects on cell growth may take many hours or (with *M. tuberculosis*) days to occur likewise, because MmpL3 is thought to be involved in cell wall biosynthesis, its inhibition would also be expected to result in observable effects on growth inhibition on a time scale of hours to days.

■ CONCLUSIONS

The results we have described above are of interest for drug discovery against tuberculosis, as well as against other bacterial, fungal, and protozoan pathogens, for several reasons. We synthesized a series of analogues of the antituberculosis drug **1** in which we varied the nature of the ethylenediamine linker to provide cationic, protonatable, and neutral species, and in addition we varied the adamantyl headgroup. The most active compound against *M. tuberculosis* was ~5× more potent than was **1** and was also less toxic to an MCF-7 human cell line. We tested all compounds against a panel of bacteria, fungi, and a protozoan parasite, and the results obtained showed that at least one cationic (or basic) group was essential for activity. The most potent activity was against *M. tuberculosis* (MIC = 0.02−0.05 μg/mL) and the intraerythrocytic form of the malaria parasite, *P. falciparum* (IC_{50} = 30 ng/mL). To explore possible targets, we tested several compounds for activity against a panel of *cis*- and *trans*-prenyl transferases (*cis*-FPPS, FPPS, DPPS, GGPPS, UPPS, CrtM, and SQS) as well as against the menaquinone biosynthesis enzymes, MenA and MenG. Activity was seen against MenA and MenG, and we proposed a structural model for the MenA active site, as well as a likely binding site for **1**. In addition, we found that menaquinone (MK-4) rescued both aerobic H37Rv *M. tuberculosis* cell growth and the activity of nonreplicating *M. tuberculosis* (streptomycin-starved 18b). We found that **1** as well as several analogues inhibited oxygen consumption in *M. smegmatis*, and there was a correlation between oxygen consumption and cell growth inhibition. We tested **1** and each of the 11 analogues for their effects on the PMF (ΔpH and Δψ) in fluorescence-based assays, as well as in some cases in intact cells (via ^{31}P NMR). The results obtained showed that **1** and the most potent cell growth inhibitors collapsed both Δψ and ΔpH, and there were good correlations between experimental and predicted cell growth inhibition results based on MenA/ΔpH (*E.coli*) and respiration/Δψ (*M. smegmatis*). Taken together, the results obtained suggested a model for **1**/analogue activity in mycobacteria in which the increase in TMM levels seen on treatment with **1** have a contribution from (indirectly) inhibiting the TMM transporter MmpL3 by blocking the PMF/ATP biosynthesis. Overall, the results are of general interest because they indicate that **1** (and its analogues) can have diverse effects: on O_2-consumption/electron transport/MenA/MenG inhibition; on Δψ, ΔpH, and ATP biosynthesis, likely helping to explain activity against non-MmpL3-containing pathogens such as *H. pylori*, *C. albicans*, and, here, *P. falciparum*. Moreover, the possibility of developing more potent compounds that can inhibit these targets is of general interest in the context of developing drug leads that are "resistance resistant", due to multitargeting.

EXPERIMENTAL SECTION

Chemical Syntheses: General Methods. All chemicals were reagent grade and were used as received. Moisture-sensitive reactions were performed under an inert atmosphere (dry nitrogen) with dried solvents. Reactions were monitored by TLC using Merck silica gel 60 F-254 thin-layer plates. Flash column chromatography was carried out on Merck silica gel 60 (230−400 mesh). ^{1}H NMR and ^{13}C NMR spectra were recorded on Varian (Palo Alto, CA) Unity spectrometers at 400 and 500 MHz for ^{1}H and at 100 and 125 MHz for ^{13}C. Coupling constants (J) are reported in hertz. High-resolution mass spectra (HRMS) were recorded in the University of Illinois Mass Spectrometry Laboratory. Elemental analyses were carried out in the University of Illinois Microanalysis Laboratory. HPLC/MS was performed using an Agilent LC/MSD Trap XCT Plus system (Agilent Technologies, Santa Clara, CA) with an 1100 series HPLC system including a degasser, an autosampler, a binary pump, and a multiple-wavelength detector. All final compounds were ≥95% pure as determined by elemental analysis, analytical HPLC/MS analysis, or qNMR analysis. qNMR spectra were recorded using Varian (Palo Alto, CA) 500 MHz Unity spectrometers with 1,3,5-trimethoxybenzene as the internal total-spin-count quantitation standard; 60° pulse excitation, 60 s recycle delay, 1.0 Hz line-broadening due to exponential multiplication, and 16 accumulations. qNMR data were processed using Mnova NMR software (Mestrelab, Escondido, CA). All NMR spectra (including qNMR spectra) are provided in the Supporting Information.

Enzyme Inhibition Assays. *MenA and MenG Inhibition.* MenA and MenG inhibition assays were carried out using *M. smegmatis* membrane fragments.[22] Mycobacterial MenA assays were conducted as previously reported.[22] In addition, we used an expressed, purified *E. coli* MenA, as described below.

MenG Assay. Vitamins K1 and K2 and kanamycin were purchased from Sigma-Aldrich (St. Louis, MO). Authentic MK9 was purchased from Toronto Research Chemicals (TRC, Canada). *S*-Adenosyl-L-[methyl-^{14}C]methionine (^{14}C-SAM) obtained from Perkin-Elmer (47 mCi/mmol). DMK8 was prepared from an *E. coli* Δ*ubiE* mutant (CGSC #11636), which accumulates DMK8, and was purchased from the *E.coli* Genetic Stock Center, Yale University (http://cgsc.biology.yale.edu).

MenG assays were conducted using the membrane fractions prepared from *M. smegmatis* grown in 7H9 medium (supplemented with oleic acid, albumin, dextrose, and 0.05% Tween 80). Washed cells were resuspended in buffer A (50 mM MOPS pH 7.9, 5 mM $MgCl_2$, 5 mM DL-dithiothreitol (DTT), 10% glycerol (V/V)) and disrupted by probe sonication on ice with a Sanyo Soniprep 150 (10 cycles of 60 s on and 90 s off). The whole cell lysate was centrifuged at 27 000*g* for 20 min at 4 °C. The supernatant was further centrifuged at 100 000*g* (for 2 h at 4 °C) in an Optima TLX Ultracentrifuge (Beckman). The membrane-enriched pellet was washed with buffer A followed by ultracentrifugation at 100 000 g. The washed pellet was resuspended in buffer A, divided into aliquots, and frozen at −80 °C. The membrane protein concentration was estimated by using a BCA protein assay kit (Pierce).

Assay mixtures (100 μL) contained 100 mM Tris-HCl pH 8.0, 1 mM DTT, 5 mM $MgCl_2$, 0.1% CHAPS, 600 ng of DMK8, 40 μM radiolabeled SAM, and varying concentrations of inhibitor **1** (0 to 25.0 μg/mL). Reactions were initiated by the addition of 50−100 μg of *M. smegmatis* membrane protein and incubated at 37 °C for 1 h. Reactions were stopped by the addition of 0.1 M acetic acid in methanol (0.5 mL), and radiolabeled products were extracted with hexane (2 × 3 mL). Pooled extracts were washed with 1 mL of water, evaporated to dryness under a N_2 stream, and dissolved in $CHCl_3/CH_3OH$ (2:1 v/v). An aliquot was subjected to liquid scintillation counting (LS 6500, Beckman Coulter); a second aliquot and authentic standards (DMK8 and MK9) were subjected to reverse-phase TLC (Whatman KC 18F Silica gel 60 A) developed in acetone/water (97:3). Standards were visualized under UV light, and distribution of radioactivity was detected by phosphorimaging (Typhoon TRIO, Amersham Biosciences) and quantified with ImageQuant TL v2005 software (Amersham Biosciences). IC_{50} values were calculated by using GraFit Software (Version 5.0.13).

Expression and Purification of EcMenA. The gene encoding EcMenA with a N-terminal strep tag was amplified by polymerase chain reaction (PCR) with forward primer 5′-GACGACGACAAGATGAGCGCGTGGAGCCATCCGCAGTTT-GAAAAAGGCGGTGGCAGCGCGGAGAATCTTTATTTT-CAGGGCGCTGGTGC-3′ and reverse primer 5′-GAGGAGAAGCCCGGTTATTATGCTGCCCACTGGCTTAGGAATAT-3′, and then cloned into the pET46 Ek/LIC vector. The recombinant plasmid was transformed to *E. coli* C43 (DE3) and the protein induced with 1 mM isopropyl thiogalactopyranoside (IPTG) at 37 °C for 5 h. The cell paste was harvested by centrifugation at 7000*g* and resuspended in buffer A containing 25 mM Tris-HCl, pH 7.5, 150 mM NaCl, and 20 mM imidazole. A cell lysate was prepared with a JNBIO pressure cell (JN-3000 PLUS), the membrane, and soluble proteins being separated by ultracentrifugation at 150 000*g* for 1.5 h. The resulting pellet was solubilized by incubation in buffer A supplemented with 1% (w/v) DDM detergent overnight at 4 °C. The latter solution was centrifuged (100 000*g* for 1 h at 4 °C in a Beckman Ti70 rotor) and the supernatant loaded onto a Ni-NTA column and washed with buffer A containing 0.05% DDM. The buffer and gradient for the Ni-NTA column were 25 mM Tris, pH 7.5, 150 mM NaCl, 0.05% DDM, and 20−500 mM imidazole. The protein was then loaded onto a Strep-Tactin (IBA) column equilibrated with washing buffer containing 100 mM Tris-HCl, pH 8.0, 150 mM NaCl, 1 mM EDTA, and 0.05% DDM and washed with five column volumes of washing buffer. EcMenA was finally eluted with eluting buffer containing 100 mM Tris-HCl, pH 8.0, 150 mM NaCl, 1 mM EDTA, 0.05% DDM, and 2.5 mM desthiobiotin. The purified protein was finally concentrated to 5 mg mL^{-1} in a 25 mM Tris-HCl, pH 7.5, 150 mM NaCl, 0.05% DDM buffer.

EcMenA Inhibition Assay. Inhibition of EcMenA was carried out using an HPLC-based protocol. Typically, 2.5 μg of EcMenA in 100 μL of reaction buffer (25 mM Tris-HCl, 0.1% Triton X-100, 250 μM $MgCl_2$, 10 mM DTT, pH = 7.5) was incubated with inhibitors for 30 min at 22 °C. 1,4-Dihydroxy-2-naphthoic acid (DHNA) and farnesyl diphosphate (FPP) were then added to the enzyme solution to a final concentration of 150 μM each. The reaction was incubated at 37 °C for 3 h before quenching with 50 μL of 0.1 M acetic acid in methanol containing 50 μM menaquinone-4 (MK-4, Sigma-Aldrich) as an internal standard. The mixture was then extracted with 600 μL of hexane by vortexing. After centrifugation, 500 μL of organic layer was collected and dried under nitrogen then dissolved in 200 μL of methanol. Twenty microliters of the methanol solution was then subjected to HPLC analysis (0.1% formic acid in H_2O to 0.1% formic acid in CH_3CN, UV: 325 nm, 250 μL/min). The amount of the MenA reaction product demethylmenaquinone-3 (DMMK-3) was determined by comparison of integrated peak areas between DMMK and the internal standard MK-4. IC_{50} values were estimated by using Origin 6.1 software to analyze the dose−response curves.

Cell Lines. *Mycobacterium tuberculosis* ATCC 27294, *Mycobacterium smegmatis* ATCC 700084, *Bacillus subtilis* subsp. *subtilis* ATCC 6051, *E. coli* ATCC 29425, and *Saccharomyces cerevisiae* ATCC 208352 were purchased from the American Type Culture Collection. The *C. albicans* strain was CAI-4; the *P. falciparum* strain was 3D7 and the human cell line MCF-7 (breast adenocarcinoma), obtained from the National Cancer Institute.

***M. tuberculosis* Growth Inhibition Assay.** All 12 compounds (**1**, **3**−**13**) were assayed for inhibition of *M. tuberculosis* cell growth as described previously.[42]

Menaquinone Rescue Experiments with *M. tuberculosis* Treated with 1. We measured the activity of **1** against both actively growing *M. tuberculosis* (H37Rv) and nonreplicating *M. tuberculosis* (streptomycin-starved 18b[28]) using a resazurin microplate reduction assay. The effects of menaquinone supplementation on the dose−response curves were investigated using medium that was supplemented with 0, 10, 100, and 1000 μM menaquinone (MK-4, Sigma-Aldrich) in the presence of between 10 ng/mL and 10 μg/mL **1**. The activity of **1** against nonreplicating 18b was determined after 7 days of drug exposure by plating the culture followed 28 days later by

CFU counting after plating serial dilutions on 7H10 agar plates (Difco) .

***Candida albicans* Growth Inhibition Assay.** *C. albicans* growth inhibition was carried out according to a reported protocol[43] except that YPD media was used instead of RPMI 1640.

***E. coli* Growth Inhibition Assay.** IC_{50} values for *E. coli* growth inhibition were determined by using a broth microdilution method. An overnight culture of *E. coli* was diluted 50-fold into fresh Luria−Bertani (LB) broth and incubated to an OD_{600} of ∼0.4. The culture was then diluted 500-fold into fresh LB medium and 100 μL inoculated into each well of a 96-well flat-bottom culture plate (Corning Inc., Corning, NY). The starting concentration of each compound was 0.3 mM, and this was 2× serially diluted to 292 nM. Plates were incubated for 3 h at 37 °C to midexponential phase. An MTT ((3-(4,5-dimethylthiazol-2-yl)-2,5-diphenyltetrazolium bromide) cell proliferation assay (ATCC) was then carried out to obtain bacterial viability dose−response curves. Briefly, 10 μL of MTT reagent was added into each well, followed by incubation for 2−4 h until a purple precipitate was visible. Then, 100 μL of detergent reagent was added, and the plates were incubated in the dark at 22 °C for 2 h. Absorbance was measured at 570 nm and a nonlinear regression analysis carried out using Origin 6.1 software.

***B. subtilis* Growth Inhibition Assay.** IC_{50} values for *B. subtilis* growth inhibition were determined by using a microbroth dilution method. A stationary starter culture of *B. subtilis* was diluted 50-fold into fresh LB broth and grown to an OD_{600} of ∼0.4. The culture was then diluted 500-fold into fresh LB medium to give a working solution, and then 100 μL of working solution was transferred to each well of a 96-well flat-bottom culture plate (Corning Inc., Corning, NY). Inhibitors were then added at 0.5 mM and 2× serial diluted to 500 nM, the volume and solvent composition constant. Plates were incubated for 12−16 h at 37 °C, and the absorbance at 600 nm was determined. A nonlinear regression analysis was carried out using Origin 6.1 to obtain the IC_{50} values.

***S. cerevisiae* Growth Inhibition Assay.** The protocol was the same as for *B. subtilis* except that YPD instead of LB was used as the culture medium, and the 96-well plates were incubated for 48 h instead of 12−16 h.

***Plasmodium falciparum* Growth Inhibition Assay.** We determined IC_{50} values for *P. falciparum* growth inhibition using the intraerythrocytic assay described previously.[44]

Human Cell Growth Inhibition Assay. The MCF-7 cell growth inhibition assay was carried out as described previously.[45] A broth microdilution method was used to determine the growth inhibition IC_{50} values. Compounds were half-log serial diluted using cell culture media into 96-well TC-treated round-bottom plates (Corning Inc., Corning, NY). Cells were plated at a density of 5000 cells/well and then incubated under the same culture conditions for 2 days at which time an MTT ((3-(4,5-dimethylthiazol-2-yl)-2,5-diphenyltetrazolium bromide) cell proliferation assay (ATCC, Manassas, VA) was performed to obtain dose−response curves.

Dehydrogenase Activities. Dehydrogenase activity in *M. smegmatis* membranes was measured by using the MTT ((3-(4,5-dimethylthiazol-2-yl)-2,5-diphenyltetrazolium bromide) reduction assay in the presence of 5 mM KCN. MTT reduction was followed at 570 nm, after addition of the different substrates (NADH, succinate, malate, or lactate).

Oxygen Consumption. Oxygen concentration was monitored at 37 °C using a YSI model 53 oxygen electrode (Yellow Springs Instrument Co., Yellow Springs, OH) equipped with a temperature-controlled 1.8 mL electrode chamber. The reaction mixture consisted of sodium phosphate buffer, pH 7.5, 50 mM NaCl, and 200−400 μg/mL membranes. The concentration of oxygen in the air-saturated buffer was taken to be 250 μM, and the reaction was initiated by injecting 200 μM NADH. The electron transport rates are expressed as mol of NADH oxidized or mol of O_2 (mol enzyme)$^{-1}$ s^{-1}. Membranes were incubated with different concentrations of inhibitors for 5 min prior to NADH addition.

Membrane Potential Measurements in Intact Cells. The effects of inhibitors on Δψ were determined by fluorescence quenching of the potential-sensitive probe 3,3′-dipropylthiodicarbocyanine (DisC3(5)). *M. smegmatis* were grown for 8 h in Middlebrook 7H9-ADC-Tween 80 medium and diluted to an OD_{600} of 0.3 in the same medium plus 10 mM glucose and 1 μM nigericin. Different concentrations of **1** and its analogues were added to the bacterial suspension, and changes in fluorescence due to the disruption of Δψ were continuously monitored with a fluorescence spectrophotometer (FLUOstar Omega, BMG LABTECH) employing an excitation wavelength of 643 nm and an emission wavelength of 666 nm, at 30 °C.

ATP/ADP Determination. *M. smegmatis* were grown for 8 h in Middlebrook 7H9-ADC-Tween 80 and diluted to an OD_{600} of 2. Different concentrations of **1** and its analogues were added and ATP/ADP ratios determined (Abcam; ADP/ATP Ratio Assay Kit, catalog number: ab65313) after 10 and 60 min of incubation at 37 °C, 200 rpm. ATP and ADP were extracted from 50 μL of cell suspension by adding trichloroacetic acid (TCA) to a final concentration of 0.5%. After 5 min, TAE (Tris−acetic acid−EDTA) buffer was added to neutralize the system by diluting the sample 5-fold. The ATP and ADP cell concentrations were measured according to the manufacturer's protocol.

Inverted Membrane Vesicles (IMVs). *E. coli* IMVs were prepared by three passages through a precooled French pressure cell at 20 000 psi. The lysate was centrifuged at 14 000*g* at 4 °C for 20 min to remove unbroken cells. The supernatant was centrifuged at 370 000*g* at 4 °C for 1 h, and the pellet, consisting of the IMVs, was washed with 50 mM MOPS−KOH (pH 7.5), 2 mM $MgCl_2$. After the second centrifugation step, membranes were resuspended in 50 mM MOPS−KOH (pH 7.5), 2 mM $MgCl_2$, 10% glycerol, and stored at −80 °C.

Assay for ATP or Succinate-Driven Proton Translocation. Proton translocation into IMVs was measured by the decrease of ACMA fluorescence. The excitation and emission wavelengths were 410 and 480 nm, respectively. IMVs (0.1 mg/mL membrane protein) were preincubated at 37 °C in 10 mM HEPES−KOH (pH 7.5), 100 mM KCl, 5 mM $MgCl_2$ containing 2 μM ACMA, and the baseline was monitored for 5 min. The reaction was then initiated by adding 1 mM ATP or 5 mM succinate. When the signal had stabilized, **1** or its analogues were added and proton translocation was measured, fluorimetrically.

Determination of Δψ Collapse in IMVs. The Δψ-sensitive fluorophore Oxonol VI (1,5-bis(5-oxo-3-propylisoxazol-4-yl)-pentamethine oxonol) was used to determine if **1** and its analogues were able to dissipate the membrane potential in IMVs. IMVs (0.1 mg/mL membrane protein) were added to assay buffer: 10 mM MOPS−KOH pH 7.5, 2 mM $MgCl_2$, 2 μM Oxonol VI. After a few seconds, 0.5 mM NADH was added to initiate respiration-dependent generation of Δψ (positive inside), and the resultant quenching of Oxonol VI fluorescence was monitored at 37 °C. The emission and excitation wavelengths were 599 and 634 nm, respectively. Uncoupling by inhibitors was estimated based on their ability to dissipate the established Δψ, measured as the dequenching of the fluorescence signal.

Determination of ΔpH by ^{31}P NMR Spectroscopy. *M. smegmatis* was grown to a cell density of 10^8 cells/mL in a total volume of 500 mL in a 4 L Erlenmeyer flask with constant shaking at 37 °C in Difco Middlebrook 7H9 media supplemented with oleic acid/albumin/dextrose and 0.05% Tween 80. Cells were harvested by centrifugation, and the pellet was washed twice with 5 mM phosphate buffer, pH 6.8. The cell pellet was then resuspended in 200 μL of the same buffer and 500 μL of the resulting cell slurry transferred to a 5 mm NMR tube. Chemical shifts were referenced with respect to 85% phosphoric acid in D_2O in a coaxial capillary. ^{31}P NMR spectra were obtained using a Varian INOVA 300 (at 121.5 MHz) using 60° pulse excitation, proton decoupling, and a 1 s recycle time. A total of 1024 scans were accumulated corresponding to approximately a 60 min total data acquisition time (without aeration). Spectra were analyzed as described elsewhere.[46] The peak corresponding to the α-phosphate of ATP (at ∼−10.5 ppm) and the inorganic phosphate peaks of interest (in the region of 0−1.5 ppm) were used to calculate the internal and external pH using the following equation, where *d* is the distance

between the α-phosphate of ATP and the inorganic phosphate peak, in ppm.

$$\mathrm{pH} = 6.75 + \log \frac{d - 10.85}{13.25 - d}$$

■ ASSOCIATED CONTENT

Supporting Information

Additional table and figures illustrating SCORECONS analysis of MtMenA, MenA/MenG inhibition, methylene blue reduction assay, $\Delta\psi$ dissipation, NMR measurement of ΔpH, ACMA fluorescence results, synthesis schemes and protocols, compound characterization and purity data, and NMR (including qNMR) spectra. This material is available free of charge via the Internet at http://pubs.acs.org.

■ AUTHOR INFORMATION

Corresponding Author

*Tel: 217-333-3374. Fax: 217-244-3186. E-mail: eoldfiel@illinois.edu.

Author Contributions

&These authors contributed equally.

Notes

The authors declare no competing financial interest.

■ ACKNOWLEDGMENTS

This work was supported by the United States Public Health Service (National Institutes of Health grants GM065307, CA158191, HL016101, and AI049151), the National Basic Research Program of China (grants 2011CB710800 and 2011CBA00805), the National Research Foundation of Korea (NRF) funded by the Korean government (MSIP, no. 2007-00559), Gyeonggi-do (no. K204EA000001-09E0100- 00110), and KISTI, and by a grant from the NIH Director's New Innovator Award Program (DP2 OD008463 to D.A.M.), the European Community's Seventh Framework Programme (Grant 260872, S.T.C.), and the Fondation Jacqueline Beytout (B.L.) X.F. was an American Heart Association, Midwest Affiliate, Predoctoral Fellow (grant 13PRE14510056).

■ ABBREVIATIONS USED

UPPS, undecaprenyl diphosphate synthase; FPPS, farnesyl diphosphate synthase; GGPPS, geranylgeranyl diphosphate synthase; CrtM, *S. aureus* dehydrosqualene synthase; MK, menaquinone; MenA, 1,4-dihydroxy-2-naphthoate polyprenyl transferase; MenG, 2-polyprenyl-1,4-naphthoquinone methyltransferase; TMM, trehalose monomycolate; IC_{50}, half maximal inhibitory concentration; MIC, minimum inhibitory concentration required to inhibit the growth of 90% of organisms; PMF, proton motive force; Mt, *M. tuberculosis*; Ms, *M. smegmatis*; Sa, *S. aureus*; Bs, *B. subtilis*; Ec, *E. coli*; Sc, *S. cerevisiae*; Ca, *C. albicans*; Pf, *P. falciparum*; MTT, 3-(4,5-dimethyl-2-thiazolyl)-2,5-diphenyl-2*H*-tetrazolium bromide; IMV, inverted membrane vesicles; TI, therapeutic index; CCCP, *m*-chlorophenylcarbonyl cyanide phenylhydrazone; ACMA, 9-amino-6-chloro-2-methoxyacridine; TLC, thin layer chromatography; THF, tetrahydrofuran

■ REFERENCES

(1) US Department of Health and Human Services Centers for Disease Control and Prevention, Antibiotic resistance threats in the United States 2013. http://www.cdc.gov/drugresistance/threat-report-2013/pdf/ar-threats-2013-508.pdf (accessed March 31, 2014).

(2) World Health Organization, Global tuberculosis report 2013. http://apps.who.int/iris/bitstream/10665/91355/1/9789241564656_eng.pdf?ua=1 (accessed March 31, 2014).

(3) *Report of Two Workshops on Novel Antimicrobial Therapeutics, National Research Council*; The National Academies Press: Washintgon, DC, 2006.

(4) Gray, K. C.; Palacios, D. S.; Dailey, I.; Endo, M. M.; Uno, B. E.; Wilcock, B. C.; Burke, M. D. Amphotericin primarily kills yeast by simply binding ergosterol. *Proc. Natl. Acad. Sci. U.S.A.* **2012**, *109*, 2234−2239.

(5) Fischbach, M. A. Combination therapies for combating antimicrobial resistance. *Curr. Opin. Microbiol.* **2011**, *14*, 519−523.

(6) Silver, L. L. Multi-targeting by monotherapeutic antibacterials. *Nat. Rev. Drug Discovery* **2007**, *6*, 126−126.

(7) Morphy, J. R. The challenges of multi-target lead optimization. *Designing Multi-Target Drugs*; Royal Society of Chemistry: London, 2012; pp 141−154.

(8) Sacksteder, K. A.; Protopopova, M.; Barry, C. E.; Andries, K.; Nacy, C. A. Discovery and development of SQ109: a new antitubercular drug with a novel mechanism of action. *Future Microbiol.* **2012**, *7*, 823−837.

(9) Martin, M. B.; Arnold, W.; Heath, H. T.; Urbina, J. A.; Oldfield, E. Nitrogen-containing bisphosphonates as carbocation transition state analogs for isoprenoid biosynthesis. *Biochem. Biophys. Res. Commun.* **1999**, *263*, 754−758.

(10) Zhang, Y.; Cao, R.; Yin, F.; Hudock, M. P.; Guo, R. T.; Krysiak, K.; Mukherjee, S.; Gao, Y. G.; Robinson, H.; Song, Y.; No, J. H.; Bergan, K.; Leon, A.; Cass, L.; Goddard, A.; Chang, T. K.; Lin, F. Y.; Van Beek, E.; Papapoulos, S.; Wang, A. H.; Kubo, T.; Ochi, M.; Mukkamala, D.; Oldfield, E. Lipophilic bisphosphonates as dual farnesyl/geranylgeranyl diphosphate synthase inhibitors: An X-ray and NMR investigation. *J. Am. Chem. Soc.* **2009**, *131*, 5153−5162.

(11) Protopopova, M.; Hanrahan, C.; Nikonenko, B.; Samala, R.; Chen, P.; Gearhart, J.; Einck, L.; Nacy, C. A. Identification of a new antitubercular drug candidate, SQ109, from a combinatorial library of 1,2-ethylenediamines. *J. Antimicrob. Chemother.* **2005**, *56*, 968−974.

(12) Tahlan, K.; Wilson, R.; Kastrinsky, D. B.; Arora, K.; Nair, V.; Fischer, E.; Barnes, S. W.; Walker, J. R.; Alland, D.; Barry, C. E.; Boshoff, H. I. SQ109 targets MmpL3, a membrane transporter of trehalose monomycolate involved in mycolic acid donation to the cell wall core of *Mycobacterium tuberculosis*. *Antimicrob. Agents Chemother.* **2012**, *56*, 1797−1809.

(13) La Rosa, V.; Poce, G.; Canseco, J. O.; Buroni, S.; Pasca, M. R.; Biava, M.; Raju, R. M.; Porretta, G. C.; Alfonso, S.; Battilocchio, C.; Javid, B.; Sorrentino, F.; Ioerger, T. R.; Sacchettini, J. C.; Manetti, F.; Botta, M.; De Logu, A.; Rubin, E. J.; De Rossi, E. MmpL3 Is the cellular target of the antitubercular pyrrole derivative BM212. *Antimicrob. Agents Chemother.* **2012**, *56*, 324−331.

(14) Makobongo, M. O.; Einck, L.; Peek, R. M.; Merrell, D. S. *In vitro* characterization of the anti-bacterial activity of SQ109 against *Helicobacter pylori*. *PLoS One* **2013**, *8*, e68917.

(15) SQ109; Global Alliance for TB Drug Development. *Handbook of Anti-Tuberculosis Agents. Tuberculosis*; Elsevier: New York, 2008; Vol. *88*, pp 159−161.

(16) Wallace, R. J., Jr.; Nash, D. R.; Steele, L. C.; Steingrube, V. Susceptibility testing of slowly growing mycobacteria by a microdilution MIC method with 7H9 broth. *J. Clin. Microbiol.* **1986**, *24*, 976−981.

(17) Gale, G. R.; McLain, H. H. Effect of ethambutol on cytology of *Mycobacterium smegmatis*. *J. Bacteriol.* **1963**, *86*, 749−756.

(18) Oldfield, E.; Lin, F. Y. Terpene biosynthesis: Modularity rules. *Angew. Chem., Int. Ed.* **2012**, *51*, 1124−1137.

(19) Meganathan, R. Biosynthesis of menaquinone (vitamin K-2) and ubiquinone (coenzyme Q): A perspective on enzymatic mechanisms. *Vitam. Horm.* **2001**, *61*, 173−218.

(20) Kurosu, M.; Narayanasamy, P.; Biswas, K.; Dhiman, R.; Crick, D. C. Discovery of 1,4-dihydroxy-2-naphthoate prenyltransferase inhibitors: New drug leads for multidrug-resistant gram-positive pathogens. *J. Med. Chem.* **2007**, *50*, 5048−5048.

(21) Kurosu, M.; Crick, D. C. MenA is a promising drug target for developing novel lead molecules to combat *Mycobacterium tuberculosis*. *Med. Chem.* **2009**, *5*, 197−207.
(22) Dhiman, R. K.; Mahapatra, S.; Slayden, R. A.; Boyne, M. E.; Lenaerts, A.; Hinshaw, J. C.; Angala, S. K.; Chatterjee, D.; Biswas, K.; Narayanasamy, P.; Kurosu, M.; Crick, D. C. Menaquinone synthesis is critical for maintaining mycobacterial viability during exponential growth and recovery from non-replicating persistence. *Mol. Microbiol.* **2009**, *72*, 85−97.
(23) Zhang, Y. H.; Cao, R.; Yin, F.; Hudock, M. P.; Guo, R. T.; Krysiak, K.; Mukherjee, S.; Gao, Y. G.; Robinson, H.; Song, Y.; No, J. H.; Bergan, K.; Leon, A.; Cass, L.; Goddard, A.; Chang, T. K.; Lin, F. Y.; Van Beek, E.; Papapoulos, S.; Wang, A. H. J.; Kubo, T.; Ochi, M.; Mukkamala, D.; Oldfield, E. Lipophilic bisphosphonates as dual farnesyl/geranylgeranyl diphosphate synthase inhibitors: An X-ray and NMR investigation. *J. Am. Chem. Soc.* **2009**, *131*, 5153−5162.
(24) Krogh, A.; Larsson, B.; von Heijne, G.; Sonnhammer, E. L. L. Predicting transmembrane protein topology with a hidden Markov model: Application to complete genomes. *J. Mol. Biol.* **2001**, *305*, 567−580.
(25) Kelley, L. A.; Sternberg, M. J. E. Protein structure prediction on the web: A case study using the Phyre server. *Nat. Protoc.* **2009**, *4*, 363−371.
(26) Lin, F. Y.; Liu, Y. L.; Li, K.; Cao, R.; Zhu, W.; Axelson, J.; Pang, R.; Oldfield, E. Head-to-head prenyl tranferases: Anti-infective drug targets. *J. Med. Chem.* **2012**, *55*, 4367−4372.
(27) Valdar, W. S. Scoring residue conservation. *Proteins* **2002**, *48*, 227−241.
(28) Sala, C.; Dhar, N.; Hartkoorn, R. C.; Zhang, M.; Ha, Y. H.; Schneider, P.; Cole, S. T. Simple model for testing drugs against nonreplicating *Mycobacterium tuberculosis*. *Antimicrob. Agents Chemother.* **2010**, *54*, 4150−4158.
(29) Felser, A.; Blum, K.; Lindinger, P. W.; Bouitbir, J.; Krahenbuhl, S. Mechanisms of hepatocellular toxicity associated with dronedarone-a comparison to amiodarone. *Toxicol. Sci.* **2013**, *131*, 480−490.
(30) Garlid, K. D.; Nakashima, R. A. Studies on the mechanism of uncoupling by amine local-anesthetics - evidence for mitochondrial proton transport mediated by lipophilic ion-pairs. *J. Biol. Chem.* **1983**, *258*, 7974−7980.
(31) Moreno-Sanchez, R.; Bravo, C.; Vasquez, C.; Ayala, G.; Silveira, L. H.; Martinez-Lavin, M. Inhibition and uncoupling of oxidative phosphorylation by nonsteroidal anti-inflammatory drugs study in mitochondria, submitochondrial particles, cells, and whole heart. *Biochem. Pharmacol.* **1999**, *57*, 743−752.
(32) Yu, E. W.; McDermott, G.; Zgurskaya, H. I.; Nikaido, H.; Koshland, D. E. Structural basis of multiple drug-binding capacity of the AcrB multidrug efflux pump. *Science* **2003**, *300*, 976−980.
(33) Haagsma, A. C.; Podasca, I.; Koul, A.; Andries, K.; Guillemont, J.; Lill, H.; Bald, D. Probing the interaction of the diarylquinoline TMC207 with its target mycobacterial ATP synthase. *PLoS One* **2011**, *6*, e23575.
(34) Moon, R. B.; Richards, J. H. Determination of intracellular pH by ^{31}P magnetic-resonance. *J. Biol. Chem.* **1973**, *248*, 7276−7278.
(35) Mukkamala, D.; No, J. H.; Cass, L. A.; Chang, T. K.; Oldfield, E. Bisphosphonate inhibition of a Plasmodium farnesyl diphosphate synthase and a general method for predicting cell-based activity from enzyme data. *J. Med. Chem.* **2008**, *51*, 7827−7833.
(36) Bonitz, T.; Alva, V.; Saleh, O.; Lupas, A. N.; Heide, L. Evolutionary relationships of microbial aromatic prenyltransferases. *PLoS One* **2011**, *6*, e27336.
(37) Meng, J.; Wang, F.; Zheng, Y.; Peng, X.; Zhou, H.; Xiao, X. An uncultivated crenarchaeota contains functional bacteriochlorophyll a synthase. *ISME J.* **2009**, *3*, 106−116.
(38) Rao, S. P.; Lakshminarayana, S. B.; Kondreddi, R. R.; Herve, M.; Camacho, L. R.; Bifani, P.; Kalapala, S. K.; Jiricek, J.; Ma, N. L.; Tan, B. H.; Ng, S. H.; Nanjundappa, M.; Ravindran, S.; Seah, P. G.; Thayalan, P.; Lim, S. H.; Lee, B. H.; Goh, A.; Barnes, W. S.; Chen, Z.; Gagaring, K.; Chatterjee, A. K.; Pethe, K.; Kuhen, K.; Walker, J.; Feng, G.; Babu, S.; Zhang, L.; Blasco, F.; Beer, D.; Weaver, M.; Dartois, V.; Glynne, R.; Dick, T.; Smith, P. W.; Diagana, T. T.; Manjunatha, U. H. Indolcarboxamide is a preclinical candidate for treating multidrug-resistant tuberculosis. *Sci. Transl. Med.* **2013**, *5*, 214ra168.
(39) Grzegorzewicz, A. E.; Pham, H.; Gundi, V. A.; Scherman, M. S.; North, E. J.; Hess, T.; Jones, V.; Gruppo, V.; Born, S. E.; Kordulakova, J.; Chavadi, S. S.; Morisseau, C.; Lenaerts, A. J.; Lee, R. E.; McNeil, M. R.; Jackson, M. Inhibition of mycolic acid transport across the *Mycobacterium tuberculosis* plasma membrane. *Nat. Chem. Biol.* **2012**, *8*, 334−341.
(40) Owens, C. P.; Chim, N.; Goulding, C. W. Insights on how the *Mycobacterium tuberculosis* heme uptake pathway can be used as a drug target. *Future Med. Chem.* **2013**, *5*, 1391−1403.
(41) Owens, C. P.; Chim, N.; Graves, A. B.; Harmston, C. A.; Iniguez, A.; Contreras, H.; Liptak, M. D.; Goulding, C. W. The *Mycobacterium tuberculosis* secreted protein Rv0203 transfers heme to membrane proteins MmpL3 and MmpL11. *J. Biol. Chem.* **2013**, *288*, 21714−21728.
(42) Gruppo, V.; Johnson, C. M.; Marietta, K. S.; Scherman, H.; Zink, E. E.; Crick, D. C.; Adams, L. B.; Orme, I. M.; Lenaerts, A. J. Rapid microbiologic and pharmacologic evaluation of experimental compounds against Mycobacterium tuberculosis. *Antimicrob. Agents Chemother.* **2006**, *50*, 1245−1250.
(43) CLSI. Reference Method for Broth dilution Antifungal Susceptibility Testing of Yeasts. In *Approved Standard-Third ed.*; Clinical and Laboratory Standards Institute: Wayne, PA, 2008.
(44) No, J. H.; de Macedo Dossin, F.; Zhang, Y.; Liu, Y. L.; Zhu, W.; Feng, X.; Yoo, J. A.; Lee, E.; Wang, K.; Hui, R.; Freitas-Junior, L. H.; Oldfield, E. Lipophilic analogs of zoledronate and risedronate inhibit Plasmodium geranylgeranyl diphosphate synthase (GGPPS) and exhibit potent antimalarial activity. *Proc. Natl. Acad. Sci. U.S.A.* **2012**, *109*, 4058−4063.
(45) Compain, J. D.; Mialane, P.; Marrot, J.; Secheresse, F.; Zhu, W.; Oldfield, E.; Dolbecq, A. Tetra- to dodecanuclear oxomolybdate complexes with functionalized bisphosphonate. *Chem.—Eur. J.* **2010**, *16*, 13741−13748.
(46) Navon, G.; Ogawa, S.; Shulman, R. G.; Tamane, T. High-resolution ^{31}P nuclear magnetic-resonance studies of metabolism in aerobic *Escherichia coli* cells. *Proc. Natl. Acad. Sci. U.S.A.* **1977**, *74*, 888−891.

B.4 References

1. Li, K., Schurig-Briccio, L.A., Feng, X., Upadhyay, A., Pujari, V., Lechartier, B., Fontes, F.L., Yang, H., Rao, G., Zhu, W., *et al.* (2014) Multitarget drug discovery for tuberculosis and other infectious diseases. *J Med Chem*: **57**, 3126-3139.

2. Zhang, Y., Fu-Yang, L., Li, K., Zhu, W., Liu, Y.L., Cao, R., Pang, R., Lee, E., Axelson, J., Hensler, M., *et al.* (2012) HIV-1 integrase inhibitor-inspired antibacterials targeting isoprenoid biosynthesis. *ACS Med Chem Lett*: **3**, 402-406.

3. Zhu, W., Zhang, Y., Sinko, W., Hensler, M.E., Olson, J., Molohon, K.J., Lindert, S., Cao, R., Li, K., Wang, K., *et al.* (2013) Antibacterial drug leads targeting isoprenoid biosynthesis. *Proc Natl Acad Sci U S A*: **110**, 123-128.